FLUID APPLICATION SYSTEM OPTIMISATION FOR HIGH SPEED GRINDING

VLADIMIR GVINIASHVILI

A thesis submitted in partial fulfilment of the requirement of Liverpool John Moores University for the degree of Doctor of Philosophy

November 2003

ABSTRACT

The thesis explores the scientific basis for the design of fluid delivery systems for grinding. It is assumed that the optimal fluid delivery system can only be designed if the physical process of the fluid behaviour in the grinding is known. A study of the factors influencing fluid flow in the grinding wheel-workpiece interface revealed the possibility to predict the flowrate that passes through the grinding zone by two new analytical models.

According to the first model it was found that the flowrate passing though the grinding zone is a function of contact pressure between grinding wheel and workpiece, wheel speed, nozzle flowrate, and fluid density.

The second model shows that flowrate through the grinding zone is a function of spindle power for fluid acceleration, wheel speed and nozzle jet velocity. Empirical loss coefficients are introduced for both models, the values lying between 0 and 1.

Based on the findings, a design criterion for optimisation of a fluid application system is proposed. The main criterion is considered to be minimum system power utilisation to satisfy the fluid requirements for grinding. In other words, an optimal fluid delivery system must deliver fluid to the grinding zone at a required flowrate and fluid velocity with minimum energy.

The new theory was experimentally validated for a range of delivery nozzles, delivery flowrates, wheel speeds and wheel types. Experiments for high speed grinding were performed in order to demonstrate the effect of delivery fluid minimisation on grinding performance of a "difficult to grind" material such as Inconel 718.

ACKNOWLEDGMENTS

I would like to thank my director of studies, Professor W.B. Rowe for his invaluable guidance and help throughout the course of the work. Thanks are also given to Dr. M. Morgan, Dr. N. Woolley and Dr. D. Allanson for their support during the research.

Acknowledgments are also extended to EPSRC for grant support and to the collaborating partners, Castrol, Dittel, Jones & Shipman, RollsRoyce, Timken and Wendt Boart for financial support, advice and practical assistance.

Finally I would like to thank everyone at AMTTREL especially Mr. P.D. Wright, Mr. P. Moran and T. Scargill for their sustained enthusiasm and help.

NOMENCLATURE

Symbol	Meaning
A	Cross sectional area.
A_1	Initial cross sectional area.
A_{exp}	Expanded cross sectional area.
a	Effective air flow thickness from the wheel surface.
α	Contraction angle of nozzle.
b	Wheel, nozzle gap and workpiece widths.
d_e	Effective diameter of a pipe.
d_n	Diameter within the nozzle.
d_o	Orifice diameter.
d_p	Pipe diameter.
F	Force.
F_c	Centripetal force
F_f	Force required for fluid acceleration within the contact zone.
F_p	Force due to atmospheric pressure.
f	Fluid friction factor.
g	gravitational acceleration
h	head pressure
h_a	Air film thickness in the contact zone.
h_s	Elemental fluid thickness on the wheel surface.
h_f	Fluid film thickness in the grinding zone.
h_g	Depth of the wheel surface grains.
h_j	Nozzle gap thickness.
K_c	Loss coefficient for contracted area.
K_f	Spindle power loss coefficient
K_g	Fluid velocity loss coefficient in the converging gap.
K_j	Jet velocity loss coefficient

K_p	Ratio of spindle power to jet power.
l_1 *to* l_2	Length of the contact pressure variation.
l_n	A length within the nozzle.
l_p	Length within a pipe.
l_s	Elemental fluid contact length on the wheel peripheral surface.
m	Mass.
$\dot{m}$	Mass flowrate
$\dot{m}_a$	Air mass flowrate
$\dot{m}_{ac}$	Air mass flowrate through the contact zone.
$\dot{m}_g$	Shoe nozzle mass flowrate passing through the gap.
$\dot{m}_j$	Jet mass flowrate
$\dot{m}_l$	Shoe nozzle leakage mass flowrate.
$\dot{m}_n$	Mass flowrate through the nozzle.
$\dot{m}_s$	Shoe nozzle mass flowrate through the wheel porous.
$\dot{m}_u$	Useful mass flowrate.
$\dot{m}_{ua}$	Actual useful flowrate after making allowance for air mixing.
n	Rotational speed of the wheel.
P	Power.
p_a	Absolute atmospheric pressure.
p_c	Contact pressure.
p_s	Pressure on the wheel surface.
P_{con}	Power loss due to a sudden contraction.
P_{exp}	Power loss due to a sudden expansion.
P_f	Spindle power due to fluid.
P_{gr}	Frictional power loss within the gradually contracted area.
P_j	Nozzle jet power.
p_{max}	Maximal contact pressure.
p_n	Pressure at nozzle inlet.
P_n	Power loss within the nozzle.
P_p	Power loss within the pipe.

P_s	Spindle power due to fluid acceleration within the shoe nozzle.
R	Gas constant (R = 287 J/kg K for air).
r	Wheel radius.
Re	Reynolds number.
r_n	Radius of the pipe at nozzle inlet.
ρ_a	Air density (1.293 kg/m^3).
ρ_{ac}	Air density in the contact zone.
ρ_f	Grinding fluid density (1000 kg/m^3 for water)
T	Absolute temperature
T_f	Turning torque on the spindle due to fluid.
v_a	Air velocity
v_{cr}	Critical wheel peripheral velocity.
$\overline{v}_{exp}$	Mean fluid velocity within expanded area
v_g	Velocity of the fluid in the converging gap.
v_{gn}	Fluid velocity through the shoe nozzle gap.
v_{in}	Fluid velocity at nozzle inlet.
v_j	Jet velocity
v_l	Velocity of the fluid leaking from the shoe nozzle.
v_p	Fluid velocity within the pipe.
v_s	Wheel peripheral velocity..
v_t	Tangential velocity of a particle.
ϕ	Wheel porosity.
η	Dynamic viscosity.

CONTENTS

LIST OF FIGURES

LIST OF TABLES

CHAPTER 1. INTRODUCTION.

1.1 Background.

Grinding is an important machining process, widely used in the production of fine tolerances and smooth finishes. Compared with many machining processes, grinding requires high energy per unit volume of material removed. The high energy is due to redundant material deformation and high friction in the cutting zone. The thermal energy is concentrated within the small grinding contact zone. This concentration of energy causes an increase in temperature that can damage the workpiece and accelerate wheel wear. Fluid delivery is very important in grinding, helping to reduce energy dissipation and prevent thermal damage by providing lubrication and cooling.

There are different types of grinding fluids, but the fundamental functions and purposes are similar. They can be subdivided into:

- Oil-based
- Water-based
- Dry (carbon and air, for example)

Each type of fluid has different properties. Oil-based and water-based fluids are the most popular with oil-based fluids usually providing enhanced lubrication effects and corrosion resistance in comparison with water-based fluids. However, water-based fluids have the advantages of high chemical stability, transparency and better cooling efficiency.

There is much empirical information available for the efficacy of different grinding fluids. However, the scientific basis of selection and design of fluid delivery systems is still in an early stage of development. There are many aspects, which need to be known before system design can be placed on a rational basis. In particular, there is a need to know how much of the grinding fluid delivered from a delivery nozzle usefully enters the grinding contact to provide lubrication and cooling of the grinding process. In other words, what is the 'useful flow-rate'? This question implies a need to understand the variables affecting useful flowrate and a need to predict useful flowrate. Following on

from these questions, it is possible to start to address the question of optimising useful flowrate and optimising system design.

One of the main aspects that need to be considered in design of a fluid delivery system is the power required by the whole process. This includes power consumption of the system itself and the power consumption due to the spindle drag of the grinding machine caused by the fluid. Generally, enhancing useful flowrate with low total power consumption implies increased efficiency of fluid delivery. It also implies energy efficiency of the grinding process.

However other parameters, such as contact pressure in the grinding wheel-workpiece interface and pressure within the delivery system are also important. High-pressure delivery systems are expensive and high pressure in the wheel-workpiece contact zone may be undesirable for size-holding depending on the particular grinding operation.

It is therefore necessary to analyse fluid behaviour in the wheel-workpiece interface, as a basis for design of an optimal fluid application system.

1.2 Aims and Objectives.

The aim was to investigate fluid behaviour in the wheel-workpiece interface and develop a method for designing an optimal fluid delivery system.

The following detailed objectives were set:

- To review previous work concerning the effect of fluid type on the grinding process, flow behaviour in the wheel-workpiece interface and the application of fluid systems and methods.

- To determine the main parameters affecting flow behaviour in the wheel-workpiece interface.

- To develop a theory for useful flowrate through the contact zone

- To undertake experiments to validate the theory for a range of wheel speeds, delivery flowrate nozzle positions and wheel types.

- Based on the findings, to develop a method for designing an optimal nozzle for fluid application.

- To conduct experiments with various nozzle designs to validate the new approach for nozzle design.

- To conduct trials for the effect of delivery flowrate minimisation on high speed CBN grinding of a "difficult to grind material" using the optimal nozzle design.

1.3 Scope of the Investigation.

A review of previous work in chapter 2 describes three aspects concerning the process fluid in grinding. The first part considers the properties of various fluids and effect of application for grinding. The second part is concentrated on the fluid functionality in the contact region between the wheel and the workpiece. The third part describes the various methods for fluid supply to the wheel-workpiece contact region.

Following a review of the literature on grinding fluids, the need to determine useful flowrate was identified. A study of the factors influencing useful flowrate led to a method for correlating useful flowrate with important parameters such as contact pressure, spindle power, wheel speed, delivery flowrate, nozzle design and wheel type.

Models for fluid flow near and through the grinding zone are presented in chapter 3. Initially the condition of the fluid interaction, including air, with the surface of the rotating wheel was defined.

Useful flowrate was determined from a consideration of the fluid energy in the wheel-workpiece interface. Accordingly, a first model correlates useful flowrate with contact pressure in the grinding wheel-workpiece interface, delivery nozzle flowrate, wheel speed, fluid mean velocity within the converging gap and the fluid density. A velocity loss coefficient was introduced, the value of which was obtained from experiments. It was assumed that the coefficient depends on the wheel geometry, jet velocity, abrasive property and fluid property. The model also gives consideration to the air-flow interaction within the contact zone between the wheel and the workpiece.

The second model predicts useful flowrate which is correlated with spindle power for fluid acceleration, wheel speed and delivery-nozzle jet velocity. Two loss coefficients are also introduced, which were calibrated experimentally. The model makes it possible to determine a suitable value of nozzle outlet gap to achieve a required fluid film thickness in the grinding zone. This leads to the optimisation of the jet velocity in relation to the power required to accelerate the fluid and the particular velocity of the wheel.

A theoretical method for nozzle design was developed based on fluid power loss within the nozzle. After the factors influencing the useful flowrate including nozzle output jet

parameters are identified, optimal nozzle design is defined as the nozzle giving least power loss. An equation is derived for calculation of power loss for a gradually converging nozzle. The power loss in the whole fluid delivery system is also considered.

An experimental rig and the equipment used during the experiments are described in chapter 4. The experimental rig allowed measurement of wheel speed, spindle power, contact pressure in the wheel-workpiece interface, useful flowrate, delivery flowrate and pressure in the fluid delivery system. Surface measuring devices are also described. Issues concerning the power meter, force table and flow meter calibration are discussed.

The experimental results are presented in chapter 5. The effect of nozzle position and nozzle distance from the wheel on useful flowrate are given for a range of delivery flowrate and wheel speed. Experiments were conducted to improve a conventional fluid delivery system by optimising delivery nozzle flowrate and jet velocity after an optimal nozzle position had been defined. An impervious aluminium disc and a porous CBN grinding wheel were tested for various delivery flowrates and nozzle gap sizes. The effects of the nozzle jet and the nozzle flowrate on useful flowrate were compared.

The models for fluid flow in the wheel-workpiece interface were validated experimentally for a range of delivery flowrate, nozzle gap size and wheel speed, for both porous and impervious wheels.

Experimental results were provided for power loss within nozzles of various designs. Experimental results for nozzle loss were compared with calculated values. Experimental power loss and theoretical power loss within the gradual contraction were also compared.

Further experiments were carried out for high speed CBN grinding of Inconel 718 using the shoe nozzle design chosen for this operation. Delivery flowrate to the nozzle was gradually reduced with the aim that the power consumption due to the fluid process as well as total power would be reduced. The effect of nozzle flowrate minimisation on the grinding performance is presented. Grinding performance was evaluated in terms of total power, power consumed due to the fluid process, specific energy, workpiece bulk

temperature, workpiece size holding, workpiece roundness, workpiece roughness and workpiece hardness.

Conclusions are summarised in chapter 6.

Recommendations for further work are given in chapter 7.

CHAPTER 2. LITERATURE REVIEW.

2.1 Grinding Fluid Selection

The fluid affects the tribological mechanism at the interface between the chip material being removed and the cutting edge material used to remove the chip. The main criteria for fluid application are the cooling and lubricating properties. However, usefulness of a grinding fluid depends not only on its behaviour in the immediate vicinity of the grinding contact but also on performance away from the region. Both aspects must be considered in the selection of a fluid. Wider considerations include chemical stability, ease of disposal, dermatological properties, and cost.

Wagner, 1950 [1] tried three grinding fluids: oil, water and air. He found that oil was the best lubricant, because there was least wear of the abrasive. With air, wear was increased, while wear was most rapid with water. It was also shown that water plus some additives gave better performance than plain water.

Outwater and Shaw, 1952 [2] used grinding forces as a measure of grinding fluid effectiveness and found that air was effective as a grinding fluid. An inert atmosphere was created using nitrogen and helium. In the inert atmosphere, grinding forces were many times greater than in air. The chip and workpiece surfaces remained clean resulting in the surfaces welding together. In air, oxygen oxidized the freshly formed surfaces and prevented welding. This example illustrates the importance of chemical activity in the grinding process.

In most cases, however, air fails to provide sufficient cooling and lubrication properties. Oil also has poor cooling properties. Chemical solutions and oil-in-water emulsions are widely used to bridge the gap between lubrication and cooling. Emulsions consist of tiny droplets of oil dispersed in water. Grinding fluid solutions often contain additives such as sulphur, chlorine or phosphorous to improve lubrication. Other ingredients are added to improve the service characteristics of the product. These include surface-active agents to enhance wetting action and detergency of the fluid and to prevent foaming. Other additives include organic and inorganic rust inhibitors, water conditioners for hard water areas, and germicides.

Tarasov, 1961 [3] discussed the effectiveness of fluid composition based on economic aspects. A richer concentration of oil in water provides better lubrication but increases cost. A rich mixture also has less cooling ability than a lean mixture. Another problem with a rich mixture is "gum loading" of the wheel face. Gum loading was found to start with jellylike particles of the compound collecting in the pores of the wheel. Fine grinding swarf then became attached to the initial deposit and reduced clearance between the abrasive grains. Sometimes transparency of an emulsion is important if it is desirable for the operator to see the work in the immediate vicinity of the wheel. Emulsions vary from milky or opaque to completely transparent, depending primarily on the size of the particles present in the water. Tarasov also observed that individual droplets in soluble-oil emulsions were generally in the range from 40 to 200 microinches in size, and somewhat smaller in chemical emulsions. Since the wavelength of visible light is from 16 to 28 microinches, the droplets in emulsions may be large enough to absorb light partly or completely so that the emulsion is either transparent or opaque. In colloidal chemical solutions and in true chemical solutions droplets are many times smaller than in emulsions. As a result of the small particle size, the solutions are transparent. In addition, Tarasov identified several types of wheel wear that occurred in grinding:

Attritious	Development of wear flat areas on abrasive grains formed mechanically or chemically.
Grain fracture	Formation of new cutting edges.
Bond Fracture	Eventually loss of remaining grain.

Ueno, 1970 [4] tested cooling ability of various fluids by heating a notched bar and welded junction of two different types of materials. Results obtained were correlated with the actual cutting process. For the experimental conditions conducted, he obtained a lower cutting zone temperature with fluids having a small heat transfer coefficient such as oil than with fluids having a large heat transfer coefficient such as water. This suggests that temperature can be reduced not only by direct cooling, but also by effective lubrication in the cutting zone.

Osman and Malkin, 1972 [5] conducted experiments for grinding with cutting oil, soluble oil, plain water and dry grinding. The three fluids were compared on the basis of

parameters such as wheel wear, surface roughness, specific energy, and G-ratio. Cutting oil gave lower roughness, larger grinding ratios, lower specific cutting energies and lower attritious wear rate of the grinding wheel grains than the other fluids. The highest roughness was generated with water at low speed and with dry grinding at high speed. With the exception of water, low speed grinding always gave slightly lower roughness than dry grinding at high speed. On the basis of G-ratio, surface roughness, and grinding wheel life, it was concluded that cutting oil was the best grinding fluid for conventional operating conditions using an aluminium oxide grinding wheel in experiments under the following conditions:

Wheel speed: 30 and 61 m/s

Table speed: 4.5 and 9.1 m/min

Depth of cut: 0.0254 mm.

Doyle and Turley, 1976 [6] studied the influence of fluid on the process of metal adhering on the workpiece surface. They found that metal particles initially adhered to a grinding wheel and subsequently adhere back to the workpiece. Microscopic and metallurgical examinations revealed considerable amount of material redeposited onto the workpiece surface when dry grinding a brass material. Consequently this increased surface roughness. With water and water-based fluids, re-deposition was reduced and almost totally eliminated by the use of oil. They reported similar results when grinding steel.

Yasui [7] 1983 studied the influence of oil, water-based fluids and dry grinding on temperature rise and forces in conventional grinding. The temperature with water-based fluids was minimal, with oil was intermediate and was highest for dry grinding. However above the boiling temperature of a water-based fluid (100°C) a catastrophic temperature rise was observed, similar to dry grinding. Boiling also resulted in a steep increase of both tangential and normal forces for the water-based fluid. Lower grinding forces were measured with oil than with the other two fluids.

Ye and Pearce, 1984 [8] compared water-based and neat oil in creep feed grinding of a nickel-based alloy with a high-porosity wheel. The fluids were compared with respect to factors such as specific energy, workpiece burn, wheel wear and surface roughness. Similarly to others, it was observed that grinding with oil resulted in less wheel profile

wear and lower surface roughness. However, a higher normal force was obtained and workpiece burn occurred at lower stock removal rates. Tangential force was 20-40 per cent lower with oil than with water. Oil was preferred for conventional grinding. Water based fluids were recommended for creep-feed grinding due to good cooling ability. It was noted that application of water gave rise to reduced wheel porosity compared with oil.

Howes, 1987 [9], 1990 [10] described the phenomenon of fluid-film boiling. He stated that below the boiling temperature coolant acts as an effective coolant and low values of thermal partitioning coefficient were obtained. However above this level, temperature rose dramatically and was nearly the same as in dry grinding. He measured boiling temperature for water-based fluids of 130°C and for oils of 300°C. He also pointed out from experience with boiler tubes, that at the transition between fluid boiling and complete fluid 'burn-out' very high heat transfer coefficients were possible.

Warren, 1994 [11] considered the cooling ability of water-based fluids. He concluded that, the best grinding performance was with oil-in-water emulsions where water was the main component. In this case, the heat transfer rate of the emulsion was almost three times higher than an equal weight of oil. In addition, it was suggested that leakage of grinding fluid into the hydraulic system of the machine must be taken into account when selecting a coolant. If leakage occurs, the fluid should not impair functioning of the oil. For instance, an alkaline solution has been known to break down some of the hydraulic oil, forming soap, thus producing sticky deposit in control ports, and shutting down the grinding machine. Warren also found that some wheel bonds were weakened by particular chemicals. Vitrified and metal bonds were generally immune to all known compounds, but resinoid, shellac, and silicate bonds were affected by alkali, and a rubber bond could be affected by oil.

Yokogawa, 1996 [12] conducted experiments using air for cooling combined with extremely small amounts of vegetable oil. Reasonably low residual stress and low surface roughness were observed using a CBN wheel at a low speed of 30 m/s.

Baheti, Guo and Malkin, 1998 [13] undertook an investigation to explore environmentally safe and hygienic alternatives to conventional soluble oils. Various

types of environmentally safe fluids were investigated including liquid nitrogen, cold air, ester oil applied in minuscule amounts, as well as dry grinding and soluble oil for comparison. The fluids were evaluated in terms of the power and specific energy, as measures of lubrication effectiveness. Grinding temperatures and energy partition to the workpiece were related to cooling effectiveness. It was demonstrated experimentally that liquid nitrogen and cold air could reduce energy partition to the workpiece. However these fluids did not provide sufficient lubrication. It was concluded that environmentally safe ester oil was capable of providing good lubrication and, when applied together with cold air, a cooling effectiveness comparable to soluble oil. Although liquid nitrogen provided better cooling, a high specific energy was observed.

Walter, 1999 [14] found that a sulphur additive in the oil reacted with the freshly generated chemically active surface of the workpiece. Calcium also existed in significant concentration in the ground surface. It was also found that an increase in feedrate leads to lower sulphur concentrations. This was explained by shorter contact time with the workpiece surface. Based on industrial experience and surface roughness observation, a sulphur concentration of 5% was recommended. In addition, it was determined that the grinding wheel specification has an influence on the generation of reaction layers.

Shaji, 2002 [15] investigated the application of graphite in grinding in comparison with conventional flood coolant application. Fine graphite powder is a high temperature solid lubricant and mixed with water-soluble oil to form a paste was applied to the grinding wheel surface. For this purpose, a special experimental set-up was developed. Lower roughness was achieved with a harder material than with a ductile material. Tangential force and specific energy were reduced under the conditions tested. However it was found that the wheel pores filled with graphite powder and with chips resulting in wheel loading.

Based on this review of previous research, it can be concluded that water-based fluids and oils are usually preferred for grinding operations. Water-based fluids are found to be good coolants. However water-based fluids are limited by the boiling temperature, which is low in comparison to oils. Although water-based fluids are superior to oils for cooling, they offer inferior lubrication. In some cases, lubrication properties can

significantly reduce contact temperature. Consequently oils often provide lower roughness.

Choosing the best fluid is a matter of selecting the characteristics to meet the requirements of the particular job. For instance, in shallow grinding, oils can give good grinding results. This is implied by the fact that friction is reduced by lubrication and prevents temperature rise. Improved lubrication can be achieved even with minimum quantity lubrication (MQL). Increase in wheel speed generates higher friction and therefore higher temperature. Under this condition, direct cooling becomes important, since the temperature cannot be suppressed only by lubrication. In this case, water-based fluids are usually preferred to oils. It must be noted that the concentration of oil in a water-based fluid significantly improves grinding performance.

For deep grinding, where the generation of heat in the contact zone may be extremely high, a fluid with a good cooling ability is of paramount importance.

Solids and gases may be used too. These coolants/lubricants are important to prevent environmental pollution. Also solids or gases may be appropriate if liquid cannot be used. Grinding of optical equipment with inert carbon dioxide is an example.

2.2 The Flow Process in the Grinding Wheel-Workpiece Interface

Grinding differs from some machining processes in the high friction experienced in the cutting zone. Grinding requires high energy input into the cutting region, where most of the energy is converted into heat. High temperature can cause workpiece damage and increased rate of wheel wear. Another important parameter is the pressure developed in the cutting region between grinding wheel and workpiece. High contact pressure can cause high normal force and size error. To some extent, a high contact pressure can be an advantage in the grinding process, which is discussed in this chapter.

Efimov et al, 1980 [16] conducted experiments to determine the influence of delivery flowrate on contact pressure for conventional low-speed shallow grinding. Various types of grinding wheel were employed during the experiments. Wheels were tested with different porosities having the same grit size and also a metal bonded wheel with no bulk porosity. He observed an increase in contact pressure with increasing delivery flowrate and reducing porosity of the grinding wheel. A wheel with no bulk porosity gave the highest contact pressure.

Khudobin, 1981 [17] found a damping effect due to the fluid between the wheel and the workpiece when sparking-out. Lower vibration amplitude was measured with fluids having higher viscosity than fluids having lower viscosity. This resulted in lower surface roughness of ground parts. It was concluded that increasing coolant pressure in the grinding arc could suppress formation of chatter marks on the ground workpiece.

Akiyama, 1984 [18] investigated the influence of the air layer and nozzle angle on fluid flow through the grinding zone. The presence of grinding fluid, was assessed by measuring the electrical resistance of the fluid passing through the contact zone. The fluid film thickness was estimated from an experimental calibration curve obtained with a device simulating the equivalent gap in the contact zone. Electrical resistance of the fluid near the wheel periphery was measured based on the assumption that the fluid sticks to the grinding wheel and is then dragged into the contact gap,. Varying delivery nozzle angle, the volumetric ratio of liquid to air was determined. The maximum value was adopted as a criterion for optimising nozzle angle.

Maksoud and Howes, 1989 [19] investigated a problem of vibration in grinding, which consequently causes waviness on the ground parts. It was shown that introducing a hydrodynamic pressure between wheel and workpiece could lead to a more stable grinding process. It was suggested that high viscosity fluids and impervious grinding wheels are possible solutions to the problem. This supports the findings by Khudobin.

Schumack et al, 1991 [20] described fluid flow under a smooth rotating wheel and workpiece at a minimal gap. Measured contact pressure was compared with predicted values. Predicted flow using lubrication theory gave reasonable agreement with experiment for low Reynolds number (laminar flow). However the model failed at high Reynolds number (turbulent flow).

Engineer, Guo and Malkin, 1992 [21] designed a rig to measure flowrate through the grinding zone in straight plunge grinding using conventional flood application at low wheel speed (30 m/s). The rig involved plates on each side of the wheel that separated useful flowrate from the flowrate that did not pass through the grinding zone. The useful flowrate was collected and weighed. Total delivered flowrate was measured by a flow-meter. Delivered flowrate was varied up to 0.24 l/min mm. Observations included the effect of work-speed, depth of cut, nozzle flowrate, nozzle position, wheel type (porosity) and dressing conditions on useful flowrate. Six vitrified wheels, all having the same abrasive grit size but different grades and structure numbers were tested. Under the experimental conditions employed, it was shown that useful flowrate significantly increased with delivered flowrate for more porous wheels and with nozzle position closer to the grinding zone. Wheel dressing conditions had only a secondary influence. Workspeed and depth of cut had virtually no effect on useful flowrate. It was found that above a particular delivered flow rate, saturation takes place. That is to say, useful flow rate could not be further increased. Accordingly, excess coolant is rejected.

Based on their experimental results Guo and Malkin [22] 1992 theoretically analysed the flow process in grinding in terms of fluid tangential velocity, radial velocity, depth of penetration into the porous wheel and useful flowrate through the grinding zone. A dimensionless effective wheel porosity parameter was introduced which was a ratio of surface porosity of the wheel to its bulk porosity. It gave a compromise solution between these two porosities, since surface porosity was higher than bulk porosity.

Creep feed wheels had much higher effective porosity than conventional wheels, which resulted in increase of useful flowrate. Based on the assumptions, it was shown that nozzle position, nozzle velocity, flowrate and effective wheel porosity are the four main factors that most significantly influence useful flowrate through the grinding zone.

Guo, Krishnan and Malkin, 1993 [23] estimated horizontal and vertical forces exerted on the workpiece by the fluid during deep grinding. At a large depth of cut, fluid at wheel speed caused significant horizontal force by impinging on the end face of the workpiece.

Brinksmeier and Minke, 1993 [24] investigated the influence of the fluid in high-speed surface grinding with electro-plated CBN wheels. The spindle power due to the fluid significantly increased with wheel velocity at a particular delivery flowrate and was 3 – 4 times higher than cutting power. High normal force was measured, caused by the fluid contact-pressure, which increased with wheel speed and delivered flowrate. However lower normal forces due to the fluid were found for a range of flow rates at a specific wheel speed. Work speed had no influence on the fluid normal force.

Okuyama et al, 1993 [25] estimated the heat transfer coefficient by heating the workpiece in the contact region between a grinding wheel and a smooth aluminium disk. The heat transfer coefficient increased with delivered flowrate. Reducing the gap size also enhanced the cooling due to high fluid velocity on the workpiece surface. However the coefficient was almost constant for a gap less than 30 μm between the wheel and workpiece. This was attributed to the limitation of the space available for fluid transport through the gap. It was concluded that further increase in delivered flowrate was unnecessary in the grinding process because the gap was assumed to be zero. Larger wheel grain size and increased wheel velocity also increased the coefficient.

Campbell, 1993 [26] investigated the effect of contact pressure on the grinding temperature. Consideration was given to fluid film boiling, above which the fluid evaporates from the cutting zone causing a dramatic increase in temperature. The temperature was comparable to dry grinding. It was suggested that the boiling

temperature of the fluid could be increased by hydrodynamic pressure in the wheel-workpiece interface. Consequently, with lower pressures, convective ability of the fluid would be better resulting in lower temperature and allowing higher material removal rates.

Campbell, 1995 [27] designed a system that measured and analysed contact zone pressure and claimed to optimise the fluid delivery conditions. This included coolant nozzle angle. Flow through the grinding zone with and without an air scraper was compared. A small nozzle angle of 5^{o} relative to a horizontal plane was recommended as optimal. An air scraper was found to be beneficial. It was assumed that pressure is the key to the existence of fluid in the grinding zone. It was assumed there is a critical wheel velocity above which measured pressure drops to ambient and there is no grinding fluid in the contact zone, since it was assumed the grinding fluid is replaced by increased air flow forced into the gap between the wheel and the workpiece.

Ganesan, 1995 [28] measured hydrodynamic forces for wheel speeds up to 48 m/s. Results indicated an increase in fluid pressure due to wheel speed. The pressure due to direct impact of the coolant jet and the cutting force were also measured. Investigation showed that the pressure force rises progressively with wheel speed. Cutting depth and feedrate had comparatively small influences. Coolant flow rate was claimed to have no influence on pressure in the contact zone. The pressure force was of comparable magnitude to the pressure due to the cutting force and in some cases higher. A smaller grain size of the grinding wheel produced higher coolant pressure. It was stated that significant hydrodynamic force (pressure) could be generated at the converging inlet to the grinding zone.

Krishnan, 1995 [29] collected the fluid passing through the contact zone for creep feed grinding. Similarly to Engineer he observed that nozzle position, wheel speed, wheel porosity and grit size significantly influence useful flowrate. In addition, grinding wheel porosity was determined using Archimedes Principle.

Metzger, 1986 [30] proposed a flowrate requirement for grinding. The minimum flowrate required, for satisfactory grinding performance was based on spindle power consumed by grinding. It was assumed that the fluid supplied should depend on this

power and should be related to maximum temperature rise of the grinding fluid in the contact zone. Consideration was given to nozzle efficiency as well as to fluid type and to fluid properties including density and specific heat capacity.

Ebbrell et al, 1997 [31] investigated the pressure distribution in the interface between a grinding wheel and workpiece with minimum gap. Air pressures in the grinding zone were found to be both higher and lower than atmospheric pressure. It was shown that air rotating with the wheel reversed direction as it approached the contact zone between wheel and workpiece. Reversing air from the contact zone impeded coolant flow from a jet pointed towards it. Reversed air is clearly shown in Figure 104.

Heinzel, 1998 [32] modelled flow between a grinding wheel and a workpiece based on pressure-induced flow. Flowrate was estimated by measuring pressure gradient in the contact zone and making assumptions concerning the gap geometry.

Klocke, 2000 [33] modelled forces due to the fluid in high-speed grinding. It was assumed that the hydrodynamic effect in grinding was similar to the effect in hydrodynamic bearings with laminar flow. The pressure in the converging gap between wheel and the workpiece was calculated using Reynolds equation. The workpiece was modelled as a stationary cylinder adjacent to a wheel with infinite radius moving at a given velocity. The flowrate was calculated as a function of the gap size and fluid velocity within the gap. In order to estimate the gap size within the grinding zone a CBN wheel was scanned using a mechanical-inductive transducer with a diamond probe. This allowed the percentage of grit material on the wheel surface to be determined and the volume of free space available for fluid transport through the grinding zone.

Hryniewicz, 2001 [34] modelled fluid flow for a rough non-porous wheel. A modified Reynolds equation was used because of the flow turbulence between the wheel and the workpiece. Satisfactory results were reported for low Reynolds number, but significant discrepancy was observed for high Reynolds number.

Ganesan 1996 [35] measured normal hydrodynamic force for various gap thicknesses between wheel and the workpiece. Hydrodynamic forces were analysed in the contact

zone by applying classical hydrodynamic theory with laminar flow. In order to fit theory to experiment, a correction factor was applied to the contact gap thickness. The value of the factor was defined from the maximum roughness of the wheel. Flowrate through the gap was defined using the same theory.

Gui, 1995 [36] unlike Metzger, included wheel velocity in a model, which was tested for high wheel speed using water-based fluids.

Inasaki, 1998 [37] defined an equivalent fluid film thickness in the contact zone between grinding wheel and workpiece. The cooling ability was determined by the magnitude of the fluid film. In order to simulate the cooling conditions in the grinding contact, two aluminium foils were inserted as electrodes into an acrylic resin workpiece at the beginning and end of a simulated grinding arc. A limitation in cooling was found after the fluid film thickness reached a particular value equal to the thickness of the thermal boundary layer. Inasaki concluded that, in order to achieve maximum cooling efficiency, the equivalent fluid film thickness should be at least equal to the thickness of the thermal boundary layer within the fluid film. The thickness of the thermal boundary layer was calculated from heat transfer across an equivalent 'solid layer' of fluid

Webster, 2002 [38] measured minimum flowrate required to avoid thermal damage for creep feed grinding at various depths of cut. Tapered workpieces were used to vary depth of cut during one grinding pass. Fluid effectiveness was assessed as rate of material removal for a corresponding spindle power.

Jin, 2003 [39] estimated the convection heat transfer coefficient of the fluid within the grinding zone from grinding temperature measurements. Very high values of the coefficient were found during the investigation. The finding underlined the importance of convection cooling particularly with large depth of cut. Large depth of cut implies either HEDG (High Efficiency Deep Grinding) or Creep Feed grinding. The convection heat transfer coefficient was also predicted using hydrodynamic and thermal modelling. It was proposed that parameters such as grinding wheel speed and fluid film thickness determined the value of the coefficient. Reasonable agreement between measured and predicted grinding temperatures was reported when using water-based fluids.

From the previous work it is noted that the investigation of fluid flow through the grinding zone is fundamental in assessing the effectiveness of fluid delivery. It is concluded that flow in the grinding zone is a mixture of air and liquid. Moreover the turbulence of the flow adds to the complexity of analysis. Many approaches to analysis include unjustifiable simplifications. The assumption of laminar flow will be shown to be unjustifiable. Taking this into account and the need to consider various aspects of system design including both cooling effectiveness and energy efficiency of the system, the mechanics of fluid delivery in grinding requires further investigation.

2.3 Fluid Application Systems and Methods

It is known that the presence of fluid in the grinding zone is critically important. It is also important to use an application system to ensure a sufficient volume of fluid passing through the contact zone. There have been various attempts to determine the most efficient fluid delivery system.

Pahlitzsch, 1953 [40] applied two different fluids separately from each other to the grinding zone. Water or water-based fluids were fed from outside and tangentially towards the grinding wheel. In addition a very small quantity of oil was supplied from inside and outwards through the pores of the grinding wheel. It was hoped that internally delivered oil would provide sufficient lubrication and keep the pores on the wheel surface free from loading with chips and debris. An external nozzle was employed mainly for cooling purposes. Pahlitzsch designed another system where both fluids were supplied from an external nozzle. Several small high-pressure oil nozzles were positioned on top of a water nozzle of rectangular cross-section. Satisfactory results were reported using this method. However it was admitted that 'two-way' fluid supply requires continuous separation of the fluids from each other, making the method complicated.

Sviridov, 1960 [41] used an ultrasonic device for cleaning the grinding wheel. Coolant was passed through the clearance between a solid object vibrating at very high frequency up to 200 kHz and a rotating wheel. It was claimed that vibrating fluid with high frequency generates a radial vibrating force on the wheel surface and removes the particles which might otherwise cause loading of the grinding wheel.

The air barrier that surrounds a rotating wheel restricts the stream of fluid from entering the grinding zone. This is especially significant at a low jet velocity and high wheel peripheral velocity, Ebbrell [31]. Fisher, 1965 [42] developed a shoe nozzle, which utilized the velocity of the wheel and the air stream to accelerate the fluid to a point where it can be diverted into the pores of the wheel face. This method only required a low delivery-system pressure, since the fluid was accelerated by the wheel, close to its peripheral speed. Due to wheel dimension changes caused by wear, the nozzle position

required frequent adjustment with respect to the wheel periphery. This was the main disadvantage of the nozzle in spite of its simplicity and low cost.

Khudobin, 1969 [43] used high-pressure jet delivery of the grinding fluid outside the grinding zone. The aim was to achieve fluid penetration with high kinetic energy directly into the wheel pores before entry into the grinding contact zone. The fluid was then carried by the rotating wheel straight into the grinding arc. It was reported that wheel loading was completely eliminated. The degree of clogging was determined by chemical analysis of the surface of the grinding wheel.

Trmal and Kaliszer, 1975 [44] investigated the effect of the air barrier surrounding the wheel on the flow stream of the supplied fluid. Experimentally, it was demonstrated that there is a critical nozzle jet velocity above which the fluid penetrates the air barrier and then clings to the wheel periphery. An air scraper was proposed to reduce the boundary layer of high-speed airflow accelerated by the wheel. The critical fluid velocity was predicted theoretically from the condition at which the momentum of the coolant equalled the momentum of the air boundary layer. The air flowrate was determined by considering wheel width, air boundary layer thickness from the wheel surface and average velocity within the layer. Agreement between theory and experiments was reported.

Graham, 1978 [45] experimented with a system where fluid was delivered from both sides of the grinding wheel. Fluid was fed to the wheel through a rigid tube which terminated almost at the wheel surface in order to reduce fluid leakage between the wheel and the tube. It was admitted that the distribution of the fluid across the width of the wheel was not always uniform. The uniformity depended on wheel width, porosity and the flowrate. Another disadvantage was that coolant mist produced by the system adversely affected the workplace environment.

Satow, 1986 [46] investigated a high-pressure coolant delivery system for high-speed precision grinding. It was concluded that a high-pressure jet was especially useful for CBN grinding at a high material removal rate. Due to the high wear resistance of a CBN wheel, dressing takes place less frequently. This means that the wheel can suffer from loading. A high-energy jet helped to clean the pores and reduce wheel loading. For

better performance, it was recommended that the nozzle jet be directed against the rotation of the wheel.

Rowe, 1991 [47] showed low heat partition ratios for CBN and diamond wheels. This suggests that coolant may account for a greater percentage of heat removed from the grinding zone when high conductivity wheels are used because there is less risk of fluid burn-out.

Yokogawa, 1993 [48] developed a dual-fluid supply system. Oil was delivered directly to the grinding zone for lubrication and water was supplied separately to the workpiece for bulk cooling. The application of water eliminated a fire hazard when using oil on its own. It was reported that the two fluids were easily separated using a centrifugal separator instead of a conventional separation tank.

Okuyama, 1993 [25] made grooves 3 mm wide and 0.5 mm deep in the wheel periphery to help transport fluid through the contact zone. A higher heat transfer coefficient was achieved with increased numbers of grooves. Also it was shown that an air scraper improved cooling efficiency in the contact zone. An air scraper was particularly significant at low coolant velocity where fluid restriction by the higher air velocity was more likely.

Mindek, 1994 [50] investigated the effect of nozzle jet thickness, jet velocity and nozzle distance from the grinding zone on the cooling ability within the contact area. Also he compared a shoe nozzle with other jet nozzles. A rig was developed to measure cooling within a simulated grinding contact. An electrical element was inserted into the workpiece to heat it. Increasing both jet thickness and jet velocity resulted in increased cooling capability although the efficiency depended on wheel speed. It was recommended that nozzle jet velocity should be approximately equal to wheel velocity for optimum cooling. In terms of cooling ability, priority was given to the circular nozzle over the shoe and other nozzle designs due to the more coherent jet. A coherent jet allowed effective delivery from a circular nozzle positioned a greater distance from the grinding zone.

Webster, 1995 [51] carried out experiments to determine the optimal design of free jet nozzles. He suggested a circular and concave form for the nozzles rather than convex, the argument being that the concave form produces a jet that is coherent for a greater distance. This allows the possibility of placing the nozzle further from the contact zone. He admitted that the critical factors for jet coherency are: contraction ratio of pipe inlet diameter to nozzle exit diameter, low surface roughness of the internal nozzle surface, and nozzle exit sharpness. It was reported that in general, higher contraction ratios gave better coherence. However, it was suggested that locating the nozzle close to the grinding zone gave best results.

Kovacevic, 1995 [52] in contradiction to Webster and Mindek recommended that grinding fluid should be supplied at higher than wheel speed to overcome the boundary layer of air.

Hiramatsu, 1998 [53] solved the problem of the air barrier around the grinding wheel by applying two coolant jets. These jets were supplied from the same manifold having a cylindrical shape with two orifices. The purpose of the first jet issuing from the upper orifice was to cut off the airflow from the wheel periphery. This enabled the second jet to deliver fluid directly to the grinding zone.

Brockhoff, 1998 [54] compared minimal quantity lubrication (MQL) with conventional flood delivery for low speed grinding (30 m/s). An ester oil was used for MQL and emulsion for flood delivery. It was observed that evaporation together with convection enabled a higher cooling performance. However for greater material removal rates and depth of cut, flood delivery gave better results than MQL. Good atomisation was achievable with MQL, necessary for effective moisturising of the cutting area. But this increases the health risk for the workers, because of dangers caused by an aerosol.

Zhang, 1998 [55] utilized an internal fluid delivery system for grinding of ceramics. The system comprised a special wheel having a chamber inside the wheel body and holes from the chamber directed outwards to the wheel. Fluid was delivered at a low pressure into the chamber and then pumped out by the rotating wheel. Satisfactory grinding performance was reported.

Delchev, 2000 [56] used a device for surface grinding and polishing machines. The device comprised of a cup in the form of a hollow truncated cone mounted against the wheel face using a conventional grinding wheel adaptor. The base of the cup included multiple apertures around the circumference. Fluid was delivered from the wheel face into the cup. Then the fluid was forced into the wheel pores from the apertures by the centrifugal effect of the rotating wheel. Thereafter the fluid spread from the pores to the wheel surface.

Ramesh, 2001 [57] designed a shoe nozzle with three adjustable orifice jets. The uppermost orifice was designed to disrupt the air barrier and create a vacuum enabling the inflow of coolant to the grinding zone. The middle orifice was aimed to apply a coolant film on the wheel surface. The lower orifice directly impinged into the grinding zone. This method was claimed to be appropriate for overcoming the air barrier surrounding the grinding wheel.

Choi, 2001 [58] used a vortex tube device with that produced cold and hot air from compressed air. The device had two tube ends, where cold air was emitted from one end and hot from the other. Cold air was supplied to the grinding zone. A nozzle with a smaller outlet diameter gave lower surface roughness than a nozzle with a larger outlet diameter.

Furutani, 2002 [59] investigated change in wheel topography during grinding and measured the hydrodynamic pressure developed between the grinding wheel and a plane surface. An additional nozzle was used to supply the fluid to the measuring point where a pressure transducer was incorporated. Spectra of the pressure were measured with an FFT analyzer. Output signal frequency was analysed and correlated with wheel loading and wheel dulling during grinding. Wheel wear was related to a change in the pressure signal caused by change in the gap between the wheel surface and the plane surface with implemented pressure sensor.

Suzuki, 2003 [60] developed a coolant supply system where ultrasonic vibration was applied to the nozzle jet. The system comprised the nozzle and ultrasonic power generator. Coolant was delivered from one side of the nozzle and vibration was applied

by an ultrasonic membrane on the opposite side of the nozzle outlet gap. Significant increase in the nozzle jet length was observed.

Ninomiya, 2003 [61] used a nozzle adjusted radially with respect to the wheel. A small clearance between wheel periphery and nozzle tip was automatically adjusted. Stagnation pressure of the nozzle jet and the reaction from the opposite side were used to control the nozzle position. It was reported that low delivery flowrate gave satisfactory results. Therefore comparatively low spindle power consumed due to fluid was monitored.

Generally, existing fluid delivery systems for grinding can be classified as either external or internal. External systems involve one of the following combinations:
high-pressure and high-flowrate,
high-pressure and low-flowrate,
low-pressure and high-flowrate,
low-pressure and low-flowrate.
Internal systems mostly use low flowrate. However, internal supply systems can be high or low pressure. As seen from previous work, application of a system depends on the particular requirements of the job. In spite of various methods and systems for fluid application, there is still a problem of workpiece thermal damage in grinding. This problem is especially critical for high-speed grinding and high material removal rates. There is, therefore, a need for further research on system requirements and performance. In particular, there is a need to know how much grinding fluid actually passes through the grinding contact zone. In some cases, most of the fluid delivery may go through the grinding contact, whereas in other cases, it is possible that very little of the fluid delivery goes through the grinding contact due to poor system design. It is therefore, important to investigate the useful flowrate passing through the grinding contact, since it is this flowrate that directly affects the grinding process. The total flowrate delivered from the nozzle may be deflected away from the grinding process and may therefore be ineffective in lubricating or cooling the cutting action. The investigation will therefore focus on useful flowrate and use this parameter as a basis for further investigation of system requirements for fluid delivery.

CHAPTER 3. THEORY.

3.1 Fluid Flow in the Grinding Wheel-Workpiece Interface

The purpose of this chapter is to derive relationships for 'useful flowrate' that can be correlated with other parameters of the grinding process and used in design of fluid delivery systems.

3.1.1 Air flow near the grinding zone and around the wheel.

At speed, air is dragged by the wheel surface. The air forms a boundary layer surrounding the wheel. At the wheel surface, boundary-layer theory states that the air travels at the same speed as the wheel [62]. At a small distance from the wheel, air flow becomes turbulent. The boundary layer of high-speed air has momentum and interferes with the delivery of grinding fluid to the grinding contact zone. Rotating the wheel at a higher speed generates a larger air-flow. Air is dragged into the converging gap between wheel and workpiece building up hydrodynamic pressure. Because only a limited quantity of air can be transported through the grinding contact, most of the air-flow is rejected and reverses direction away from the grinding zone. In some cases, reverse air-flow can significantly influence the delivery of grinding fluid by restricting flow towards the grinding area [31]. This is especially critical with a low-velocity delivery jet and low flowrate when grinding at high wheel speeds.

In order to penetrate the air boundary the momentum of the delivery grinding fluid should be higher than momentum of the air. If the momentum of the grinding fluid and momentum of the air lie in the same plane, are parallel and directed against each other, then the requirement is that,

$$\dot{m}_a v_a < \dot{m}_j v_j \tag{1}$$

where $\dot{m}_a$ is the air flowrate, $\dot{m}_j$ is the jet flowrate, v_a is the air velocity and v_j is the coolant jet velocity.

Using a Pitot tube to measure pressure head, the air velocity may be related to the head according to:

$$v_a = \sqrt{2gh\frac{\rho_f}{\rho_a}} \qquad (2),$$

where g is the gravitational acceleration, h is the head measured using a Pitot tube. The density, ρ_f is 1000 kg/m^3 for water and ρ_a is 1.293 kg/m^3 for air. Air flowrate is

$$\dot{m}_a = \rho_a abv_a \qquad (3),$$

where, a is the air flow thickness and b is the wheel width.

Although, the air surrounding the wheel has a high velocity, air pressure at the wheel surface is lower than atmospheric [31]. The problem of getting the grinding fluid into the grinding zone can be partially solved by positioning the nozzle above the reversed air flow. In this region, grinding fluid remains close to the wheel due to the low pressure as explained below. Grinding fluid is dragged together with air into the grinding gap. If the wheel velocity is too high, there is a danger of grinding fluid being thrown tangentially from the wheel surface before it reaches the grinding zone. Grinding fluid will be thrown tangentially outwards when the inward radial force due to reduced pressure provides insufficient centripetal acceleration to hold the grinding fluid close to the wheel surface.

It may be shown that there is a critical wheel speed above which fluid is no longer retained on the wheel peripheral surface. Above this speed grinding fluid will be thrown off tangentially.

Rotating the wheel at a higher speed generates a larger air flowrate surrounding the wheel. This causes increase in dynamic pressure at the wheel peripheral surface. However, in opposition to the high stagnation (dynamic) pressure, static pressure of the air at the wheel surface is lower than atmospheric [31].

It is clear that any particle of a fluid applied on to the wheel periphery, is accelerated and tends to be thrown tangentially from its surface at velocity v_t. This reduces pressure between the wheel peripheral surface and particles of a fluid (both air and grinding fluid). However, there is a force due to atmospheric pressure being higher than the pressure at the wheel surface. This pressure force acts radially inwards towards the wheel-centre, tending to hold fluid particles close to the wheel surface. The presence of a reduced pressure zone surrounding the wheel provides an explanation for the orbital motion of fluid and other particles that can often be clearly seen within a thin layer surrounding a grinding wheel.

For the simplicity of theoretical analysis a fluid layer on the wheel surface of small length l_s, thickness h and width b is treated as a solid body as illustrated in Figure 1.
Orbital motion of a particle requires continuous change of direction. Therefore the object has to be continuously accelerated towards the centre of rotation. This centripetal acceleration requires a centripetal force F_c according to Newton's Second Law of Motion. The acceleration is provided by the atmospheric pressure force F_p for an elemental volume of air or any other particle.

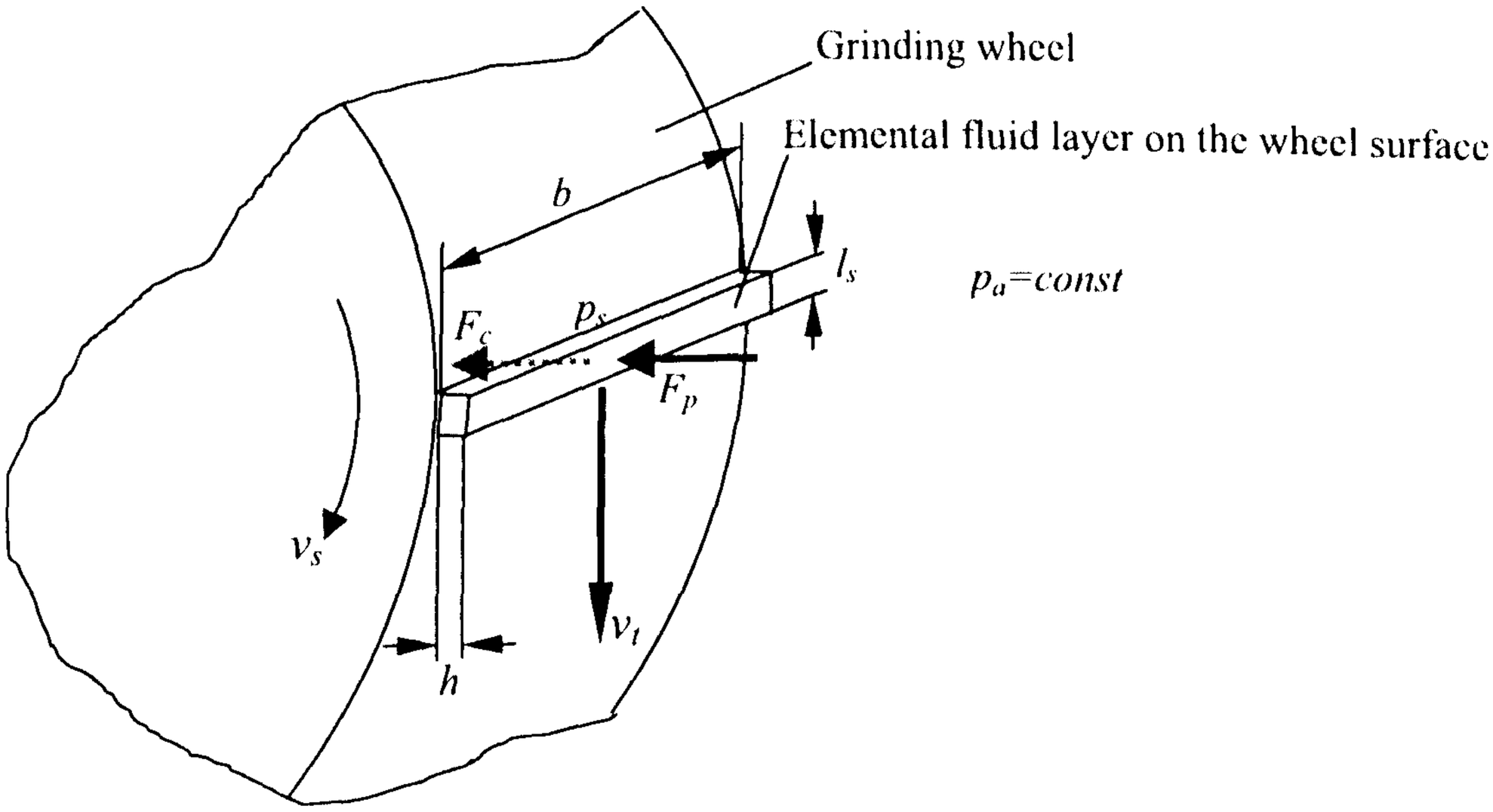

Figure 1: Movement of a fluid layer on the surface of a rotating wheel.

Based on the above description of the mechanics of rotation, the minimum centripetal force necessary to hold a particle of fluid mass, on the peripheral surface of a rotating wheel is

$$F_c = \frac{\rho h_s b l_s v_s^2}{r} \quad (4),$$

where ρ is fluid density, v_s is the linear wheel speed and r is the wheel radius. Gravitational forces are neglected due to their relatively low magnitude in comparison to inertial forces.

The centripetal force is provided by the difference between atmospheric pressure p_a and pressure p_s in the region immediately adjacent to the wheel surface. If atmospheric pressure is assumed to be distributed uniformly around the wheel, the maximum force pushing the fluid towards a small area of the wheel surface of length l_s around the wheel and wheel width b is

$$F_p = (p_a - p_s) b l_s \quad (5),$$

The condition for the fluid remaining attached to the wheel is,

$$F_c \leq F_p \quad (6),$$

Increase in wheel speed will require increase in the force necessary to keep the fluid on the wheel surface. However this force cannot be increased significantly since it mainly depends on atmospheric pressure. For the equilibrium condition,

$$F_c = F_p \quad (7),$$

The wheel peripheral velocity to hold the fluid on the wheel surface at wheel peripheral velocity v_s must be less than the critical velocity v_{cr},

$$v_{cr} = \sqrt{\frac{r(p_a - p_s)}{\rho h_s}} \qquad (8),$$

This is the critical wheel velocity beyond which the fluid will be thrown away from the wheel surface. Equation 8 provides an explanation of why some particles of either fluid or swarf are entrained while others are thrown off at a tangent.

3.1.2 Useful flowrate based on fluid pressure in the contact zone.

It will be shown that flowrate through the grinding zone depends on contact pressure, delivery flowrate, wheel velocity, fluid mean velocity within the converging gap and fluid density. The basis of a simplified model is shown schematically in Figure 2. The following analysis is based on conservation of energy for incompressible flow. Viscous forces are ignored in this region on the basis that the flow is highly turbulent and inertial forces are much more significant. Viscous losses are accommodated by use of loss coefficients. The model seeks to overcome the complexities of attempting to solve the full Navier-Stokes Equations in favour of identifying major controlling relationships between flowrate and power in the turbulent boundary layer. The resulting equations will be tested by experimentation.

Fluid energy is considered at two regions *A* and *B*. For conservation of energy, the fluid power (energy per unit time) at *A* is equal to the fluid power at *B*, plus frictional losses between *A* and *B*. It is assumed that the fluid enters region *A* at jet velocity v_j and mass flowrate $\dot{m}_j$. At A, the fluid is accelerated by the grinding wheel to a velocity v_g, which is less than v_s. In the region of A, it is assumed the fluid has only kinetic energy and no pressure energy. When the fluid arrives at B, located just before the grinding arc, it is assumed the velocity of useful flowrate passing into the grinding contact is equal to wheel velocity v_s. However due to the small gap within the grinding contact, only a

limited amount of incompressible fluid enters the zone. A large part of the fluid is rejected from entering the grinding zone, causing pressure rise at B. Therefore kinetic energy of the fluid is partially converted into pressure energy. It is assumed that the maximum pressure p_c occurs at Point B and the useful flowrate $\dot{m}_u$, which proceeds beyond this point, is entirely transported through the grinding zone. Rejected fluid from the grinding area is the difference between jet flowrate and useful flowrate $\dot{m}_j - \dot{m}_u$.

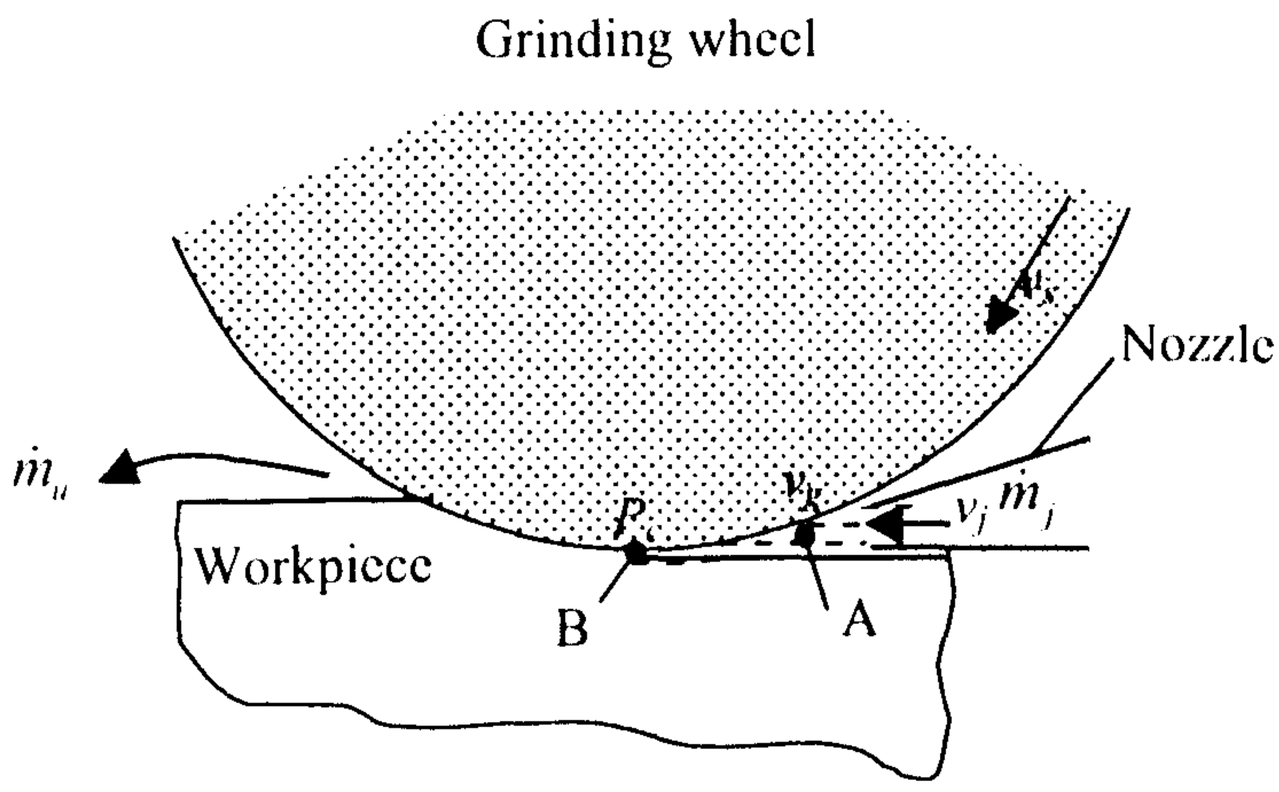

Figure 2. Contact pressure and the useful flowrate through the contact zone

According to the above assumptions, the rate of kinetic energy of the grinding fluid at A is,

$$\frac{\dot{m}_j v_g^2}{2} \tag{9}$$

The rate of kinetic energy of the useful flowrate at B is

$$\frac{\dot{m}_u v_s^2}{2} \tag{10}$$

and the rate of pressure energy at B is

$$\frac{(\dot{m}_j - \dot{m}_u)p_c}{\rho_f} \tag{11}$$

The pressure of the grinding fluid within the contact zone is assumed to be equal to air pressure within the contact zone because the fluid is a mixture of both air and grinding fluid.

Conservation of energy between *A* and *B* requires that,

$$\frac{\dot{m}_j v_g^2}{2} = \frac{\dot{m}_u v_s^2}{2} + \frac{(\dot{m}_j - \dot{m}_u)p_c}{\rho_f} + Losses \tag{12}$$

The energy loss due to viscosity is assumed to be low compared with the other fluid energy terms as previously stated. Average fluid velocity v_g in the converging gap is related to the wheel velocity.

$$v_g = K_g v_s \tag{13}$$

K_g has a value between 0 and 1. The coefficient is the ratio of average fluid velocity within the converging gap to the wheel peripheral velocity. It is assumed that K_g depends on the wheel geometry, jet velocity, abrasive property and fluid property. The value giving best agreement will be determined from experiments.

After substituting Equation 13 into Equation 12 and rearranging, the useful flowrate is,

$$\dot{m}_u = \dot{m}_j \frac{\rho_f (K_g v_s)^2 - 2p_c}{\rho_f v_s^2 - 2p_c} \tag{14}$$

Equation 14 does not take into account, the effect of air flowrate interfering with the flow of grinding fluid in the converging region towards the contact zone.

As previously stated, flow through the grinding zone is a two-phase mixture of air and grinding fluid. Although in reality, the flow is turbulent, for calculation purposes, these fluids are treated as two fluids flowing together along two paths within the grinding gap. Accordingly, mass flowrate of air through the contact zone is:

$$\dot{m}_{ac} = \rho_{ac} h_a b v_s \tag{15}$$

where h_a is the air film thickness and ρ_{ac} is the air density in the contact zone. Air velocity is assumed to be equal to wheel velocity. Air is compressible and is significantly affected by hydrodynamic pressure in the contact zone. Air density can be expressed as,

$$\rho_{ac} = \frac{p_a}{RT} \tag{16}$$

where T is absolute temperature and R is the gas constant. For air R = 287 J/kg K.

Grinding with impervious wheels allows calculation of the gap thickness available for the maximum fluid transport through the contact zone. For an impervious wheel, no fluid will penetrate deeper than the surface porosity of the wheel. It is assumed that if the grinding fluid does not fill the grinding gap then the rest of the gap area is filled by air. Therefore, if the grinding fluid film thickness h_f is determined experimentally, the air film thickness h_a can be calculated as a difference between gap thickness h_g and grinding fluid film thickness h_f.

$$h_a = h_g - h_f \tag{17}$$

Accordingly, the film thickness of the grinding fluid may be related to useful flowrate.

$$h_f = \frac{\dot{m}_u}{\phi \rho_f b v_s} \tag{18}$$

where $\dot{m}_u$ is the useful mass flowrate measured from experiment, ρ_f is the density of the grinding fluid and ϕ is the wheel surface porosity defined as the ratio of the void volume to the total volume at the surface. Definition of the surface porosity is illustrated schematically in Figure 90 (Appendix). Total volume is calculated from the sum of the grain and the void volumes. For porous wheels, wheel surface porosity is approximately equal to the overall wheel porosity. However, surface porosity is obviously different from bulk porosity for an impervious wheel. For a porous wheel surface porosity can be different from bulk porosity due to the effect of dressing and wheel wear. More precisely,

$$\phi = \frac{surface\ void\ volume}{surface\ void\ volume + grain\ volume} \tag{19}$$

The surface void volume, grain volume and hence the gap thickness h_g can be found by scanning the wheel surface [63].

From Equations 16 to18, mass flowrate of air through the contact zone is,

$$\dot{m}_{ac} = (h_g - \frac{\dot{m}_u}{\phi \rho_f b v_s}) \frac{p_c}{RT} b v_s \tag{20}$$

As the result of air mixing with the grinding fluid, the useful flow of grinding fluid through the grinding zone is further reduced. Actual useful flowrate is the difference between useful flowrate of grinding fluid and flowrate of air in the grinding contact.

$$\dot{m}_{ua} = \dot{m}_u - \dot{m}_{ac} \tag{21}$$

where, $\dot{m}_{ua}$ is the actual useful flowrate after making allowance for air mixing.

From experiments, it will be shown that the flowrate of air is low in comparison to the flowrate of grinding fluid and makes little change to the useful flowrate. Therefore Equation 14 can be used which is simple and will be shown to give satisfactory results. Equation 14 may be rearranged to yield maximum fluid pressure in the contact zone.

$$p_{\max} = \frac{\rho_f v_s^2}{2}\left(\frac{K_g^2 \dot{m}_j - \dot{m}_u}{\dot{m}_j - \dot{m}_u}\right) \tag{22}$$

If the pressure profile within the contact arc from l_1 to l_2 is known, the normal force between the wheel and the workpiece due to grinding fluid pressure can be calculated by integration, assuming pressure across the wheel width is constant.

$$F = b\int_{l_1}^{l_2} p_c\, dl \tag{23}$$

3.1.3 Useful flowrate based on spindle power.

The kinetic energy of the grinding fluid as it passes through the grinding contact is provided partly by energy from the delivery jet and partly from spindle power. The useful flowrate that passes through the contact zone is, therefore, a function of the additional spindle power required for fluid acceleration. The useful flowrate is also a function of wheel speed and delivery jet velocity as follows.

Useful flow is illustrated schematically in Figure 3. The analysis of useful flow is based on the momentum equation for incompressible flow. An assumption is made that the useful mass flowrate $\dot{m}_u$ passing through the wheel-workpiece interface enters the contact zone with the jet velocity v_j and is accelerated up to wheel velocity v_s . This assumption is based on the fact that the useful flow is carried in the pores of the wheel similar to the fixed-displacement pump.

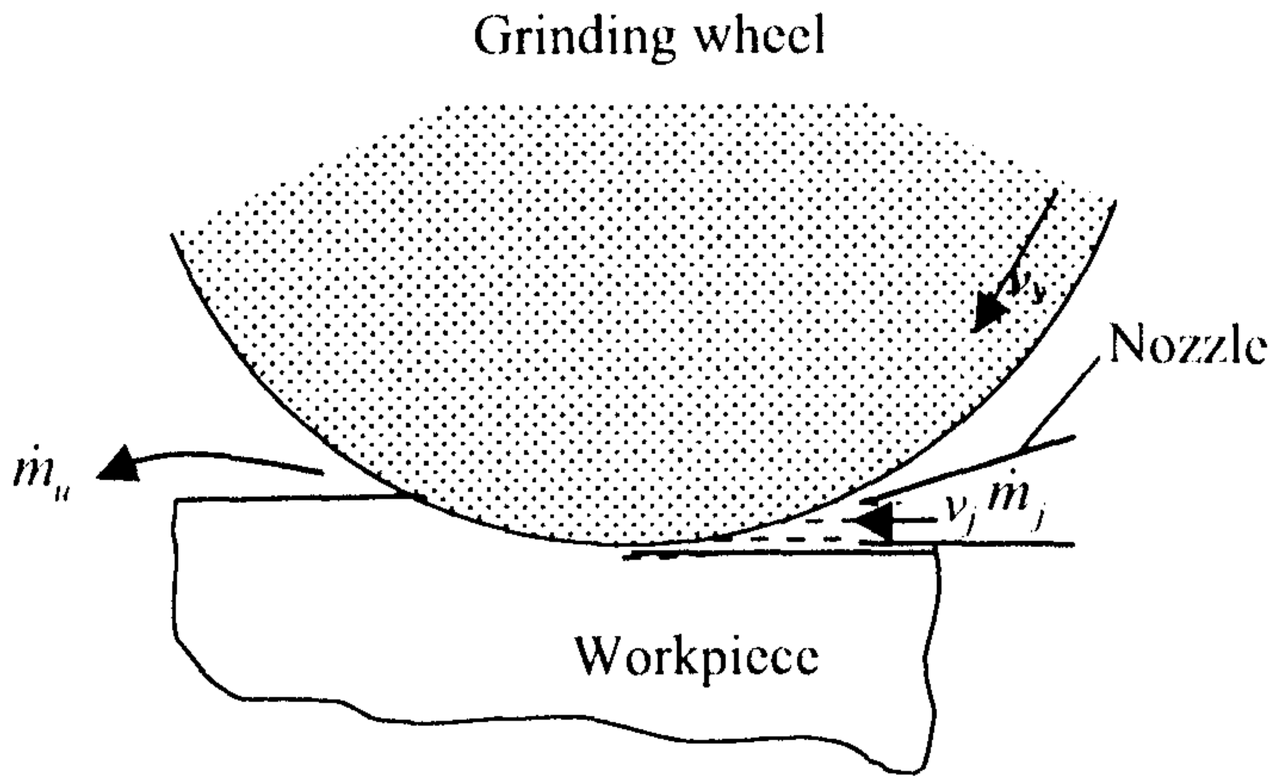

Figure 3: Useful flowrate through the contact zone

According to Newton's Second Law, the force to accelerate the fluid is related to the rate of change of fluid momentum.

$$F_f = \dot{m}_u (v_s - v_j) \tag{24}$$

The acceleration force is applied in the form of a turning moment or torque T_f on the rotating wheel of radius r. The torque required is,

$$T_f = \dot{m}_u (r \times v_s - r \times v_j) \tag{25}$$

This approach applies equally to a stream of fluid moving in the curved path of the wheel-workpiece contact [62].

Writing the wheel radius in terms of wheel peripheral velocity and rotational speed,

$$T_f = \dot{m}_u \times \left(\frac{v_s}{2\pi n} \times v_s - \frac{v_s}{2\pi n} \times v_j \right) \tag{26}$$

where n is the rotational speed of the wheel. The power required to cause the rate of change of momentum of the fluid is therefore,

$$P_f = \dot{m}_u \left(v_s^2 - v_j v_s \right) \tag{27}$$

This is the spindle power required to accelerate the useful flow to wheel speed. The increased spindle power due to the drag of the fluid jet can be measured. Rearranging Equation 27, useful mass flowrate through the contact zone is a function of wheelspeed, jet velocity and measured increase in spindle power due to the fluid.

$$\dot{m}_u = \frac{P_f}{v_s^2 - v_j v_s} \tag{28}$$

Jet velocity v_j can be expressed in terms of the jet flowrate $\dot{m}_j$ delivered through the nozzle, fluid density ρ_f and the nozzle outlet cross-sectional area A

$$\dot{m}_u = \frac{P_f}{v_s^2 - \left(\frac{\dot{m}_j}{\rho \times A} \right) . v_s} \tag{29}$$

Equation 29 is an ideal case when no losses occur. In a real grinding process there are frictional losses, which significantly influence spindle power. The losses need to be taken into account.

For practical purposes, Equation 28 must be modified taking into account the power loss coefficient K_f and the jet velocity loss coefficient K_j.

$$\dot{m}_u = \frac{K_f P_f}{v_s^2 - (K_j v_j) v_s} \tag{30}$$

The loss coefficient K_f allows for the power required to overcome frictional drag of the fluid caused by contact with the workpiece surface and by shear losses within the fluid. The velocity coefficient K_j is the nozzle jet velocity correction factor, which can be viewed as an efficiency of the jet. In other words, K_j represents the fraction of the jet velocity, which contributes to the change of momentum. The coefficient values lie between 0 and 1. The values are to be determined from experiment.

In practice, peripheral speed of the wheel is usually much higher than the jet velocity. This means the wheel has to accelerate the useful flowrate to its peripheral speed as the fluid enters the contact zone. Accordingly, spindle power increases to a higher level. With a large difference between the two velocities, the velocity of the nozzle jet is negligible and Equation 30 can be simplified to,

$$\dot{m}_u = \frac{K_f P_f}{v_s^2} \tag{31}$$

If the jet velocity is higher than the peripheral speed of the wheel, the kinetic energy of the fluid will try to accelerate the wheel. This results in a decrease in spindle power, as shown from experiments. For high jet velocities, Equation 30 must be used.

The spindle power to accelerate the fluid including the effect of the loss coefficients is,

$$P_f = \frac{\dot{m}_u}{K_f}(v_s^2 - v_s K_j v_j) \tag{32}$$

The nozzle jet power including the loss coefficient is,

$$P_j = \frac{K_j \dot{m}_j v_j^2}{2} \tag{33}$$

If the spindle power for fluid acceleration is K_p times the jet power,

$$P_f = K_p P_j \tag{34}$$

so that,

$$\frac{\dot{m}_u}{K_f}(v_s^2 - v_s K_j v_j) = \frac{K_p K_j \dot{m}_j v_j^2}{2} \tag{35}$$

Equation 35 is quadratic with respect to v_j as a variable. By solving the quadratic equation, the jet velocity can be calculated for the required condition as,

$$v_j = v_s \frac{\sqrt{\dot{m}_u^2 K_j^2 + 2\dot{m}_u \dot{m}_j K_p K_f} - \dot{m}_u K_j}{\dot{m}_j K_p K_f} \tag{36}$$

Equation 36 allows the jet velocity to be determined for any ratio of P_f to P_j using values of loss coefficients determined from experiments.

It is considered that the value of the loss coefficient K_f may depend on the topography of the wheel and on the fluid properties. The loss coefficient K_j will depend on the value of Reynolds Number. The coefficients need calibration for an appropriate range of conditions. The magnitudes of the coefficients will be determined from the experiments.

It was found from experiments, for the condition where jet power was equal to spindle power for the fluid that jet velocity was approximately equal to the wheel velocity.

After substituting experimental values into Equation 36, this result was confirmed.

$$v_j \approx v_s \text{ when } P_j = P_f \tag{37}$$

It is intended to show by consideration of the experimental results that it is possible to optimise the jet velocity in relation to the power required to accelerate the fluid and the particular velocity of the wheel.

If $v_j \approx v_s$ and $P_j \approx P_f$, then the ratio of the jet thickness h_j to the fluid film thickness h_f in the grinding zone may be found by the Equation 38.

$$\frac{h_j}{h_f} = 2\frac{(1-K_j)}{K_f} \tag{38}$$

Substitution of experimentally determined values of the coefficients into Equation 38 gives the approximate required thickness of the nozzle outlet gap to achieve the corresponding fluid film thickness for the prescribed conditions. For the above values of loss coefficients,

$$h_j \approx 2.2h_f \tag{39}$$

It is tentatively concluded that if the jet velocity is equal to the wheel velocity, the spindle power to accelerate the fluid for these conditions will be equal to the jet power. Therefore the model also makes it possible to determine a suitable value of nozzle outlet gap to achieve a required fluid film thickness in the grinding zone.

In order to ensure a sufficient volume of coolant in the grinding zone, it is recommended that the wheel surface pores should be filled with the coolant. Therefore, by taking into account the wheel surface porosity ϕ, the mean fluid film thickness h_f may be related to the average depth of the wheel surface grains h_g,

$$h_f = \phi h_g \tag{40}$$

The analysis based on spindle power takes into account both air and grinding fluid flows through the grinding zone. This can be explained by the fact that any change of fluid ratio will affect the spindle power. For example, if the grinding gap is filled with grinding fluid, spindle power will be a maximum. Spindle power will decrease as the grinding fluid supply is reduced to zero. At this condition, the spindle power as monitored will be the power caused by the friction of the wheel with air, friction of the motor bearings and the spindle bearings. This power is interpreted as the no-load power.

3.1.4 Combined model.

It has been shown that useful flowrate can be predicted by two different approaches. Combination of the two approaches allows prediction of useful flowrate, spindle power to overcome fluid drag or maximum contact pressure if one of the three is known. For example, substituting Equation 30 into Equation 22 allows calculation of maximum contact pressure after monitoring the spindle power during spark out. In practice, spindle power can be easily monitored since it does not require a special rig. Moreover most grinding machines already have a built-in power meter, which makes the task easier.

3.2 Methods for Design of Conventional Fluid Application Systems.

The supply of sufficient grinding fluid for the process may be critical. The volume of fluid required may depend on the quality requirements of the particular job. For example, if a low contact temperature is the main requirement, a higher delivery flowrate is often used. Delivery jet velocity also has a critical importance. Jet flowrate and jet velocity both affect the process power demand, as will be shown from experiments. Increasing supply flowrate requires higher power consumption for the fluid supply system. Reduction of the supply flowrate may cause undesirable problems such as thermal damage to the workpiece and increased wheel wear. Excessive flowrate and incorrectly designed systems may waste large amount of energy, cause environmental pollution and significantly affect the total cost of the product. It is important to take into account all necessary aspects for the design of an optimal fluid supply system in relation to the particular type of grinding process and product requirements.

3.2.1 Slot nozzle and orifice nozzle.

If the delivery flowrate, jet velocity and nozzle position are already determined, the next task is to design the fluid supply system. The required jet velocity can be achieved simply by using an appropriate outlet gap cross sectional area of the nozzle. However, it is important that the fluid is delivered to the cutting zone at the required velocity and flowrate with minimum energy losses in the whole system. These losses occur as the fluid is transported through the system between the pump and the nozzle. Losses in standard pipes, bends and fittings can be estimated from texts on hydraulics. Values may be obtained experimentally for turbulent flow and can be calculated for laminar flow. In most cases, flow in the supply system is turbulent. Turbulent fluid flow, especially in non-standard shapes, is complex. Use of devices within the system such as refrigerators and filters, often does not allow theoretical solution. The same applies to the delivery nozzle, where shape and size vary depending on the workpiece shape and the particular requirements of the grinding process.

A simple and accurate approach to the problem is to consider the energy of the flow at inlet and at outlet of the nozzle. The losses are the difference between these energies. Accordingly, the fluid energy at nozzle inlet consists of pressure energy with pressure p_n and kinetic energy with inlet velocity to the nozzle v_{in}.

$$\frac{\dot{m}_n p_n}{\rho_f} + \frac{\dot{m}_n v_{in}^2}{2} \tag{41}$$

The mass flowrate through the system is constant and can be calculated either using the cross sectional area and velocity at nozzle outlet or at nozzle inlet,

$$\dot{m}_n = \rho_f h_j b v_j = \rho_f \pi r^2 v_{in} \tag{42}$$

The fluid energy just after the nozzle exit neglecting the vena contracta is.

$$\frac{\dot{m}_n v_j^2}{2} \tag{43}$$

The pressure energy at this point is zero since the pressure is atmospheric pressure. For conservation of energy, the fluid energy at nozzle inlet is equal to the fluid energy at outlet plus loss of energy within the nozzle.

$$\frac{\dot{m}_n p_n}{\rho_f} + \frac{\dot{m}_n v_{in}^2}{2} = \frac{\dot{m}_n v_j^2}{2} + Loss \tag{44}$$

This allows determination of energy loss for any shape and size of nozzle. In practice, as will be shown from the experiments, mass flowrate through the system, fluid pressure and cross sectional areas can be easily measured. Jet velocity can be then calculated by substituting obtained values into Equation 45.

$$v_j = \frac{\dot{m}_n}{\rho_f \times outlet\ gap\ area} = \frac{\dot{m}_n}{\rho_f h_j b} \tag{45}$$

The nozzle inlet velocity can be calculated from Equation 46.

$$v_{in} = \frac{\dot{m}_n}{\rho_f \times inlet\ gap\ area} = \frac{\dot{m}_n}{\rho_f \pi r_n^2} \tag{46}$$

Lower energy loss from Equation 44 corresponds to a more efficient nozzle design.

3.2.2 Theoretical method for nozzle energy loss estimation.

Energy loss can be estimated using a method by which the loss in every section of the nozzle is individually estimated and the results summed to give the total loss within the nozzle. For this purpose, the nozzle is divided into elementary geometrical shapes, for which cross sectional areas and volume can be easily calculated. In practice, cross sectional areas are usually assumed to be rectangular or circular. If the magnitude of the

cross sectional area is constant along the nozzle within the given interval, then standard terms can be used to calculate the frictional loss in each interval. For example, Darcy's equation determines frictional losses in pipes for turbulent flow. This equation can be used for cylindrical shapes within the nozzle. It is also assumed that the same method would give negligible discrepancy for a rectangular shape. It has to be assumed that the cross-sectional shape changes very slowly with distance, otherwise substantial losses will occur at the transition point. For example, at the transition from a pipe to an orifice, a substantial loss occurs. Losses due to sudden contractions or expansions can also be estimated.

The loss of energy per unit time in terms of pressure head is,

$$P = \dot{m}gh \tag{47}$$

The frictional power loss within a circular pipe of length l_p and diameter d_p is,

$$P_p = \dot{m}g\left(\frac{4fl_p}{d_p}\cdot\frac{v_p^2}{2g}\right) \tag{48}$$

where f is the flow friction factor determined experimentally, v_p is the mean velocity of the fluid in the pipe and g is the value of gravitational acceleration.

Friction factor can also be defined from the empirical Blasius equation for turbulent flow in smooth pipes.

$$f = 0.079/\mathrm{Re}^{0.25} \tag{49}$$

The Reynolds number *Re* is a measure of flow turbulence,

$$\mathrm{Re} = \rho_f v_p d_e/\eta \tag{50}$$

where d_e is effective diameter of a pipe and η is the dynamic viscosity.

$$d_e = \frac{4 \times Cross\ section\ area}{Wetted\ perimeter} \tag{51}$$

Equation 51 can be used to define effective diameter for any shape of cross sectional area.

Usually there are transitions along the nozzle as the fluid flows from a particular size of cross sectional area to another. These transitions can be either contraction or expansion, and cause additional energy loss. The power loss due to a sudden expansion is,

$$P_{\exp} = \dot{m}_n g\left(\frac{\bar{v}_{\exp}^2}{2g}\left(\frac{A_{\exp}}{A_1} - 1\right)^2\right) \tag{52}$$

where A_1 is the initial cross sectional area, A_{exp} is the expanded cross sectional area and $\bar{v}_{\exp}$ is the mean fluid velocity within expanded area.

The power loss due to a sudden contraction is,

$$P_{con} = \dot{m}g\left(K_c \frac{\bar{v}_{con}^2}{2g}\right) \tag{53}$$

where K_c is a loss coefficient, which is determined experimentally depending on the ratio of the contracted area to the initial area.

In practice, the nozzle shape often comprises a gradual contraction towards the outlet gap. In this case there is no standard equation that describes the problem. Only experimental values of the loss are known which are determined for limited range of sizes and contracted angles of the nozzle. Moreover, the data having been obtained for a fluid having particular properties may be unsuitable for another application.

The frictional loss within this type of nozzle can be estimated by integrating the Darcy equation along the gradual contraction. According to the Darcy equation, the power loss for a circular pipe, expressed in terms of mass flowrate, is

$$P_p = \dot{m} g \left(\frac{32 f l_p \dot{m}^2}{g \pi^2 \rho_f^2 d_p^5} \right) \tag{54}$$

Reynolds number for a circular cross sectional area, expressed in terms of mass flowrate, is

$$\mathrm{Re} = \frac{4\dot{m}}{\eta \pi d_e} \tag{55}$$

The nozzle diameter can be expressed in terms of length l_n along the nozzle

$$d = d_o + 2 l_n \tan\alpha \tag{56}$$

where d_o is orifice diameter and α is contraction angle.

Substitution of Equation 56 into 55, then 55 into 49 will give the friction factor for turbulent flow for a cylindrical cross section. Substituting Equations 49 and 56 into 54 and then integrating along l_n, frictional power loss can be defined within the contracted area.

$$P_{gr} = 1.8 \frac{\eta^{0.25} \dot{m}_n^{2.75} g}{g \rho_f^2 \pi^{1.75}} \int_{l_{n1}}^{l_{n2}} \frac{dl_n}{\left(d_o + 2 l_n \tan\alpha\right)^{4.75}} \tag{57}$$

This method defines only the frictional loss within the nozzle. However, it will be shown experimentally that the total loss is higher than predicted by Equation 57. It is assumed that this loss is caused by additional loss due to shape contraction and turbulence of the flow.

3.2.3 Shoe nozzle.

The flow behaviour within a shoe nozzle is different from flow in slot and orifice nozzles. The principle of the shoe type nozzle is that the flow is accelerated by the grinding wheel. It is also found that there is a substantial side flow leakage between the wheel and the shoe. Very low pumping energy is needed for a shoe nozzle, whereas for slot and orifice nozzles, the flow energy is supplied in entirety by the pump motor. The flow exits from the shoe nozzle in three ways: flowrate $\dot{m}_s$ into the pores of the wheel, gap flowrate $\dot{m}_g$ passing through the gap between the shoe nozzle and the wheel and leakage flowrate $\dot{m}_l$ leaking around the side of the wheel. Therefore the total flowrate from the shoe nozzle is

$$\dot{m} = \dot{m}_s + \dot{m}_g + \dot{m}_l \tag{58}$$

It is assumed that the velocity of the fluid penetrating into the wheel is equal to the wheel peripheral velocity. The velocities of leakage flow and gap flow are both less than wheel velocity and are unequal to each other. The energy of fluid flow from a shoe nozzle is the sum of energy from the pump and energy provided by the spindle motor. For conservation of energy for flow between the shoe nozzle inlet and outlet,

$$\frac{\dot{m}v_{in}^2}{2} = \frac{\dot{m}_s v_s^2}{2} + \frac{\dot{m}_g v_{gn}^2}{2} + \frac{\dot{m}_l v_l^2}{2} - P_s + Loss \tag{59}$$

Accordingly, the fluid energy per unit time at the shoe nozzle inlet is equal to the energy per unit time of the fluid ejected from the nozzle, minus spindle power due to fluid acceleration plus loss within the nozzle. The energy of the flow ejected from the nozzle is the sum of kinetic energy of fluid absorbed into the wheel, kinetic energy of the fluid passing through the nozzle gap and kinetic energy of the leakage flow. The number of variables does not allow a similar approach to be employed for slot and orifice nozzles. The minimisation of spindle power was considered, since spindle power can be a major problem for a shoe nozzle. Therefore, spindle motor power as well as pumping power and losses can be reduced by optimal design of a shoe nozzle.

CHAPTER 4. EXPERIMENTAL EQUIPMENT.

4.1 Grinding Machines.

4.1.1 Surface grinding machines.

Initial experiments were conducted on a conventional surface grinder having low peripheral wheel speed and low spindle power. The machine parameters are described in Table 1.

Machine	Elliot 618, surface-grinding machine
Spindle motor power	1.1 kW (continuous power)
Spindle speed	2700 rpm
Longitudinal travel	480 mm
Cross traverse of head	190 mm
Vertical traverse of head	290mm
Maximum wheel size	200 mm x 25 mm
Grinding wheel used	A60KVMOS3710, diameter 167.5 mm, width 25 mm

Table 1. Elliot 618 surface-grinding machine specification.

Further experiments were carried out on an Abwood Series 5020 surface grinding machine (See Figure 96). This machine allowed higher spindle power and wheel speed. A larger diameter grinding wheel was used on the machine in order to achieve a high peripheral speed. For this purpose, the machine was modified to accept a larger wheel diameter. This included manufacturing a new wheel guard. The vee belt, which transmitted rotation from the motor to the spindle was replaced by a toothed belt. A toothed belt prevented any possible sliding due to the mechanical load during the experiments. This allowed constant rotational speed of the wheel. Rotational speed of the motor was controlled by the built in optical sensor. The parameters of the machine are described in Table 2.

Machine	Abwood series 5025 surface-grinding machine
Spindle motor power	2.2 kW (continuous power) 8 kW (instantaneous power)
Spindle speed	Variable up to 6000 rpm
Longitudinal travel	530 mm
Cross traverse of head	260 mm
Vertical traverse of head	350
Maximum wheel size	400 mm x 25 mm
Grinding wheel used	390 mm x 23 mm aluminium disc and CBN porous wheel.

Table 2. Abwood series 5025 surface-grinding machine specification.

4.1.2 Cylindrical grinding machine.

Grinding trials on a difficult-to-grind material (Inconel 718) were carried out on a Suprema cylindrical-grinding machine (See Figure 97).

The machine included a high-pressure low flowrate fluid delivery system and also a lower pressure high flowrate system. The high-pressure system producing the high jet velocity was only used for grinding wheel surface cleaning purposes. Use of the high-pressure system was not found to be necessary as the lower pressure system provided sufficient cleaning of the wheel surface. Only a limited proportion of the capability of this system was used during the experiments, since satisfactory results were achieved with low delivery flowrate.

4.2 Fluid Delivery Systems.

Two fluid delivery systems were employed during experiments on the surface grinding machines. The first was a high flowrate system with a high-power fluid supply pump (See Figure 96). The system included the main pump, which delivered fluid to the machine and a secondary pump transporting the recycled fluid from the tank into the primary filter. The primary filter was a centrifugal type, which separated the heaviest particles of the grinding swarf from the coolant. After rough filtering fluid was

transported via the main pump through a fine filter. Fine filtering was necessary to avoid blockage of the nozzle with a small thickness of outlet gap (0.15 mm). The parameters of the system are described in Table 3.

Main pump power	8.6 kW
Secondary pump power	1.1 kW
Main pump control device	Jaguar VXM 750.
Tank capacity	700 Litre
Primary filter type	Centrifugal
Secondary filter type	Mesh type

Table 3. High flowrate fluid delivery system specification.

The second fluid delivery system was high pressure and low flowrate. It was a conventional high velocity water jet system designed for cleaning purposes within a domestic environment. The system comprised a special nozzle design for producing a flat jet, which was approximately equal to the grinding wheel width. A tank was used for the fluid recycling. The parameters of the system are described in Table 4.

Model of the system	DYNAMIC 4600X-TRA
Pump power	2.1 kW
System pressure	120 bar
Jet type	Flat and divergent
Design of the nozzle	Special, with hole of diameter 1.2mm
Tank capacity	110 litre

Table 4. High pressure low flowrate fluid delivery system specification.

The system did not include any filtering device since it was designed for water utilisation directly from the tap.

4.3 Grinding Wheels.

4.3.1 Aluminium knurled disc.

A special aluminium disc of 390 mm diameter and 23 mm width was manufactured in order to achieve high circumferential speed (See Figure 105). Fine knurling was applied to the disc periphery to represent the abrasive surface of a real grinding wheel. The knurled surface allowed measurement of void volume between grains. These data were used for determining maximal flowrate available for transporting through the grinding zone.

Rotational stresses in the aluminium disk were calculated to ensure the safety due to the stresses caused by the high rotational speed.

Tangential and radial stresses in the disc are presented in Figure 4 for a peripheral wheel speed of 120 m/s.

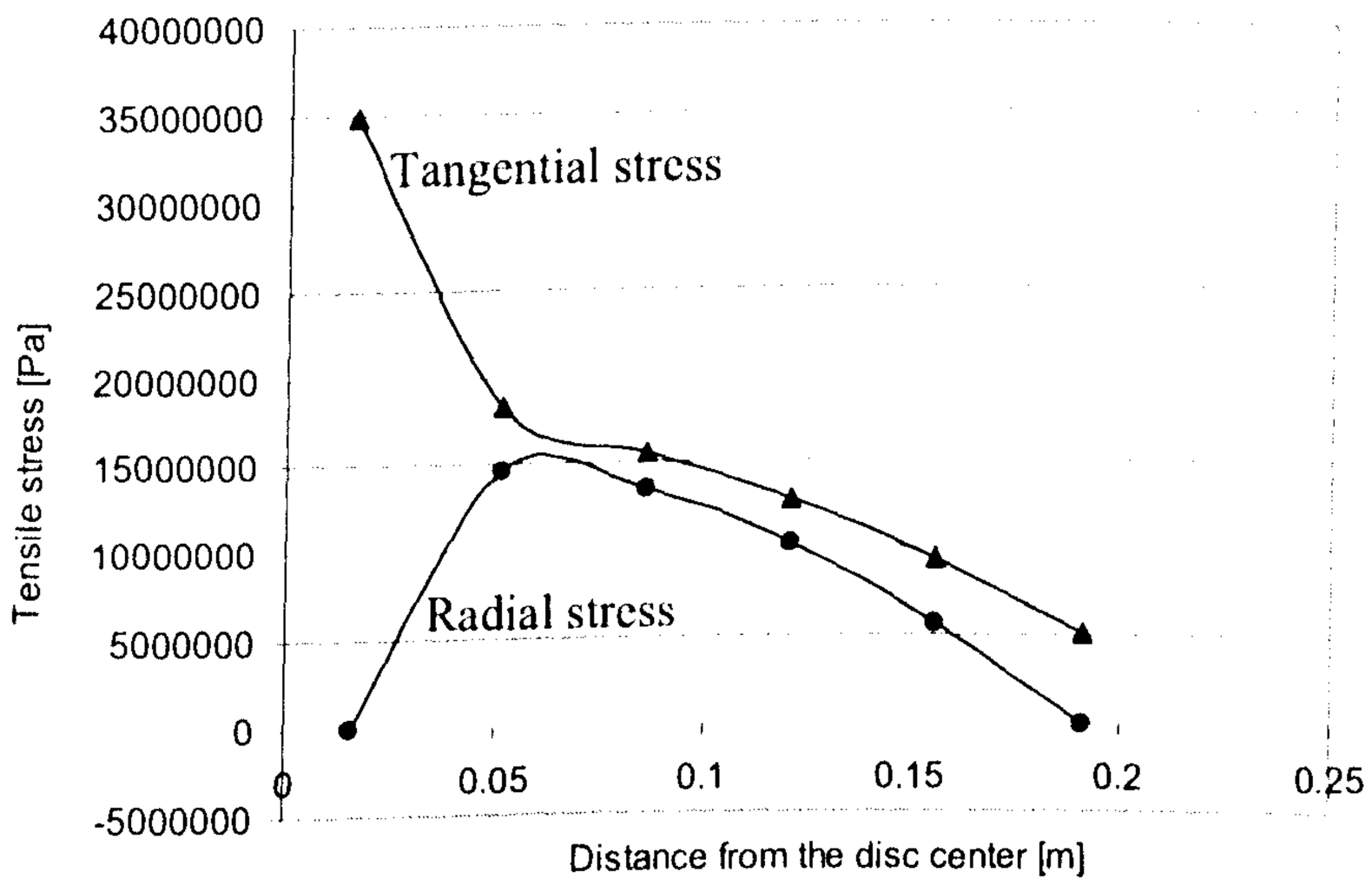

Figure 4. Stresses due to rotation in the aluminium disc (*Line of best fit*).

Theoretical predictions, as well as experimental trial confirmed that stresses, which occurred during rotation, were acceptable for the aluminium material and satisfied the safety requirements in the experiments.

4.3.2 CBN grinding wheel.

A porous high speed CBN grinding wheel 23 mm width and diameter 449 mm was also employed in the experiments. The wheel was initially designed for use with grinding machines having a large diameter spindle adapter. For this reason a special adapter was manufactured in order to allow the grinding wheel to be mounted on the Abwood surface grinding machine. The drawing of the adapter is shown in Figure 106.

4.4 Measuring Devices.

4.4.1 Power meter.

Spindle motor power was measured during the experiments using a Siemens Model B1081 function meter. The power meter measured the power in a single phase of the three-phase supply. Total power was determined by multiplying the single-phase power by three. In order to ensure the accuracy of measurement, the function meter was calibrated using a force table. The force table was also calibrated initially. Tangential grinding force and spindle motor power signals were measured at the same time for a range of depths of cut. Tangential force was used to calculate turning moment on the spindle and determine power rise during grinding. Due to the small contact length, it was assumed that the tangential force consists only of one vector parallel to the surface of the force table. Power from the force table was calculated from,

$$P = Fv_s \tag{60}$$

where F is tangential grinding force and v_s is grinding wheel peripheral velocity. For simplicity, workpiece velocity was excluded from the calculation, since it was negligible in comparison with wheel velocity. The power signal from the function meter and the power determined from the force table are shown below.

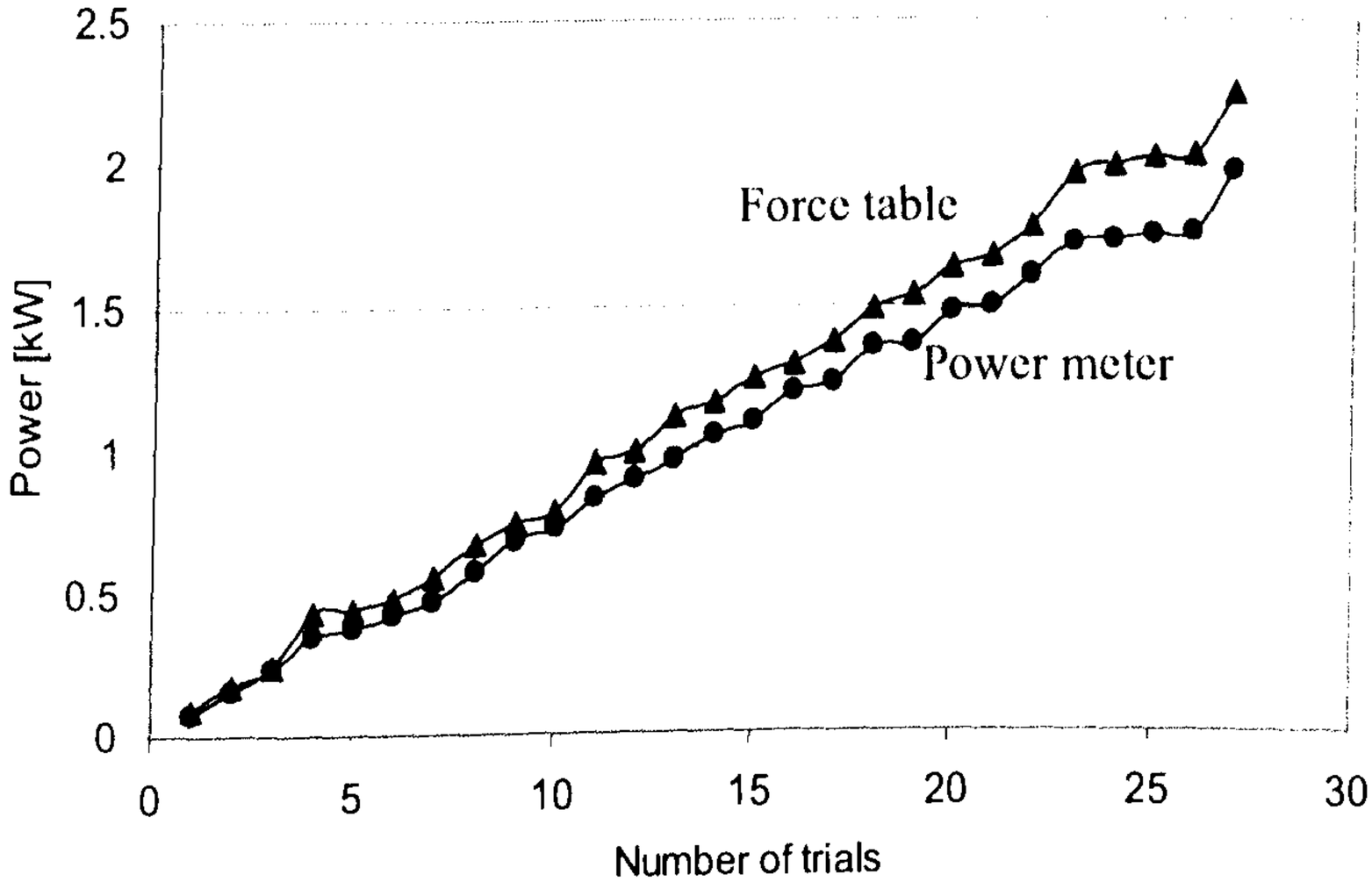

Figure 5. Comparison of the function meter power to the force table power *(Line of best fit).*

It can be seen from the graph that the power determined from the force table and power measured by the function meter differ by approximately 10%. It is assumed that the calibration results are correct, since the power from the force table was determined after its calibration based on the fundamental physical law of the gravity.

4.4.2 Force table.

A Kistler force table was used to calibrate the power measured by the function meter. The force table was calibrated by applying weights. Although, only the tangential direction of the force table was used during the experiments, the device was calibrated in both, horizontal and vertical directions. A special puller was manufactured for tangential force measurement. Weights were simply placed on the force table for vertical force measurement. Measurements were taken by increasing weights up to 10.5 kg in increments of 100 gram. Every 100 gram weight gave 45 mV output voltage, which corresponds to 0.981 *N* of force. Force was calculated from,

$$F = mg \tag{61}$$

The calibration is shown below.

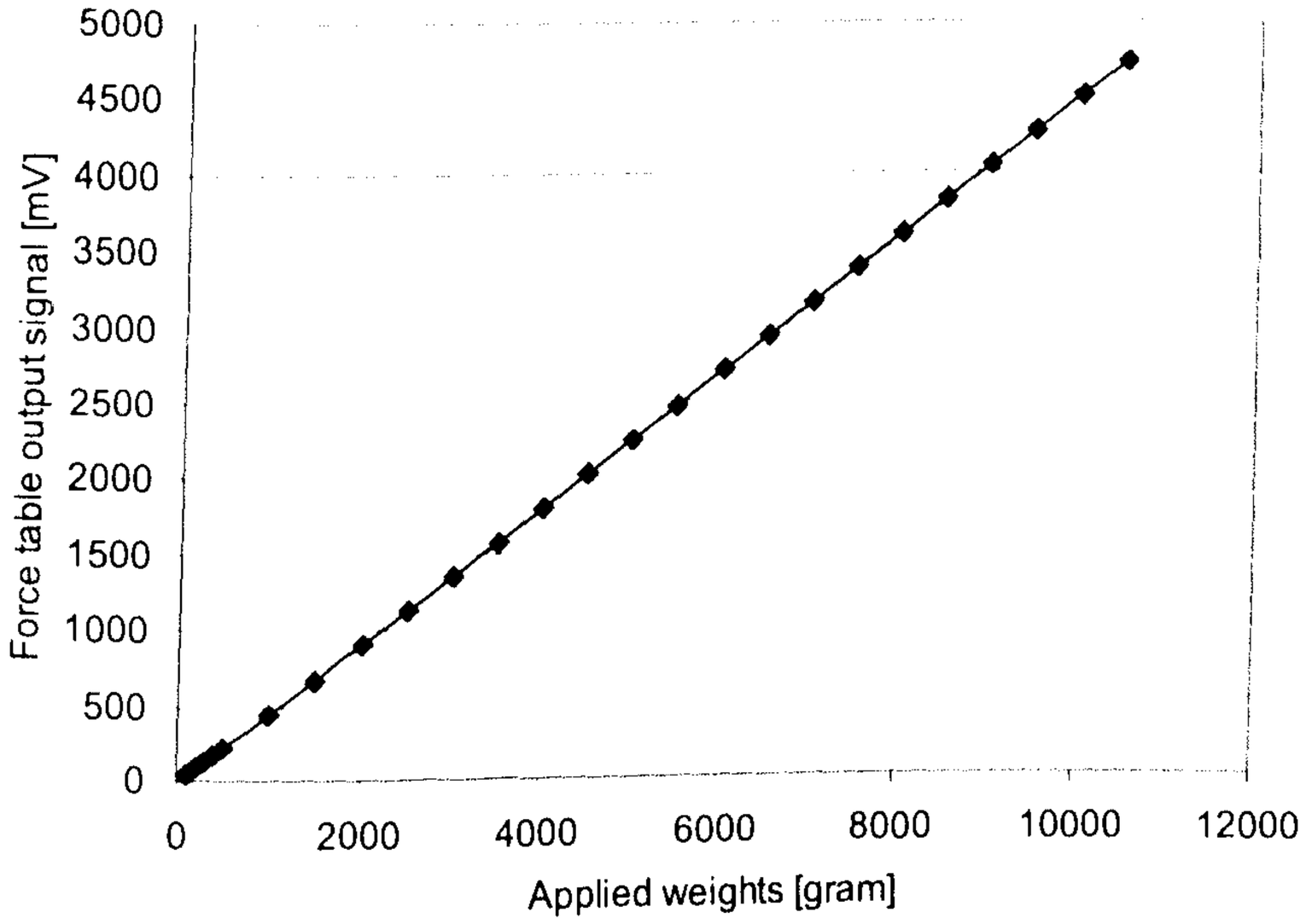

Figure 6. Force table calibration *(Line of best fit)*.

It can be seen that the output signal is linear for the range of applied weights.

4.4.3 Pressure transducer.

All pressure measurements during the experiments were carried out with the "ESI" (Ellison Sensors International) pressure transducer. The accuracy of the pressure signal was confirmed by the calibration certificate provided by the company. According to the certificate the parameters of the pressure transducer are described below.

Pressure transducer model	HI2002
Serial number	01415
Pressure range	0 – 25 bar
Supply voltage	13 – 30 V
Output signal	0 – 10 V dc
Linearity of the output signal	+/- 0.05 %

Table 5. Pressure transducer specification.

4.4.4 Flowmeter.

A turbine type flowmeter Series FTB 791 was used throughout the experiments. The parameters of the flowmeter are described below.

Flowmeter model and size	FTB 791, ½ inch
Linear flowrate range	3.8 – 37.9 l/min
Maximum flowrate	56.8 l/min
Pressure rating	103 bar

Table 6. Flow-meter specifications.

The flow-meter was calibrated for the grinding fluid "Castrol Hysol X" used during the experiments. Grinding fluid dispensed through the flow-meter was collected after fixed period of time and weighed using balance scales. The volumetric flowrate was determined with approximately 1% accuracy assuming fluid density equal to water density since the fluid contained only 10% oil. Density was required since the monitoring data of the flowmeter was given in volume per unit time in the specifications. The fluid density assumption was also confirmed by fluid volume measurement using a calibrated vessel.

Calibration results are shown below.

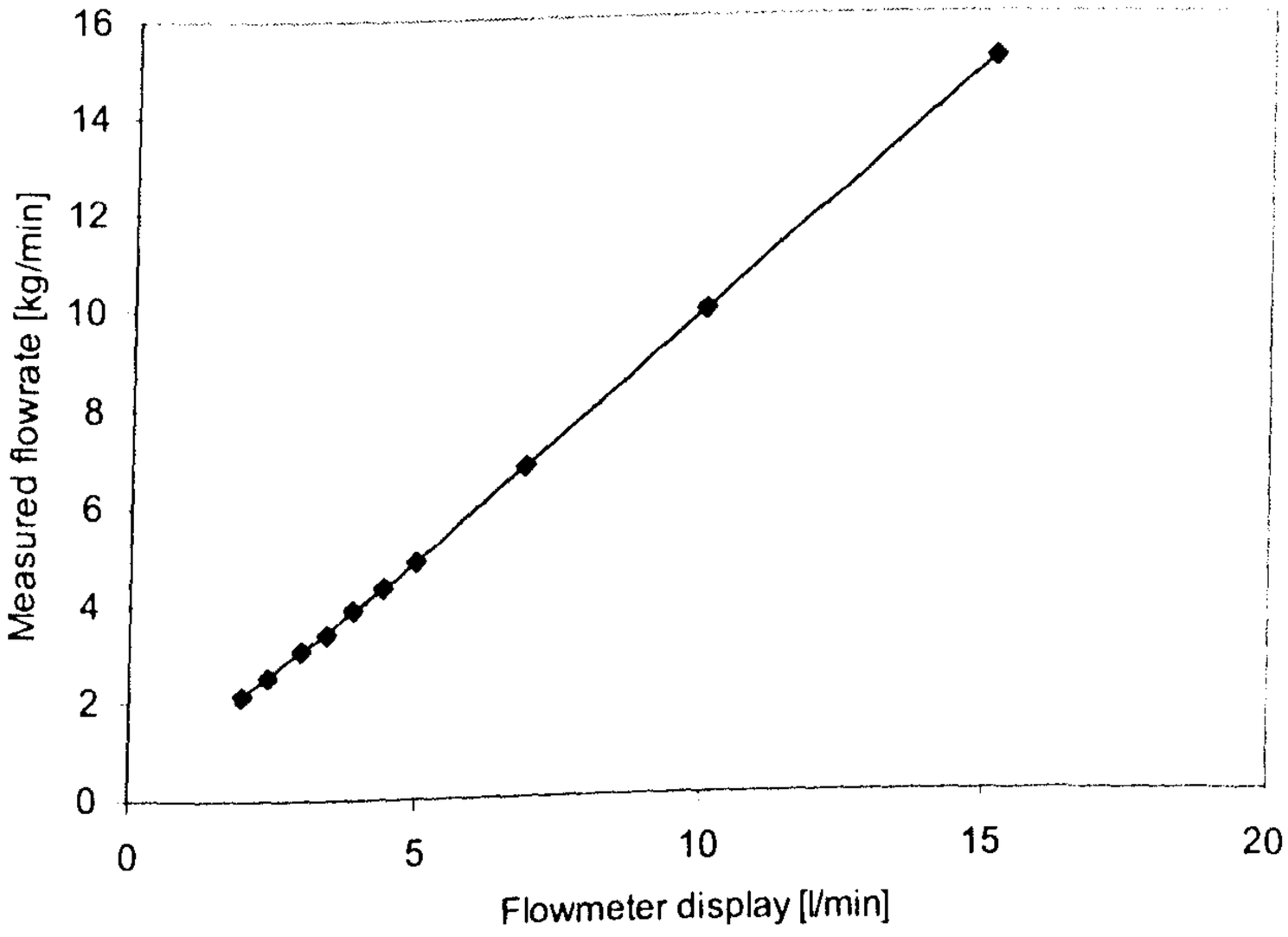

Figure 7. Flowmeter calibration chart *(Line of best fit)*.

Calibration of the flow-meter was discontinued beyond 15 l/min since good agreement with the factory calibration was observed.

4.4.5 Fluid concentration measuring device.

It was important that the properties of the fluid were kept constant during the experiments. The fluid viscosity was one of the main factors affected by the oil concentration. Concentration of oil was measured using a Hand Refractometer Model DR 50-80. The device measured percentage of oil solution in water.

4.4.6 Surface measuring devices.

Roughness of the ground parts and the grinding wheel topography were measured using a Taylor Hobson Talysurf 120 (3D) instrument (See Figure 98). The instrument employed an inductive transducer for detecting the heights and depths of the surface. A single traverse of the diamond contact probe could gather 120 000 data points, which allowed high accuracy of measurement. The distance between the traverses (increment) was 50μm, length and the width of the measured area was 5mm. The data were analysed with the appropriate software included in the instrument software. A scanned surface of the aluminium knurled disc and CBN porous grinding wheel are shown in Figure 8 and Figure 9.

Roundness of the ground parts was measured on a Taylor Hobson Talyrond.

Hardness was measured on a Leitz Mini-load Hardness Tester.

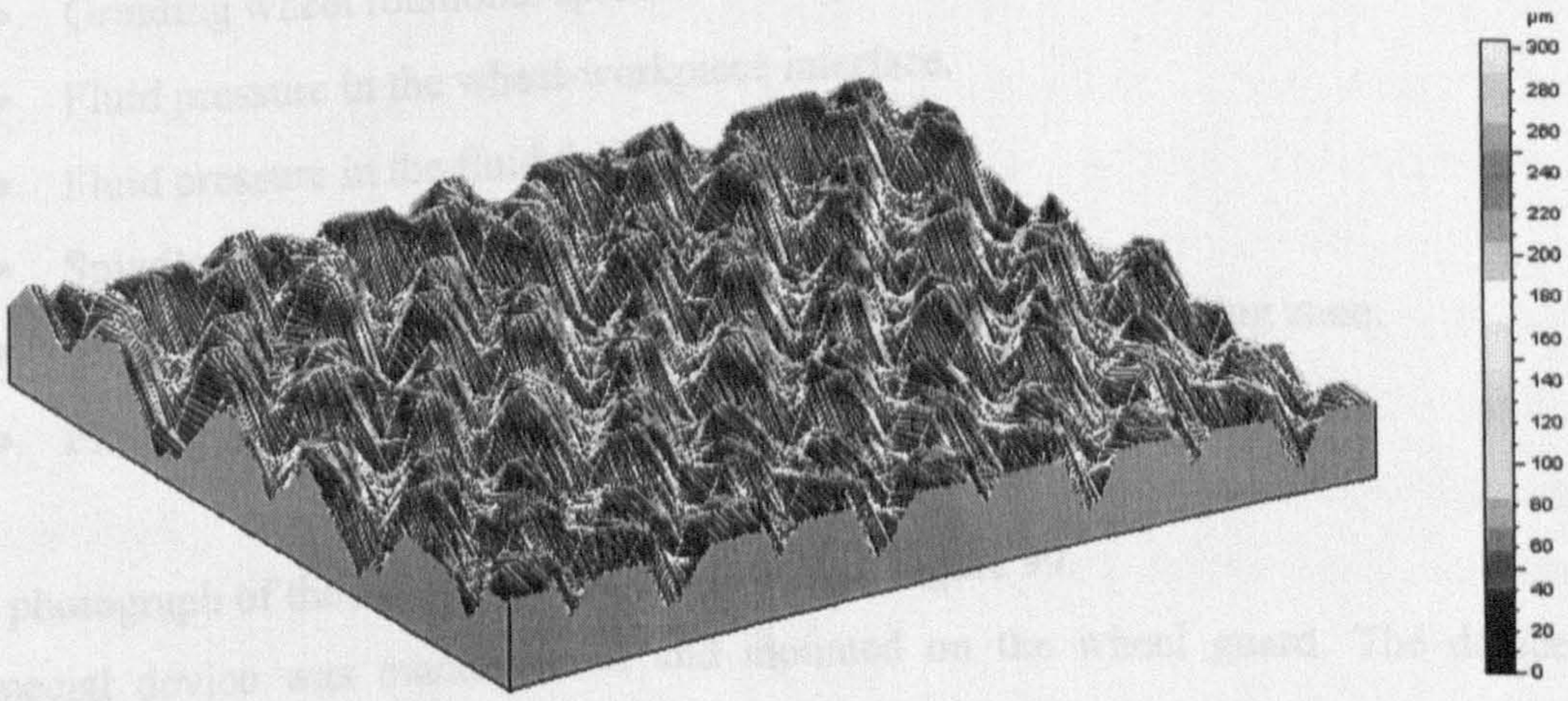

Figure 8. Aluminium knurled disc surface.

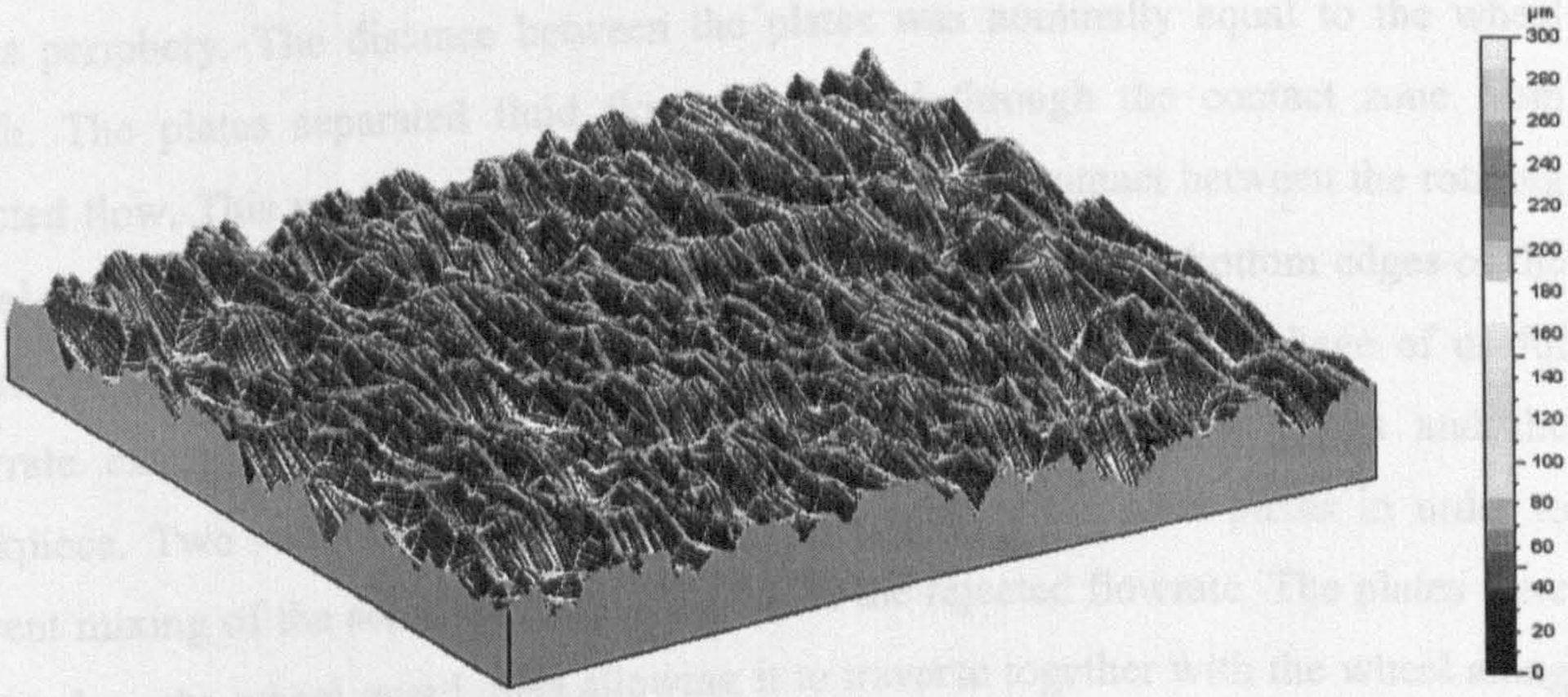

Figure 9. CBN porous grinding wheel surface.

4.5 Experimental Rig for the Surface-Grinding Machine.

Although preliminary trials were conducted on the Elliot grinding machine, the main experimental rig was built on the Abwood grinding machine in order to assess fluid behaviour in high-speed grinding and to correlate the results with the theoretical model.
The rig allowed measurement of various parameters, which were:

- Grinding wheel rotational speed.
- Fluid pressure in the wheel-workpiece interface.
- Fluid pressure in the fluid delivery system.
- Spindle motor power consumed due to delivery fluid.
- Supply flowrate and useful flowrate passing through the grinding zone.
- Fluid temperature and oil concentration in the fluid.

The photograph of the experimental rig is shown in Figure 99.
A special device was manufactured and mounted on the wheel guard. The device allowed adjustment of nozzle position towards the wheel and use of a wide range of nozzles of various types, design and size.
A rig was built to separate useful flowrate from total delivered flowrate (See Figure 100).

The device comprised two parallel plates positioned against the wheel and fitted closely to its periphery. The distance between the plates was nominally equal to the wheel width. The plates separated fluid flow that passed through the contact zone from rejected flow. This method did not actually allow physical contact between the rotating wheel and the experimental rig. Rubber seals were attached to the bottom edges of the plates contacting both sides of the workpiece. The seals prevented leakage of useful flowrate exiting the contact zone through the space between the plates and the workpiece. Two rubber plates were placed both sides of the steel plates in order to prevent mixing of the separated useful flow with the rejected flowrate. The plates were mounted on the wheel guard, thus allowing it to traverse together with the wheel along the workpiece. A scraper plate was positioned near the fluid exit from the wheel to prevent fluid recirculation around the wheel. Ejected useful flowrate was drained into a bucket through a special channel and was weighed using balance scales.

Flowrate that passed through the contact zone was collected for 1 minute. Trials were repeated three times in order to determine an average value of useful flowrate.

A carbon workpiece material was used instead of metal because the knurled aluminium grains are much softer than real grinding wheel grains (See Figure 100). The workpiece width was equal to the wheel width (23 mm). One side of the carbon was insulated and attached by adhesive to a metal base-plate and held on the magnetic table of the grinding machine. Electrical current was passed through the aluminium disc and the carbon workpiece. This allowed detection of the moment at which the disc contacted the workpiece. The clearance between wheel and workpiece was controlled roughly by measuring electrical resistance of the coolant in the gap.

A hole of 0.7 mm diameter was drilled vertically into the workpiece so that the hole was positioned radially towards the wheel for hydrodynamic pressure measurement in the contact zone. Pressure was measured by connecting the hole to a pressure sensor. Contact pressure, spindle power, useful flowrate and delivery flowrate were measured at the same time.

4.6 Experimental Rig for the Cylindrical Grinding Machine.

The rig has been designed for the Suprema cylindrical grinding machine in order to determine the effect of the delivery fluid minimisation on the grinding performance of the "difficult to grind material" Inconel 718.

The rig allowed measurement of various parameters, which were:

- Grinding wheel rotational speed.
- Workpiece rotational speed.
- Fluid pressure in the fluid delivery system.
- Supply flowrate.
- Fluid temperature and oil concentration in the fluid.
- Workpiece bulk temperature.
- Grinding power.
- Spindle motor power consumed due to delivery fluid.

A special shoe nozzle was designed for the experiments. The design of the shoe nozzle was based on a concave shaped shoe plate. It was aimed that the concave contraction between the plate and the wheel surface would minimise the power loss within the nozzle. The shoe plate was positioned close to the wheel surface (maximum separation 5mm) to reduce swirling of the fluid within the nozzle. The nozzle outlet edge was positioned close to the grinding zone, since this position was found to achieve maximum useful flowrate. A picture of the nozzle is shown in Figure 101.

The grinding parameters used during the experiments are shown in Table 7.

Dressing direction	Up
Dressing overlap	2 (0.055 mm/rev, 8.47 mm/s)
Dressing increment	2 μm
Dresser rotational speed	42 m/s (5348 rpm)
Number of passes	10 passes
Wheel speed	120 m/s
Workpiece speed	262 rpm

Dwell	None
Infeed rate	0.014 mm/s
Depth of material removed	0.2mm (off diameter)
Workpiece diameter	34.85 mm
Grinding wheel type	CBN B151 – 150 VR
Grinding wheel width	21mm

Table 7. Grinding parameters for high speed CBN grinding of Inconel 718.

A drawing of a specimen workpiece is shown in Figure 102.

CHAPTER 5. EXPERIMENTAL RESULTS AND DISSCUSSIONS.

5.1 Effects of Jet Nozzle Position on Useful Flowrate.

Experiments were conducted using rectangular cross-section jet nozzles. It was aimed to achieve maximum efficiency of the fluid delivery system due to the nozzle position when the remaining parameters are fixed. These parameters are mainly wheel speed, wheel type, fluid type and jet nozzle design. The efficiency due to the nozzle position may be evaluated by the amount of the flowrate passing through the grinding zone. This flowrate is termed the useful flowrate. However other parameter such as fluid pressure in the grinding zone and power consumed due to the fluid process also play significant roles depending on the particular grinding operation. Experiments were conducted in order to investigate the effect of nozzle distance from the wheel surface on the flowrate passing through the contact zone between grinding wheel and the workpiece. Preliminary experiments were conducted on an Elliot 618 surface grinding machine for a low rotational grinding wheel peripheral speed of 23.7 m/s. An aluminium oxide grinding wheel A60KVMOS of diameter 167.5 mm was used. The grinding fluid was Castrol Hysol X with 10 % concentration of oil. The nozzle was conventional with a rectangular outlet cross sectional area, 23 mm gap width and 0.8 mm gap thickness. The sketch of the experimental arrangement is shown in Figure 10.

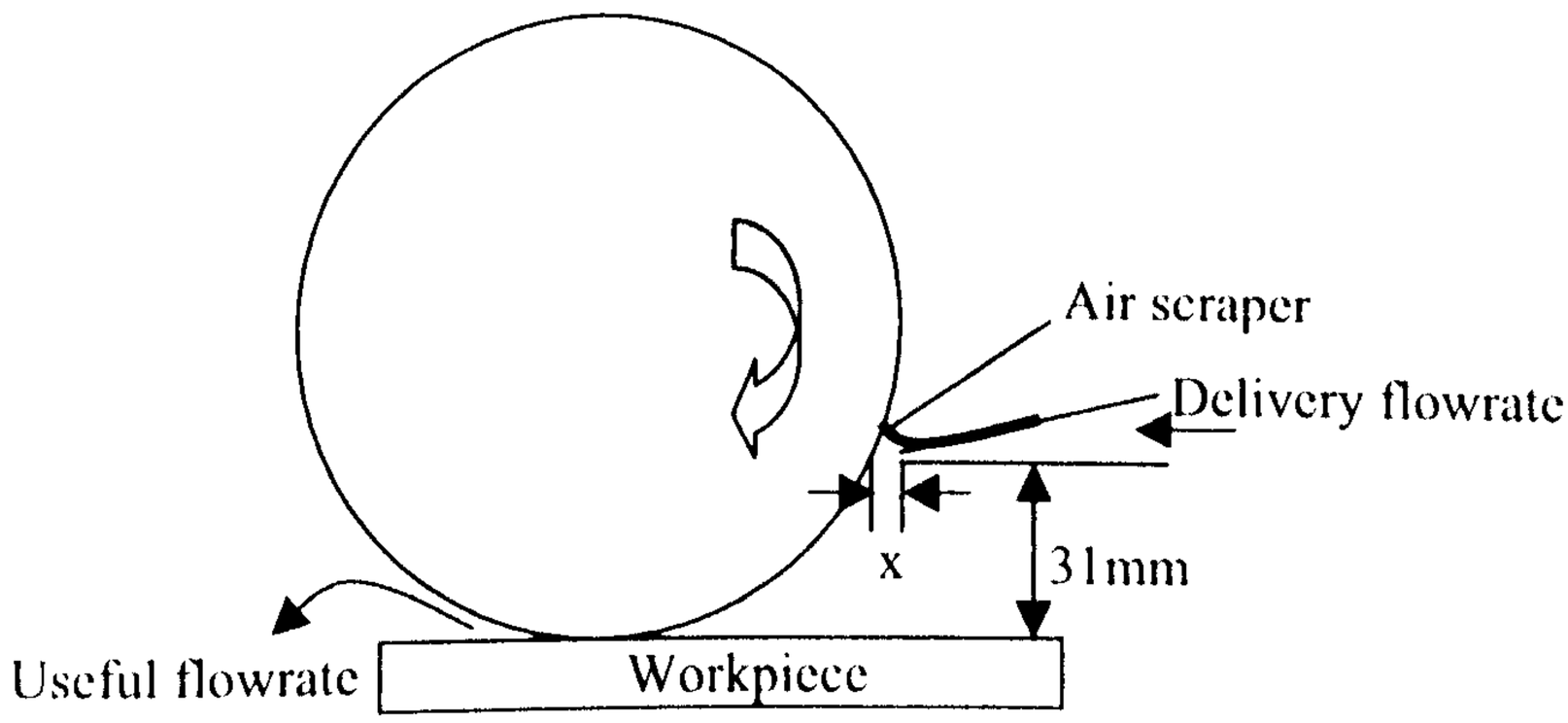

Figure 10. The experimental arrangement for the investigation of the effect on useful flowrate of nozzle distance from the wheel.

The nozzle was positioned horizontally with 0^{o} angle towards the workpiece. Distance between the nozzle and the workpiece, delivery flowrate and wheel speed was kept constant. Only the nozzle distance "x" from the wheel was varied during the experiments. Useful flowrate was measured for two conditions: with and without an air scraper. Flowrates are expressed per unit width of the wheel and nozzle as below.

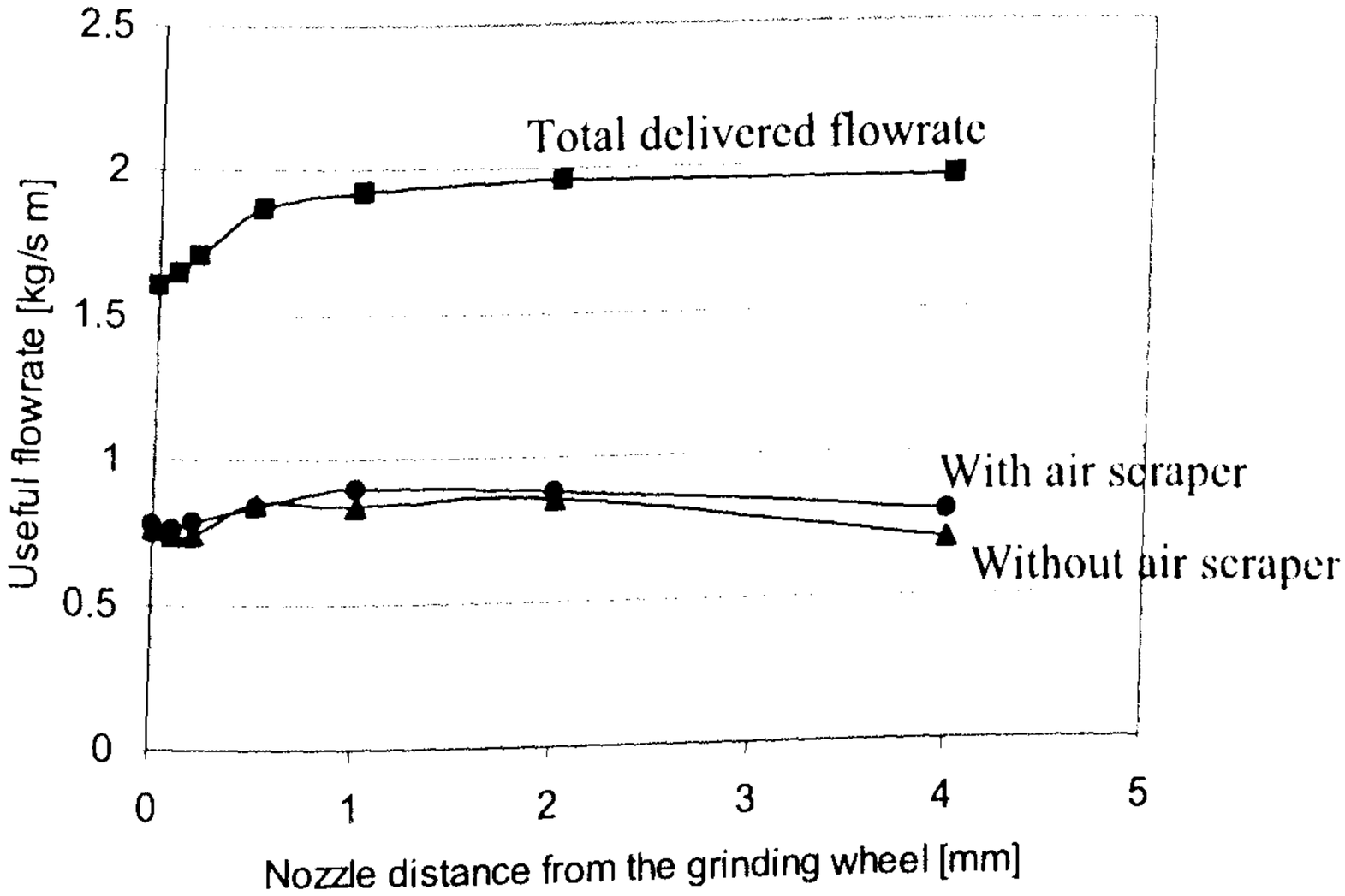

Figure 11. The effect of nozzle distance from the wheel periphery on useful flowrate *(Line of best fit)*.

Total measured delivery flowrate and useful flowrate with and without scraper versus nozzle distance are plotted together and shown in Figure 11. It can be seen that total flowrate was reduced with reduction of the clearance between the wheel surface and the nozzle outlet edge. This was caused due to the gap blockage by the wheel that restricted the fluid exit from the nozzle. On the other hand fluid was forced into the wheel pores, which prevented further decrease in useful flowrate. The air scraper had little influence on useful flowrate except at the greatest nozzle distance from the wheel. However, use of an air scraper may be important if distant nozzle positioning is required at high wheel speed and low delivery flowrate.

Further experiments were conducted on Abwood surface grinding machine, which allowed variable high peripheral wheel speed up to 120 m/s and variable supply flowrate. A large diameter aluminium knurled disc was used for this purpose. The width of the wheel was equal to the nozzle outlet gap width and was 23mm. The nozzle gap

thickness was 0.45 mm. Three nozzle positions were tested in order to determine the effect of the nozzle position on useful flowrate for a range of wheel speeds and supply flowrates. These nozzle positions are illustrated in Figure 12.

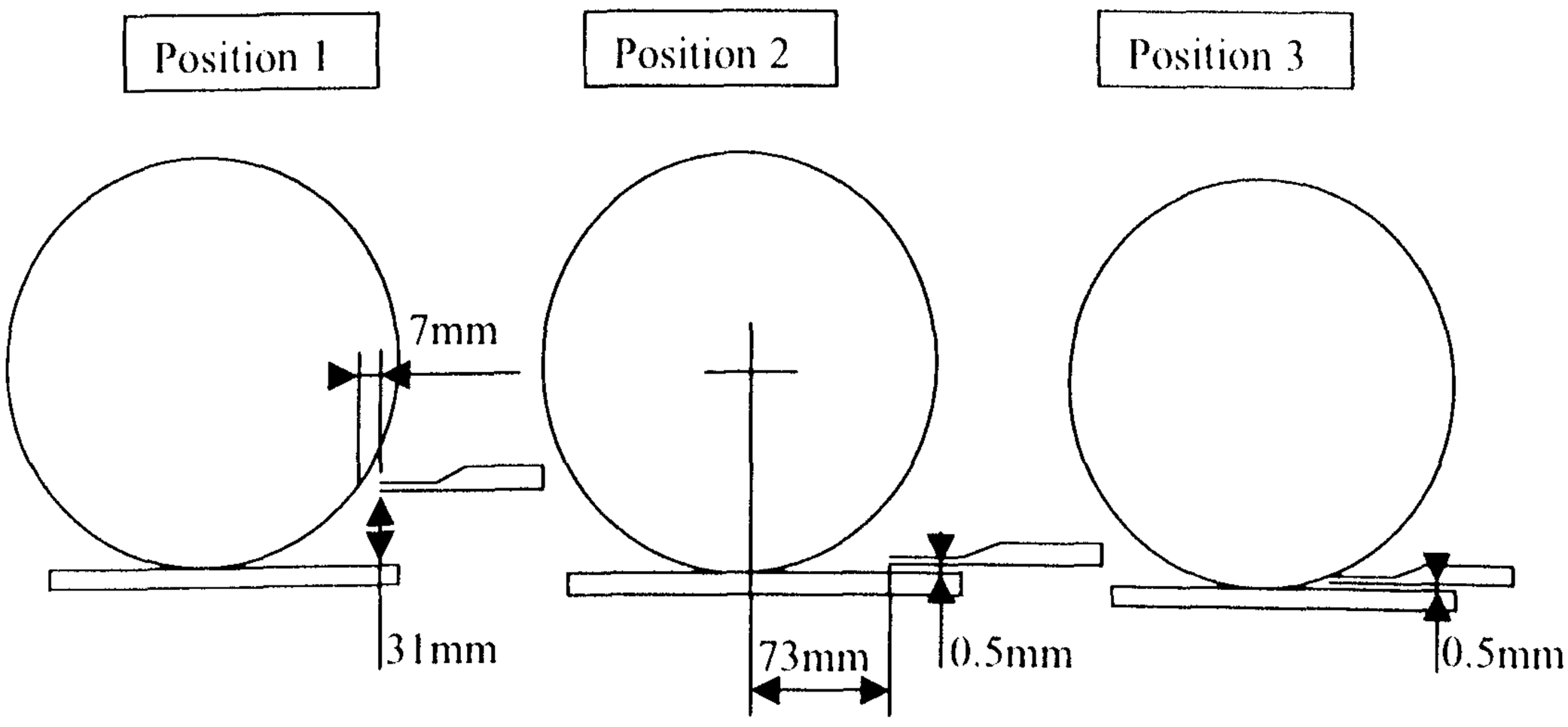

Figure 12. Positions of the nozzle for the experiments.

Position 1 is typical of a set-up used in conventional grinding. By using this position it is intended that grinding fluid will penetrate the air barrier surrounding the wheel, adhere to its periphery and be carried into the grinding zone.

Position 2 is used when a more distant location from the grinding contact is required. This may depend on the specific shape of the ground workpiece or design of the grinding machine. Position 2 requires the reverse flow from the air barrier in the converging wedge between the wheel and the workpiece to be overcome. Overcoming reverse air flow shown in Figure 104 requires greater coherence of the nozzle jet.

Position 3 does not require high jet coherence since the nozzle is positioned close to the grinding zone. Very close positioning of the nozzle to the wheel utilizes the air scraper effect, which greatly diminishes the air barrier problem. However, it may not always be possible to employ this position due to the specific technical limitations of a particular grinding operation.

Useful flowrate for the three nozzle positions are plotted against wheel peripheral velocity at a particular supply flowrate. Experimental results are presented below.

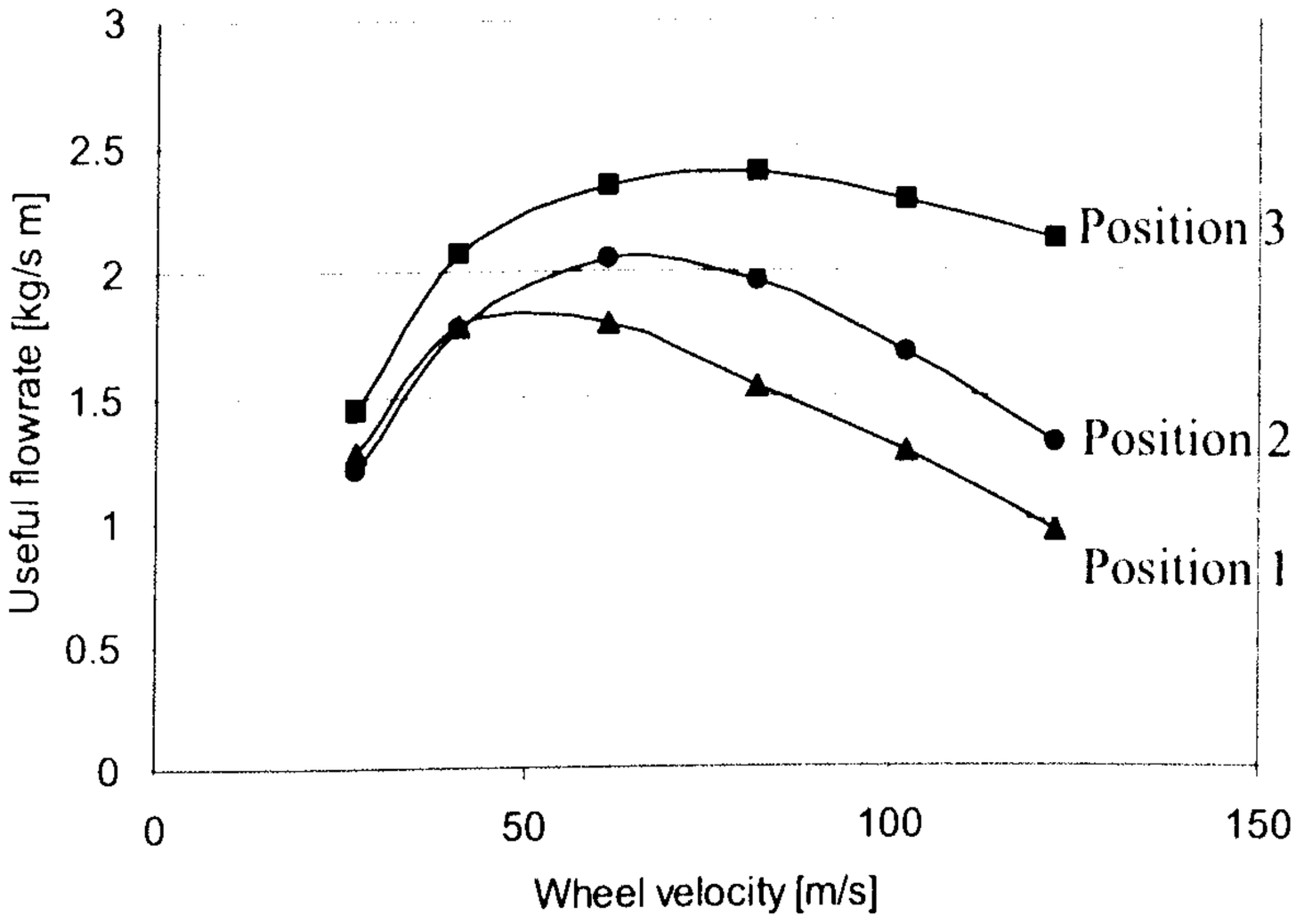

Figure 13. The effect of nozzle position on useful flowrate for 2.8 kg/s m supply flowrate *(Line of best fit)*.

Figure 13 shows results for a supply flowrate of 2.8 kg/s m, the lowest used in the experiments. At low wheel speeds, an increase in wheel speed results in increase of useful flowrate for all nozzle positions. This can be explained due to the wheel pumping effect on the grinding fluid passing through the contact zone between the wheel and the workpiece. The nozzle position closest to the contact zone gave the greatest useful flowrate. After reaching a particular wheel speed, useful flowrate starts to decrease. Lower useful flowrate at Positions 1 and 2 was achieved than at Position 3 especially for higher wheel speeds. Figure 13 shows that more supply flowrate is wasted at Position 1 than at the other two positions.

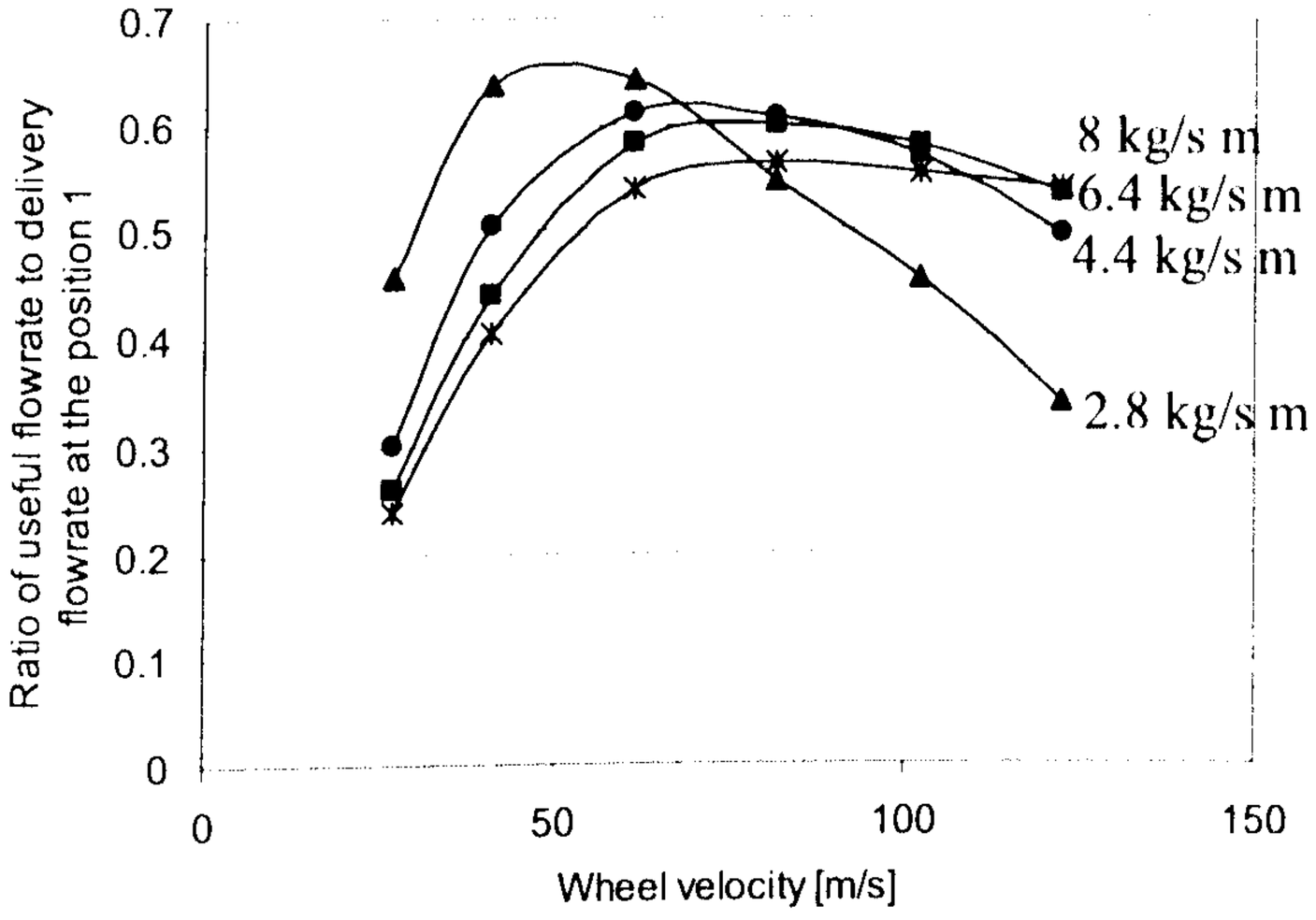

Figure 14. Ratio of useful flowrate to delivery flowrate for Position 1 for a range of delivery flowrate *(Line of best fit)*.

Figure 14 shows the ratio of useful flowrate to supply flowrate for Position 1. The maximum value for the four values of supply flowrate varies between 55 and 65%. From Figure 13, it was seen that more of the flowrate passed through the contact zone at Position 2 than at Position 1. The lowest useful flowrate at Position 1 for the high wheel speeds suggests that the fluid is ejected from the wheel surface before it reaches the contact zone. This is possibly due to low fluid energy in comparison to the air flow energy, which prevents fluid penetration through the air barrier surrounding the wheel. Furthermore fluid is easily ejected tangentially from the wheel surface due to high rotational speed of the wheel as discussed in Chapter 3.

Position 2 is better than Position 1 since the nozzle jet is directed towards the contact zone and located tangentially towards the wheel surface. Therefore, when the fluid enters the converging gap in the wheel-workpiece interface it is accelerated tangentially by the wheel and propelled through the grinding zone by the pumping action of the pores in the wheel surface. However, because of the distance of the nozzle position from the contact zone, forward motion of the fluid may be restricted by reverse air flow from the converging gap.

Position 3 is the most efficient position. The advantages of Position 3 are:

- Close location to the area where the wheel pumping action occurs.
- The short length of the jet does not require the jet to maintain coherence for a great distance.
- The edge of the nozzle acts as an air scraper.

- Fluid is not ejected prematurely from the wheel surface and is not restricted by reverse air flow.

The advantage of Position 3 is confirmed in Figure 15, which shows a high efficiency of supply flowrate utilisation at this position. The utilisation ratio varies between 76 and 85%.

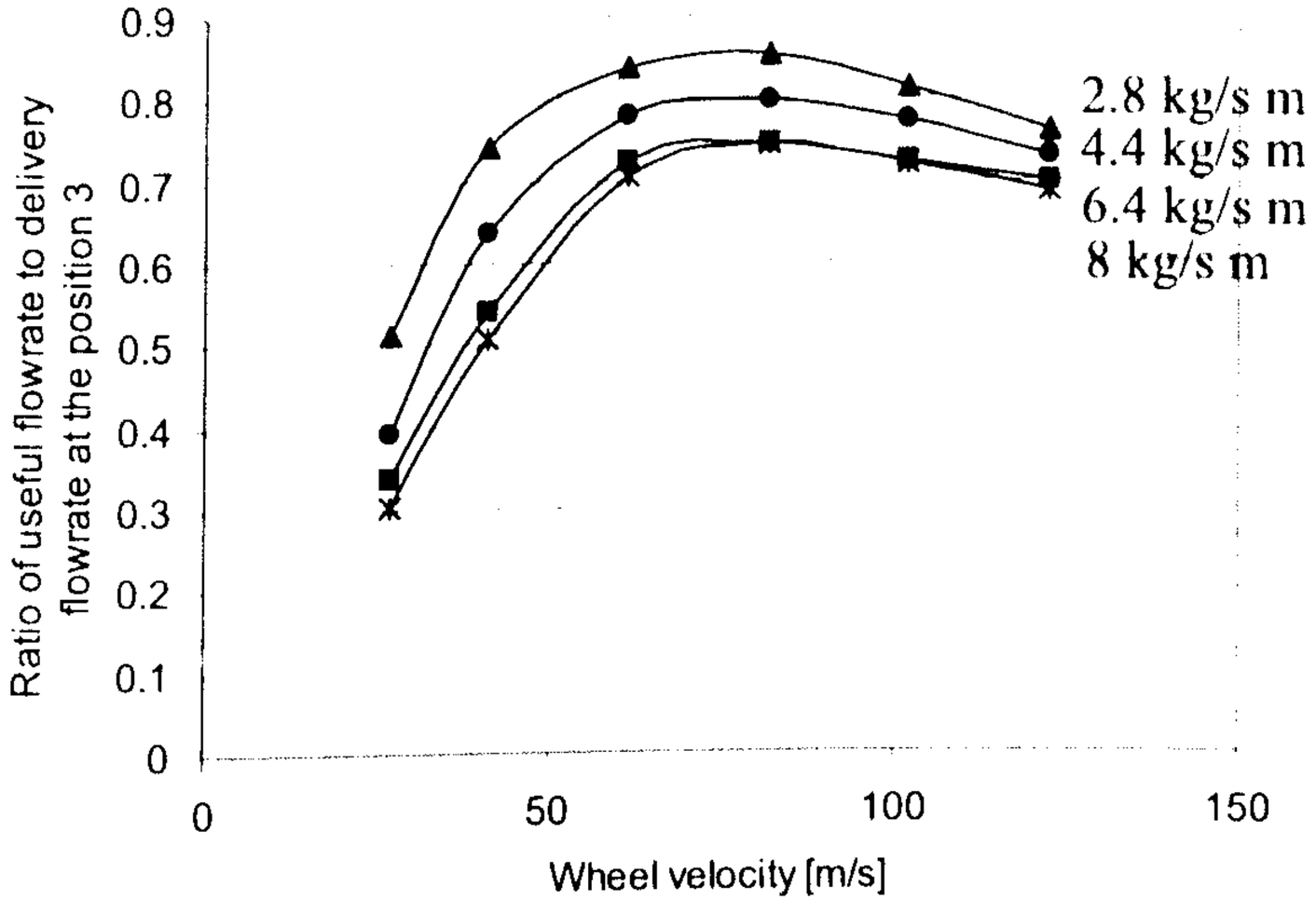

Figure 15. Ratio of useful flowrate to supply flowrate at Position 3 for a range of supply flowrates *(Line of best fit)*.

It can be seen that even at the lowest supply flowrate the percentage of the useful flowrate does not drop as markedly in comparison to Position 1 shown in Figure 14. Experimental results for increased supply flowrate are shown in Figure 16, Figure 17 and Figure 18.

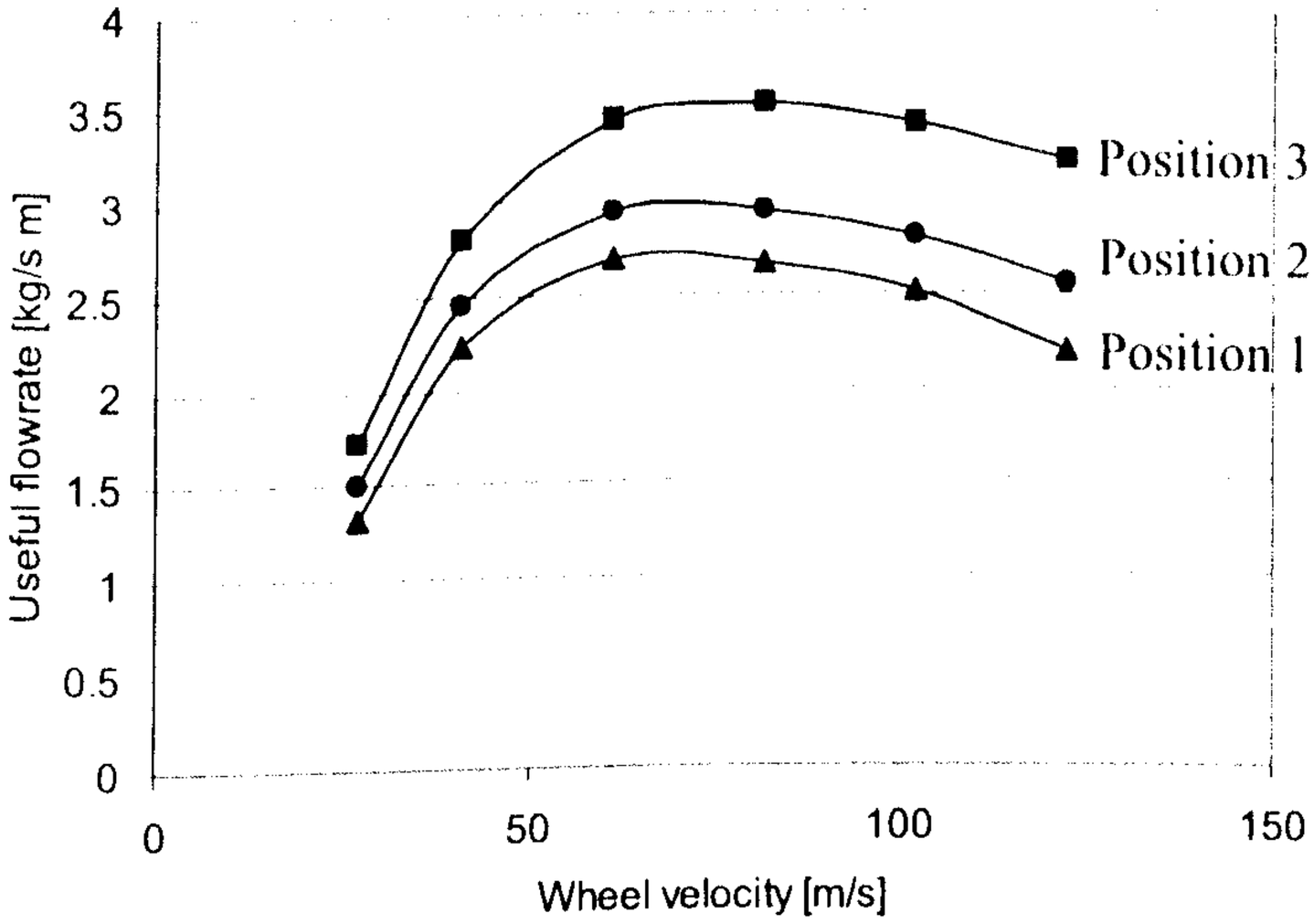

Figure 16. The effect of nozzle position on useful flowrate for 4.4 kg/s m supply flowrate *(Line of best fit)*.

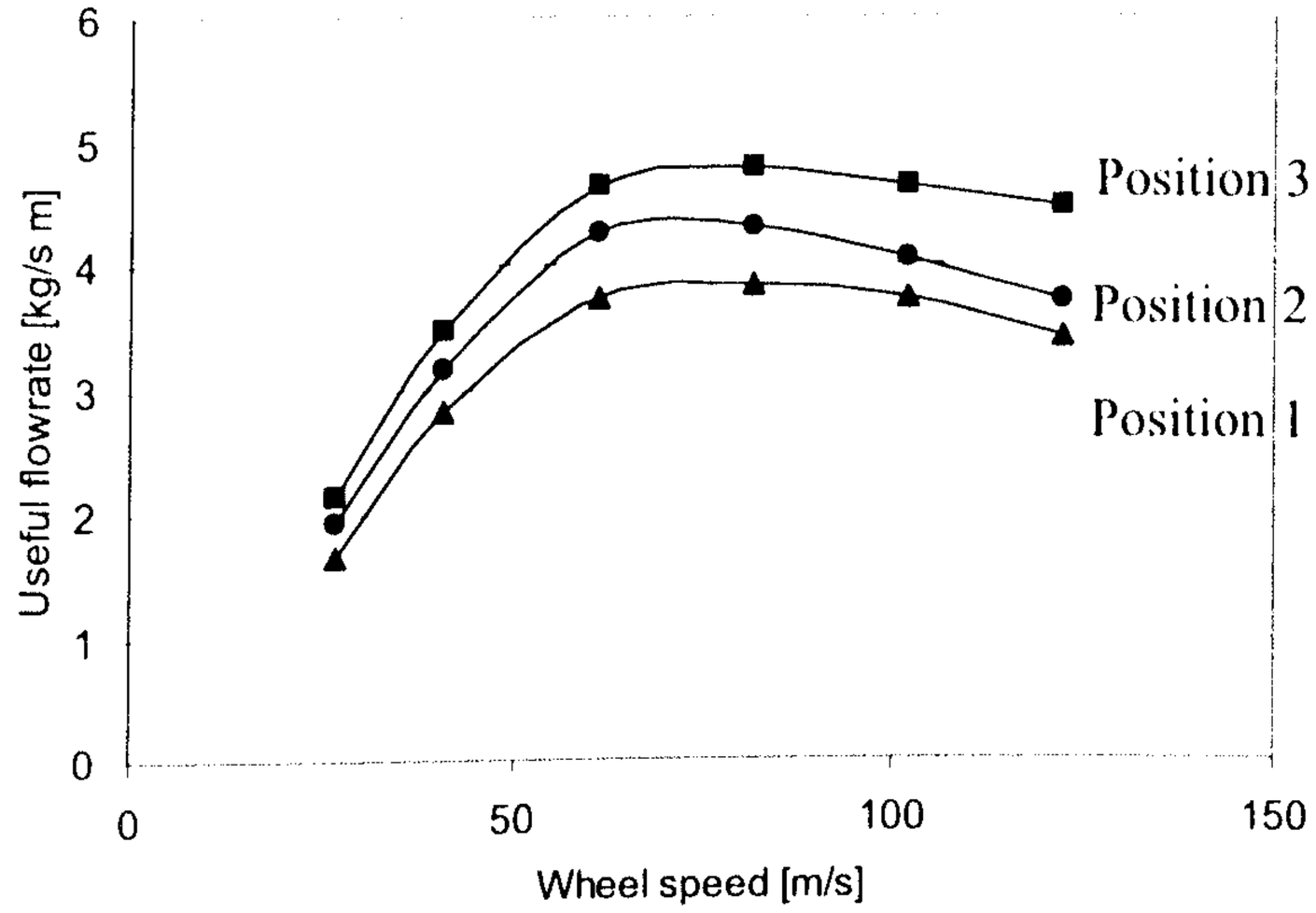

Figure 17. The effect of nozzle position on useful flowrate for 6.4 kg/s m supply flowrate *(Line of best fit)*.

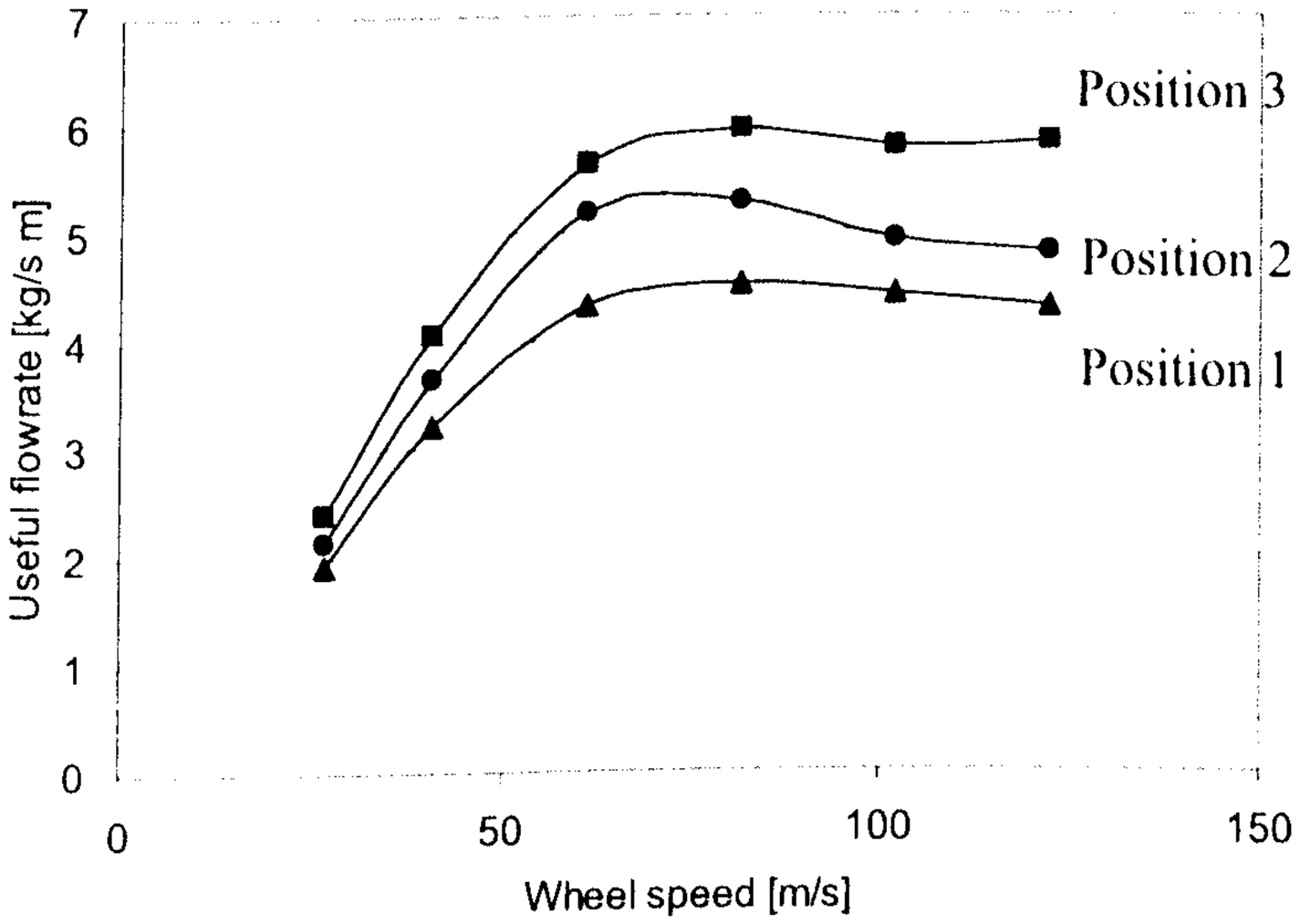

Figure 18. The effect of nozzle position on useful flowrate for 8 kg/s m supply flowrate *(Line of best fit)*.

It can be seen that increased supply flowrate results in greater useful flowrate for all three positions. As would be expected, a higher mass flowrate having greater momentum more easily overcomes the air barrier, thus increasing the flow through the contact zone. However, Position 1 still gives the lowest useful flowrate and Position 3 the highest useful flowrate for the same supply flowrate.

5.2 The Effect of Nozzle Flowrate and Jet Velocity on Useful Flowrate.

Higher useful flowrate may be achieved by increasing supply flowrate. Obviously this is the simplest solution to the problem. However employing this approach tends to reduce the usefulness of the supply fluid, since a large quantity of the flowrate may bypass the grinding zone. If the fluid is pumped at high pressure, the rejected flowrate represents a waste of energy. Increased waste of grinding fluid into the external environment may also result increasing total cost of the grinding process and causing environmental pollution. A number of important parameters affecting the fluid process have to be taken into account in order to achieve maximum efficiency of the fluid delivery system. Experiments were conducted to improve a conventional fluid delivery system by optimising delivery nozzle flowrate and jet velocity. This method can significantly increase efficiency of the fluid delivery process. An impervious aluminium disc and a porous CBN grinding wheel were tested for various delivery flowrates and nozzle gap sizes. Three nozzles having 0.15mm, 0.4mm or 2mm gap thickness were employed during the experiments and all of 23mm slot width. Position 3 for the nozzles was chosen for the experiments. In order to compare performance of the nozzles, jet power for all three nozzles was kept constant. Equal jet power was achieved by varying the jet flowrate and jet velocity. As a result, the nozzle with thicker gap produced higher flowrate and lower jet velocity, the nozzle with smaller gap produced lower flowrate and higher jet velocity.

Nozzle gap size mm	Jet power P_j =0.088kW/m		Jet power P_j =1.1kW/m		Jet power P_j =4kW/m		Jet power P_j =11.2kW/m		Jet power P_j =32.1kW/m	
	$\dot{m}_j$ kg/sm	v_j m/s	$\dot{m}_j$ kg/sm	v_j m/s	$\dot{m}_j$ kg/sm	v_j m/s	$\dot{m}_j$ kg/sm	v_j m/s	$\dot{m}_j$ kg/sm	v_j m/s
0.15	1.6	10.6	3.6	24.2	5.7	37.7	8	53	11.3	75.4
0.4	3	7.6	7	17.4	10.9	27.2	15.2	38	21.7	54.3
2	8.9	4.5	20.4	10.2	32	16				

Table 8. Nozzle jet velocity and jet mass flowrate for various nozzle gap sizes at constant jet powers.

5.2.1 Useful flowrate for the impervious knurled disc varying nozzle gap size.

The peripheral surface of an aluminium disc was knurled to represent an impervious grinding wheel. A groove was ground into the carbon workpiece by the disc and fixed in this position to represent the grinding arc. Trials were carried out for each nozzle. Flowrate supplied to the nozzle and wheel speed were varied during the experiments. Useful flowrate was collected and weighed for a range of jet flowrates. The maximum flowrate that can be transported by the surface pores of the wheel through the grinding zone was calculated and compared with measured useful flowrate. Maximum available useful flowrate for the impervious wheel was defined assuming that the space between the knurled grains was filled with grinding fluid. The ratio of useful flowrate to jet flowrate is shown in Figure 19 with the smallest nozzle gap used during the experiments. At low wheel speed, it was found that maximum percentage of the fluid was transported through the grinding zone at lowest jet flowrate. However after a particular wheel speed, for a particular jet flowrate, the ratio starts to drop and is least at the highest wheel speed. This is expected due to the ability of the increased air flow at higher wheel speed to dominate the grinding fluid flow by interfering and mixing with it in the converging gap. Although increased jet flowrate gives a lower utilisation ratio, the situation is less sensitive to the effect of higher wheel speeds. It appears that the maximum utilisation ratio achievable with the impervious wheel is approximately 46%. This compares with 85% in Figure 15 for the porous wheel.

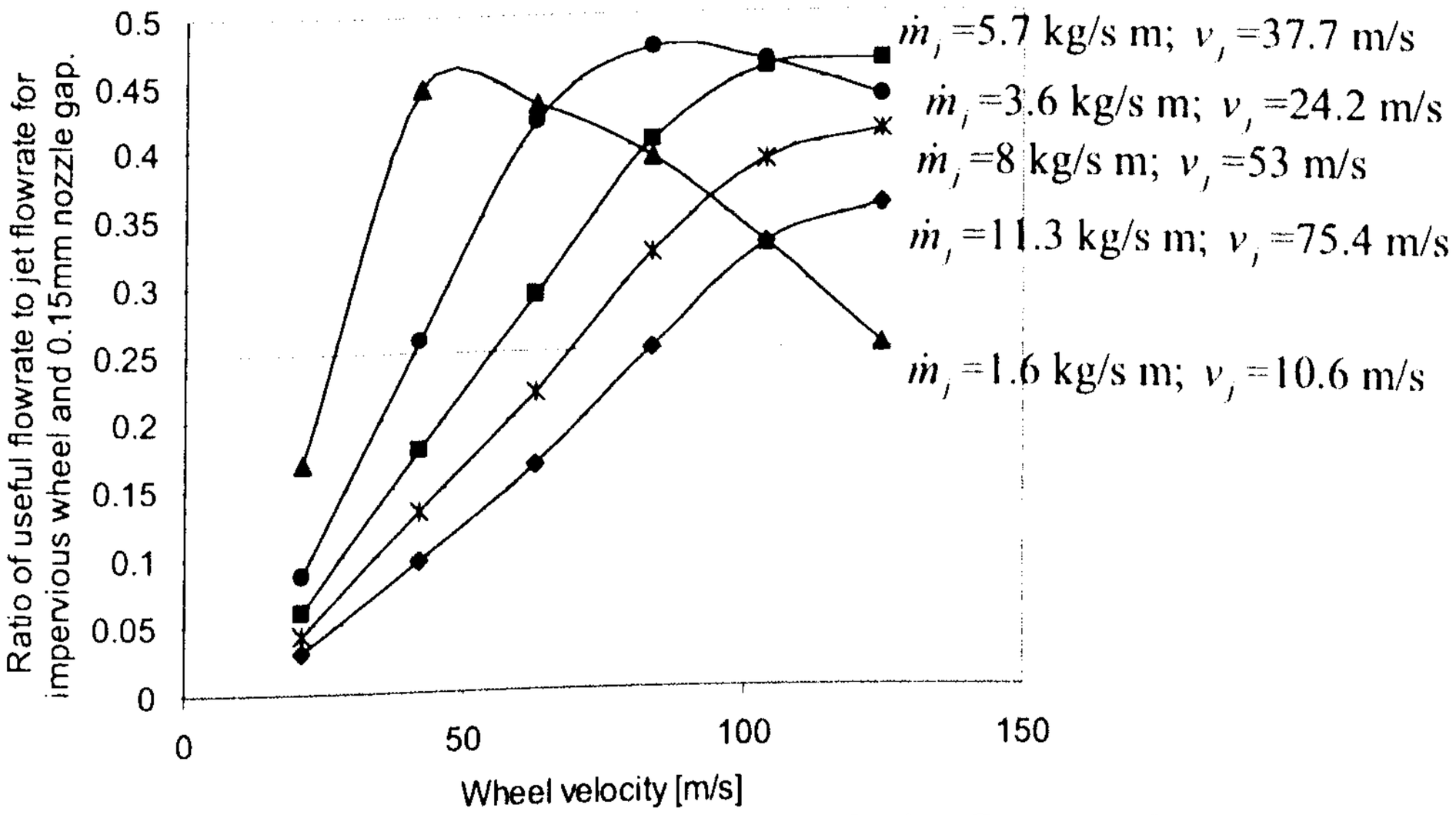

Figure 19. Ratio of useful flowrate to supply jet flowrate for an impervious disc and a 0.15mm gap nozzle *(Line of best fit)*.

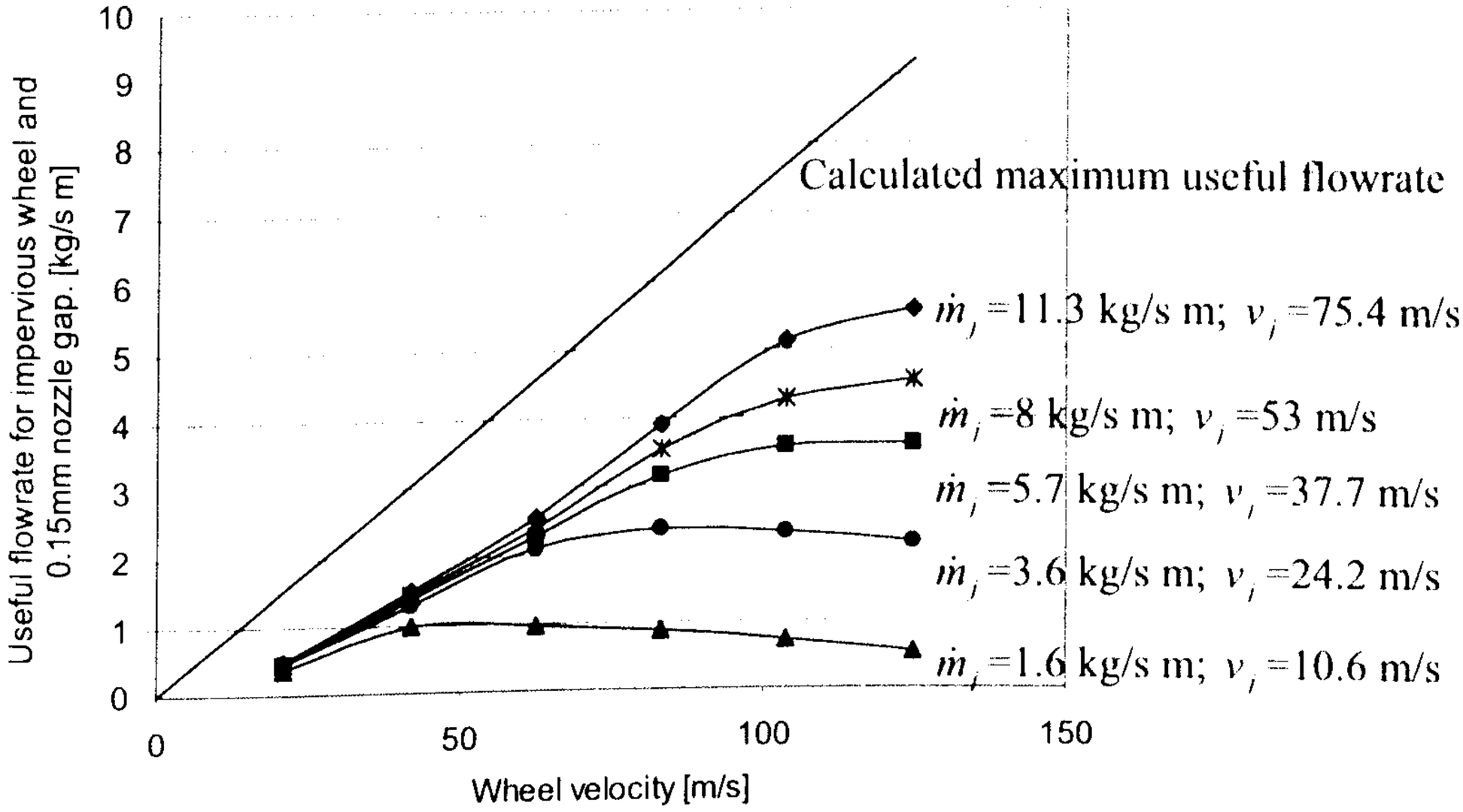

Figure 20. Measured and calculated maximum useful flowrates for the impervious disc with 0.15mm gap nozzle *(Line of best fit)*.

Useful flowrate is plotted in Figure 20 for the range of supply flowrates together with calculated maximum useful flowrate. It is shown that increase in wheel speed at low wheel speed results in linear increase in useful flowrate. This is in agreement with the expected wheel pumping effect in the wheel-workpiece interface. For a particular jet flowrate, further increase of useful flowrate ceases at a specific wheel velocity. This transition occurs at lower wheel velocity for the lower jet flowrate and higher wheel velocity for the higher jet flowrate. This means that increased wheel speed allows more fluid transport through the grinding zone as far as fluid is delivered efficiently to the contact zone where the pumping action occurs. From the design point of view, it is important that the nozzle design should be capable of operating below or at the transition wheel speed. This has implications for the minimum nozzle gap and jet velocity.

Although higher jet flowrate allows more fluid to be carried through the contact zone, the contact gap was not filled fully with grinding fluid at any jet flowrate using a 0.15mm gap nozzle. If the gap is not filled with grinding fluid or work material removal, it is probably filled with the air. This suggests that air mixes with the grinding fluid creating a two-phase flow, which is consequently transported by the rotating wheel.

Figure 21 shows the ratio of useful flowrate to jet flowrate with a 0.4mm gap nozzle.

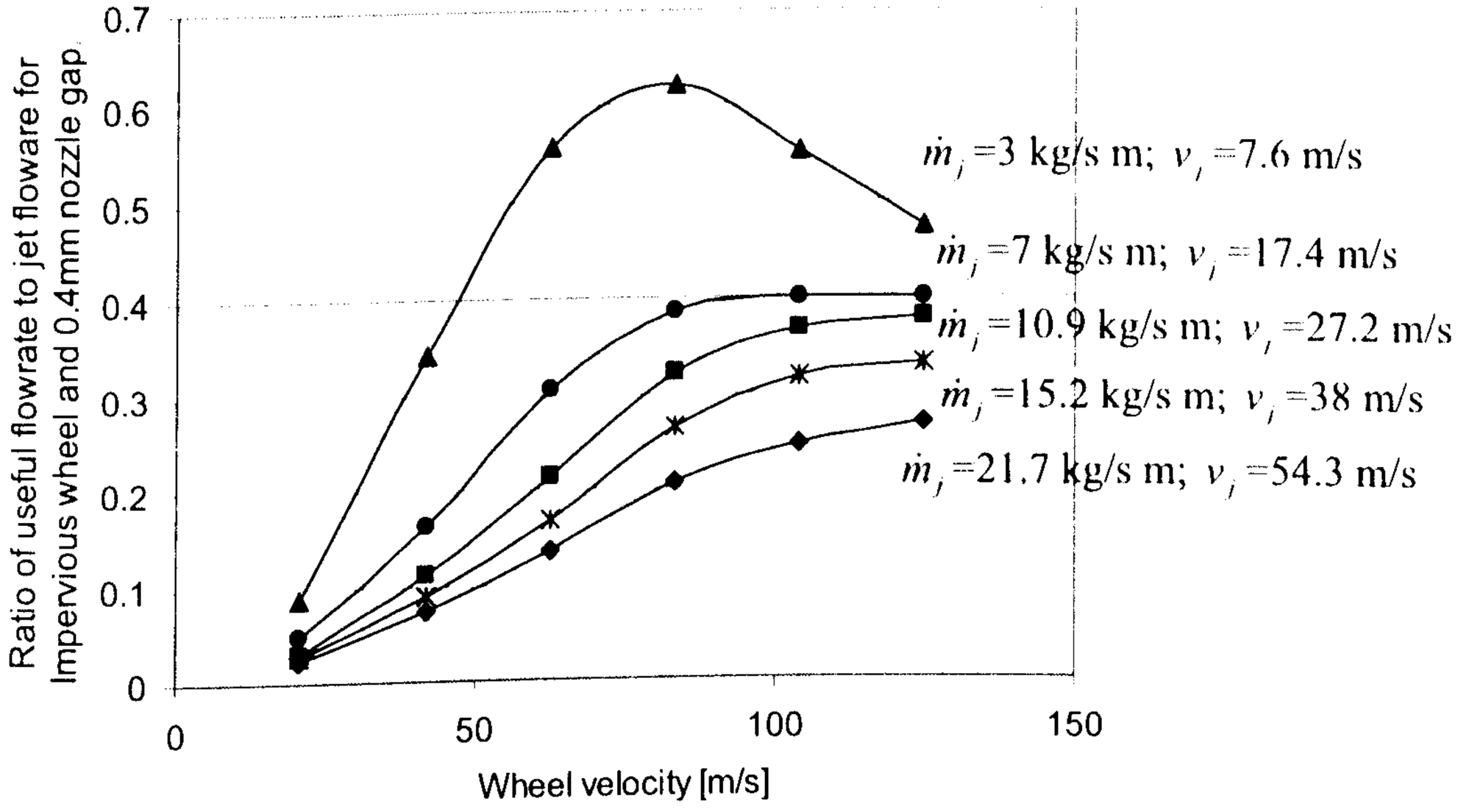

Figure 21. Ratio of useful flowrate to jet flowrate for the impervious disc with 0.4mm gap nozzle *(Line of best fit)*.

It can be seen that the ratio for the lowest jet flowrate tends to drop after the transition wheel speed as with the previous nozzle. The utilisation ratio for the larger gap size is less sensitive to the air flow than for the smaller gap nozzle in spite of lower jet velocity. This is also attributed to the effect of higher jet flowrate. However for a bigger gap and a higher jet flowrate more fluid is wasted than for a smaller gap and a lower jet flowrate. This can be seen by comparing ratios for the two nozzles in Figure 19 and Figure 21 where the jet powers for both nozzles are equal as shown in Table 8. On the other hand the nozzle with bigger gap size and higher jet flowrate produces slightly higher useful flowrate, which is shown in Figure 22.

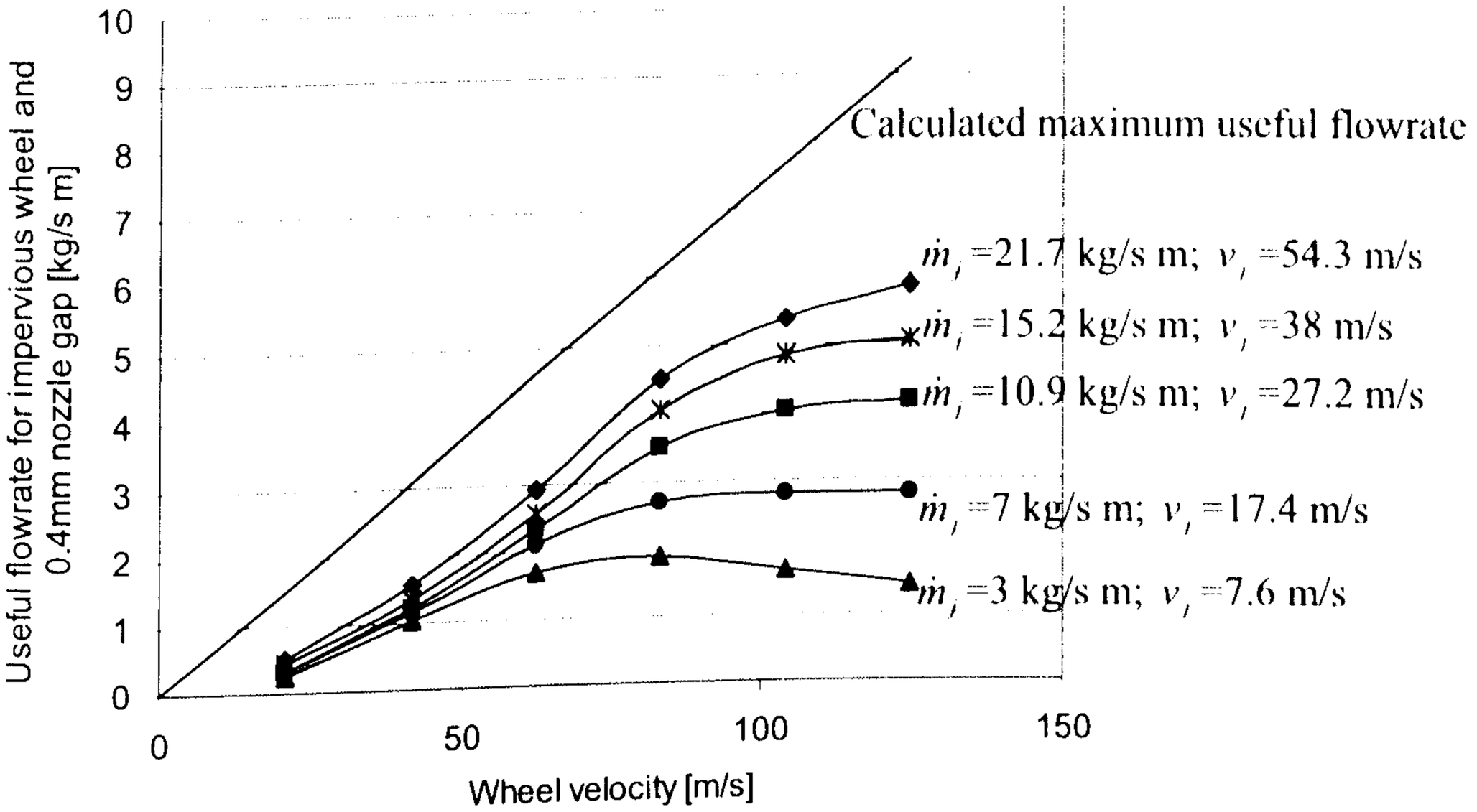

Figure 22. Measured and calculated maximum useful flowrates for the impervious disc with 0.4mm gap nozzle *(Line of best fit)*.

The ratio of useful flowrate to jet flowrate for the nozzle with the largest gap size of 2mm is shown in Figure 23. As expected, the biggest gap size and largest jet flowrate rejects the largest quantity of grinding fluid. The utilisation ratio is especially low at lowest wheel speed and highest jet flowrate. Figure 23 shows that less than 5 % of fluid passed through the grinding zone at minimum wheel speed and maximum jet flowrate. A significant decrease in ratio for lowest jet flowrate is also observed above the transition wheel speed. This tends to support the argument that the passage of grinding fluid can be disrupted by air flow, not only because of lower jet flowrate but also due to lower jet velocity.

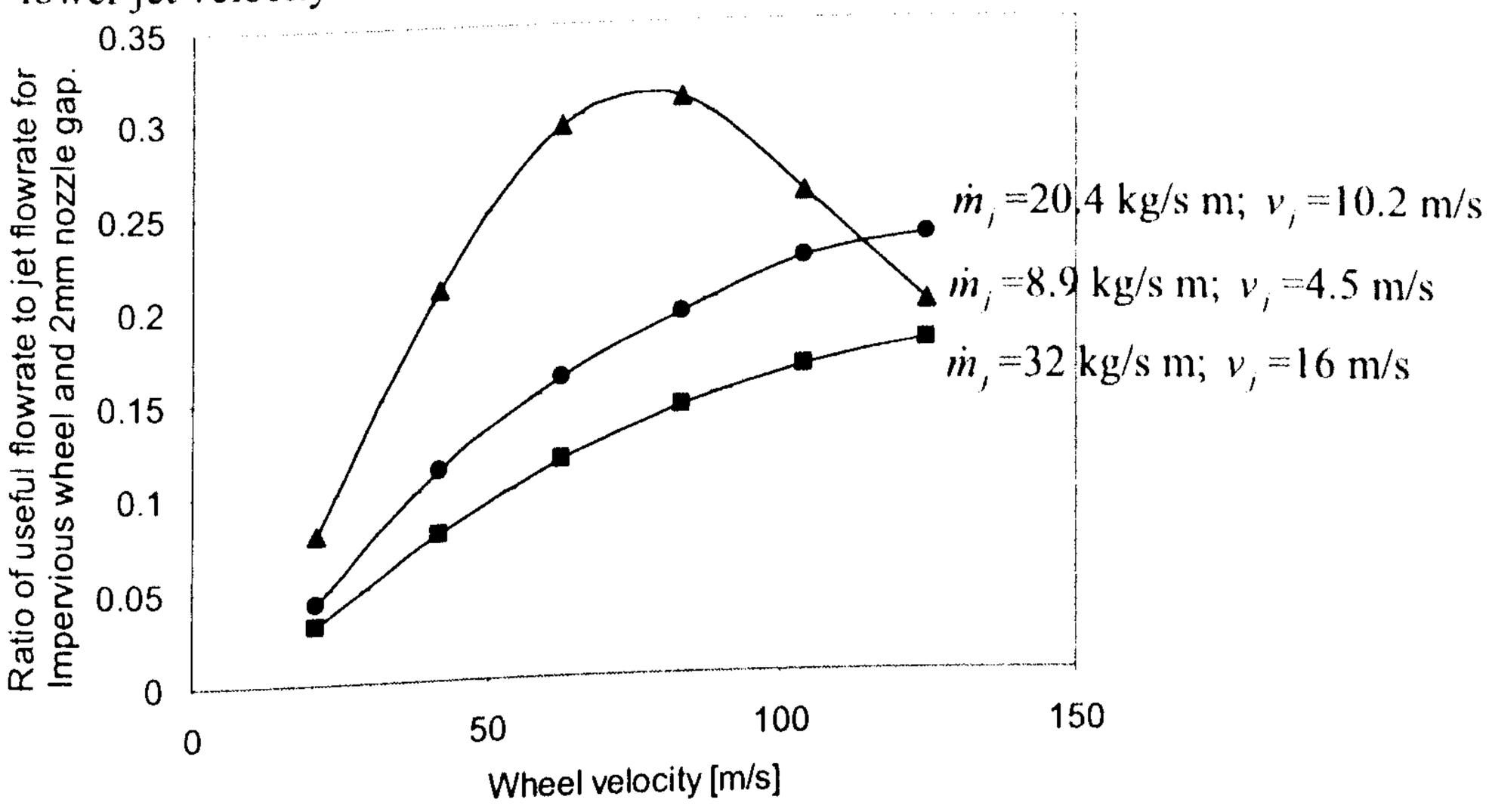

Figure 23. Ratio of useful flowrate to jet flowrate for the impervious disc with a 2mm gap nozzle *(Line of best fit)*.

In spite of the low utilization ratios, Figure 24 shows that the nozzle with the largest gap and highest flowrate produces a higher useful flowrate than the other two nozzles.

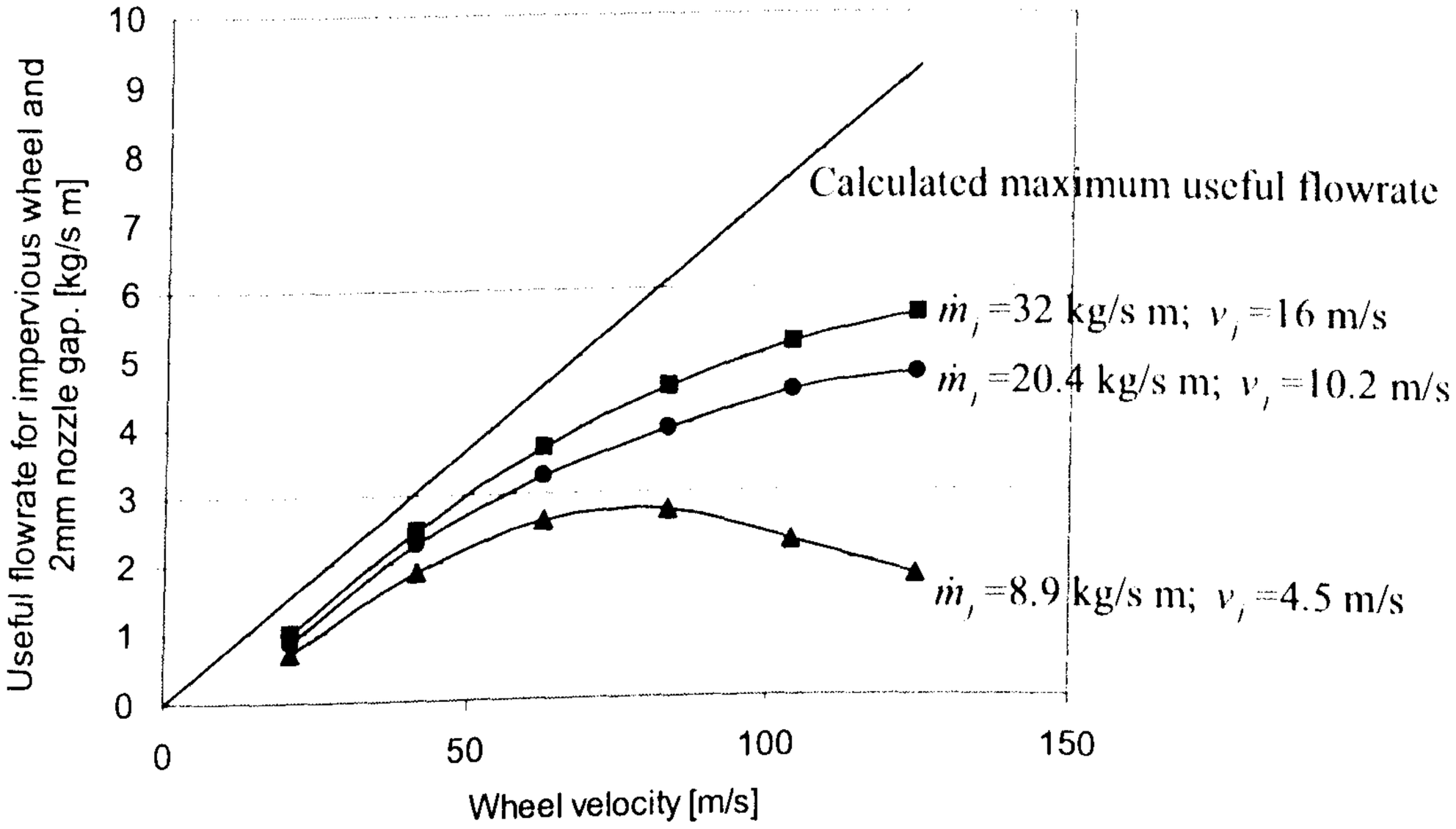

Figure 24. Measured and calculated maximum useful flowrates for the impervious disc with a 2mm gap nozzle *(Line of best fit)*.

Although maximum useful flowrate was achieved for this nozzle, the gap in the wheel workpiece interface still was not completely filled with grinding fluid. This suggests there is always possibility for the air interfering and mixing with the grinding fluid by creating a two-phase fluid.

5.2.2 Useful flowrate for a porous vitrified CBN grinding wheel.

Similar experiments to those on the impervious wheel were conducted for the porous CBN wheel. The same nozzles were employed at the same jet flowrates, jet velocities and jet powers, which are shown in Table 8. With the porous wheel, it was not possible to calculate a maximum theoretical useful flowrate, since the fluid could penetrate deeper into the wheel body. Instead, optimum useful flowrate was calculated assuming the condition at which only the surface pores were filled with fluid. Surface porosity was determined by scanning the wheel peripheral surface as previously described. The ratio of useful flowrate to jet flowrate for a porous CBN wheel is shown in Figure 25. Compared with the results for the impervious wheel, the utilisation ratio for the porous

wheel is more sensitive to wheelspeed at low jet flowrate and high wheel speed. As argued previously, this is consistent with the disruptive effect of airflow. However, the utilisation ratio for the porous wheel becomes higher than for the impervious wheel as jet flowrate increases. This can be seen by comparing Figure 19 with Figure 25.

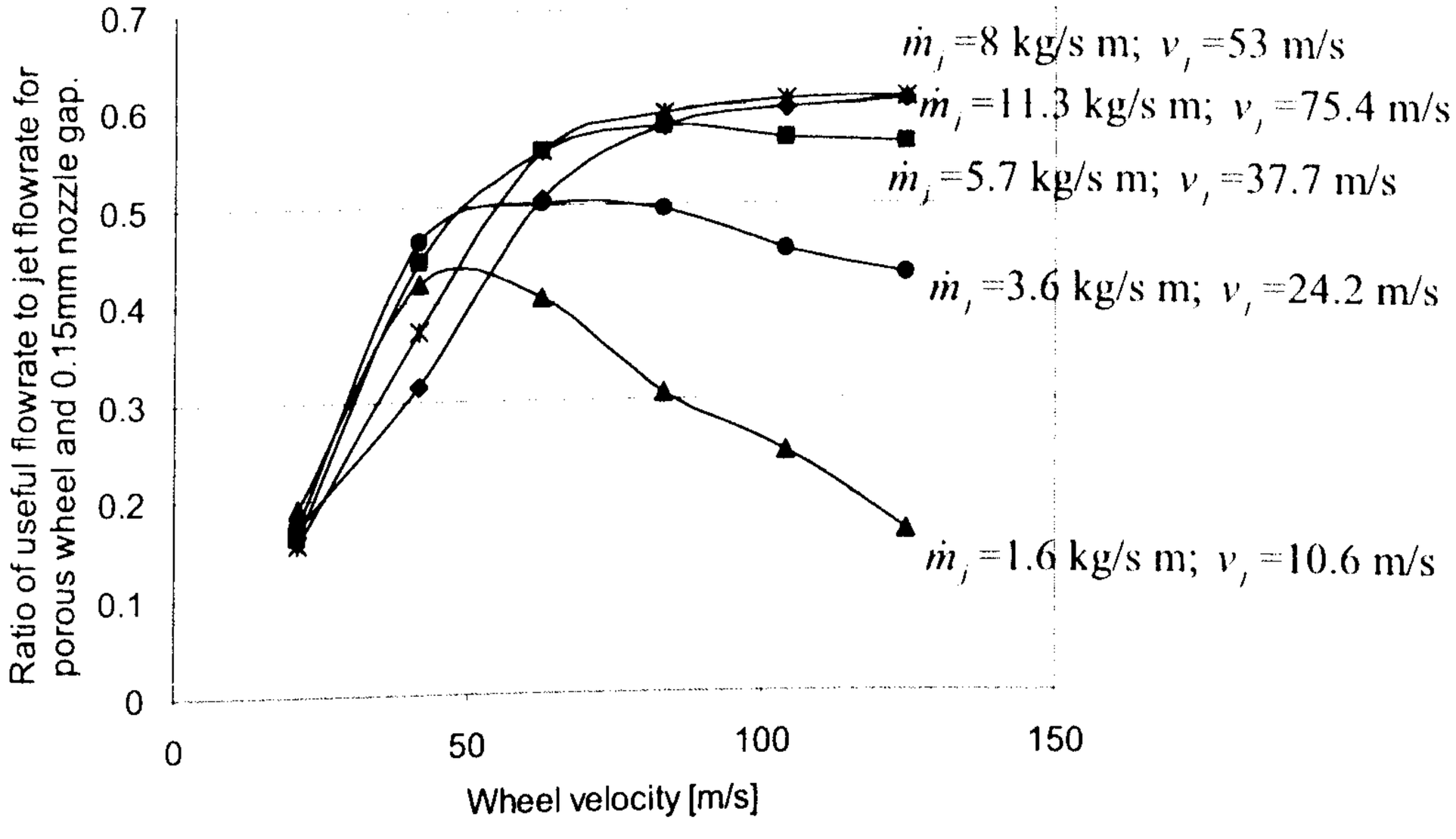

Figure 25. Ratio of useful flowrate to nozzle jet flowrate for a porous CBN grinding wheel with a 0.15mm gap nozzle *(Line of best fit)*.

Accordingly, useful flowrate for a porous wheel is lower than for an impervious wheel at lower jet flowrate. Conversely, useful flowrate for a porous wheel is higher than for an impervious wheel at higher jet flowrate. This also can be seen by comparing Figure 20 with Figure 26. Low useful flowrate for the low jet flowrate with a porous wheel can be explained by the easier access of air to displace the grinding fluid, since there is more space available in the wheel sub-surface due to the wheel pores. On the other hand, a porous wheel has a higher potential to carry fluid within its pores, which results in increased useful flowrate for the higher jet flowrate.

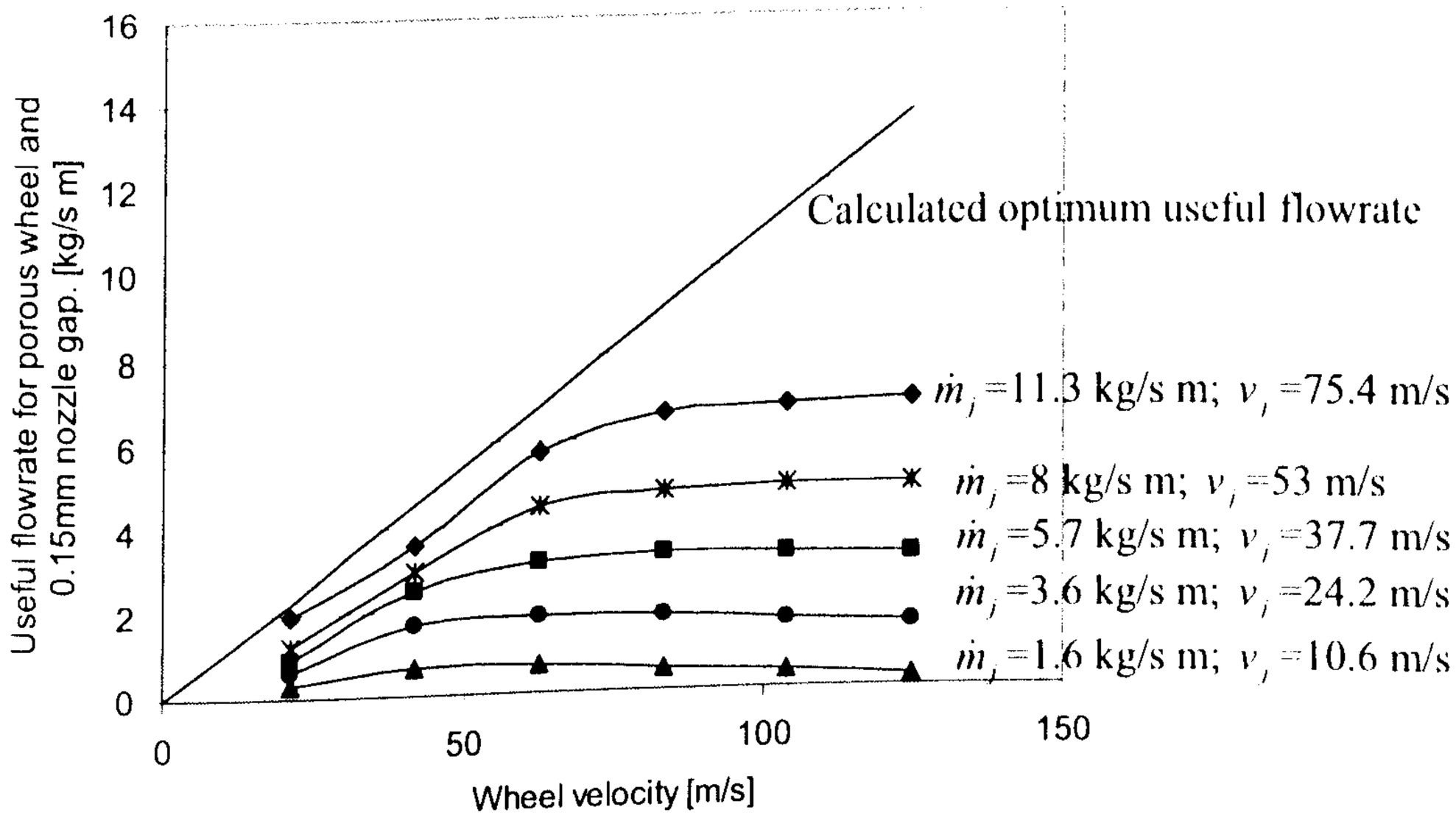

Figure 26. Measured and calculated optimum useful flowrates for a porous CBN grinding wheel with a 0.15mm gap nozzle *(Line of best fit)*.

Figure 27 shows results for utilisation ratio for a nozzle with a 0.4mm gap. This nozzle also gives a low ratio at lower jet flowrate and high wheel speed, but a higher ratio at high jet flowrate and high wheel speed. Due to the higher flowrate and ability of a porous wheel to contain more fluid, the ratio for this nozzle tends to be higher than the ratio for the previous nozzle especially at higher jet flowrate using the same porous wheel. The breaks in the graphs are due to the limitations of the grinding machine and measuring devices.

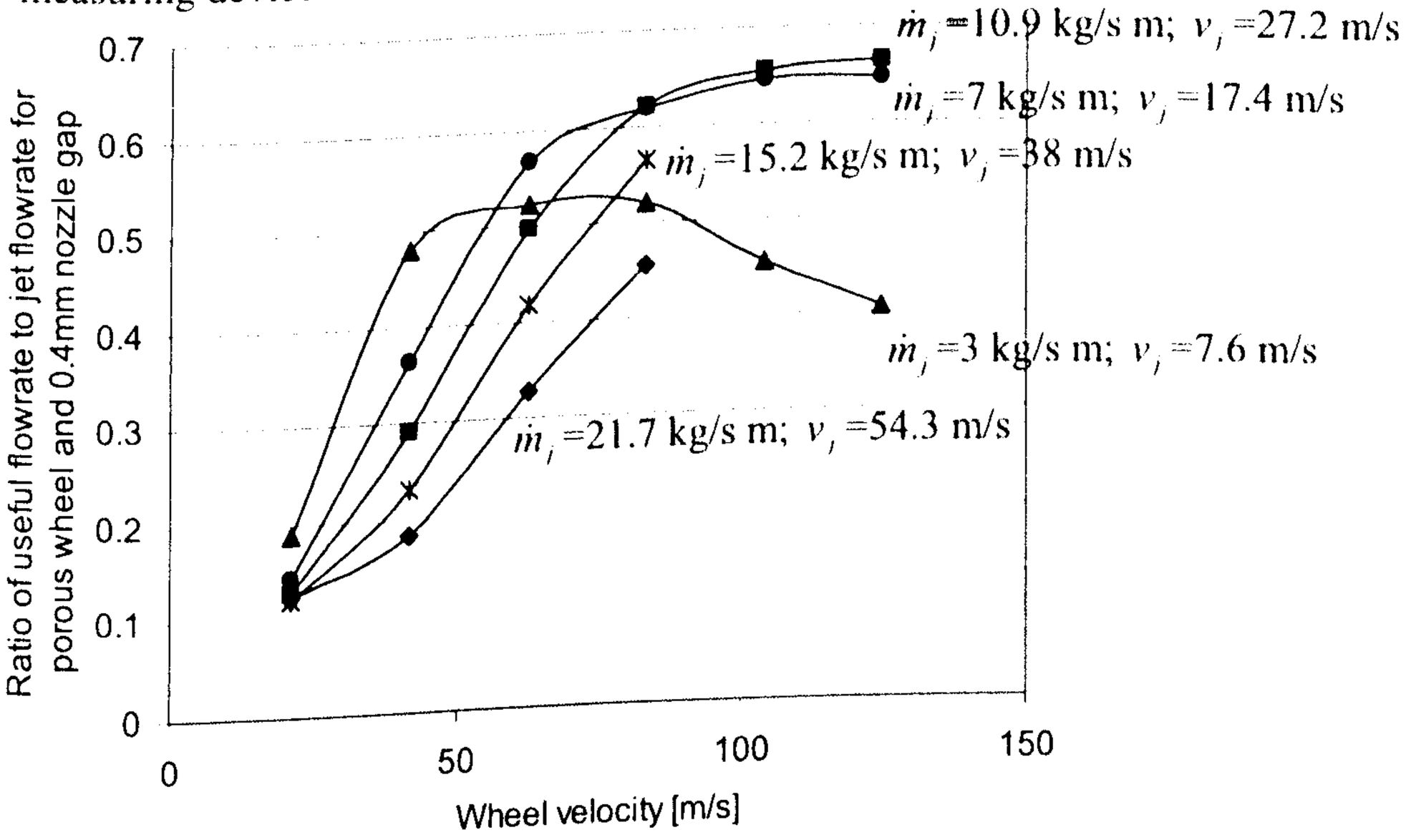

Figure 27. Ratio of useful flowrate to jet flowrate for a porous CBN grinding wheel with a 0.4mm gap nozzle *(Line of best fit)*.

The ability of a porous wheel to transport more fluid through the grinding zone is confirmed in Figure 28. It can be seen that the useful flowrate is actually higher than the assumed optimum flowrate. This means that the grinding fluid has penetrated deeper into the wheel than the depth of the surface pores.

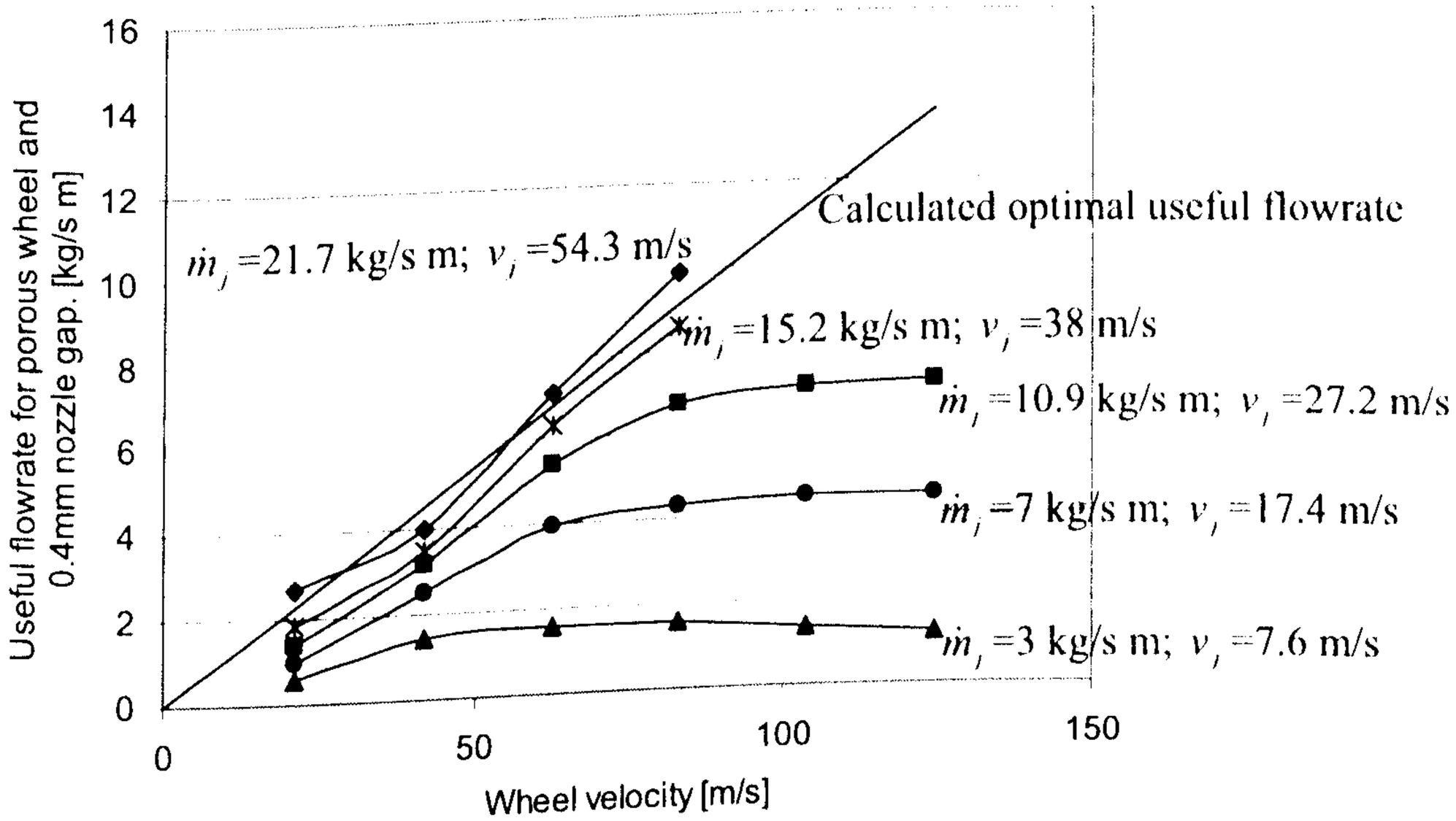

Figure 28. Measured and calculated optimum useful flowrates for a porous CBN grinding wheel with a 0.4mm gap nozzle *(Line of best fit)*.

As expected, a nozzle with a 2mm gap gave the lowest utilisation ratio as shown in Figure 29. As with the impervious wheel, the utilisation ratio dropped after the transition wheel speed was reached. This occurs with a low jet velocity in spite of a high jet flowrate. However, the 2 mm nozzle with the porous wheel gave a higher utilisation ratio than with the impervious wheel.

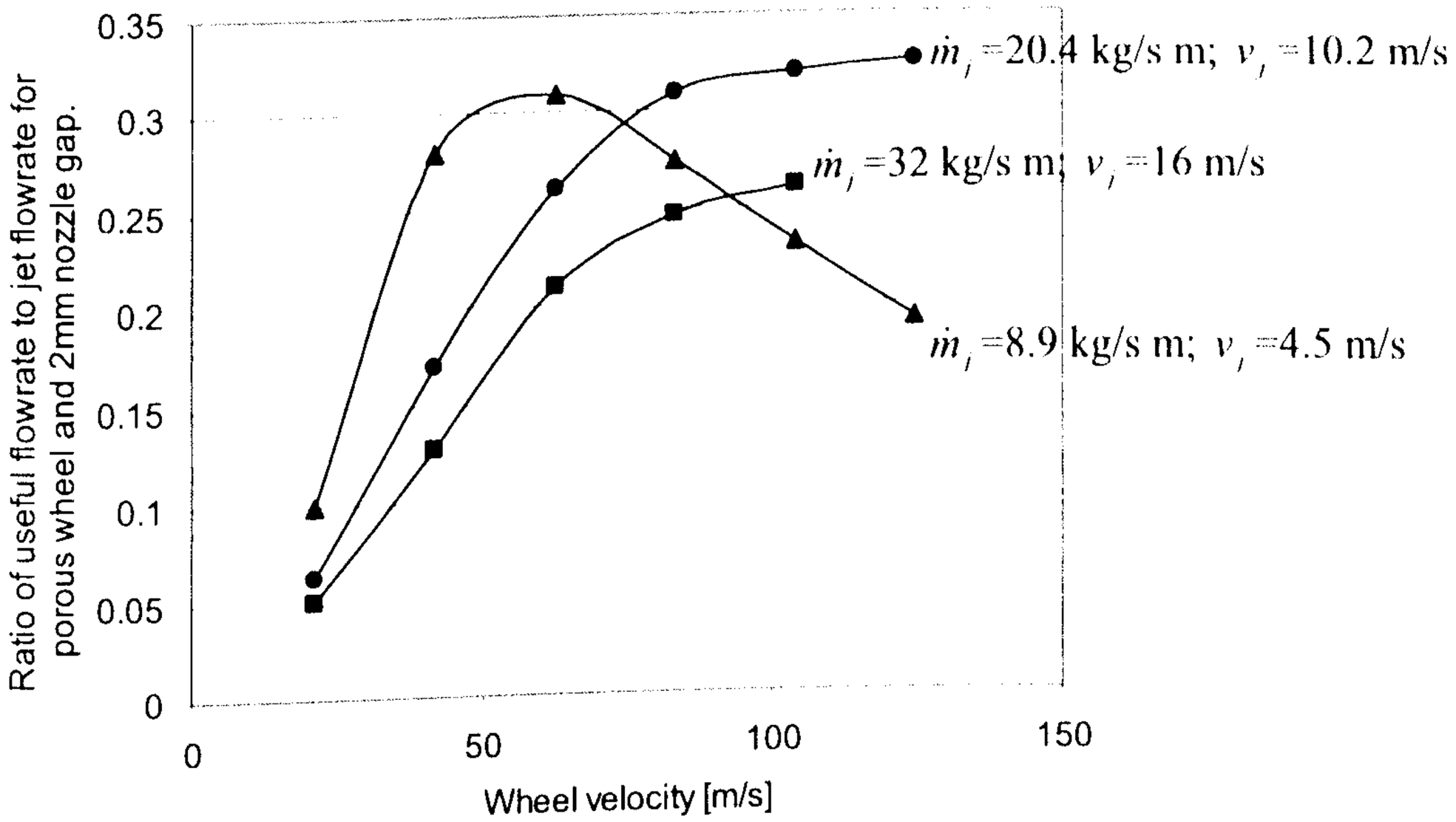

Figure 29. Ratio of useful flowrate to delivery jet flowrate for the porous CBN grinding wheel with a 2mm gap nozzle *(Line of best fit)*.

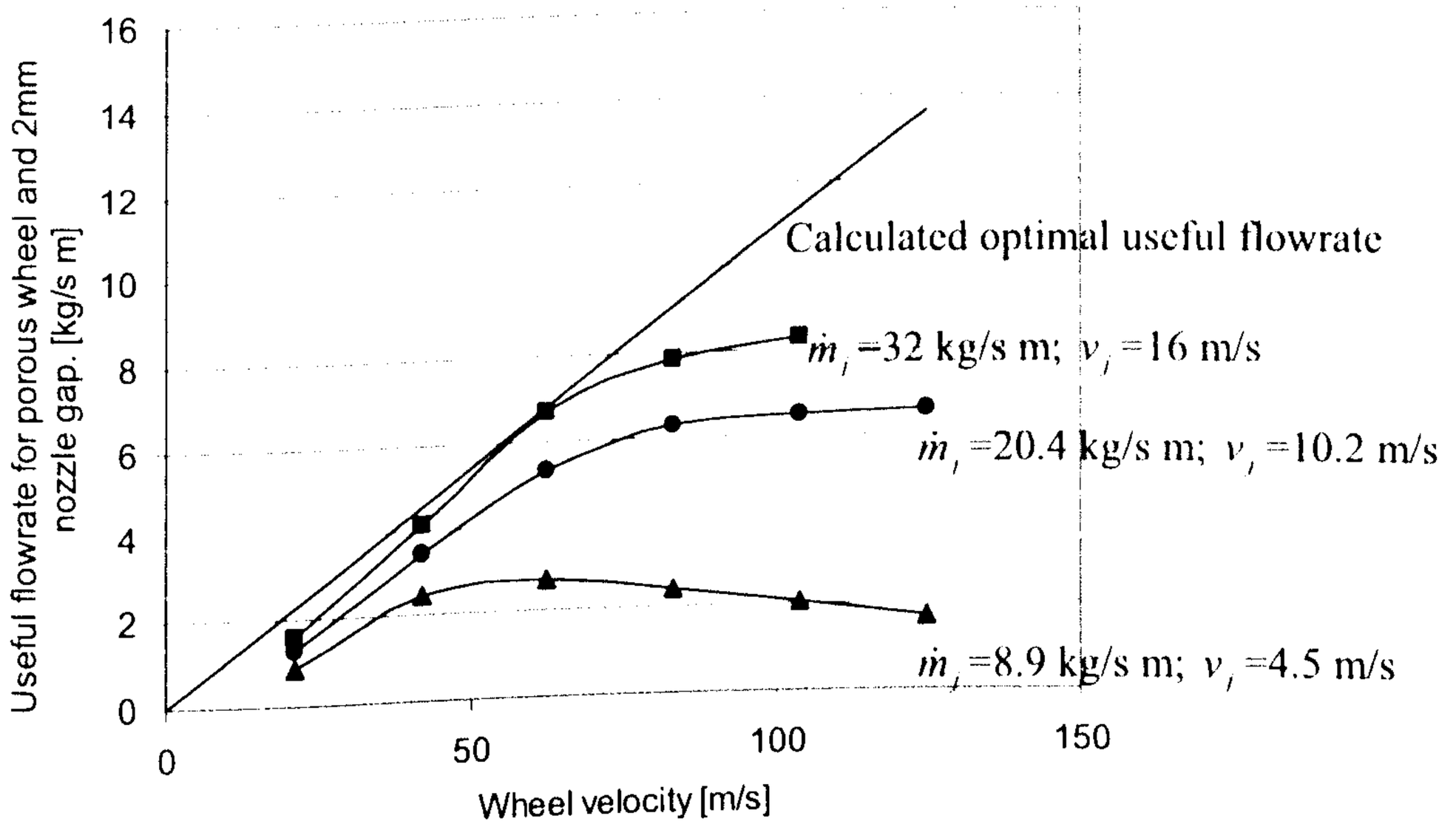

Figure 30. Measured and calculated optimum useful flowrates for the porous CBN grinding wheel with a 2mm gap nozzle *(Line of best fit)*.

The maximum useful flowrate in Figure 30 resulted when the largest jet flowrate was applied to the porous wheel. This is the advantage of the porous wheel compared to an impervious wheel in its ability to carry more grinding fluid.

Generally, the selection of nozzle jet velocity and jet flowrate depend on the particular grinding conditions and requirements. If economy plays a dominant role then a nozzle with a small gap may be necessary to achieve a reasonable velocity at low flowrate. If a high quantity of useful flowrate is required in order to prevent workpiece damage due to high contact temperature, than the nozzle gap size needs to be increased. Higher jet flowrate can also be achieved from a nozzle with a smaller gap size. However, high flowrate for a smaller gap will result in very high jet velocity. This may cause significant increase of nozzle power consumption and misting of the environment. Useful flowrate can also be increased by employing a high-porosity wheel. High-porosity wheels are able to carry larger volumes of fluid due to bulk penetration. However excessive penetration of grinding fluid deeper than the surface pores may not be useful for the process even if the fluid is transported through the grinding zone. This is because grinding fluid carried deeper than the wheel pores are unlikely to have sufficient access to the workpiece surface to provide efficient cooling and lubrication [37].

5.3 Useful Flowrate and Contact Pressure in the Wheel-Workpiece Interface.

An important parameter affecting useful flowrate is the contact pressure in the wheel-workpiece interface. Due to contact pressure, fluid can penetrate into the wheel resulting in increase of useful flowrate. On the other hand contact pressure tends to reject fluid from the grinding zone, resulting in reduced utilisation ratio. The magnitude of the contact pressure depends on various parameters of the grinding operation as discussed in Chapter 3.

Experiments were conducted to validate the theoretical relationships between the contact pressure, useful flowrate, jet flowrate, jet velocity, wheel peripheral velocity and wheel type.

5.3.1 Contact pressure and useful flowrate for the impervious knurled disc using nozzles of various gap sizes.

Contact pressure for the impervious wheel was measured for the range of jet flowrates versus wheel velocity shown in Figure 31. Although the pressure varies along the contact area between the wheel and the workpiece, only the maximum pressure is given. The maximum fluid pressure occurred at the beginning of the contact zone of the wheel and the workpiece.

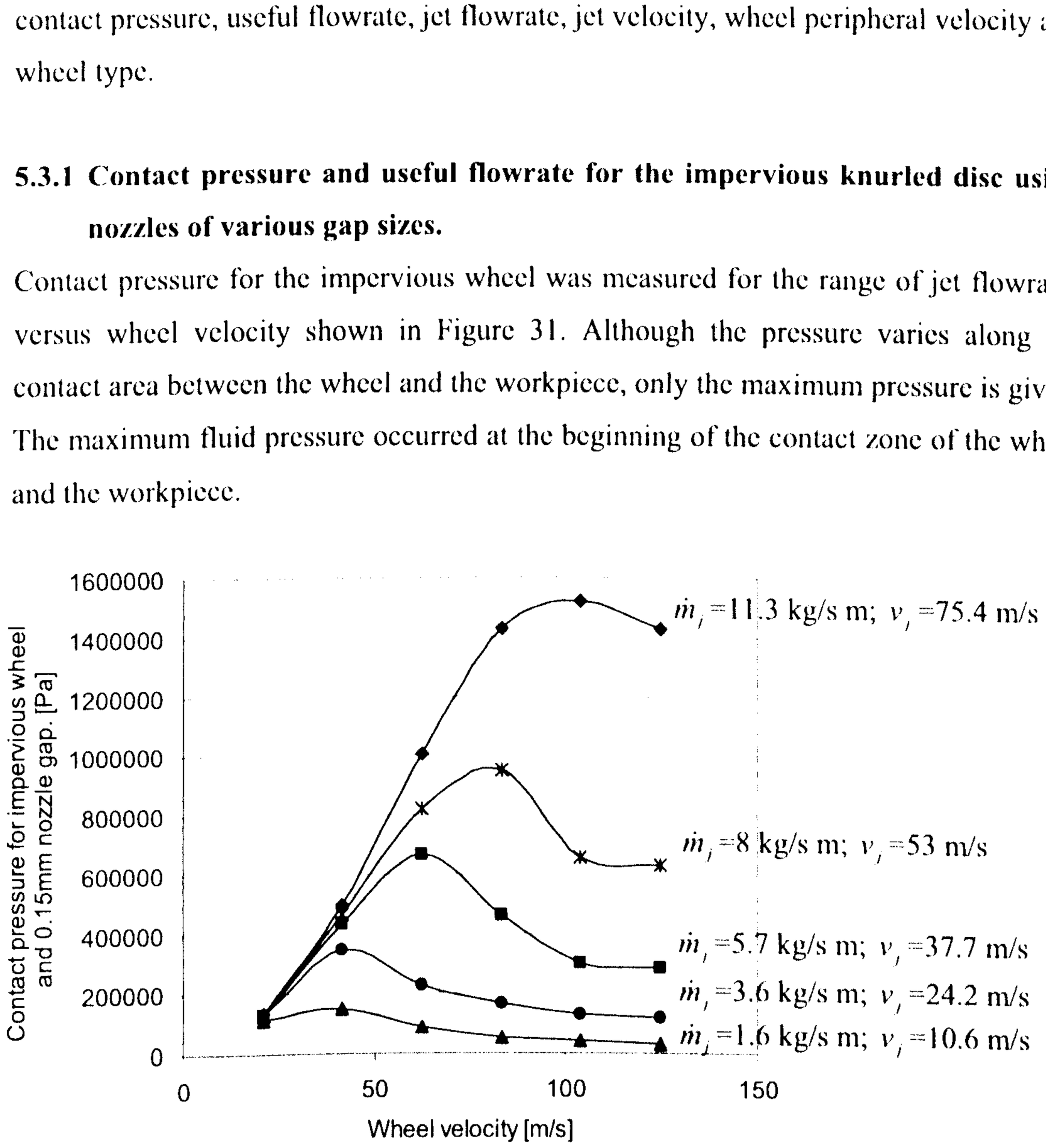

Figure 31. Contact pressure for the impervious disc with a 0.15mm gap nozzle *(Line of best fit).*

It can be seen that the larger jet flowrate gave higher contact pressure. Increase in wheel speed results in increased hydrodynamic contact pressure, since the wheel drags more fluid into the converging gap. Consequently, the fluid builds up more pressure in the converging gap just before the contact zone. However, with further increase of the wheel speed, pressure drops after reaching the maximum and then tends to level off. The drop in pressure occurs at a lower wheel velocity for a smaller jet flowrate and at a higher wheel velocity for a larger jet flowrate. This occurs because the wheel pumps the fluid through the grinding zone faster than it is delivered. Consequently, a starvation effect occurs accompanied by significant reduction in pressure. Support for this argument can be seen from Figure 31 by comparing various jet flowrates. If the grinding fluid is not supplied fast enough, more air is pumped through the contact zone together with the grinding fluid. Compressibility of the air tends to stabilise the pressure for further increase of wheel speed. The level for the stable pressure region varies depending on jet flowrate and jet velocity. Figure 32 shows that the pressure shown in Figure 31 dropped at the same wheel speed as useful flowrate started to fall. Pressure and useful flowrate both depend on jet flowrate and jet velocity. Theoretical useful flowrate calculated from Equation 14 is plotted in Figure 32 together with measured useful flowrate. Measured values of the contact pressure were substituted into Equation 14 for the useful flowrate calculations.

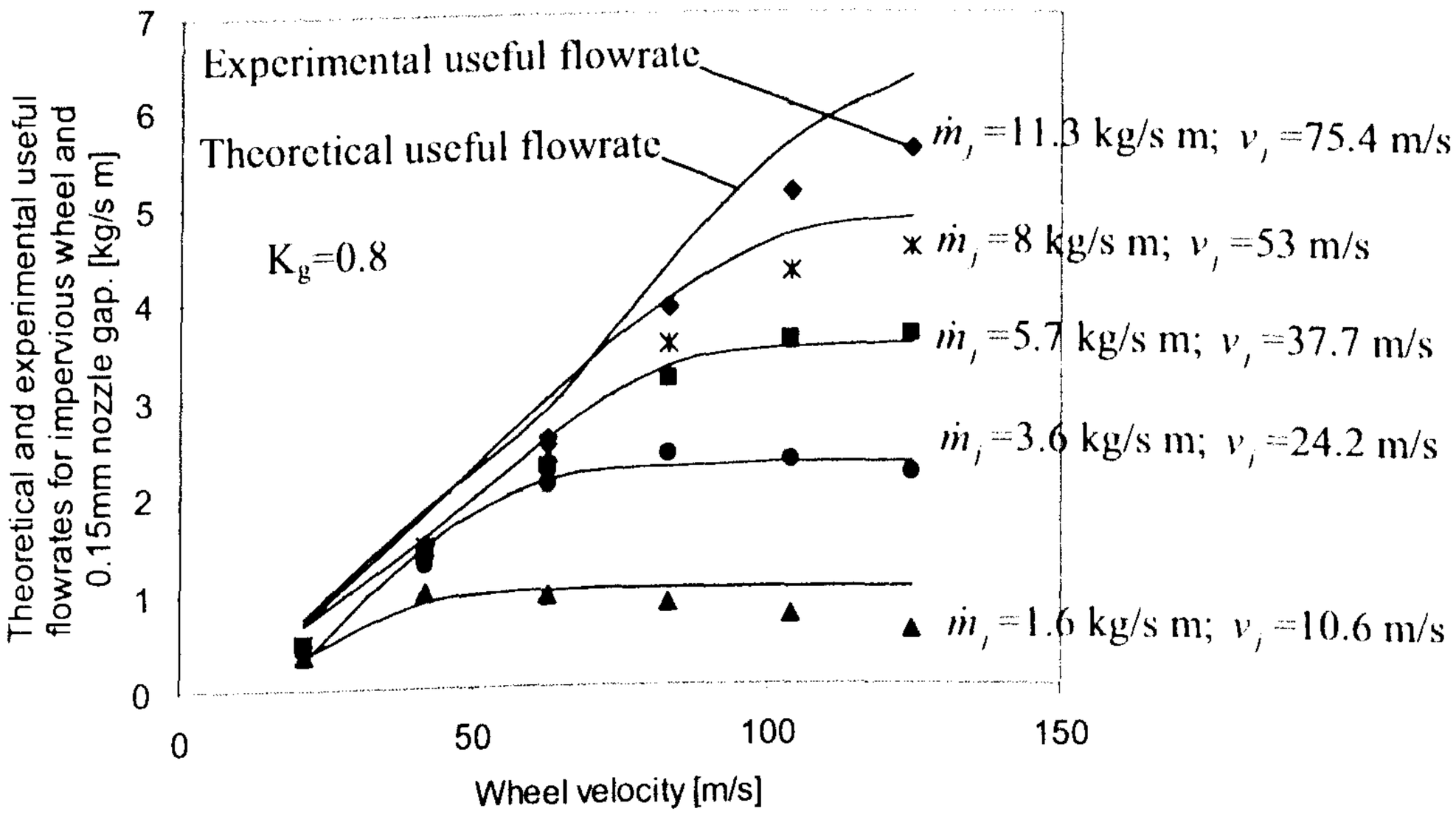

Figure 32. Measured useful flowrates and calculated values based on contact pressure for the impervious disc with a 0.15mm gap nozzle *(Experimental fit)*.

The fluid velocity coefficient K_g required for the model was determined experimentally for all three nozzles and for both the impervious and the porous wheels. The values of the coefficients are listed in Table 9.

K_g	0.15mm nozzle gap	0.4mm nozzle gap	2mm nozzle gap
Impervious wheel	0.8	0.7	0.5
Porous wheel	0.8	0.8	0.55

Table 9. Fluid velocity coefficients in the converging region with impervious and porous wheels for the range of nozzle gap sizes.

Two theoretical useful flowrates are plotted in Figure 33. One calculated from the Equation 14 neglecting air flow and the other from Equation 21 taking air flow into account in the maximum pressure region of the contact zone.

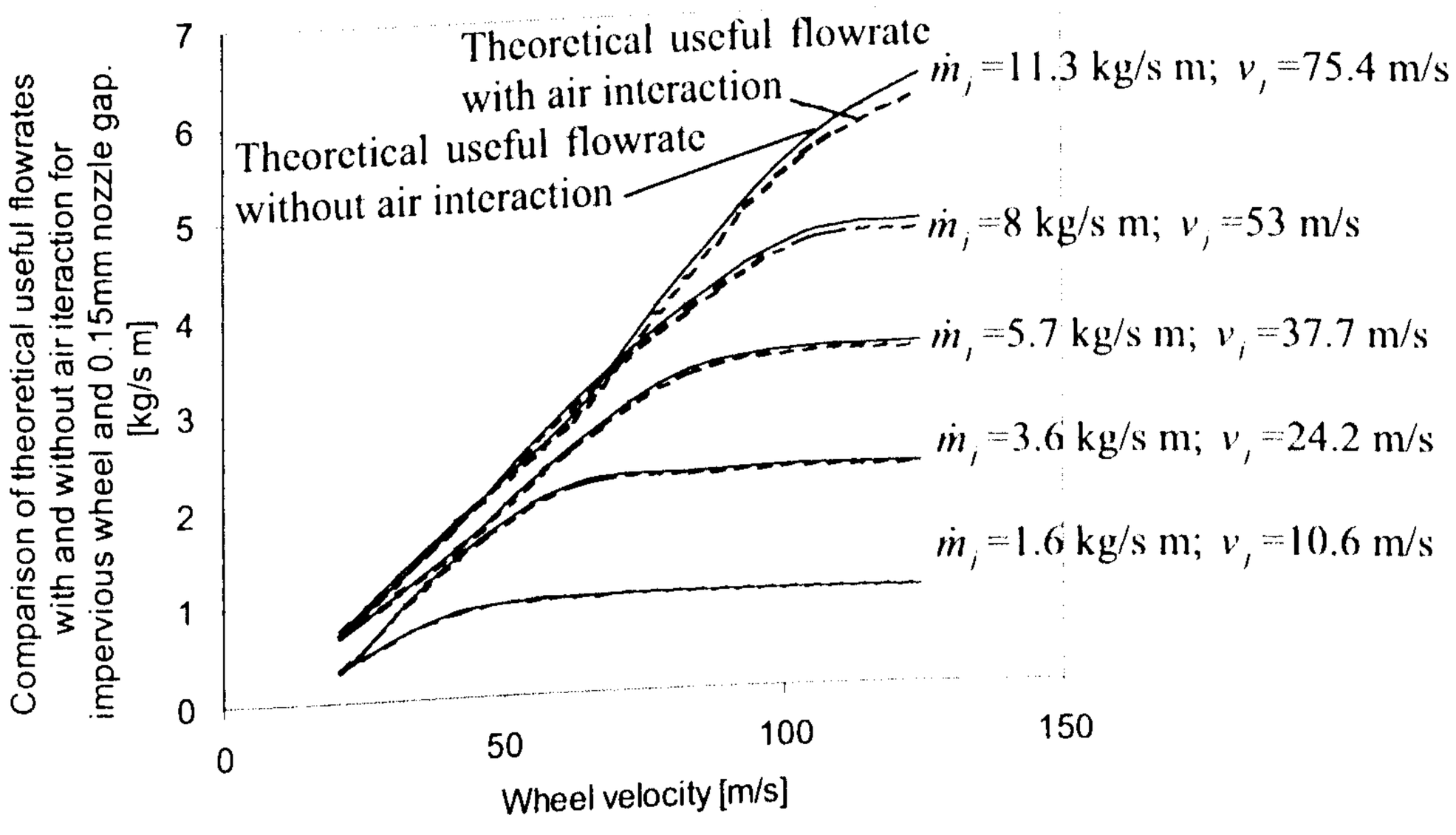

Figure 33. Calculated useful flowrates based on contact pressure with and without air interaction for the impervious disc with a 0.15mm gap nozzle.

The air flowrate was calculated at the point where the maximum pressure occurs taking into account the increased density due to its compressibility. Experimental values of

pressure and useful flowrate were used for the air flowrate calculations from Equation 20. It can be seen from Figure 33 that air after it enters the minimum gap in the contact zone is not able to significantly replace the grinding fluid from the grinding zone even if the air density due to the maximum pressure is increased. However, influence of the air is significant in the converging region due to the mixing with the grinding fluid. The influence of the air on the delivery grinding fluid is shown in Figure 104. From Figure 32, it can be seen that very good agreement between theory and experiment is achieved using the empirical values of the loss coefficient. It is considered that the agreement is sufficiently good to conclude that the useful flowrate model is valid.

In Figure 34 measured values of maximum contact pressure are shown for the nozzle with a 0.4mm gap. A larger gap size as in the previous case gives high flowrate and lower jet velocity for the constant jet power (see Table 8). By comparing Figure 34 with Figure 31 it can be seen that due to the increased jet flowrate the contact pressure is higher for the 0.4mm nozzle than for the 0.15mm nozzle. The drop in pressure also occurs at higher wheel velocity, since more fluid is delivered which allows an extended range for the wheel pumping action.

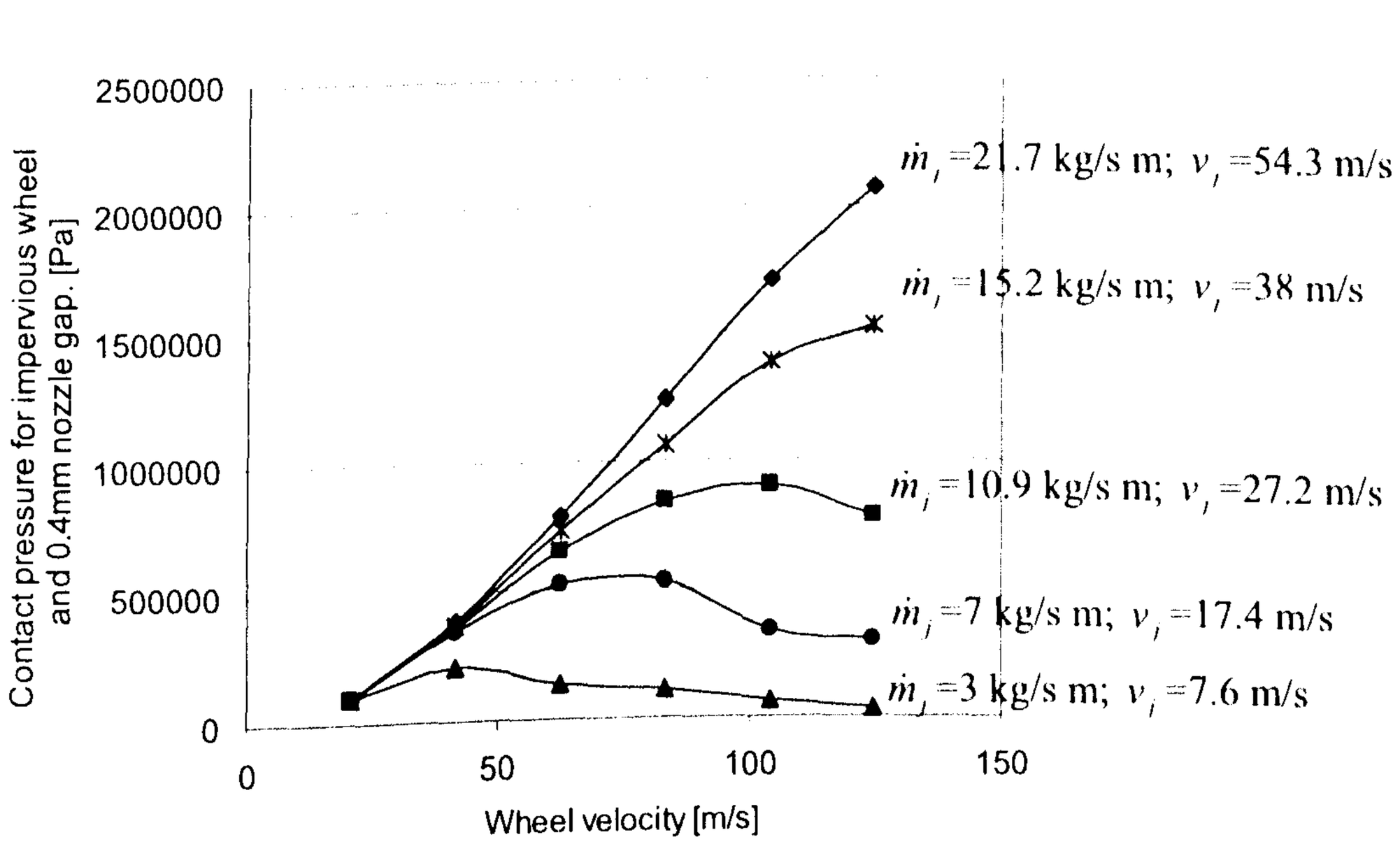

Figure 34. Contact pressure for impervious aluminium disc employing nozzle with 0.4mm gap *(Line of best fit)*.

Theoretical and experimental useful flowrates for a 0.4mm nozzle are plotted in Figure 35. The value of the velocity coefficient is listed in Table 9.

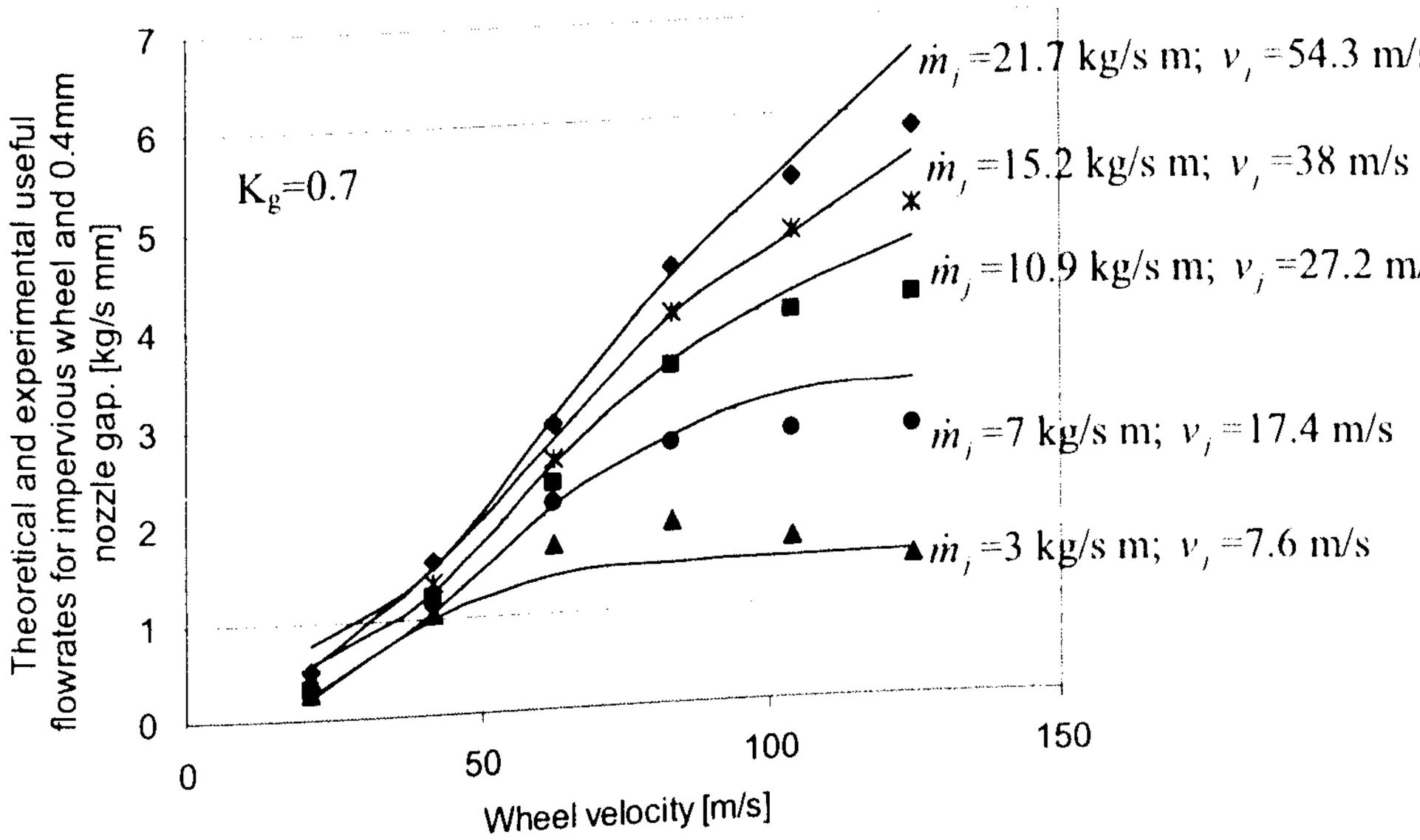

Figure 35. Experimental and theoretical useful flowrates based on contact pressure for the impervious disc with a 0.4mm gap nozzle *(Line of best fit)*.

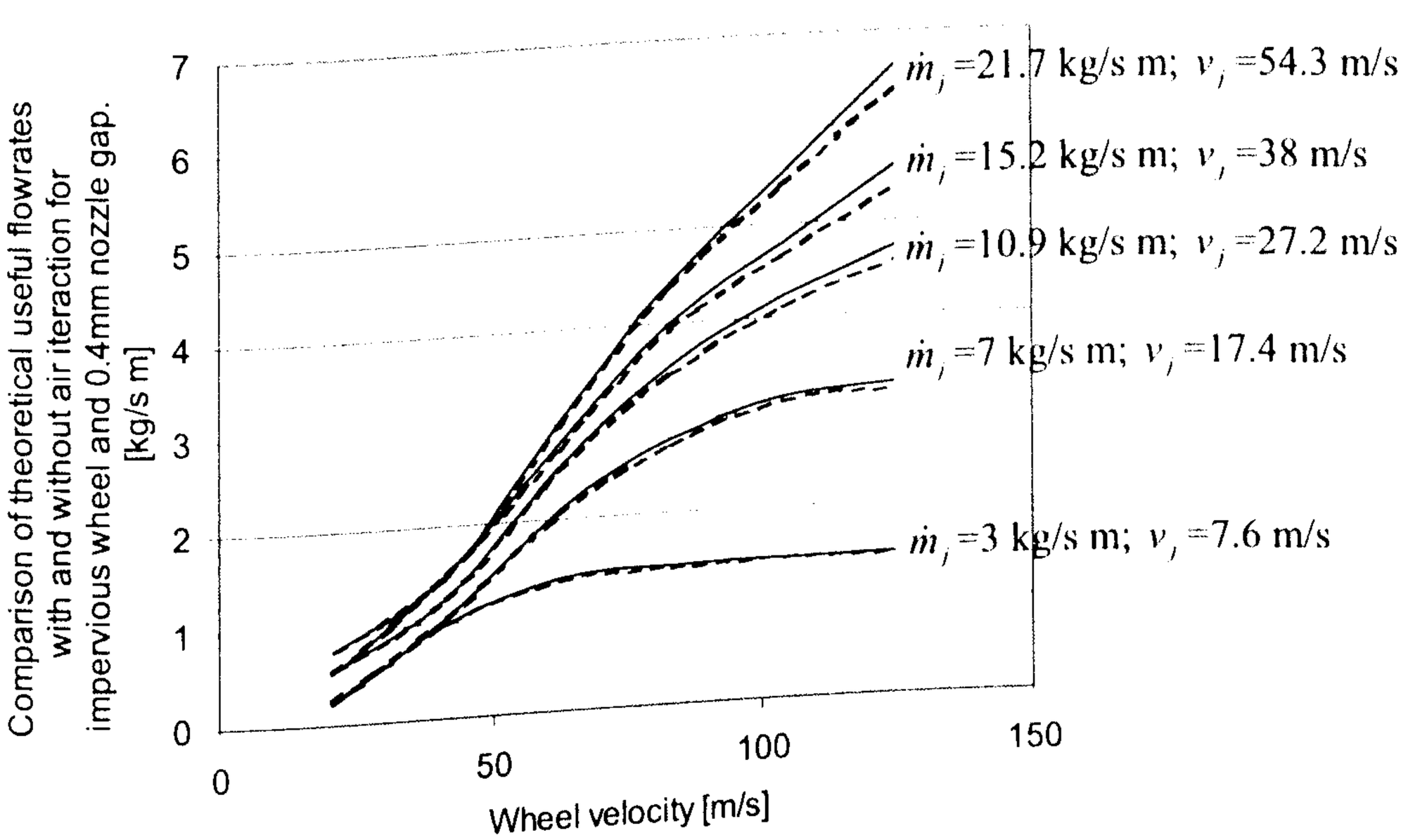

Figure 36. Calculated useful flowrates based on contact pressure with and without air interaction for the impervious disc with a 0.4mm gap nozzle.

For the nozzle with a 0.4mm gap it can be seen from the Figure 36, as previously for the smaller gap, that air mixed with the grinding fluid within the contact zone has negligible ability to replace the grinding fluid.

Maximum experimental contact pressure for the nozzle with a 2mm gap is shown in Figure 37. This nozzle allows highest flowrate but lowest jet velocity. As mentioned previously, the measurements for the higher flowrate were discontinued due to limitations of the measuring equipment and the grinding machine. It can be seen that the largest flowrate for this nozzle results in a peak maximum pressure value at the highest wheel velocity. However, the lowest jet velocity results in lowering the magnitude of the contact pressure in comparison to other nozzles. This confirms that the starvation effect can occur not only due to the low quantity of delivery flowrate, but also due to the speed at which it is delivered.

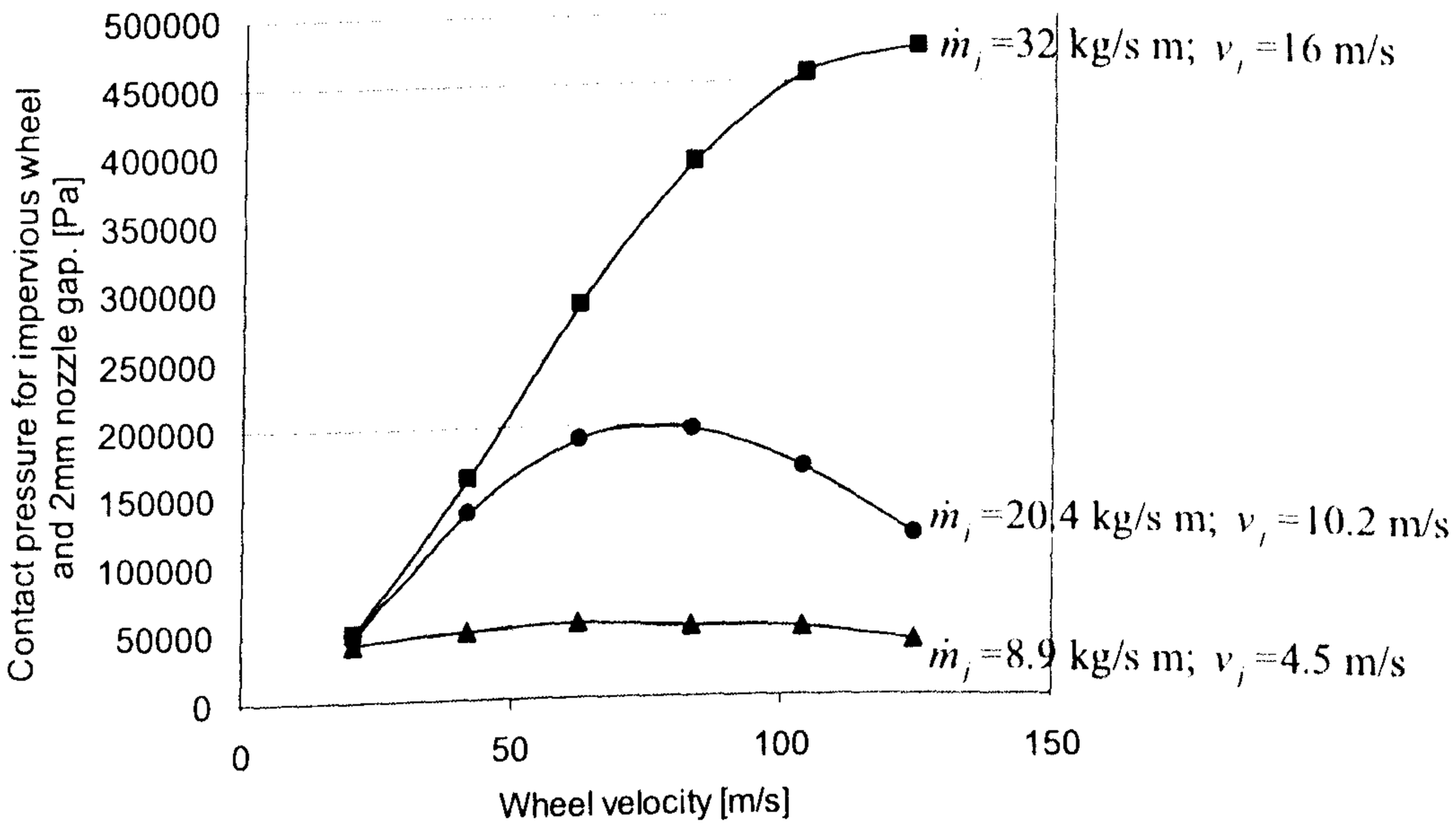

Figure 37. Contact pressure for the impervious disc with a 2mm gap nozzle *(Line of best fit).*

Theoretical useful flowrate was also calculated for the nozzle with a 2mm gap and plotted together with experimentally measured useful flowrate, as shown in Figure 38. The coefficient substituted into the theoretical model for this nozzle with the impervious wheel was chosen from Table 9.

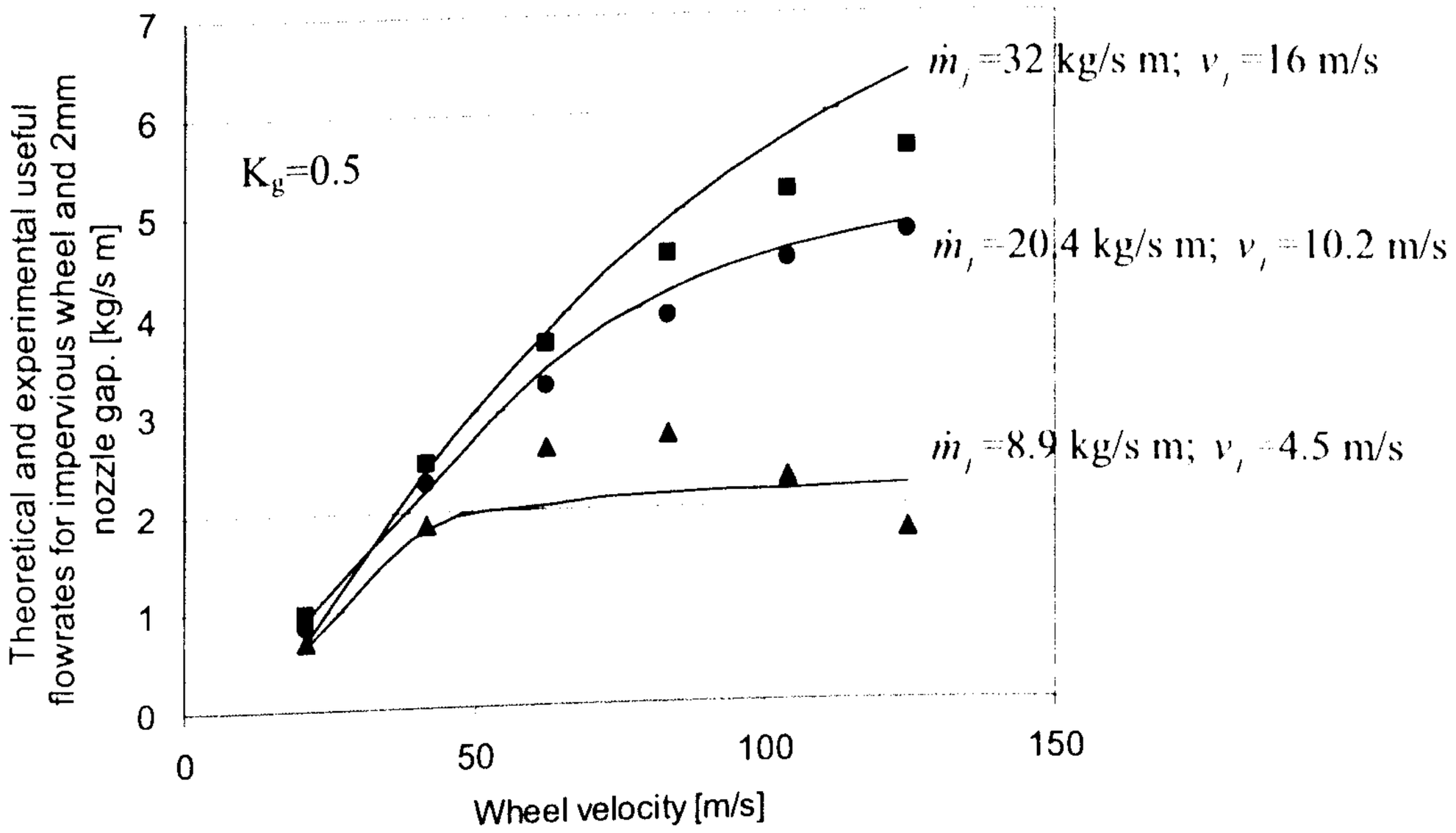

Figure 38. Measured and theoretical useful flowrates based on contact pressure for the impervious disc with a 2mm gap nozzle *(Experimental fit)*.

Theoretical flowrates with and without air flow present in the contact zone are plotted in Figure 39. It can be seen that due to high flowrate air in maximum contact pressure region had virtually no influence on the grinding fluid.

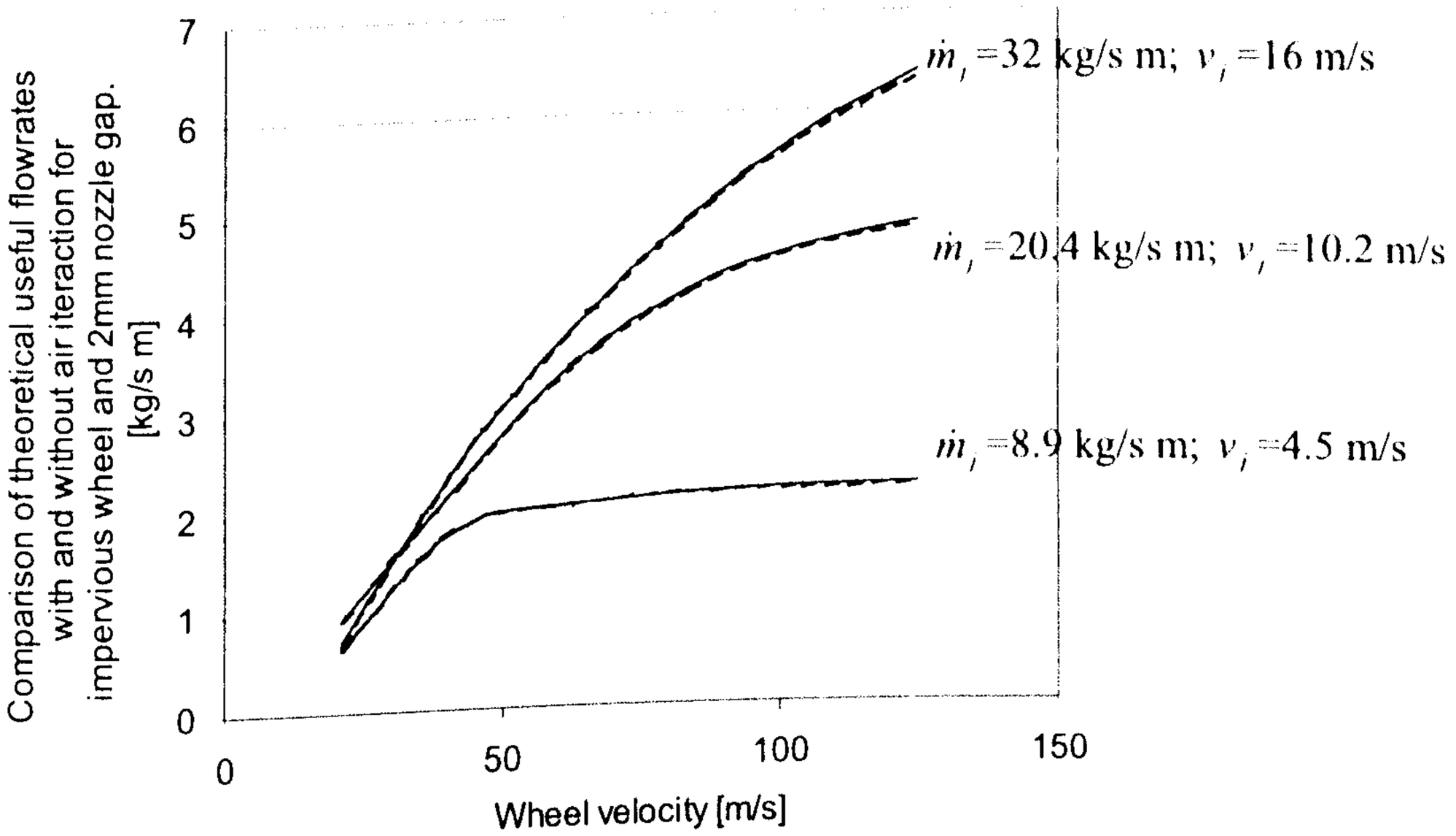

Figure 39. Theoretical useful flowrates based on contact pressure with and without air interaction for the impervious disc with a 2mm gap nozzle.

5.3.2 Contact pressure and useful flowrate for the porous vitrified CBN grinding wheel using various size nozzles .

Experiments were conducted for the CBN porous grinding wheel for all three nozzles. Experimentally measured maximum contact pressure for the porous wheel with a 0.15mm nozzle gap is shown in Figure 40. By comparing Figure 40 with Figure 31 it can be seen that the contact pressure is significantly lower for the porous wheel than for the impervious wheel. The peak pressure for a porous wheel occurs at a lower wheel velocity compared with the case of the impervious wheel. The reason for that is the bulk porosity of the porous wheel, which reduces pressure build up. This is because the fluid penetrates deep into the wheel after it is squeezed into the converging gap. It is an advantage of the porous wheel that it can carry more fluid and at the same time reduce the tendency to develop a high normal force due to the fluid pressure in the contact zone.

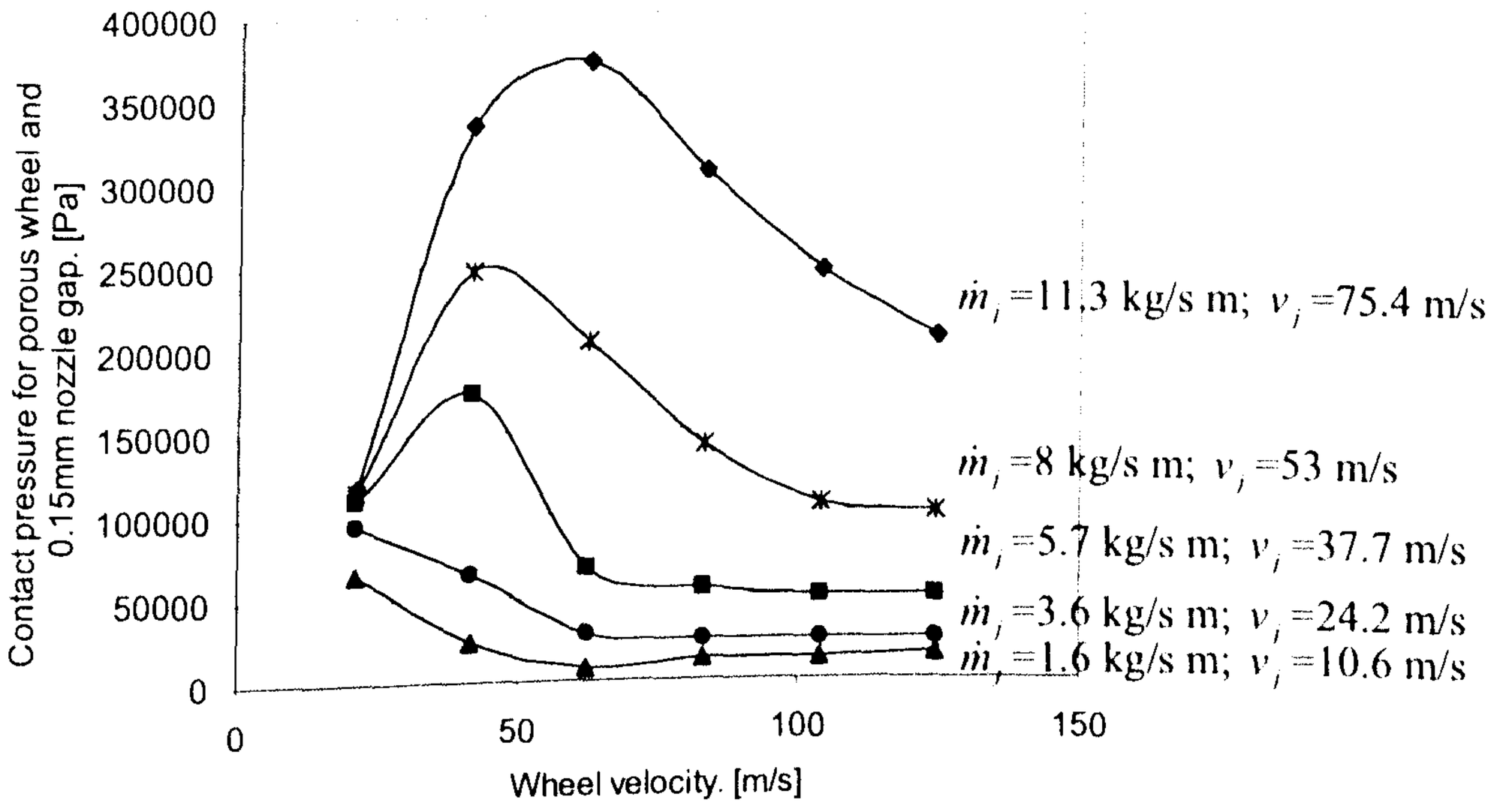

Figure 40. Contact pressure for a porous CBN grinding wheel with a 0.15mm gap nozzle *(Line of best fit)*.

Theoretical useful flowrates from Equation 14 for a porous wheel and a 0.15mm nozzle gap are shown in Figure 41 together with measured useful flowrates. The velocity coefficient K_g used for the calculation is also listed in Table 9. As in the previous cases for the impervious wheel, agreement is qualitatively good particularly at higher jet

flowrates. At low jet flowrates, agreement is not quite as good. It is considered that this may be due to air interfering with the grinding fluid in the converging region.

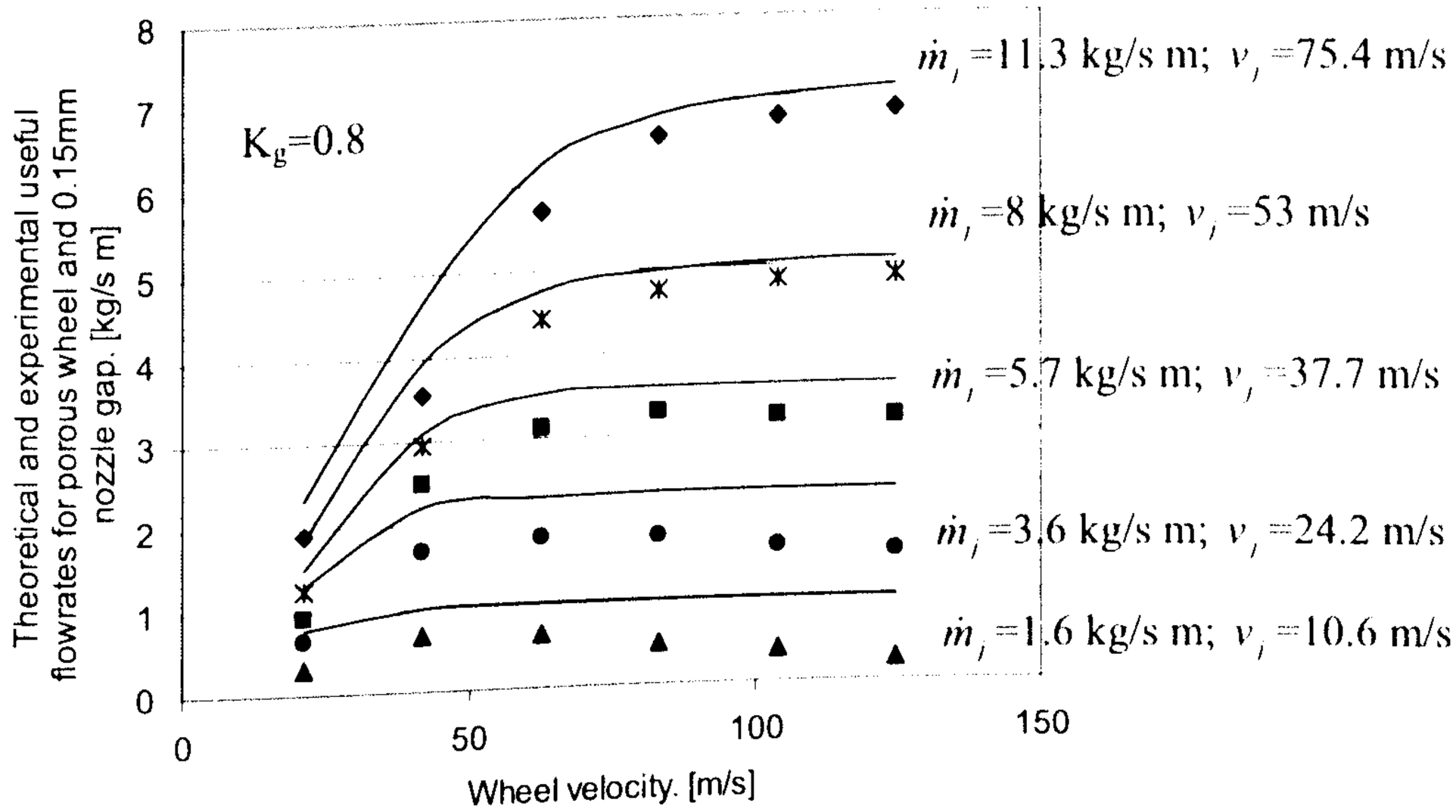

Figure 41. Experimental and theoretical useful flowrates based on contact pressure for a porous CBN grinding wheel with a 0.15mm gap nozzle *(Experimental fit)*.

The air flowrate in the contact zone in the region of maximum pressure was not calculated for the porous wheel since the bulk porosity of the wheel did not allow determination of a boundary for the air flow thickness in the wheel-workpiece contact region. Air flowrate calculations for impervious disc are described for the 0.15mm nozzle. Same method was used for 0.4mm and 2mm nozzles.

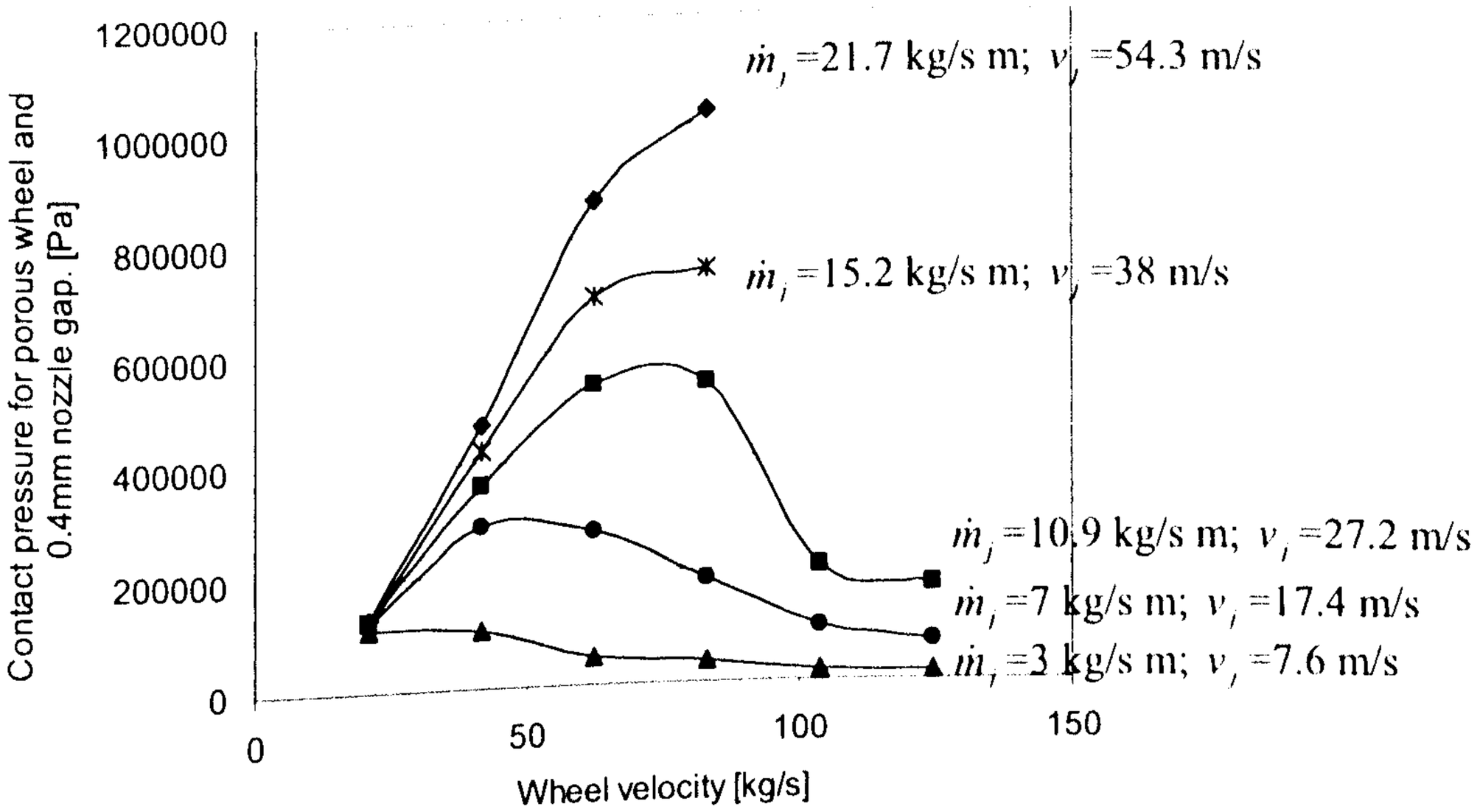

Figure 42. Contact pressure for the porous CBN grinding wheel with a 0.4mm gap nozzle *(Line of best fit)*.

As expected, higher jet flowrate from the 0.4mm nozzle gap results in a higher contact pressure than the 0.15mm nozzle gap for the porous wheel. This is shown in Figure 42. The peak value occurs at a higher wheel velocity with higher jet flowrate.

Theoretical and experimental useful flowrates for 0.4mm nozzle gap are shown in Figure 43.

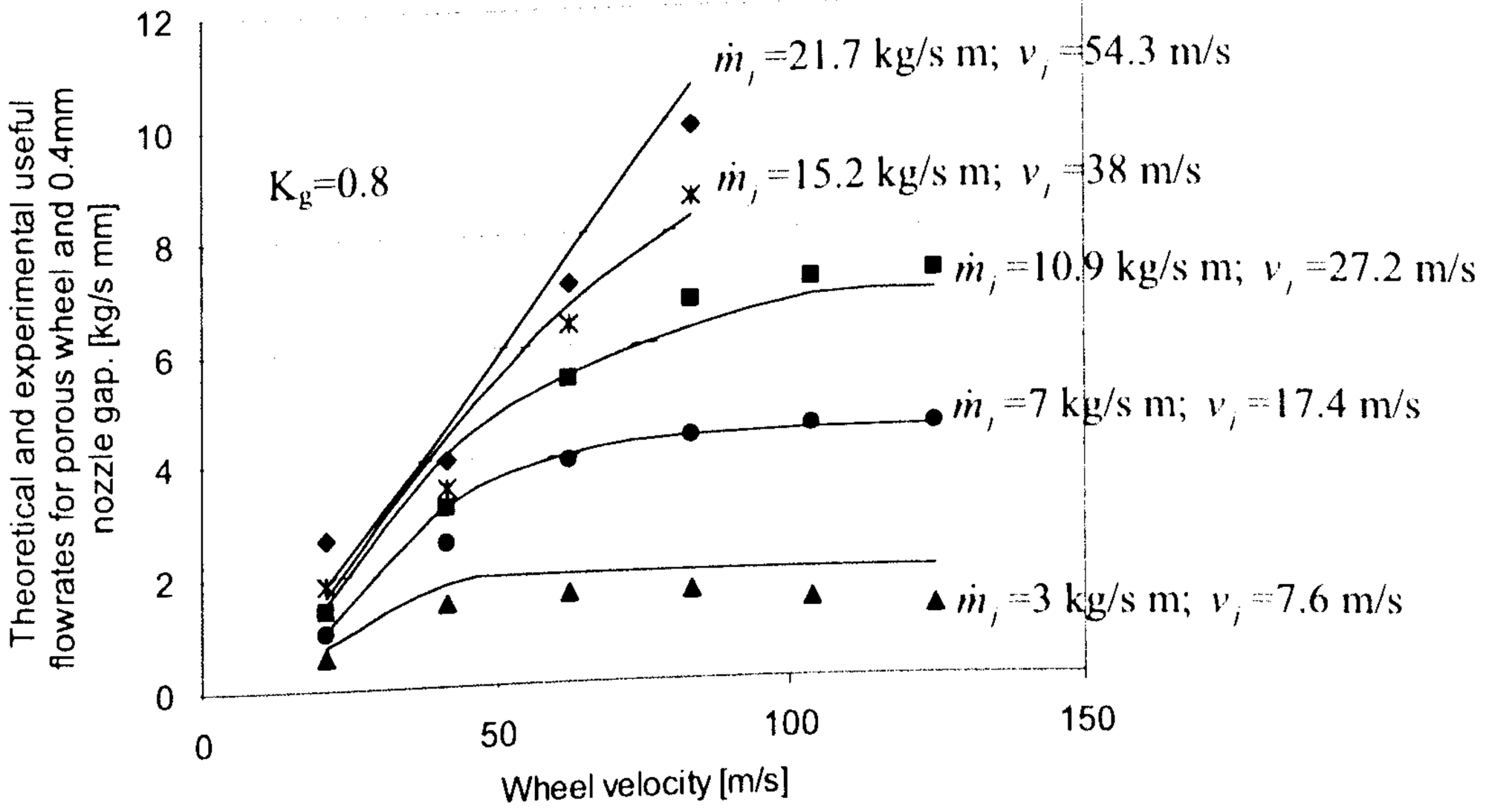

Figure 43. Experimental and theoretical useful flowrates based on contact pressure for a porous CBN grinding wheel with a 0.4mm gap nozzle *(Experimental fit)*.

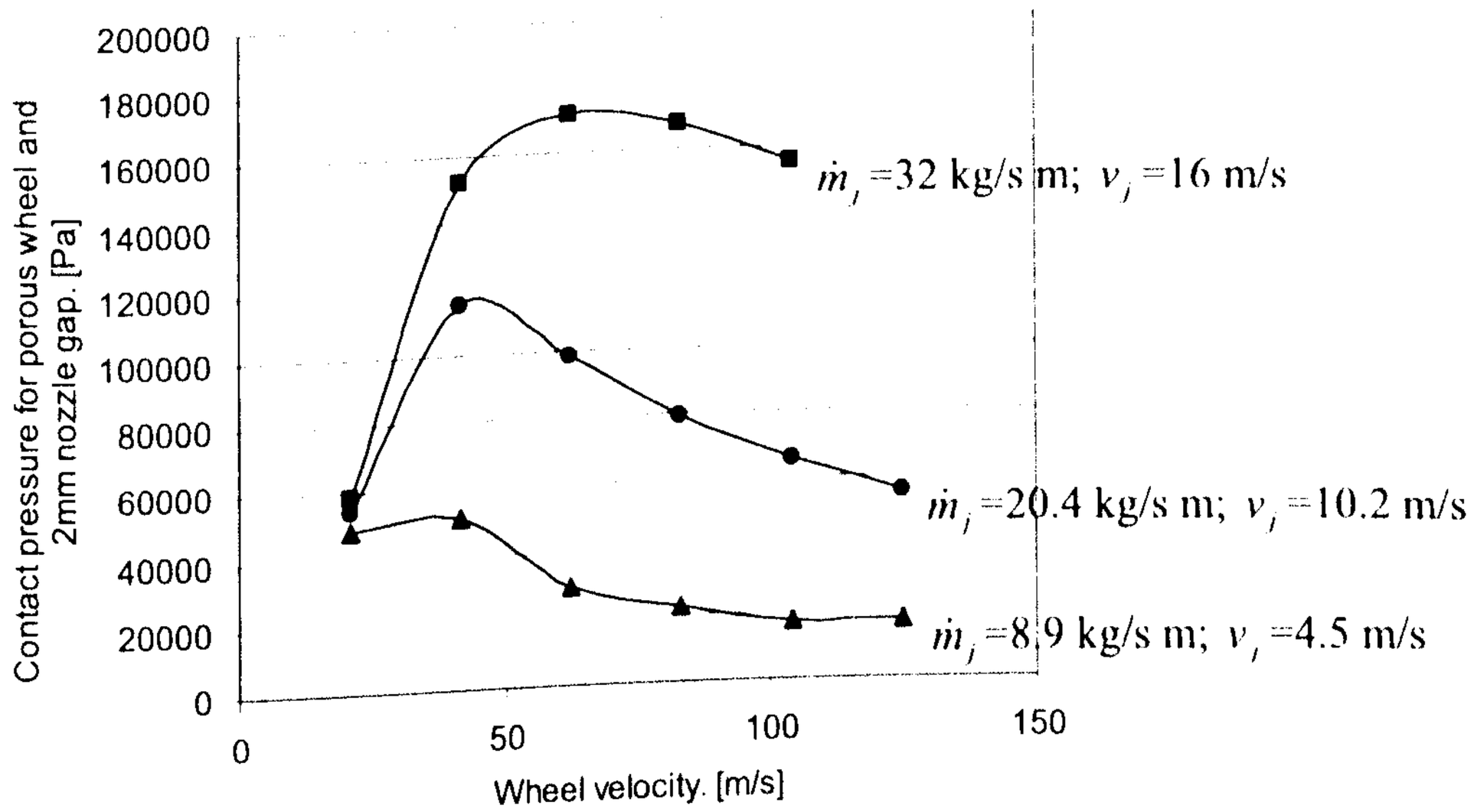

Figure 44. Contact pressure for a porous CBN grinding wheel with a 2mm gap nozzle *(Line of best fit)*.

Experimental contact pressure for a 2mm nozzle gap is shown in Figure 44. Although the jet flowrate was high, lower contact pressures are observed from Figure 42 in comparison with the 0.4mm nozzle gap. As with the impervious wheel this corresponds to the fact that the jet speed is lower than the wheel speed pumping the fluid through the grinding zone, which consequently causes lower contact pressure.

Theoretical useful flowrate for the 2mm nozzle gap and experimentally measured useful flowrate are plotted together in Figure 45.

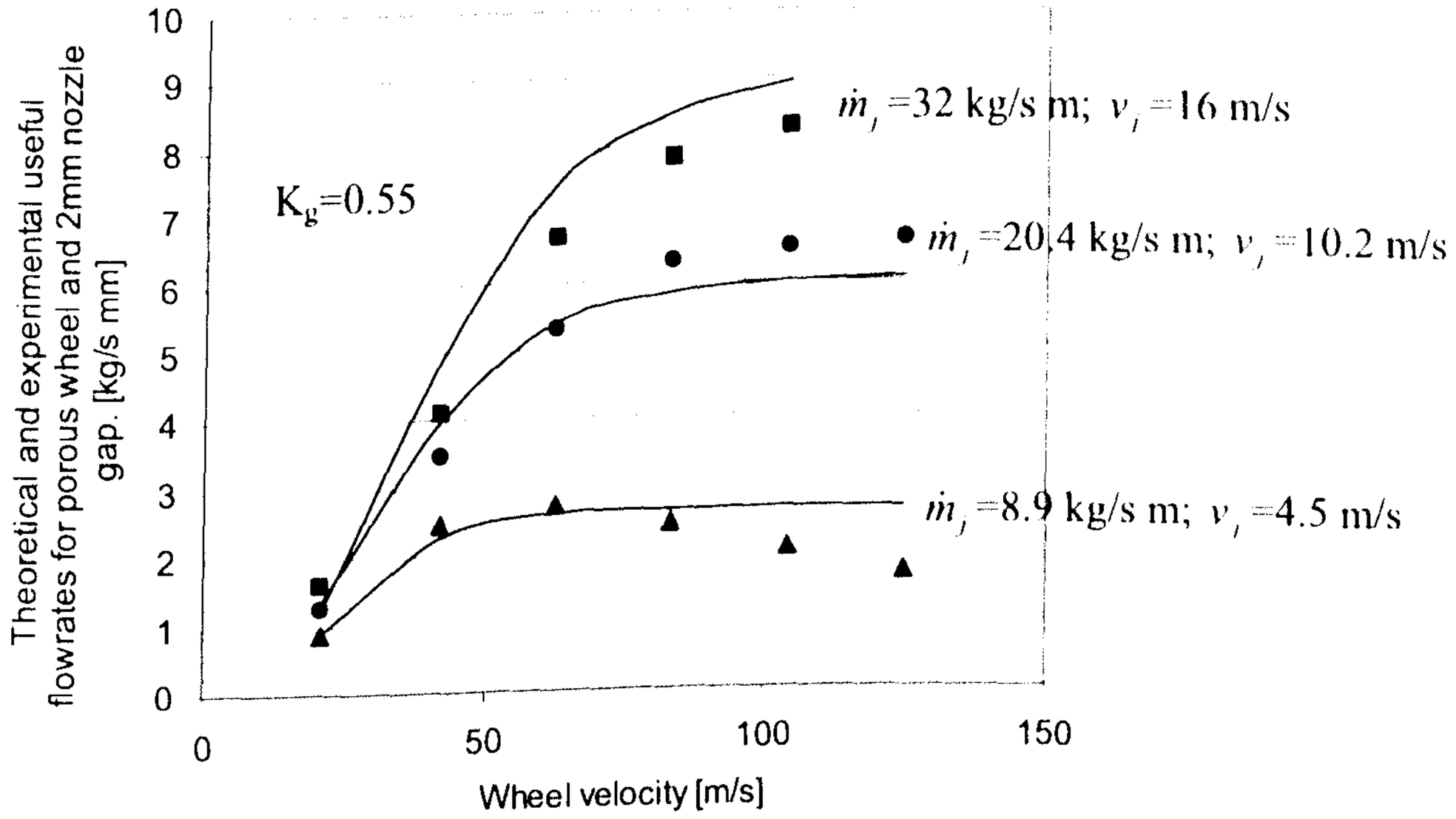

Figure 45. Experimental and theoretical useful flowrates based on contact pressure for a porous CBN grinding wheel with a 2mm gap nozzle *(Experimental fit)*.

Analysing the results, it can be said that the impervious wheel produces higher contact pressure than the porous wheel at the same fluid delivery conditions. In some cases, a high contact pressure can be desirable depending on the particular requirements for the grinding process. In most of cases, it is undesirable due to the additional normal force developed and added to the normal grinding force. The low contact pressure and high useful flowrate for the porous wheel indicates the ability to fill its pores efficiently with grinding fluid. In comparison, an impervious wheel provides only a limited volume for fluid containment within the contact zone. For calculation purposes, the impervious wheel allows the space occupied by the air and the grinding fluid to be estimated. Density of the air is increased in the minimum gap region due to the contact pressure which is equal to the grinding fluid pressure. Taking increased density into account, air

flowrate as shown above was very low, which indicates inability of the air to force the grinding fluid out from the contact region. However, it is apparent that air is present in the grinding gap because of the partial filling of the contact gap by the grinding fluid. This means that air is mixed with the grinding fluid initially, probably due to flow turbulence in the converging region between the wheel and the workpiece. If the converging region is filled with grinding fluid there is less potential for air mixing. An example, is the result for useful flowrate using the 2mm nozzle gap with the impervious wheel. Apparently, this nozzle produced a thicker jet, which better filled the converging region and consequently resulted in maximum fluid film thickness in the contact region.

5.4 Useful Flowrate and Spindle Power Due to the Fluid.

Spindle power consumed by the fluid process is also an important parameter in grinding. As described in the theory, the spindle power to accelerate the grinding fluid is proportional to the flowrate passing through the grinding zone. Inefficiently delivered fluid may cause a high spindle power demand, which increases the total cost of the grinding operation. Experiments were conducted in order to validate the relationships described from theory between spindle power consumed by the fluid, jet velocity, jet flowrate and wheel speed. Three nozzles with different gap sizes were tested for both the impervious wheel and the porous grinding wheel.

5.4.1 Spindle power and useful flowrate for the impervious knurled disc using nozzles of differing gap sizes.

Experimental and theoretical useful flowrates for the impervious wheel employing the nozzle with 0.15mm gap are plotted together in Figure 46. Theoretical useful flowrate is calculated from the Equation 30. The power loss coefficient K_f and the jet velocity loss coefficient K_j necessary for the calculations were determined experimentally and are shown in Table 10. The value of K_f varies between 0.4 and 0.5 across the range of nozzles, the two different wheels and the various flowrates and velocities. This is a reasonably close banding of the power loss coefficient and gives confidence in the nature of the assumptions employed in the modelling. The value of K_j varies between 0.2 and 0.45. This coefficient tends to be slightly lower than the other coefficient. This might be expected given the dispersion losses usually experienced following the exit of fluid from a jet. However, the banding of the values is still close enough to suggest that the modelling approach is the most reasonable way forward.

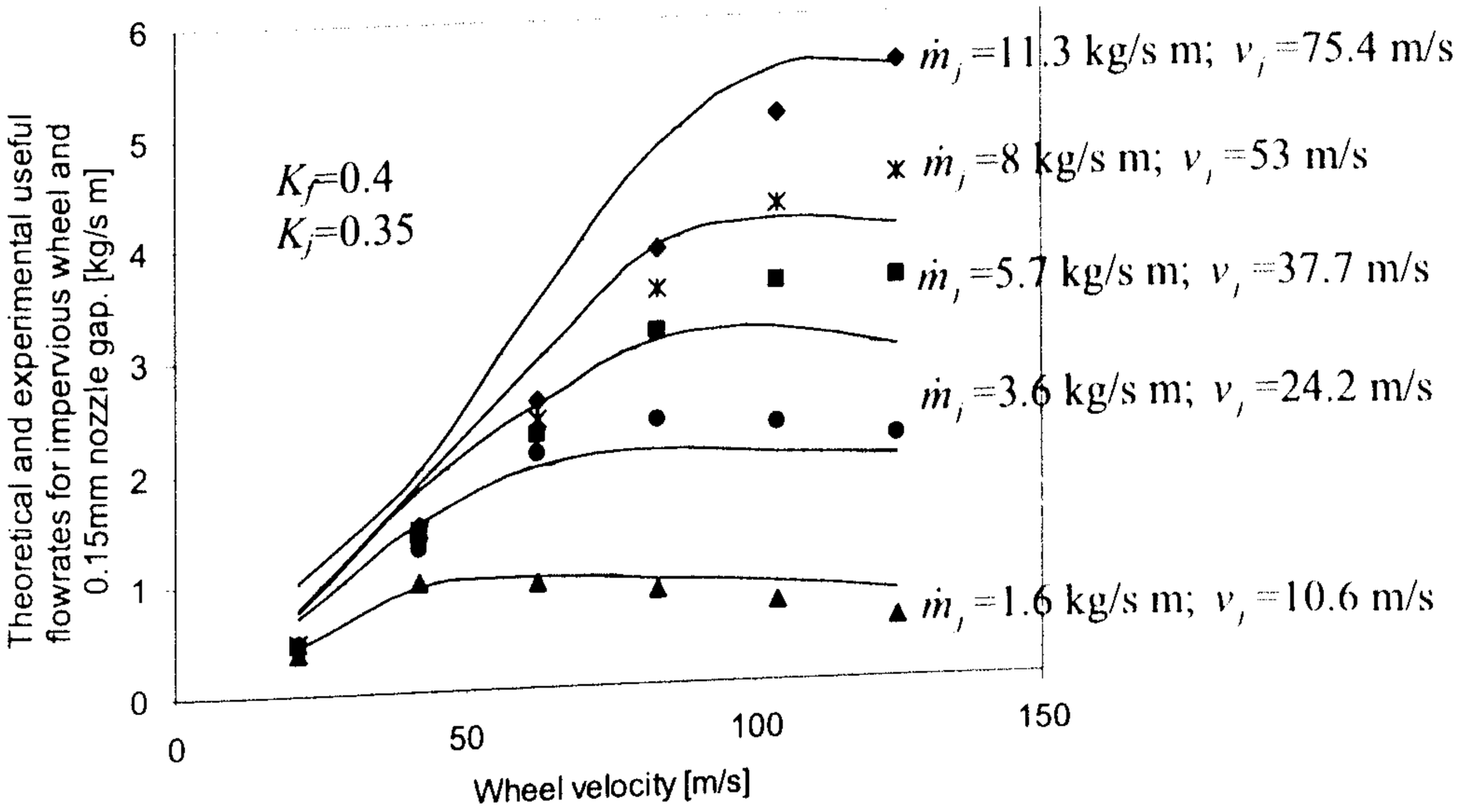

Figure 46. Experimental and theoretical useful flowrates based on spindle power for the impervious disc with a 0.15mm gap nozzle *(Experimental fit)*.

	0.15mm nozzle gap	0.4mm nozzle gap	2mm nozzle gap
Impervious knurled disc			
K_f	0.4	0.35	0.4
K_j	0.35	0.3	0.2
Porous CBN grinding wheel			
K_f	0.45	0.5	0.4
K_j	0.4	0.45	0.35

Table 10. The power loss coefficients and the jet velocity loss coefficients for impervious and porous wheels using nozzles of various gap size.

Experimentally measured spindle power consumed by the fluid was substituted into Equation 30, which is shown in Figure 47. It can be seen that spindle power exponentially increases with increasing of wheel velocity. Higher jet flowrate also results in elevated spindle power. This problem is especially critical when high wheel speed and high jet flowrate are used together. Therefore reduction of jet flowrate is recommended in order to reduce the spindle power consumed by the fluid.

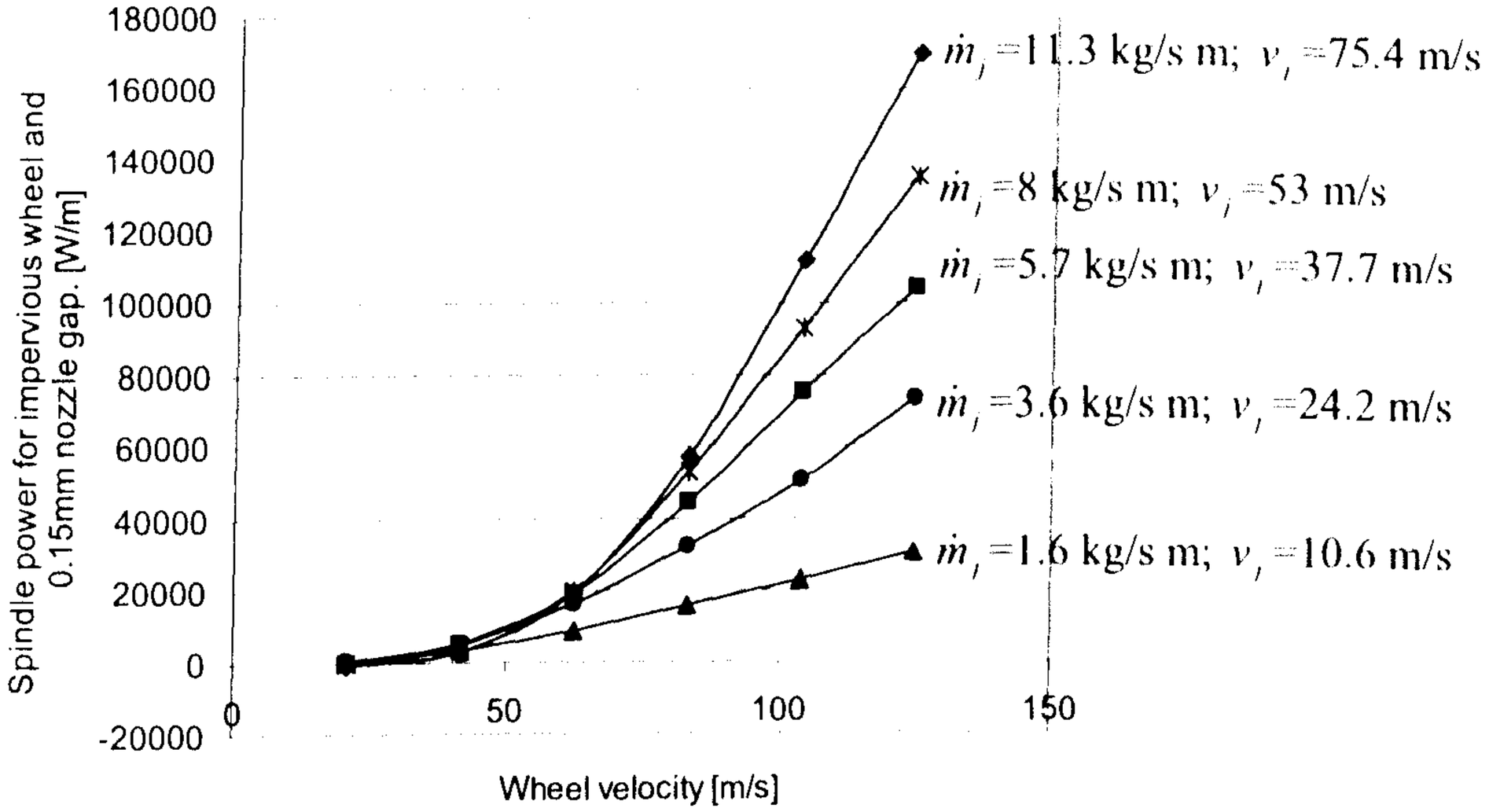

Figure 47. The effect of wheel velocity on spindle power consumed due to the fluid for the impervious disc with a 0.15mm gap nozzle *(Line of best fit)*.

However, reduction of jet flowrate can cause workpiece damage due to high contact temperature especially at high wheel speeds.

It is shown in Figure 48 that spindle power does not increase exponentially with increased jet flowrate. This is because increase in jet flowrate results in increase in jet velocity. High jet velocity can accelerate the wheel if it is directed tangentially in the same direction. This effect is seen particularly Figure 49 and in Figure 49 to cause a negative spindle power increase with increasing jet velocity approaching values of maximum jet velocity and minimum wheel speed.

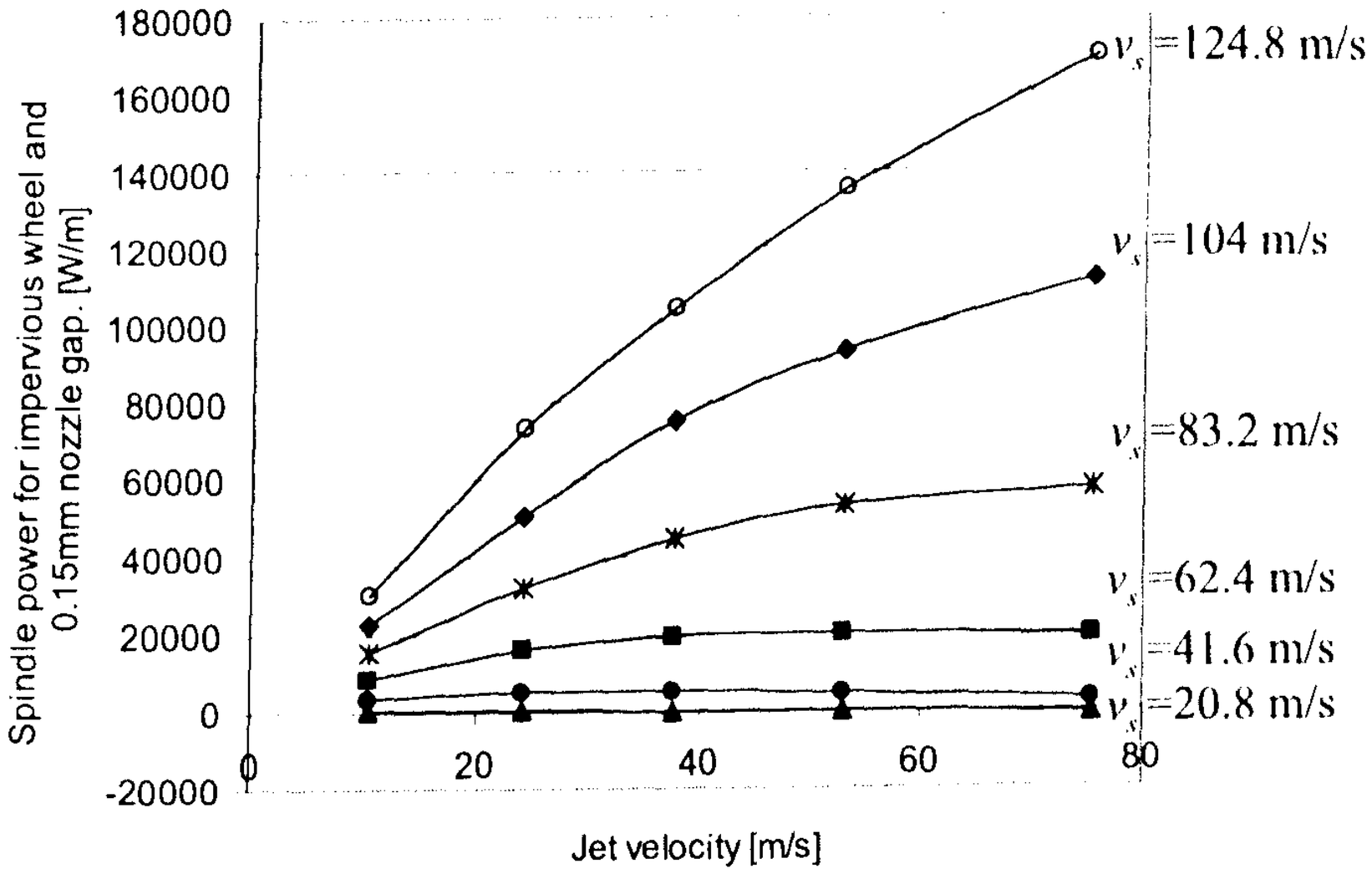

Figure 48. The effect of jet velocity on spindle power consumed due to fluid for the impervious disc with a 0.15mm gap nozzle *(Line of best fit)*.

In order to demonstrate the effect of the jet velocity on spindle power, jet power and spindle power are plotted together in Figure 49. It can be seen that high jet flowrate results in high jet velocity and both result in exponential increase in jet power. When the jet velocity reaches the wheel peripheral velocity, the spindle power required to accelerate the fluid starts to decrease. At this point jet power is approximately equal to the spindle power. After this point the spindle power levels off, since the fluid jet directed tangentially towards the wheel periphery tries to accelerate the wheel and the spindle. Further increase in jet velocity and jet flowrate show that the rate of increase in jet power becomes much higher than the rate of decrease of the spindle power. This is an important conclusion since this argument is used to assist in the formulation of an optimisation criterion.

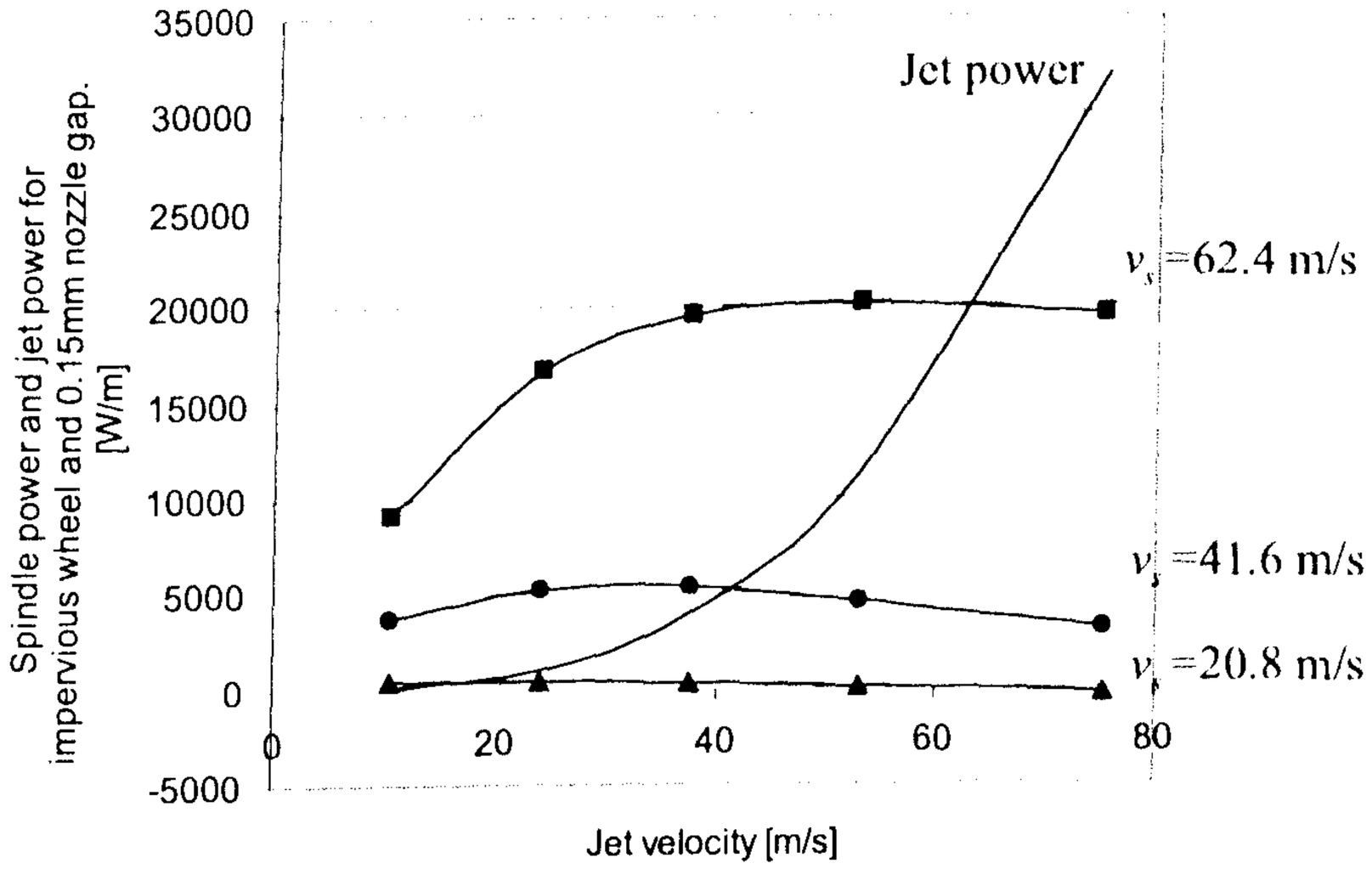

Figure 49. Relationship between jet power and spindle power consumed due to fluid for the impervious disc with a 0.15mm gap nozzle *(Line of best fit)*.

Experimental and theoretical useful flowrates are plotted in Figure 50 for the nozzle with 0.4mm gap. Theoretical useful flowrate was calculated from Equation 30 and the coefficients were as given in Table 10.

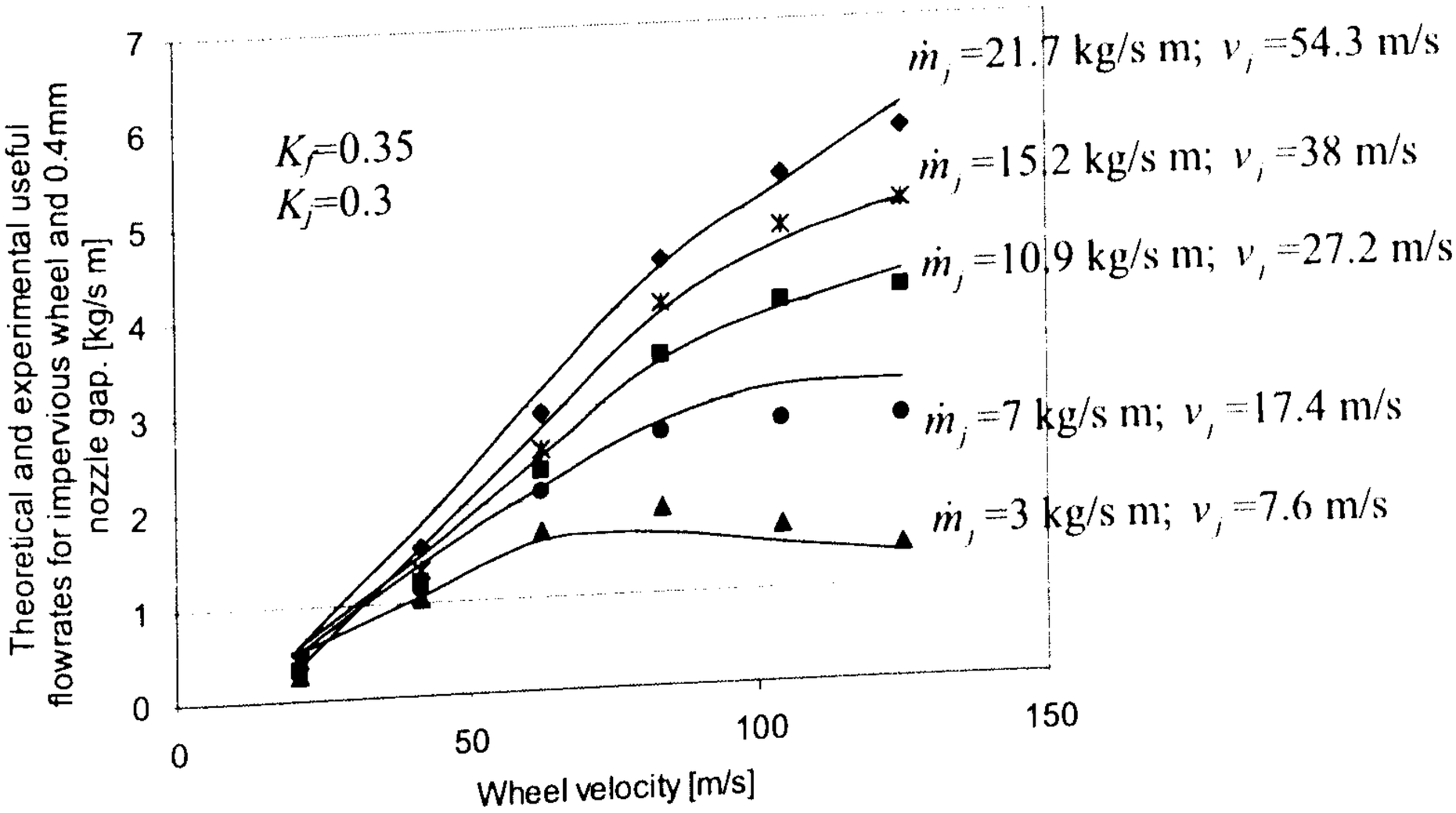

Figure 50. Experimental and theoretical useful flowrates based on spindle power for the impervious disc with a 0.4mm gap nozzle *(Experimental fit)*.

Experimental spindle power used for the calculations is plotted versus wheel peripheral velocity and is shown in Figure 51. Higher flowrate from the nozzle with 0.4mm gap produced higher spindle power than the nozzle with 0.15mm gap, though the corresponding jet powers were the same for both nozzles. This can be seen comparing Figure 51 with Figure 47.

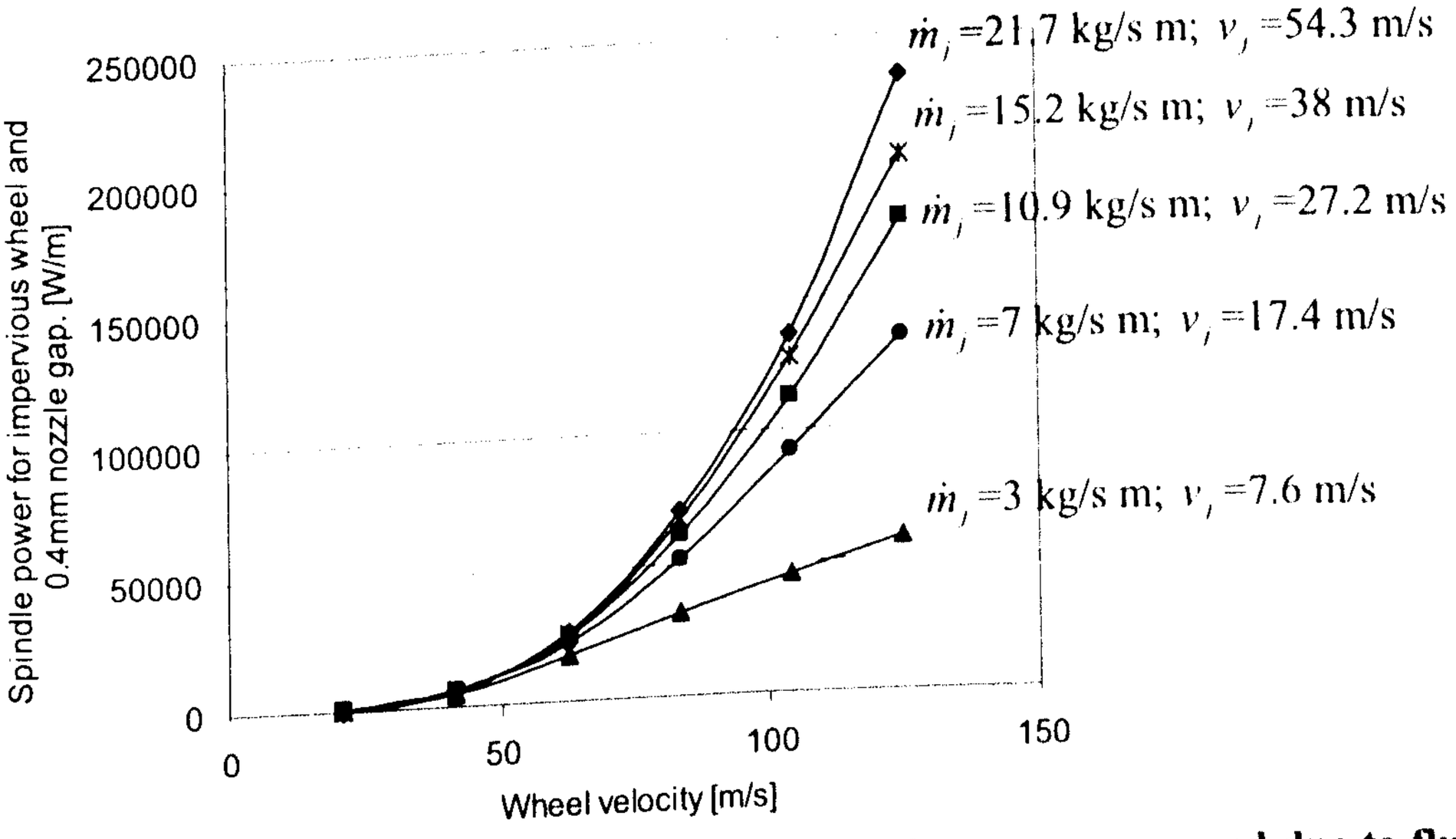

Figure 51. The effect of wheel velocity on spindle power consumed due to fluid for the impervious disc with a 0.4mm gap nozzle *(Line of best fit)*.

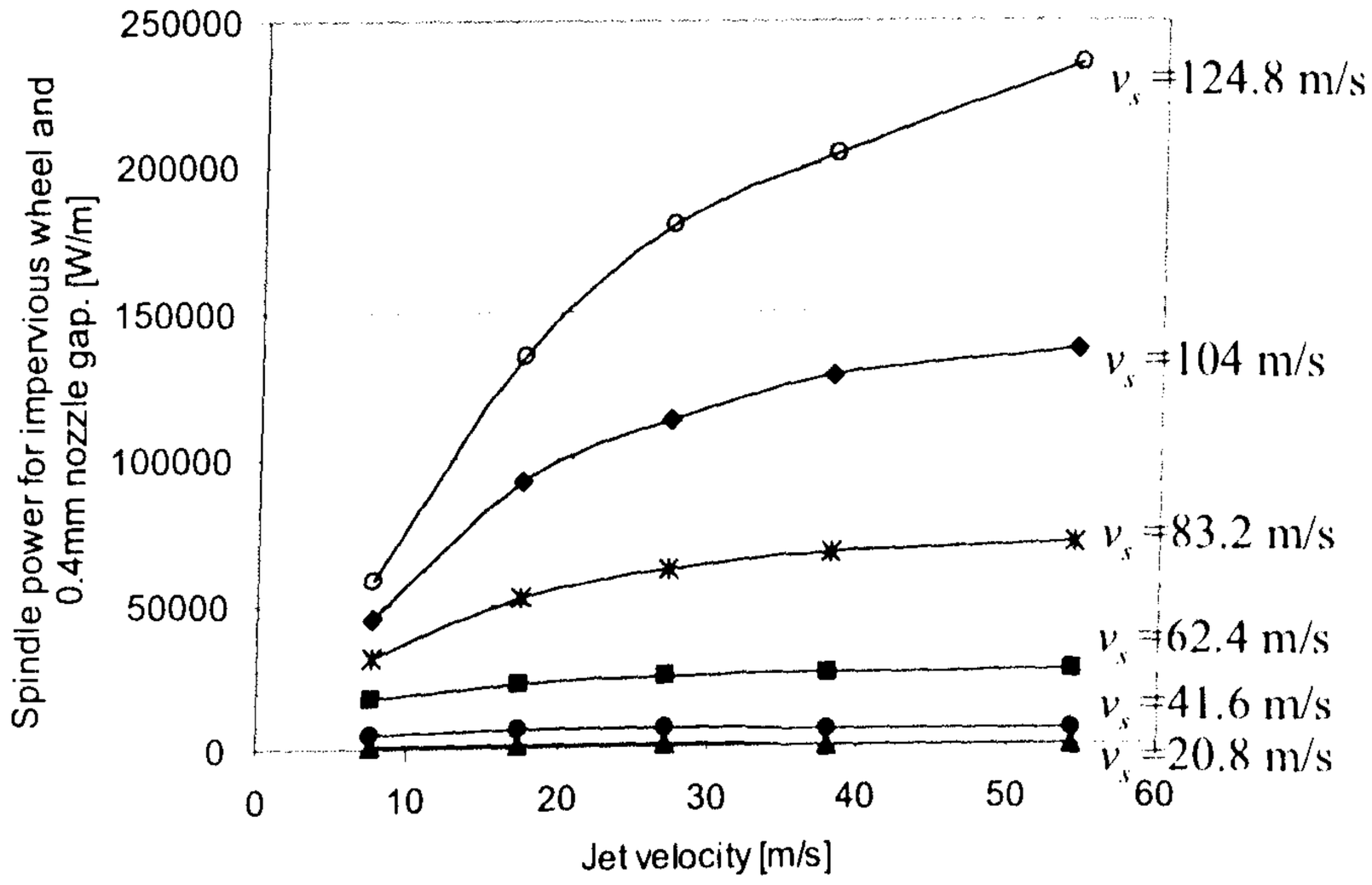

Figure 52. The effect of jet velocity on spindle power consumed due to fluid for the impervious disc with a 0.4mm gap nozzle *(Line of best fit)*.

As with the smaller nozzle, the rate of increase in spindle power was reduced by increasing jet velocity as shown in Figure 52.

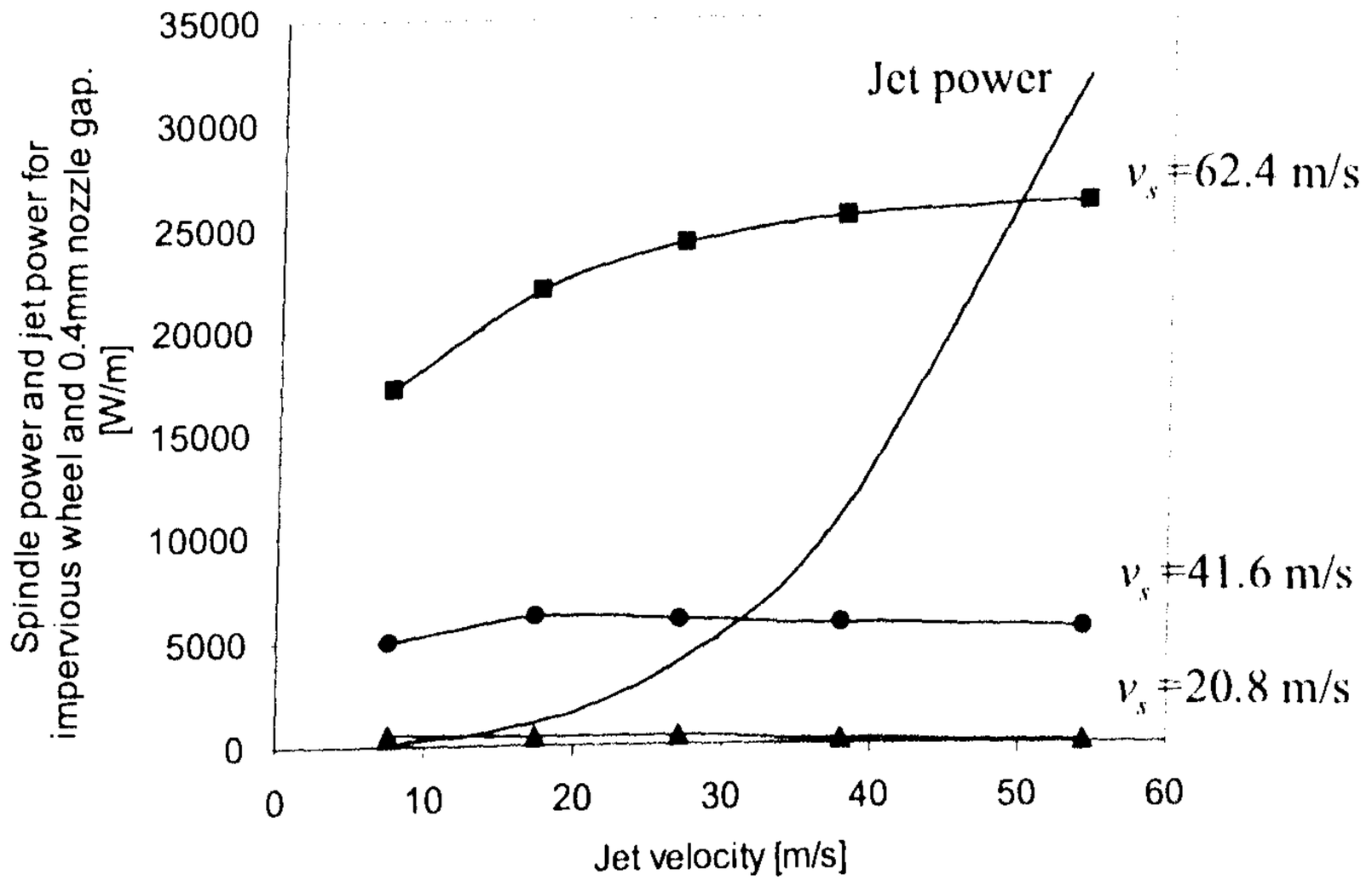

Figure 53. Relationship between jet power and spindle power consumed due to fluid for the impervious disc with a 0.4mm gap nozzle *(Line of best fit)*.

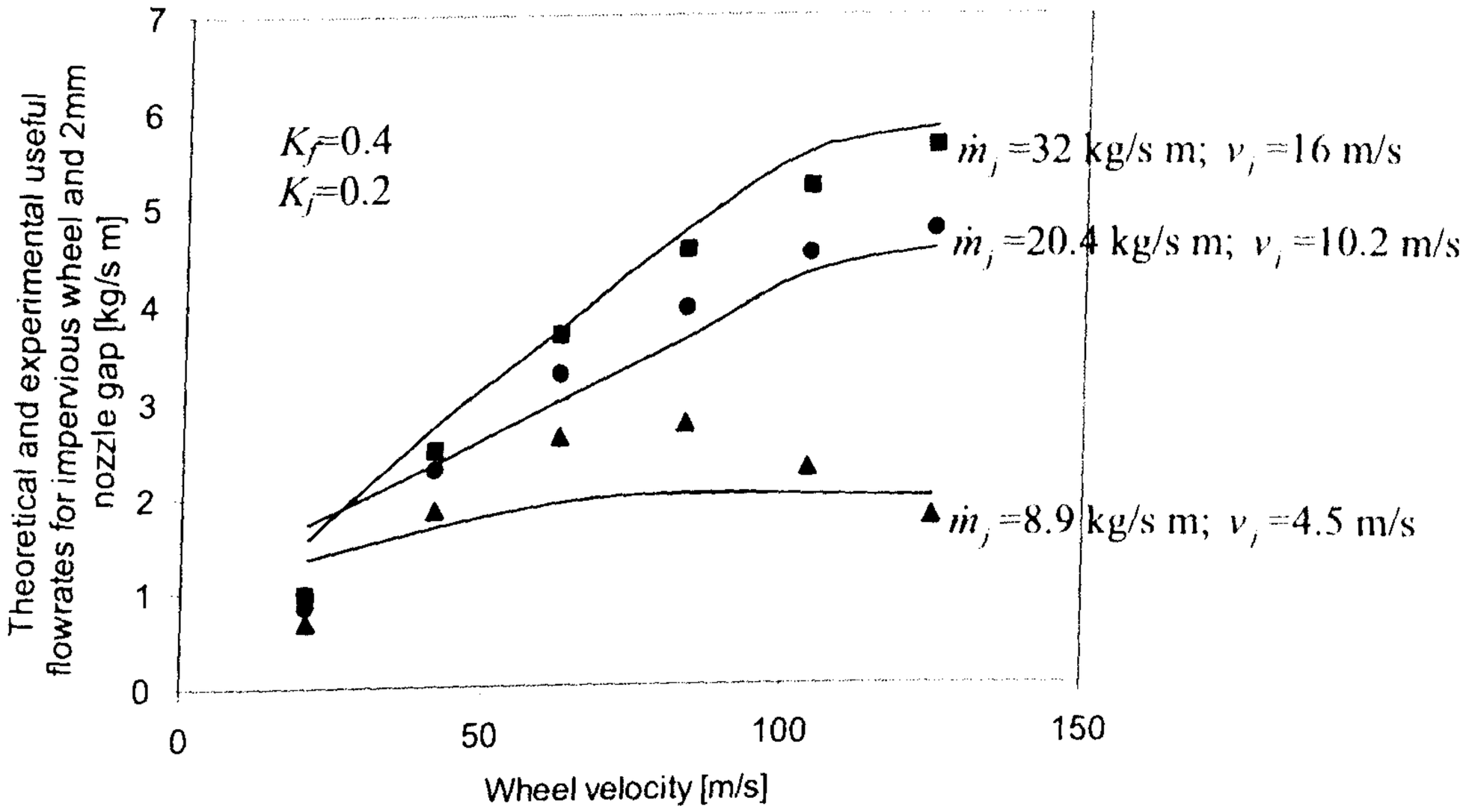

Figure 54. Experimental and theoretical useful flowrates based on spindle power for the impervious disc with a 2mm gap nozzle *(Experimental fit).*

Figure 53 shows that the spindle power starts to decrease after the point where the jet velocity is equal to wheel peripheral velocity. However in comparison to the nozzle with thinner gap and lower flowrate, the decrease of spindle power for the nozzle with thicker gap starts at a lower jet velocity at lower wheel speeds. This may be due to less interaction of air with the fluid thus enhancing the ability of the grinding fluid to exert traction on the wheel.

Comparison of theoretical and experimental useful flowrates for the nozzle with a 2mm gap is shown in Figure 54. Coefficients were selected from Table 10. The experiments were discontinued as with other trials due to the grinding machine and the measuring devices range limitations.

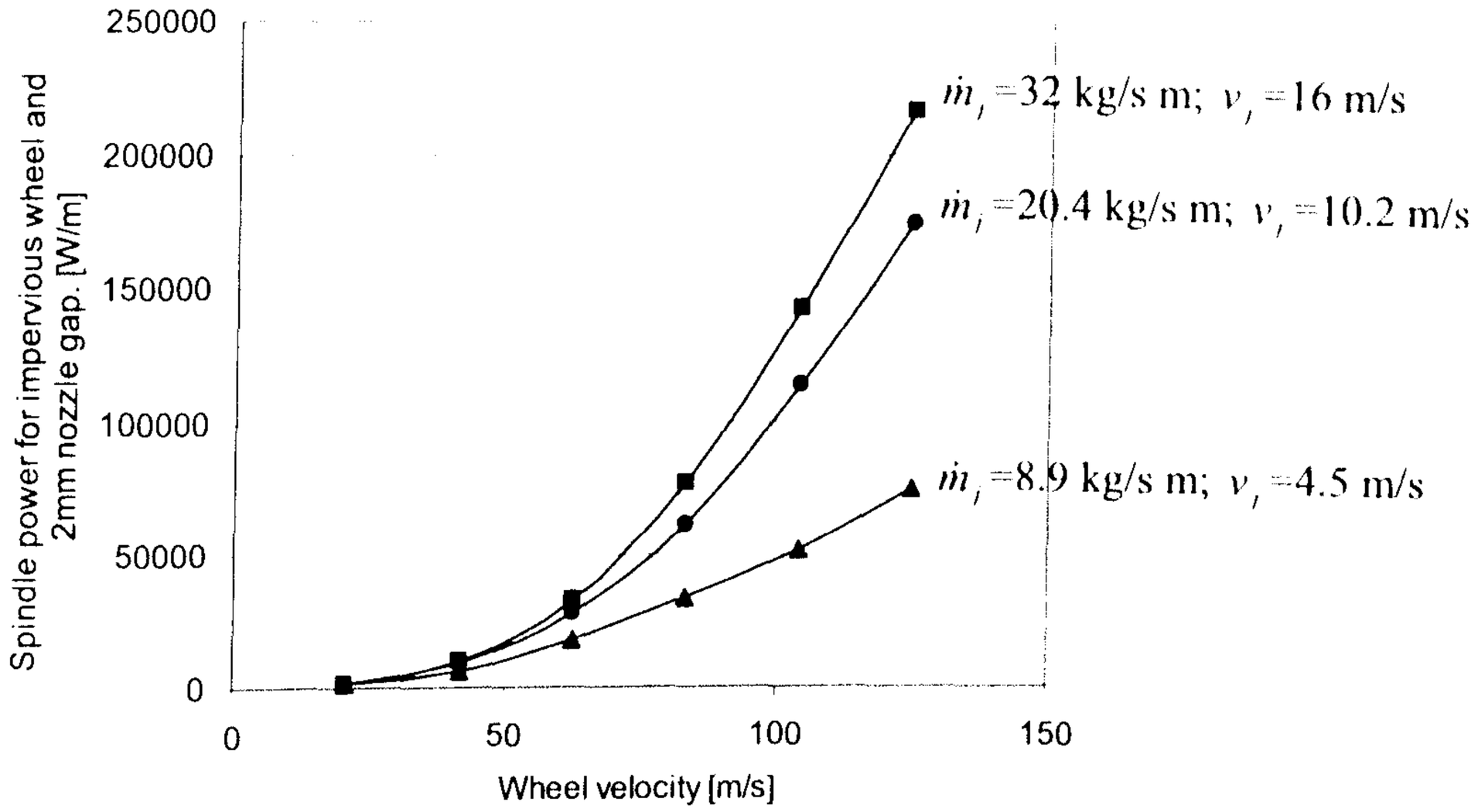

Figure 55. The effect of wheel velocity on spindle power consumed due to fluid for the impervious disc with a 2mm gap nozzle *(Line of best fit)*.

The spindle power observed for this nozzle is the highest in comparison to the previous two nozzles for corresponding values of jet power shown in Figure 55. This confirms that the jet velocity is the factor that reduces the spindle power whereas jet flowrate tends to increase spindle power. Jet flowrate tends to increase useful flowrate and hence increases spindle power. These findings are in agreement with Equation 27 which forms the basis of the spindle power model.

Spindle power versus jet velocity is also plotted in Figure 56 for the range of wheel speeds. It can be seen that low jet velocity and high jet flowrate for the larger gap nozzle have less ability to reduce spindle power.

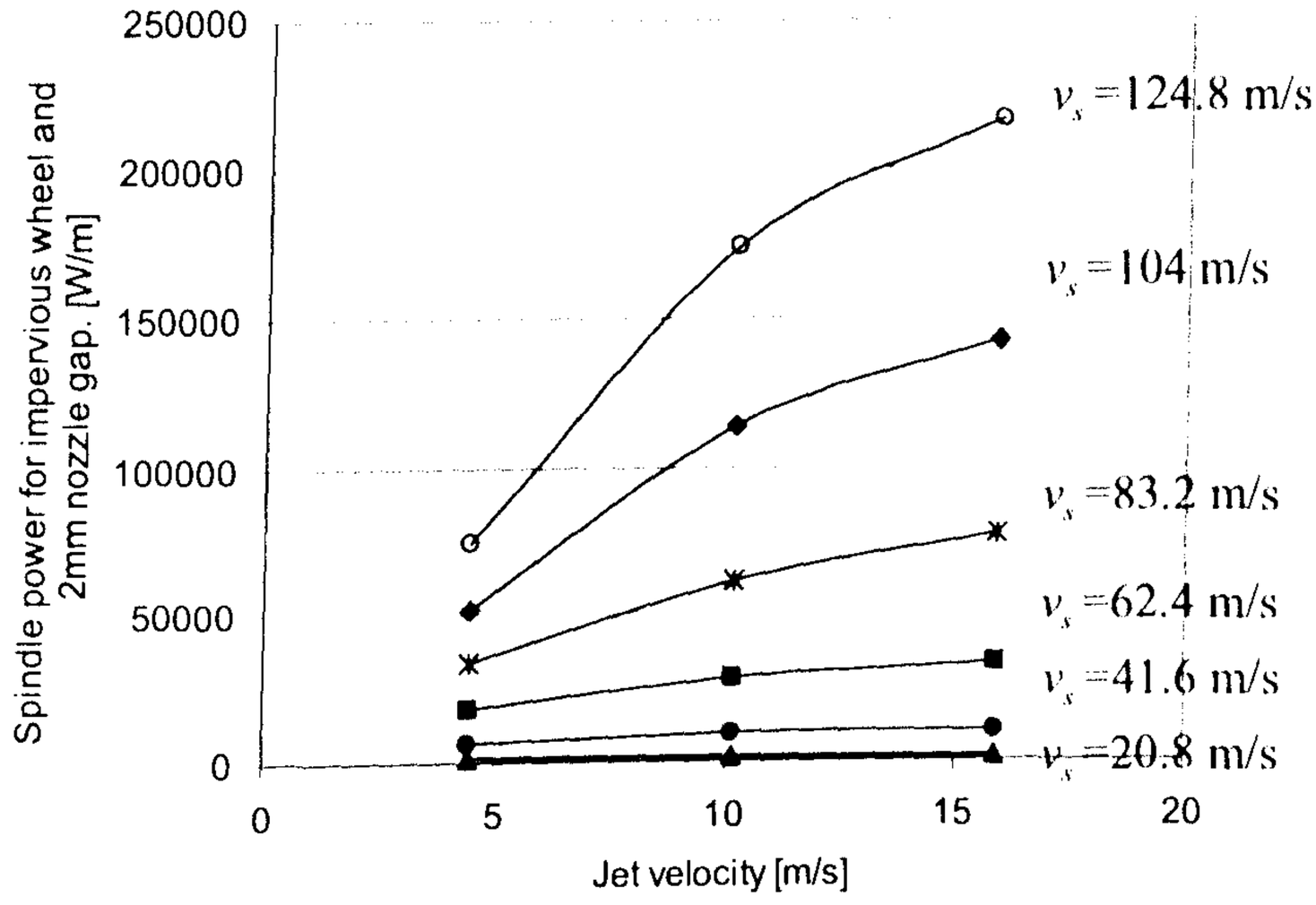

Figure 56. The effect of jet velocity on spindle power consumed due to fluid for the impervious disc with a 2mm gap nozzle *(Line of best fit)*.

In Figure 57, it is observed that the high flowrate with this nozzle starts to decrease spindle power for case of the lower jet velocity at the point where jet power was equal to spindle power.

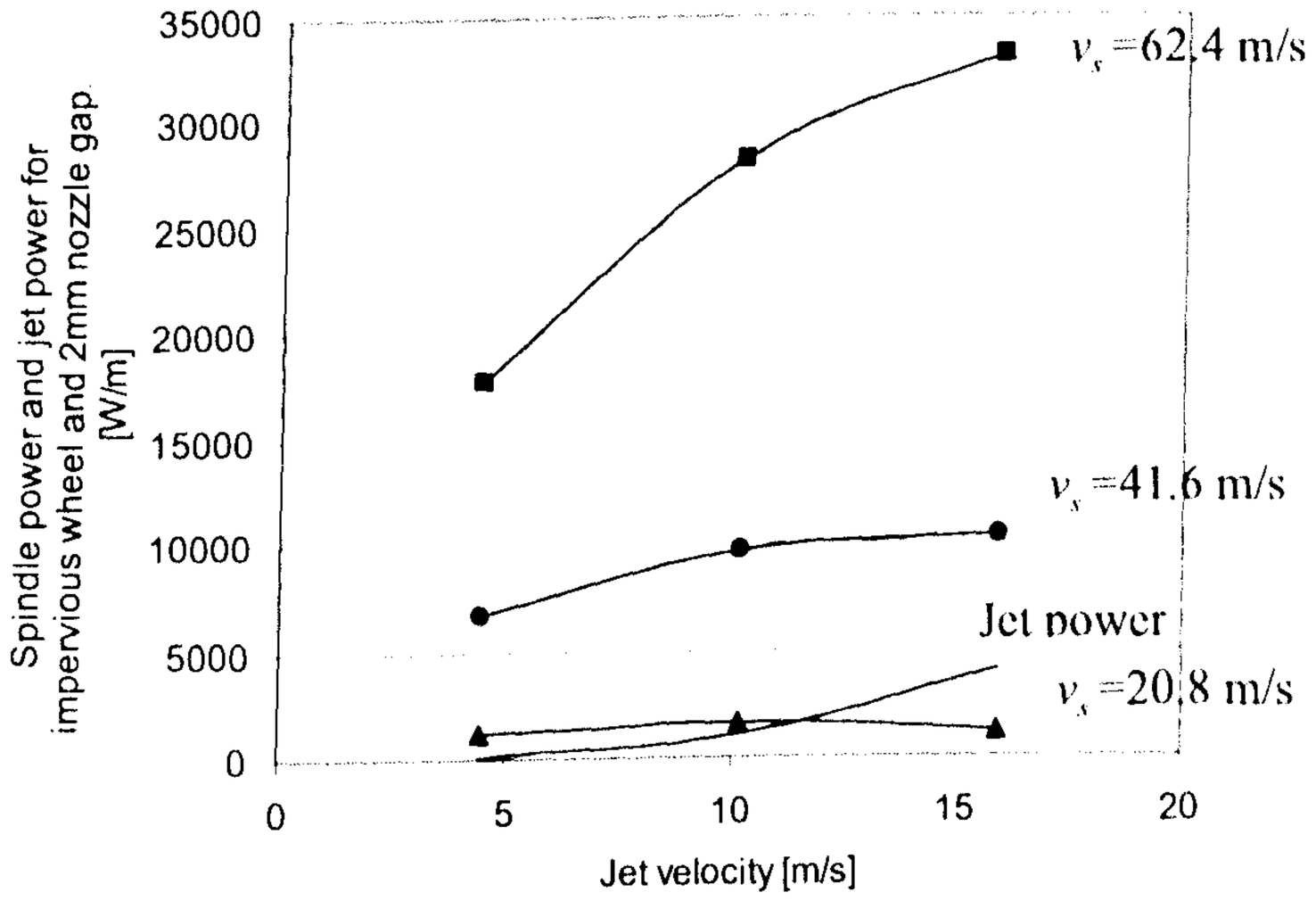

Figure 57. Relationship between jet power and spindle power consumed due to fluid for the impervious disc with a 2mm gap nozzle *(Line of best fit)*.

The results show that spindle power is reduced with high jet velocity but is increased with high jet flowrate. This problem becomes critical at higher wheel speeds. It is possible to reduce the spindle power by reducing the nozzle outlet gap size without change in jet power. In Figure 58, jet power for two nozzles with different gap size are plotted together with corresponding spindle power for the same wheel speeds. Jet power for the two nozzles is equal at different jet velocities. A horizontal line drawn through the two jet power lines indicates the corresponding jet velocities for equal jet power. It can be seen that the nozzle with a smaller gap reduced may spindle power more than the nozzle with a larger gap for the same jet power. Therefore, if the spindle power is reduced without a change in jet power, the total power due to the fluid process is also reduced. However caution has to be taken since the small nozzle gap size gives low jet flowrate, which may reduce the useful flowrate and may cause workpiece damage due to elevated contact temperature.

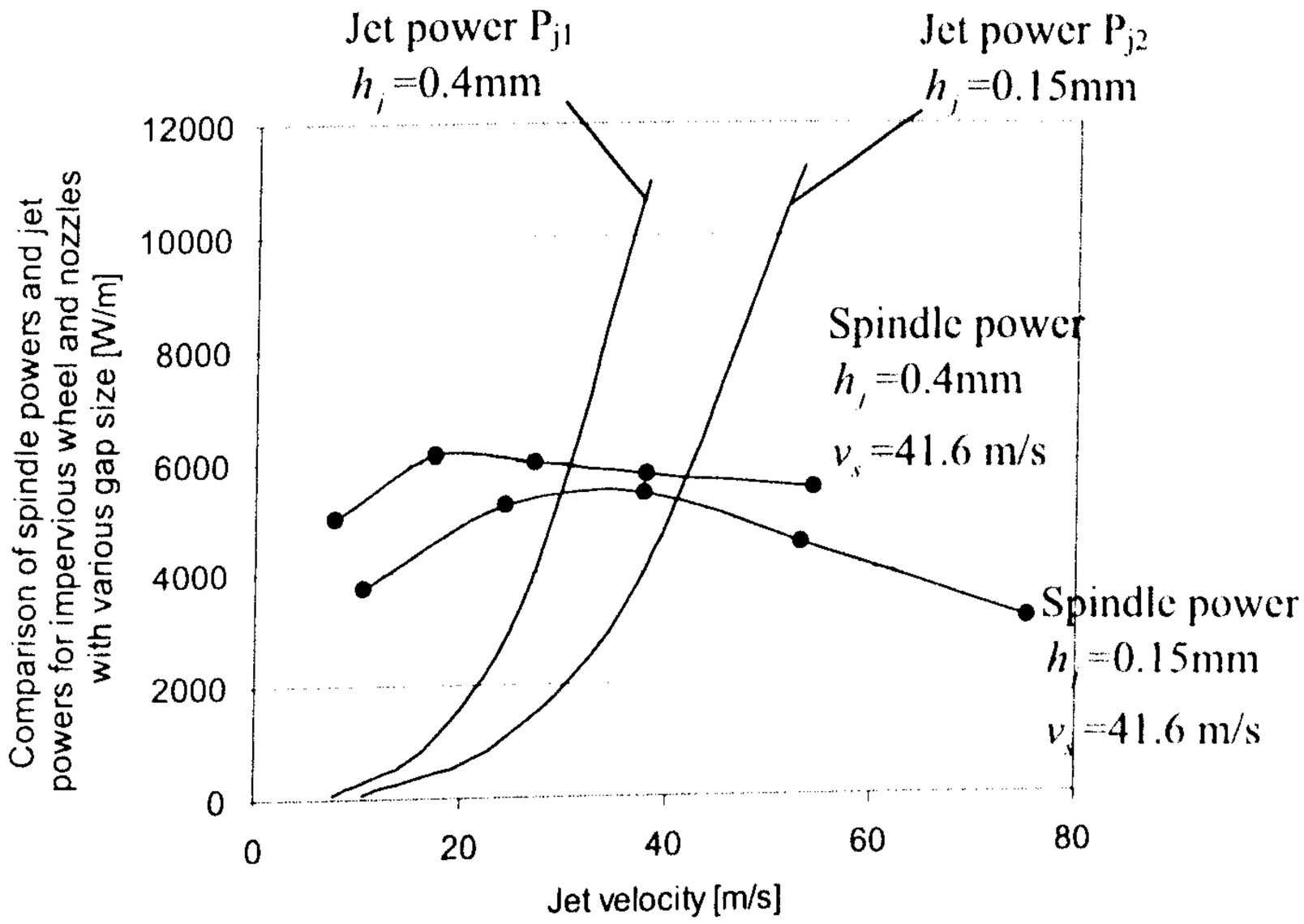

Figure 58. The effect of nozzle gap size on jet power and spindle power consumed due to fluid for the impervious disc *(Line of best fit)*.

5.4.2 Spindle power and useful flowrate for the porous vitrified CBN grinding wheel using nozzles of differing gap sizes.

Theoretical and experimental useful flowrates using a nozzle with 0.15mm gap are plotted together in Figure 59. Calculations were made from Equation 30. Coefficients were chosen from Table 10. As expected, the porous wheel gave a higher useful flowrate than the impervious wheel for the same nozzle.

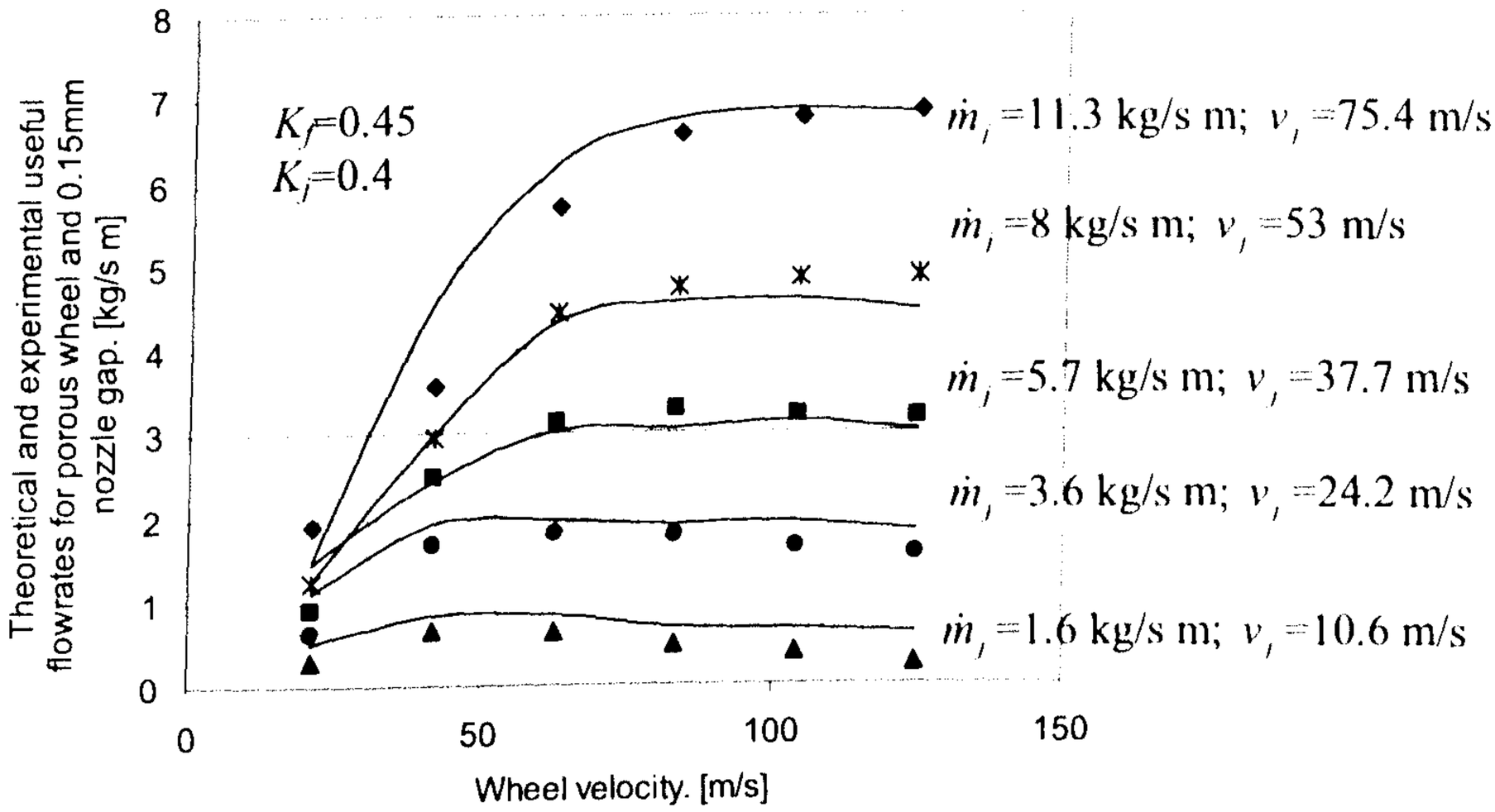

Figure 59. Experimental and theoretical useful flowrates based on spindle power for the porous CBN grinding wheel with a 0.15mm gap nozzle *(Experimental fit)*.

The higher flowrate for the porous wheel in comparison to the impervious wheel resulted in higher spindle power consumed due to fluid transport through the contact zone, as shown in Figure 60. As with the impervious wheel, spindle power is greatest at the largest jet flowrate and highest wheel speed.

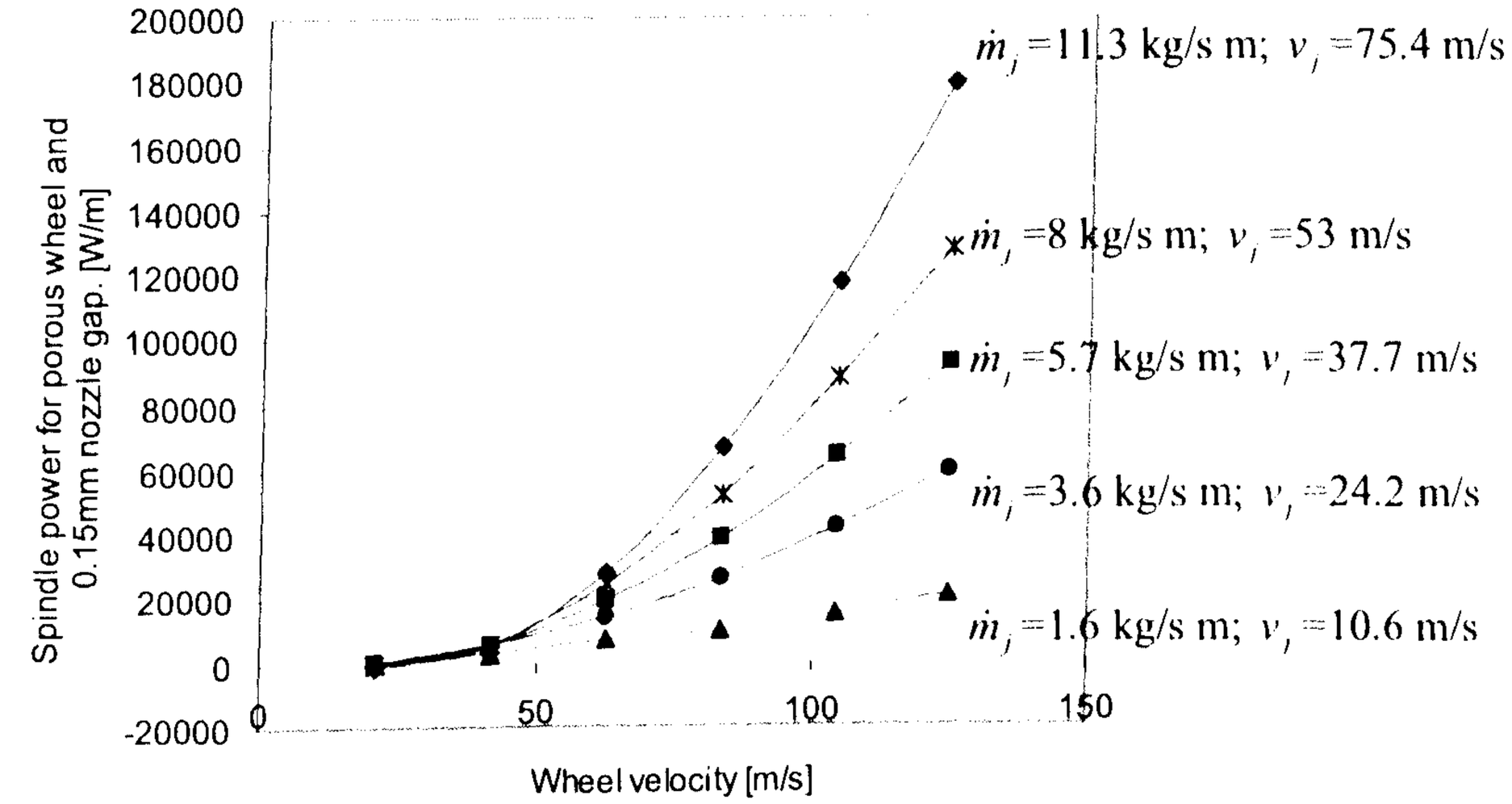

Figure 60. The effect of wheel velocity on spindle power consumed due to fluid for the porous CBN grinding wheel with a 0.15mm gap nozzle *(Line of best fit)*.

Figure 61, confirms that increasing jet velocity with the jet stream directed tangentially towards the wheel limits the rate of increase of spindle power.

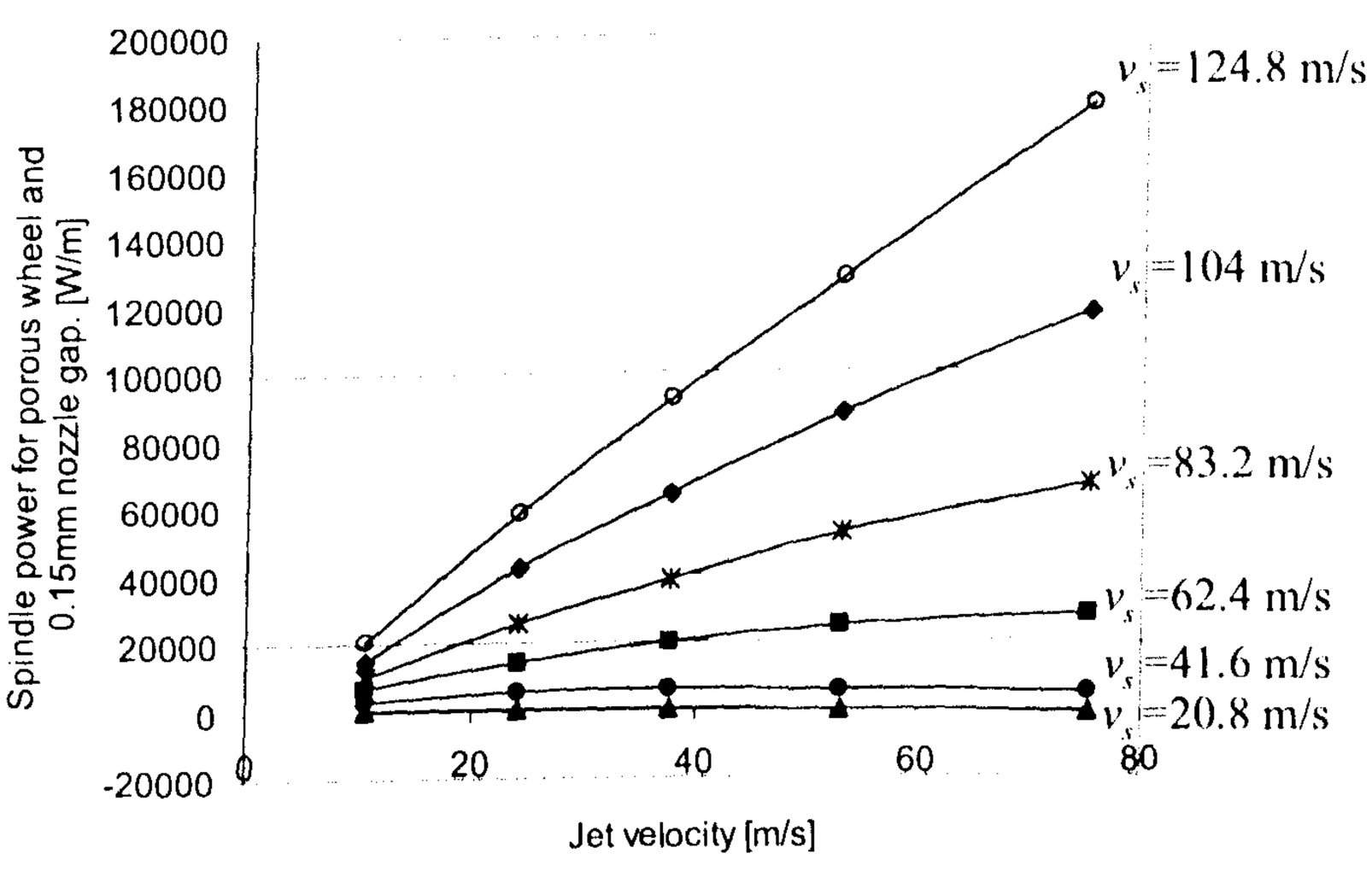

Figure 61. The effect of jet velocity on spindle power consumed due to fluid for the porous CBN grinding wheel with a 0.15mm gap nozzle *(Line of best fit)*.

Figure 62 shows that as the jet power approaches the spindle power, the spindle power starts to decrease similar to previous cases described above. When the jet and the spindle powers are equal, the jet velocity is approximately equal to the wheel peripheral velocity.

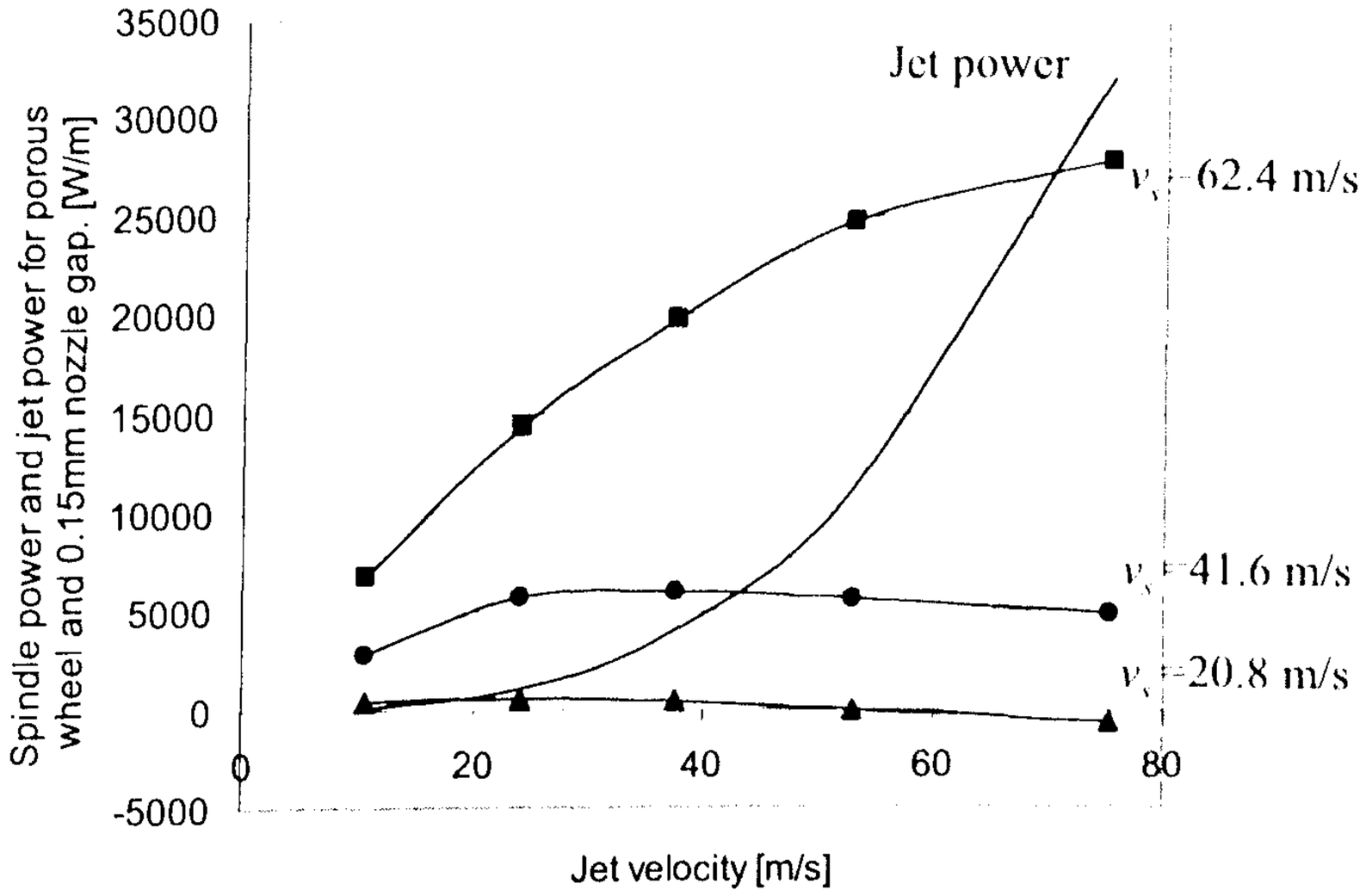

Figure 62. Relationship between jet power and spindle power consumed due to fluid for porous CBN grinding wheel employing nozzle with 0.15mm gap *(Line of best fit)*.

The nozzle with 0.4mm gap produced higher flowrate than the nozzle with 0.15mm gap. Theoretical and experimental results are shown in Figure 63. Calculations were made similarly to the other nozzles. Values of power K_f coefficient and jet velocity coefficient K_j are listed in Table 10.

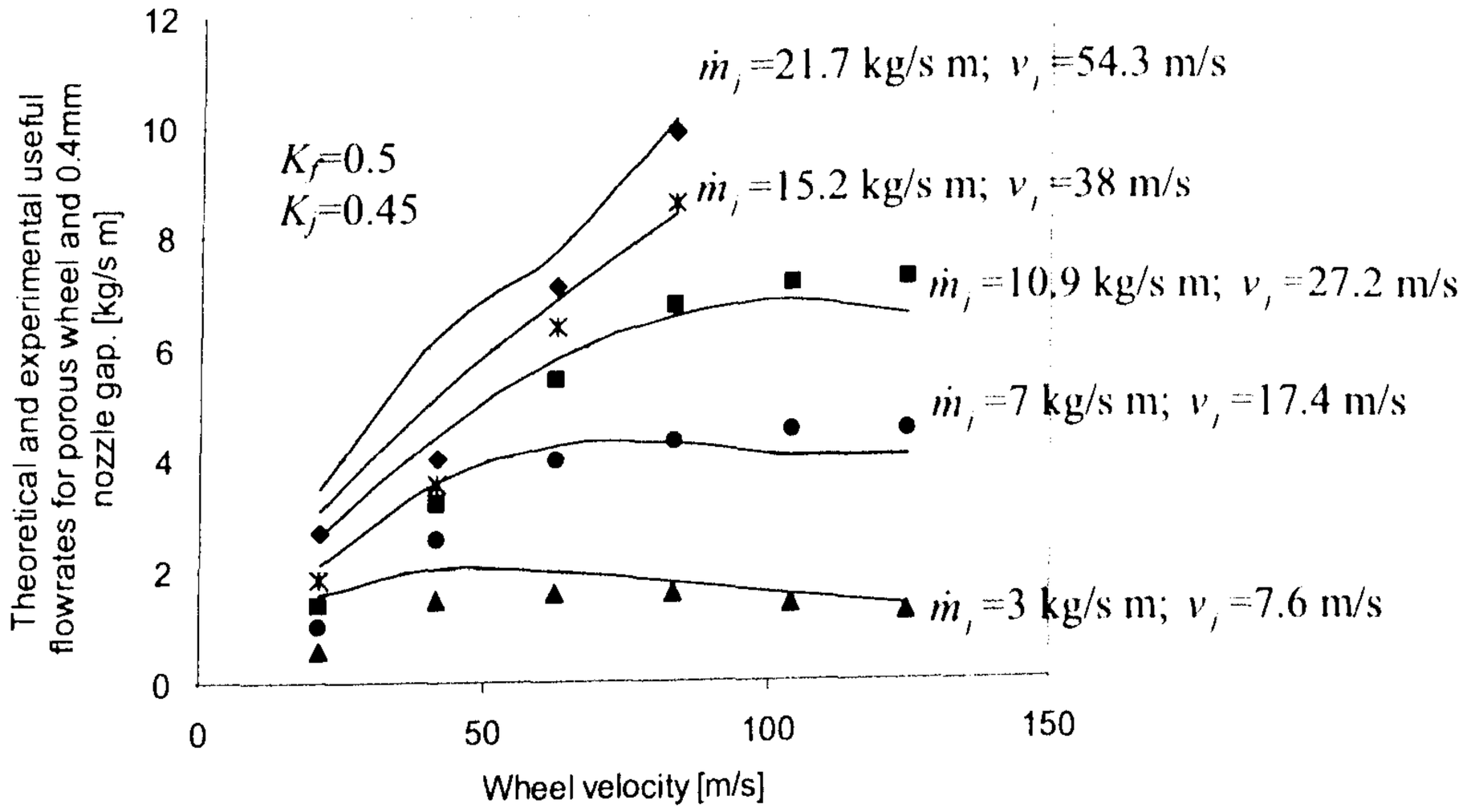

Figure 63. Experimental and theoretical useful flowrates based on spindle power for the porous CBN grinding wheel with a 0.4mm gap nozzle *(Experimental fit)*.

Figure 64 for a 0.4 mm nozzle shows that higher flowrate and lower jet velocity resulted in higher spindle power than the results for the 0.15 mm nozzle shown in Figure 62.

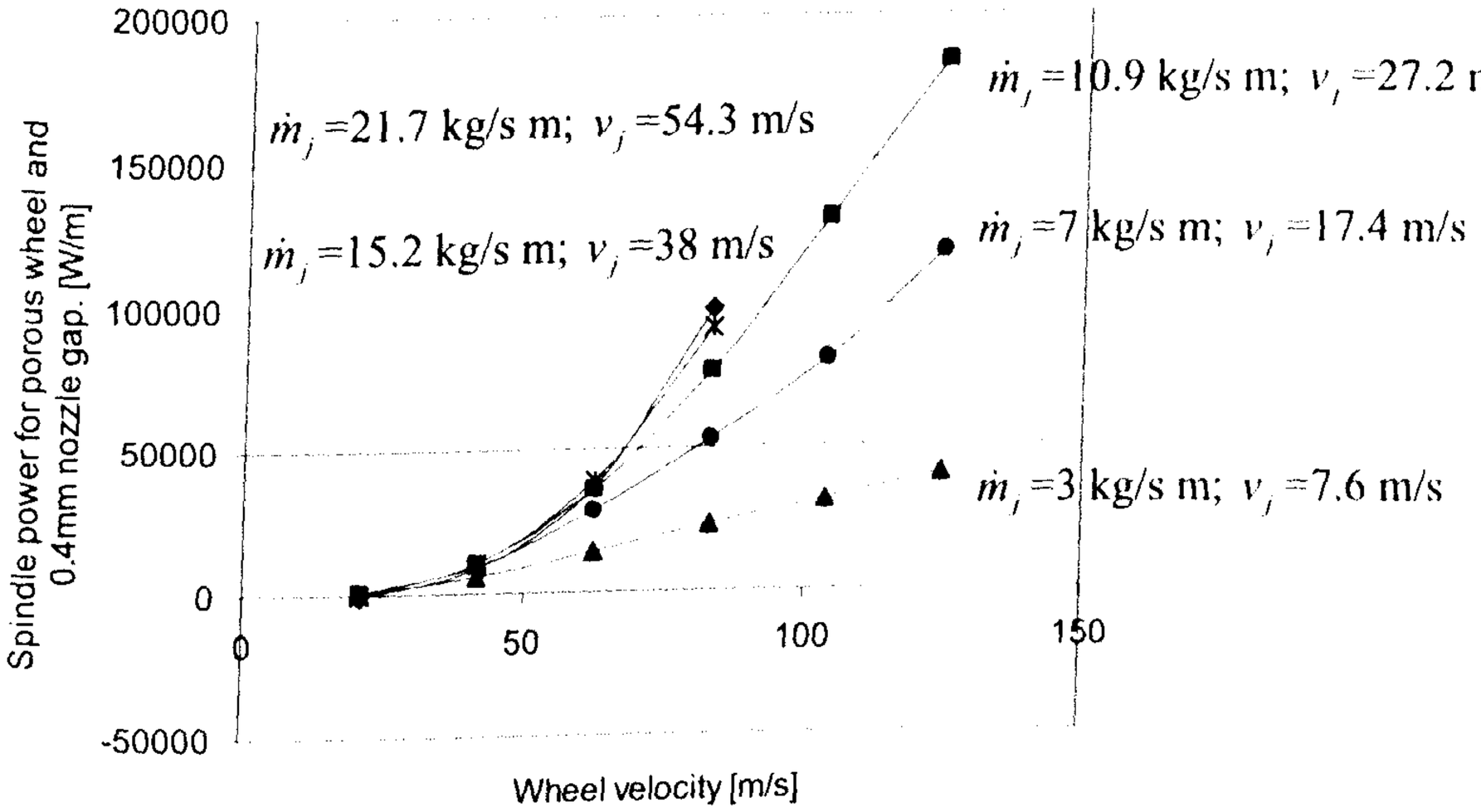

Figure 64. The effect of wheel velocity on spindle power consumed due to fluid for the porous CBN grinding wheel with a 0.4mm gap nozzle *(Line of best fit)*.

Figure 65 shows that the nozzle with 0.4mm gap size still possesses sufficient jet velocity to limit spindle power.

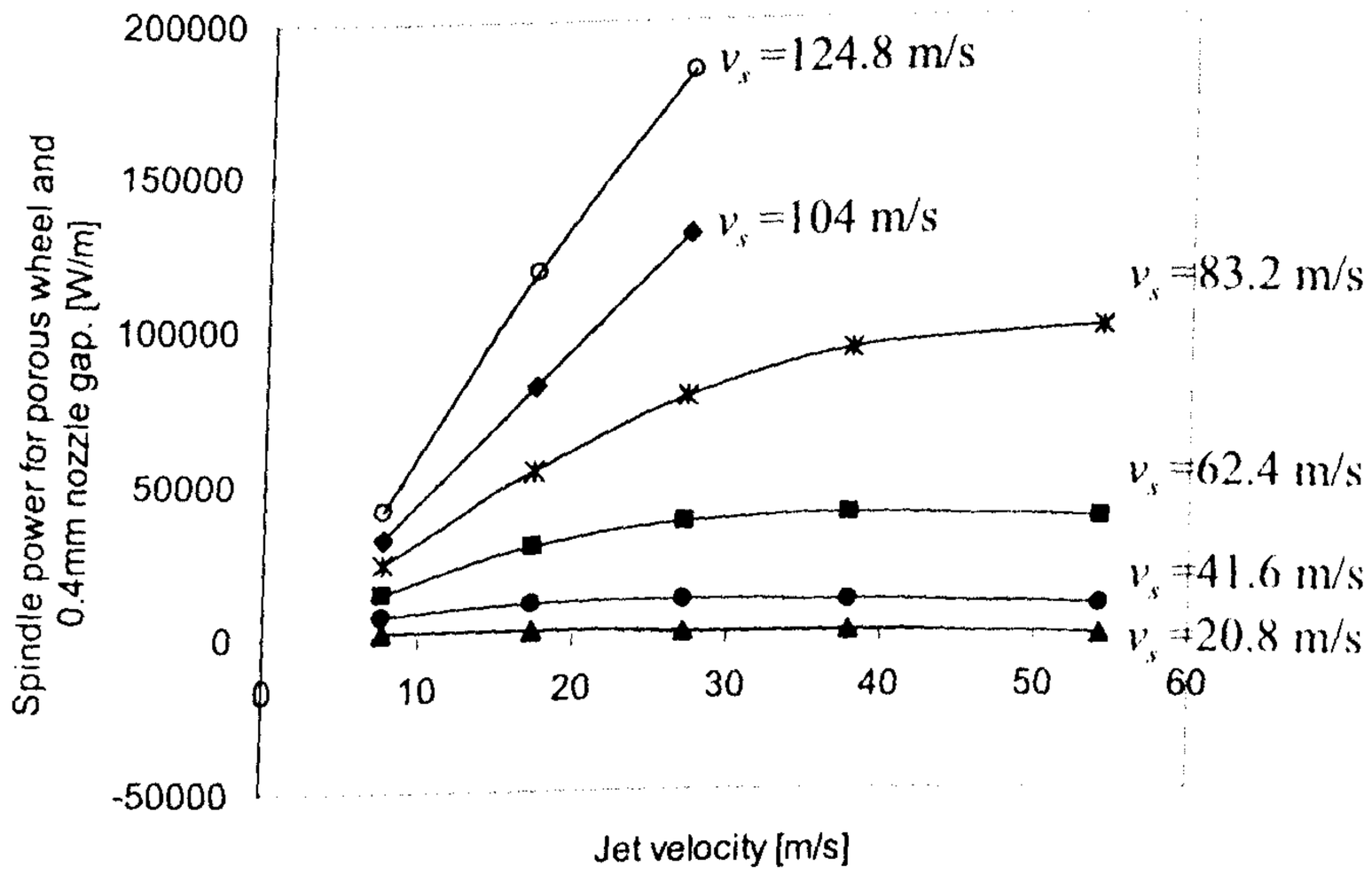

Figure 65. The effect of jet velocity on spindle power consumed due to fluid for the porous CBN grinding wheel with a 0.4mm gap nozzle *(Line of best fit)*.

Comparison of spindle power and jet power using the 0.4mm gap nozzle with the porous wheel is shown in Figure 66. As with the impervious wheel maximum spindle power occurs at a slightly lower jet velocity when the jet power is equal to spindle power. As described previously this is attributed to the effect of the air interaction with the grinding fluid. A larger jet flowrate is likely to be less sensitive to the air flow.

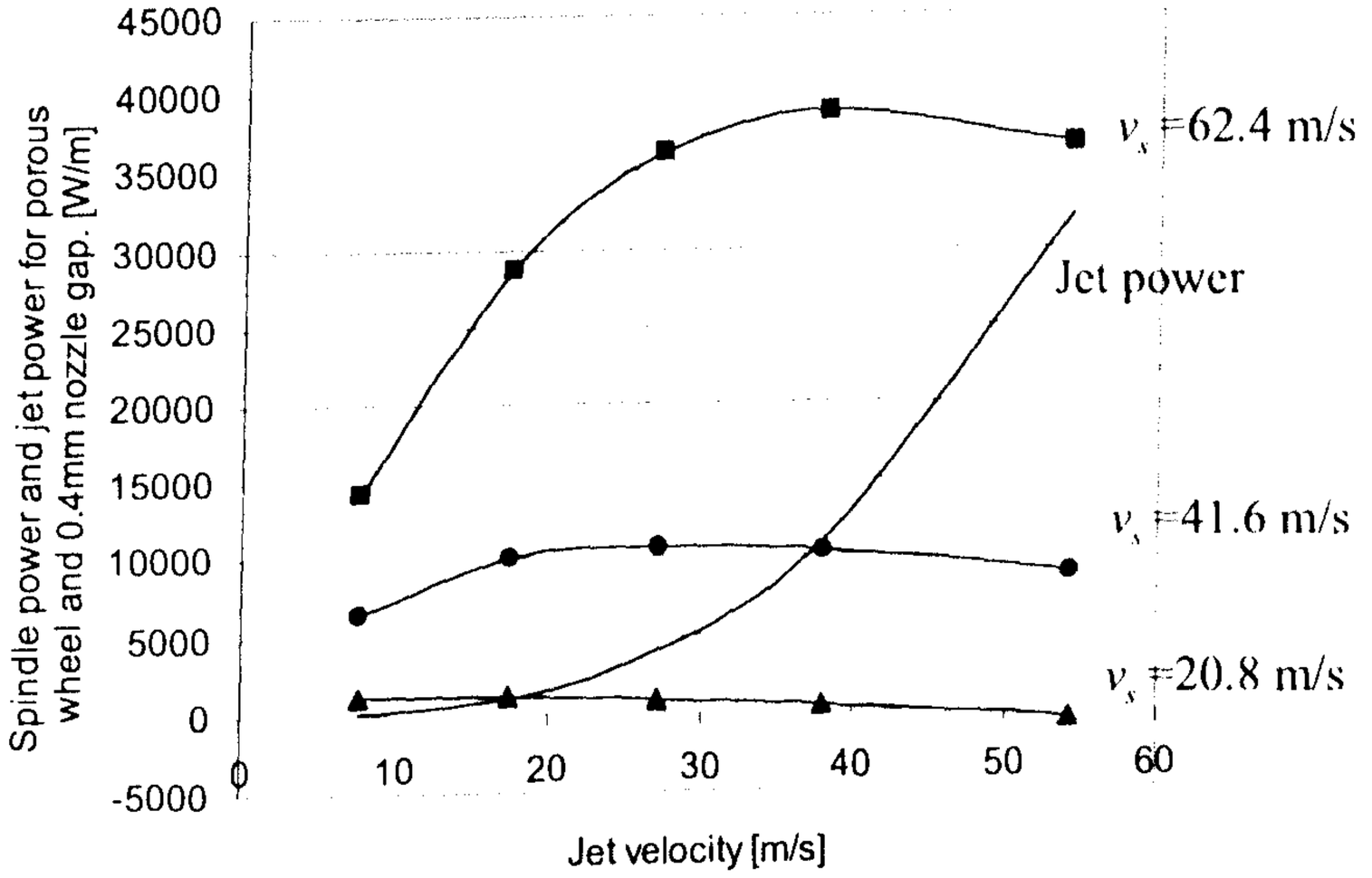

Figure 66. Relationship between jet power and spindle power consumed due to fluid for the porous CBN wheel with a 0.4mm gap nozzle *(Line of best fit)*.

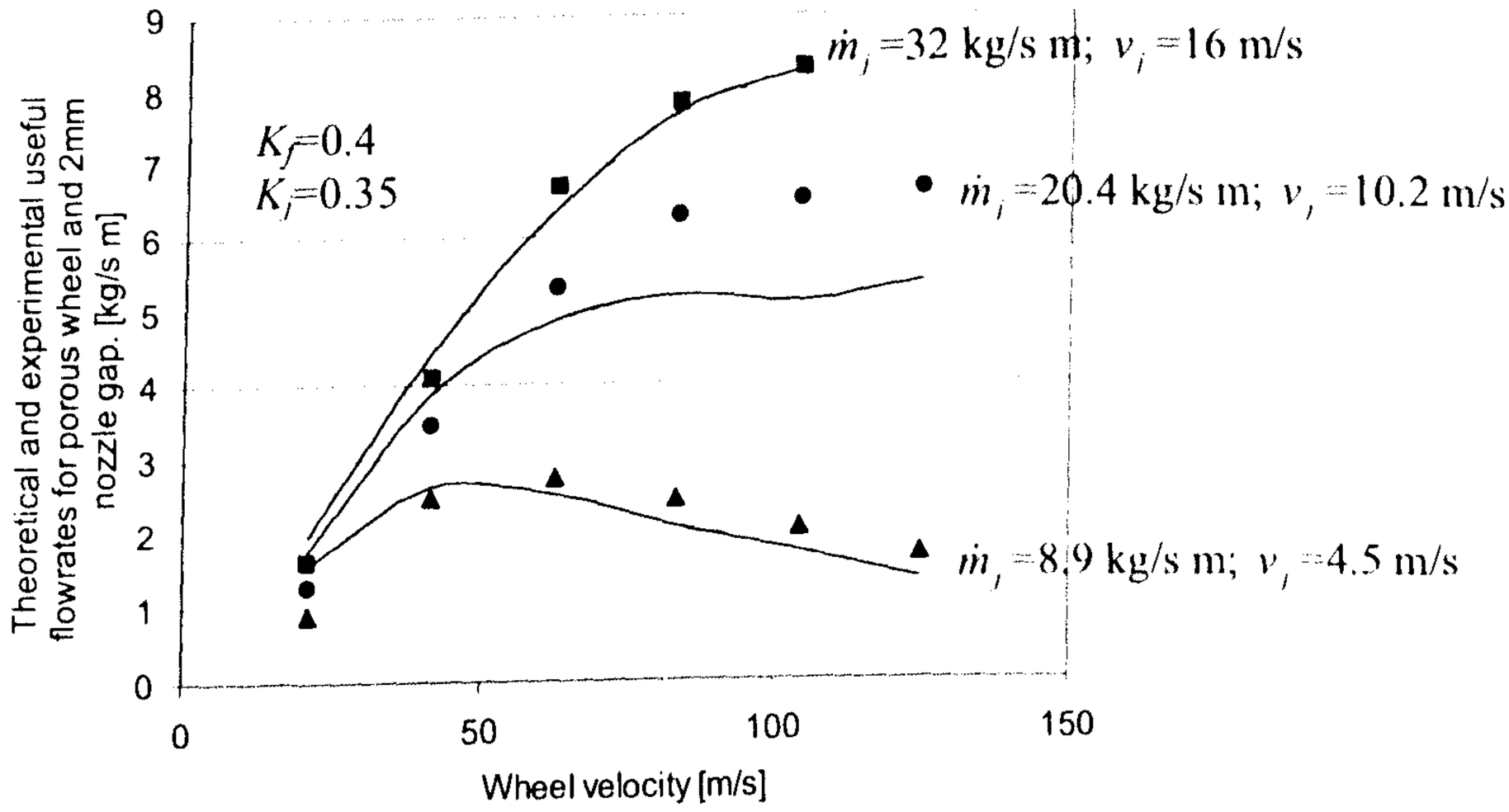

Figure 67. Experimental and theoretical useful flowrates based on spindle power for the porous CBN wheel with a 2mm gap nozzle *(Experimental fit)*.

Theoretical and experimental useful flowrates for the nozzle with 2mm gap and the porous wheel are shown in Figure 67. Coefficients used for the calculation of theoretical useful flowrate are listed in Table 10. Spindle power versus wheel speed for the range of jet flowrates is shown in Figure 68. As expected, the largest jet flowrate gave the highest spindle power, though the jet powers were equal.

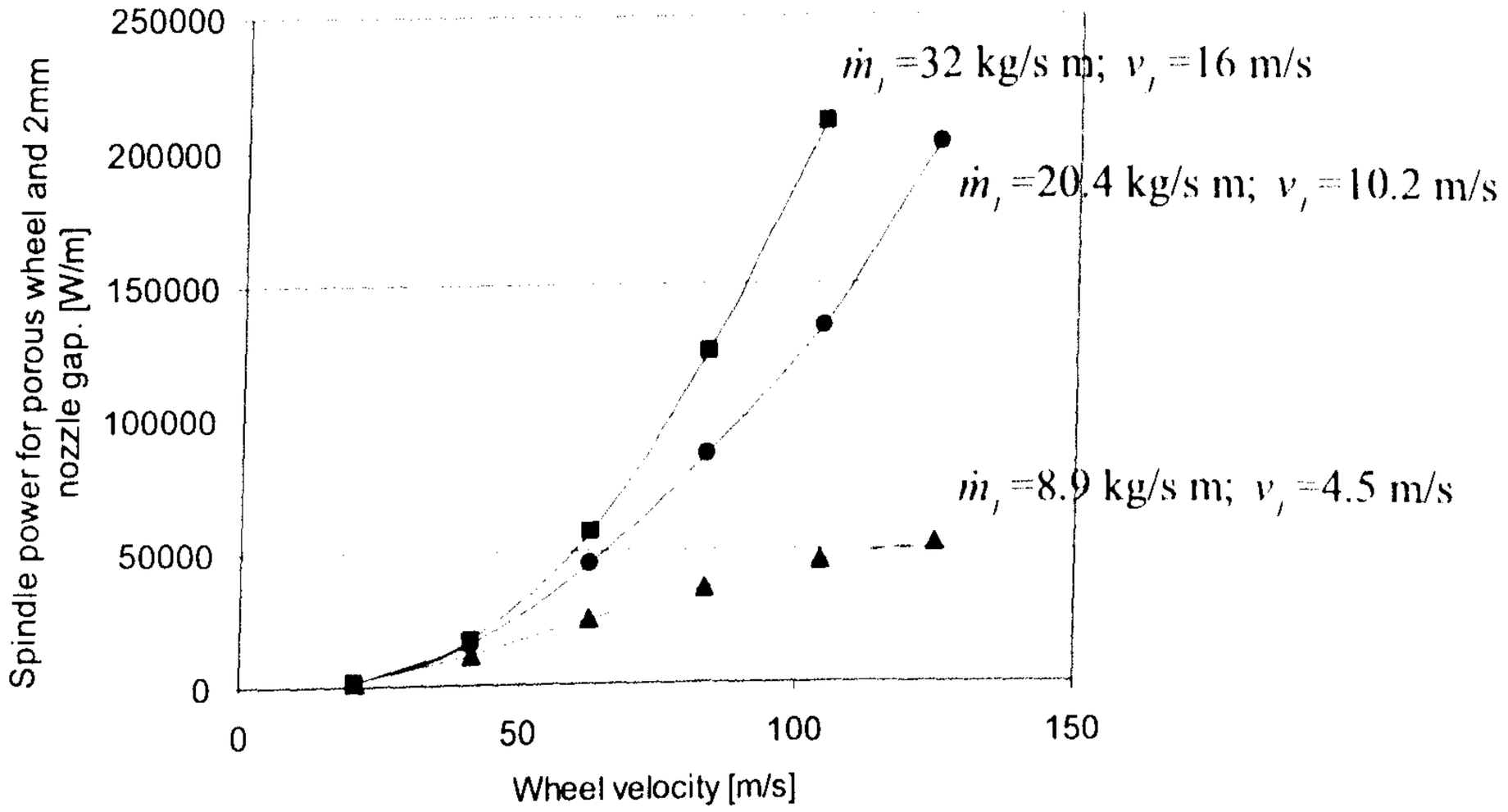

Figure 68. The effect of wheel velocity on spindle power consumed due to fluid for the porous CBN grinding wheel with a 2mm gap nozzle *(Line of best fit)*.

In spite of the lowest jet velocities and largest jet flowrates from this nozzle, maximum spindle power is limited by increasing jet velocity as shown in Figure 69.

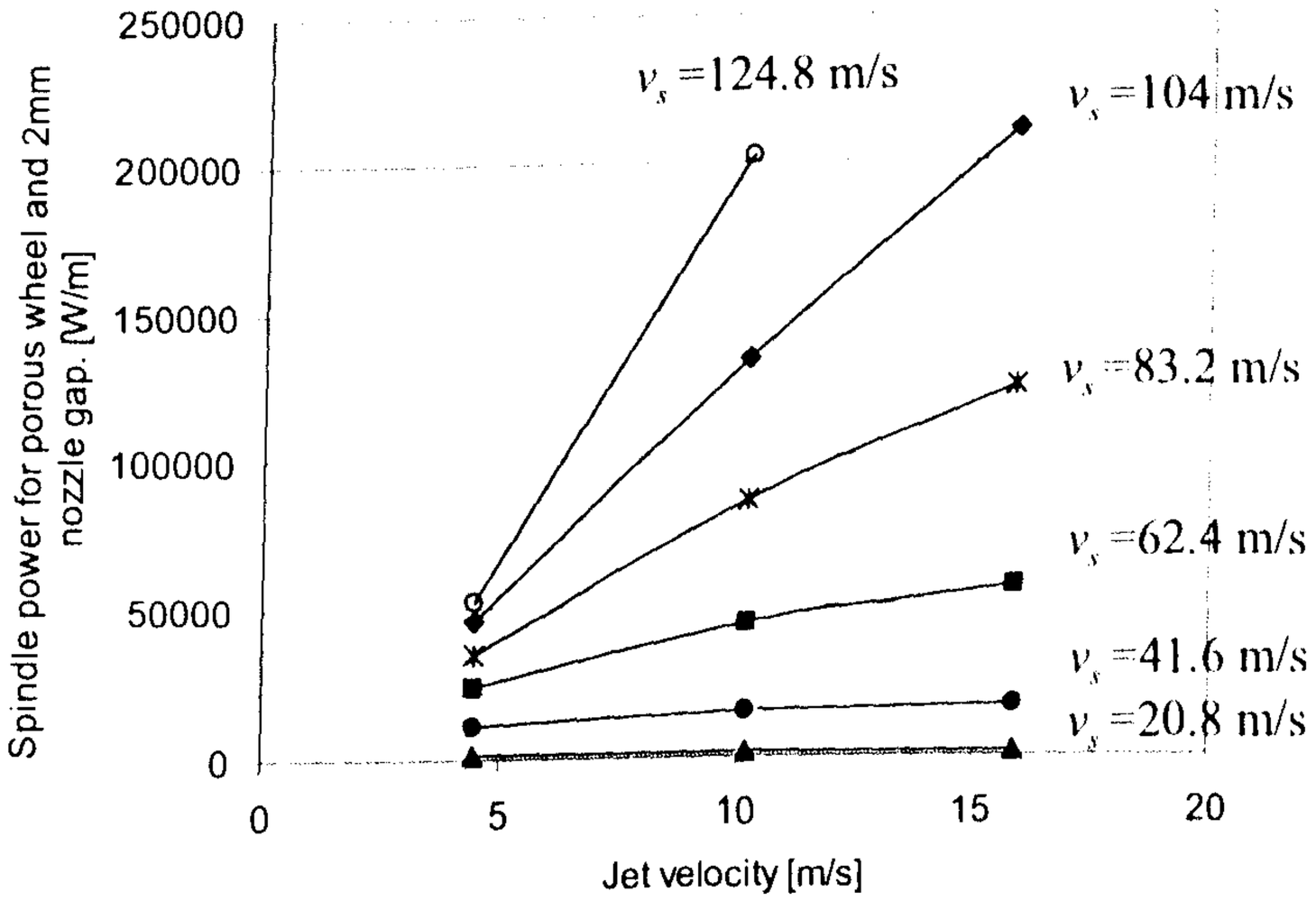

Figure 69. The effect of jet velocity on spindle power consumed due to fluid for the porous CBN grinding wheel with a 2mm gap nozzle *(Line of best fit)*.

Figure 70 shows that the 2mm nozzle does not significantly affect the spindle power due to low jet velocity.

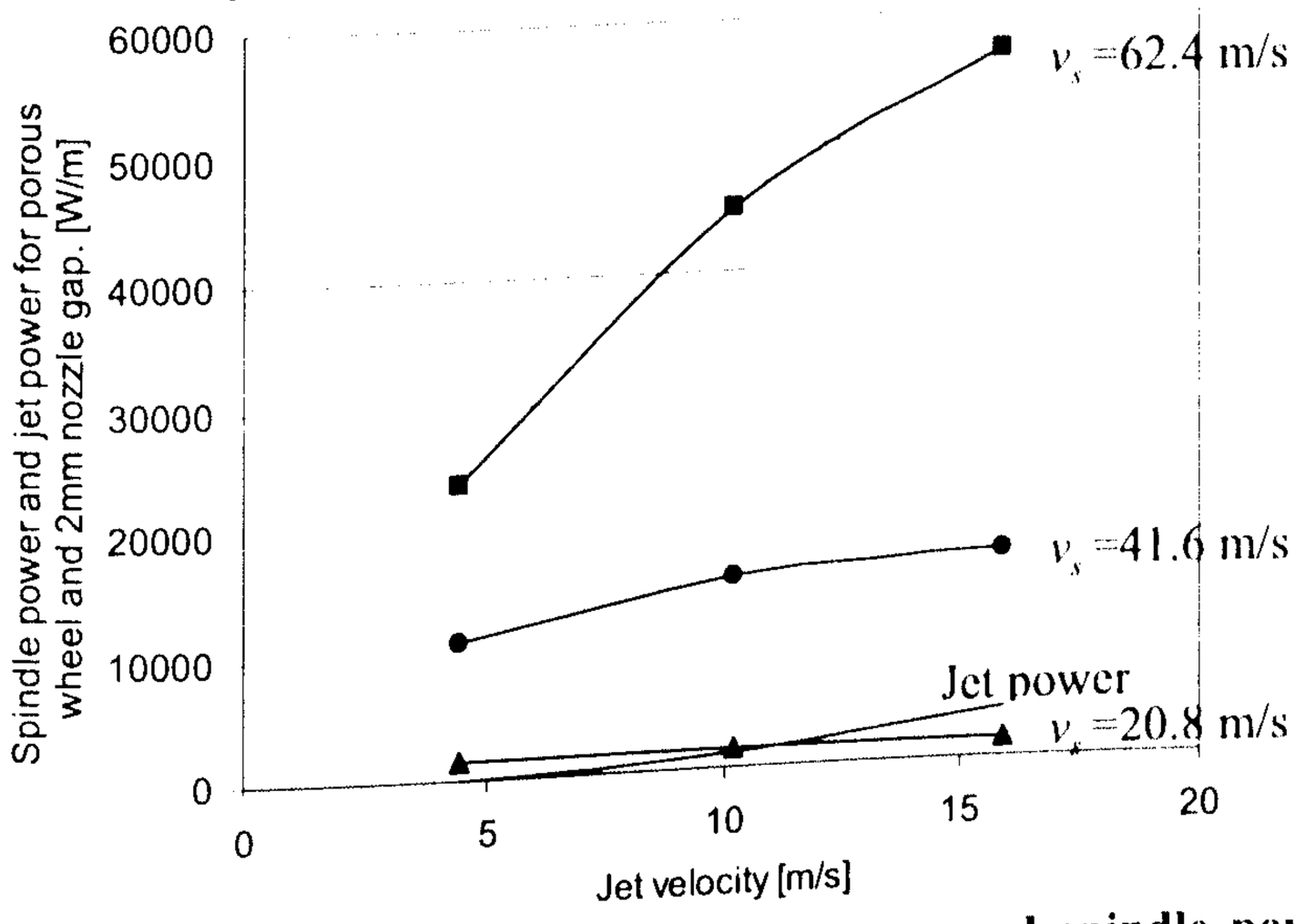

Figure 70. Relationship between jet power and spindle power consumed due to fluid for the porous CBN wheel with a 2mm gap nozzle *(Line of best fit)*.

Figure 71 confirms that the total power consumed due to fluid process, which is spindle power and jet power, can be reduced by reducing the nozzle outlet gap size. This condition is applicable only if the nozzle jet is directed tangentially towards the wheel periphery.

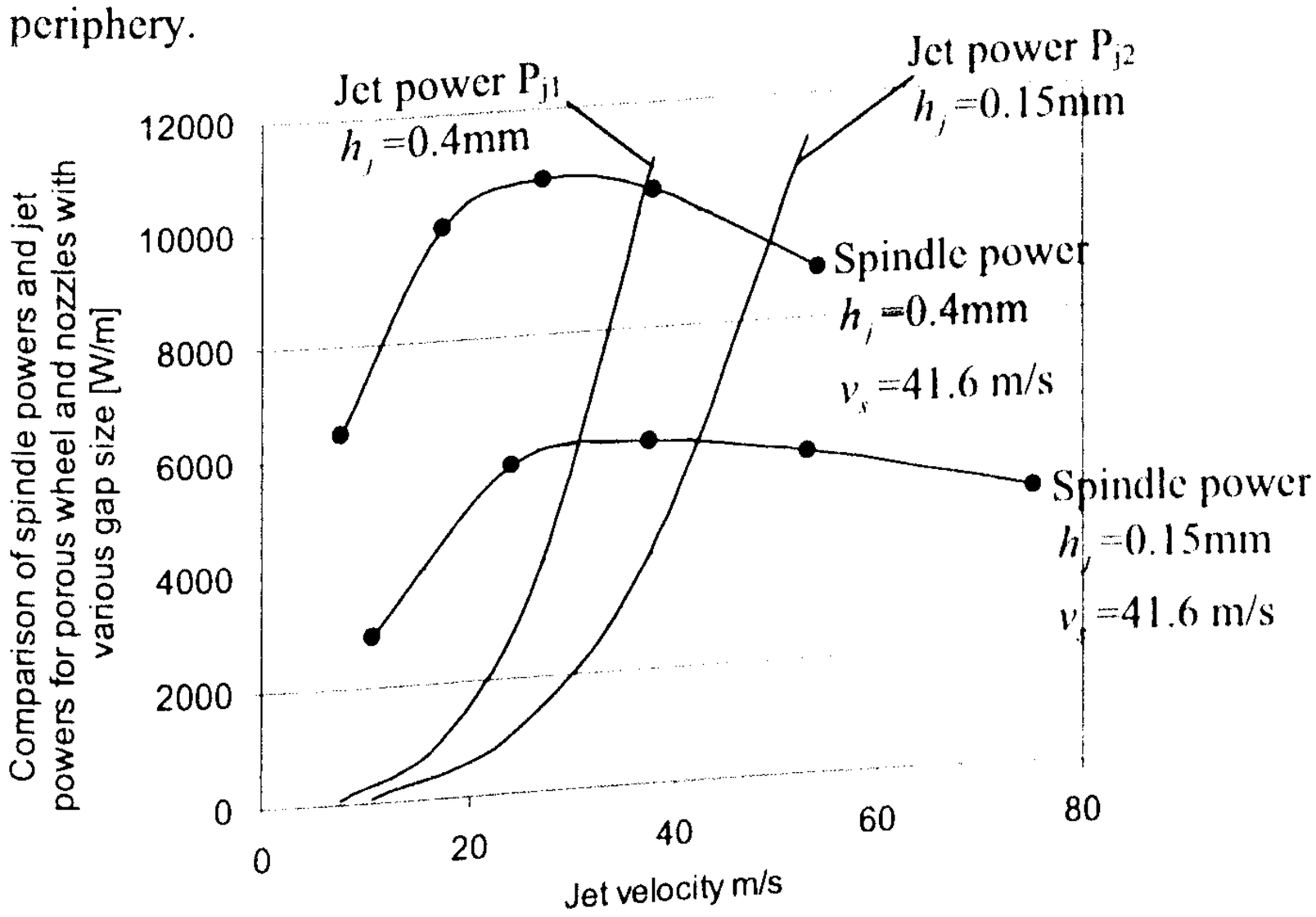

Figure 71. The effect of nozzle gap size on jet power and spindle power consumed due to the fluid for the porous CBN grinding wheel *(Line of best fit)*.

Jet power and spindle power for both nozzles are shown in Figure 71. The values of total combined jet and spindle power due to the fluid are compared in Figure 72.

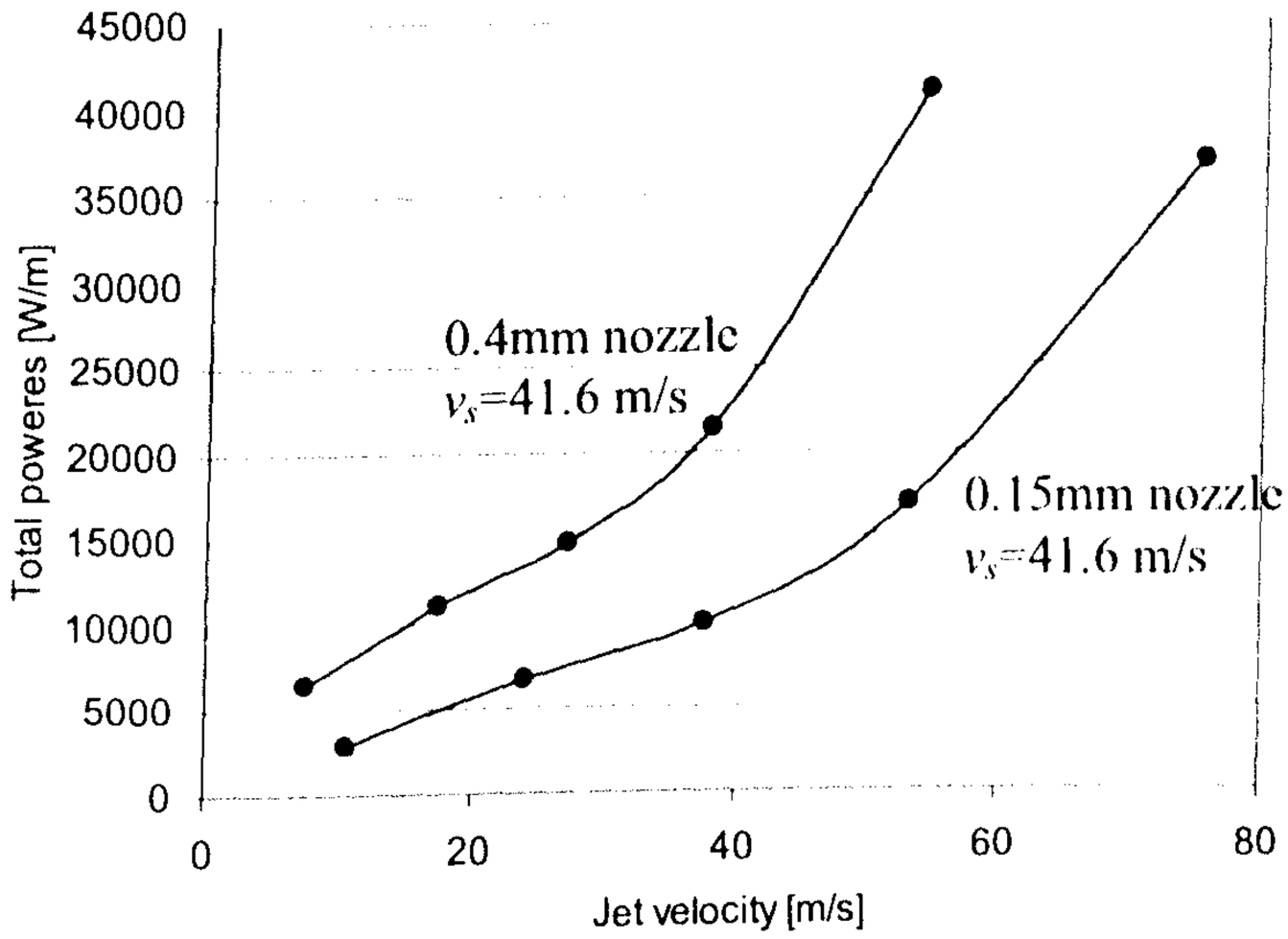

Figure 72. Comparison of total jet power and spindle power for the nozzles with 0.15mm gap and 0.4mm gap and a porous CBN grinding wheel *(Line of best fit)*.

The small size of nozzle gap gives least total power although it should be recalled that this is at the cost of reduced useful flowrate.

5.5 Nozzle Losses.

The next objective is to investigate losses within the nozzle and make suggestions for efficient of the fluid delivery from the nozzle. As discussed previously, the losses in standard pipes, bends and fittings can be estimated from texts on hydraulics. However in non-standard shapes the losses have to be determined individually for every part of the chain within the system. Shape and size of a delivery nozzle vary depending on workpiece shape and on the particular requirements of the grinding process. A simple and accurate approach has been used by considering the energy of the flow at inlet and at outlet of the nozzle. The losses for the range of nozzles of various designs were determined from the difference between these energies. Fluid pressure at the nozzle inlet and the flowrate through the nozzle were measured. After measuring the cross sectional areas of the nozzle inlet and outlet, the fluid velocities were also determined. These data were substituted into Equation 44 for calculation of power loss within the nozzle. This is regarded as the experimental power loss. Total power and the loss within a nozzle having a long thin slot is shown in

Figure 73. A schematic drawing of the nozzle is shown in Figure 91.

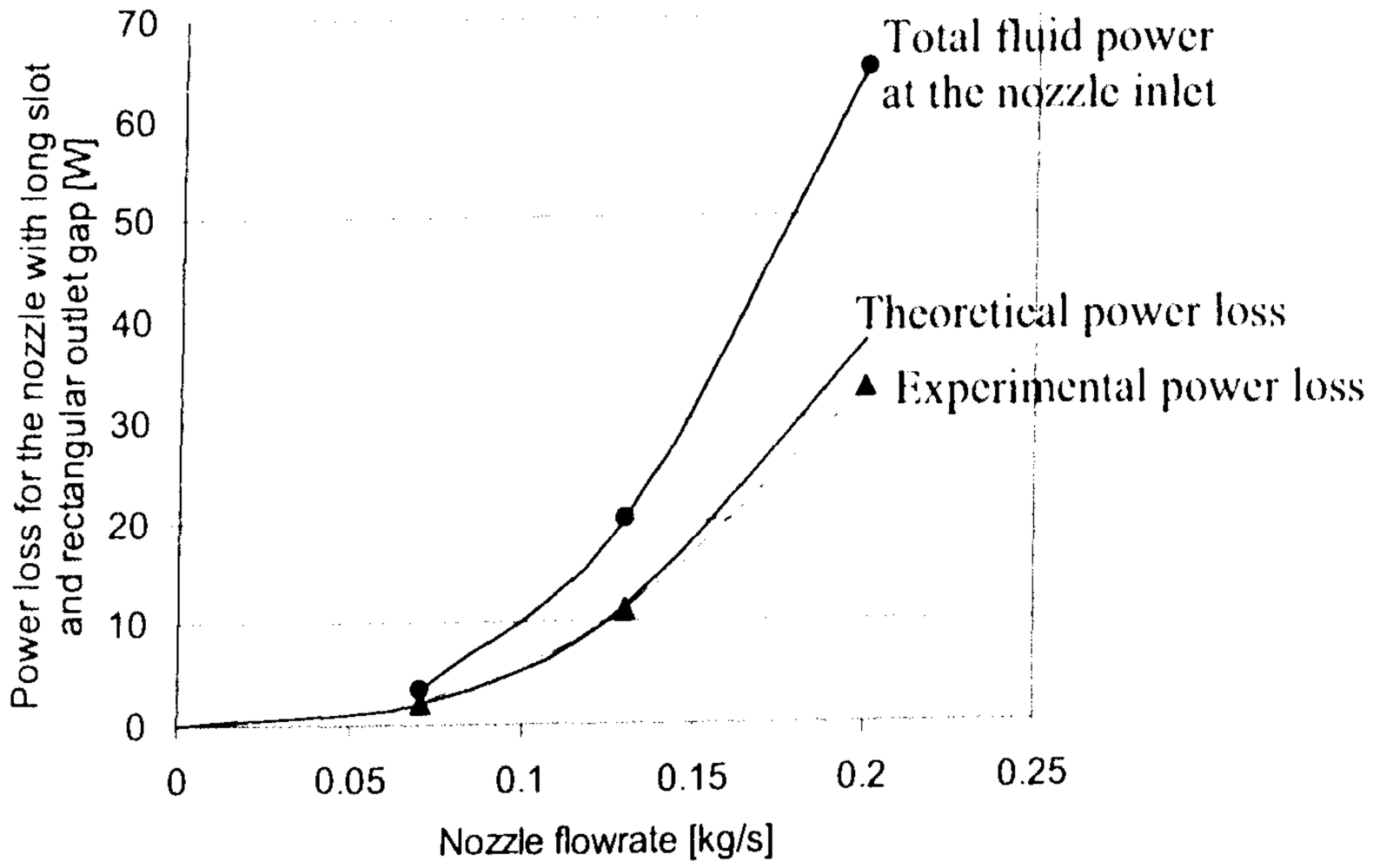

Figure 73. Theoretical and experimental power loss compared with total fluid power at the inlet of a long slot nozzle having a rectangular outlet gap *(Line of best fit)*.

Total power of the fluid was determined from the sum of kinetic and pressure energies per unit time at nozzle inlet. Theoretical power loss is shown together with experimental power loss. In order to estimate the loss, the nozzle was divided into three elementary sections. The first section comprised the pipe attached to the second section of rectangular shape, which carried fluid into the third section having a long thin rectangular gap. The frictional loss was calculated individually for every section. In addition, the loss due to expansion between the first and second sections was calculated. The loss due to the contraction between the second and the third sections was also calculated. The calculated losses were summed to give the total theoretical power loss. Although this method allows loss estimation without undertaking experimental measurements, it cannot always give satisfactory results because of the complexity of the fluid flow within the nozzle. From Figure 73 it can be seen that the fluid jet possesses reduced power because of the power loss within the nozzle. Jet power is the difference between the total power and the power loss.

Total power, together with experimental and theoretical power losses are shown in Figure 74 for the nozzle with a gradual contraction of 23° and rectangular outlet gap. A schematic drawing of the nozzle is shown in Figure 92.

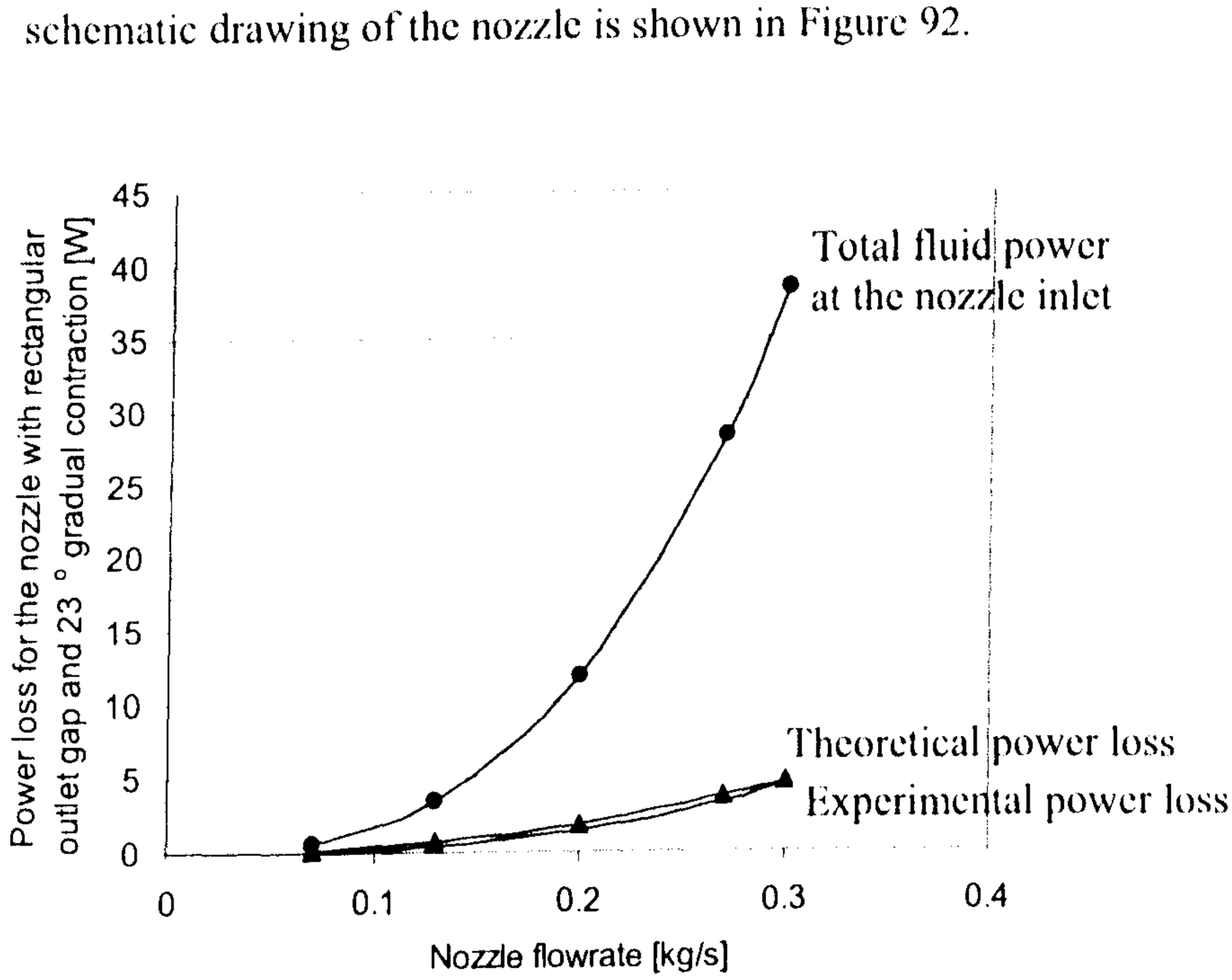

Figure 74. Theoretical and experimental power losses together with total fluid power at the inlet of a nozzle having a rectangular outlet gap and a 23° gradual contraction *(Line of best fit)*.

Total power, experimental and theoretical power losses are plotted in Figure 75 for the nozzle with a gradual contraction of 13° and a rectangular outlet gap. A schematic drawing of the nozzle is shown in Figure 93.

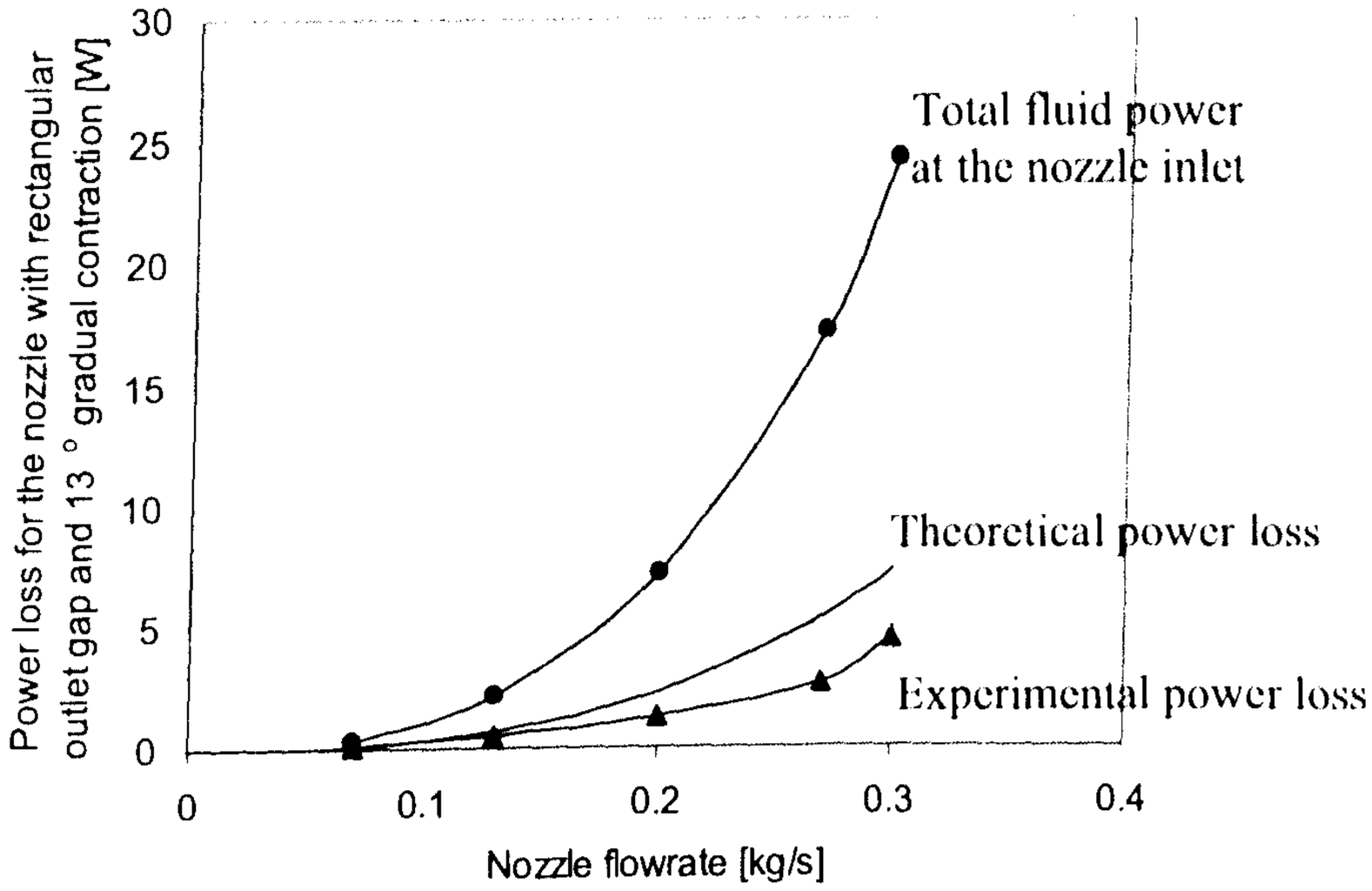

Figure 75. Theoretical and experimental power losses together with total fluid power at the inlet of the nozzle having a rectangular outlet gap and 13° gradual contraction *(Line of best fit)*.

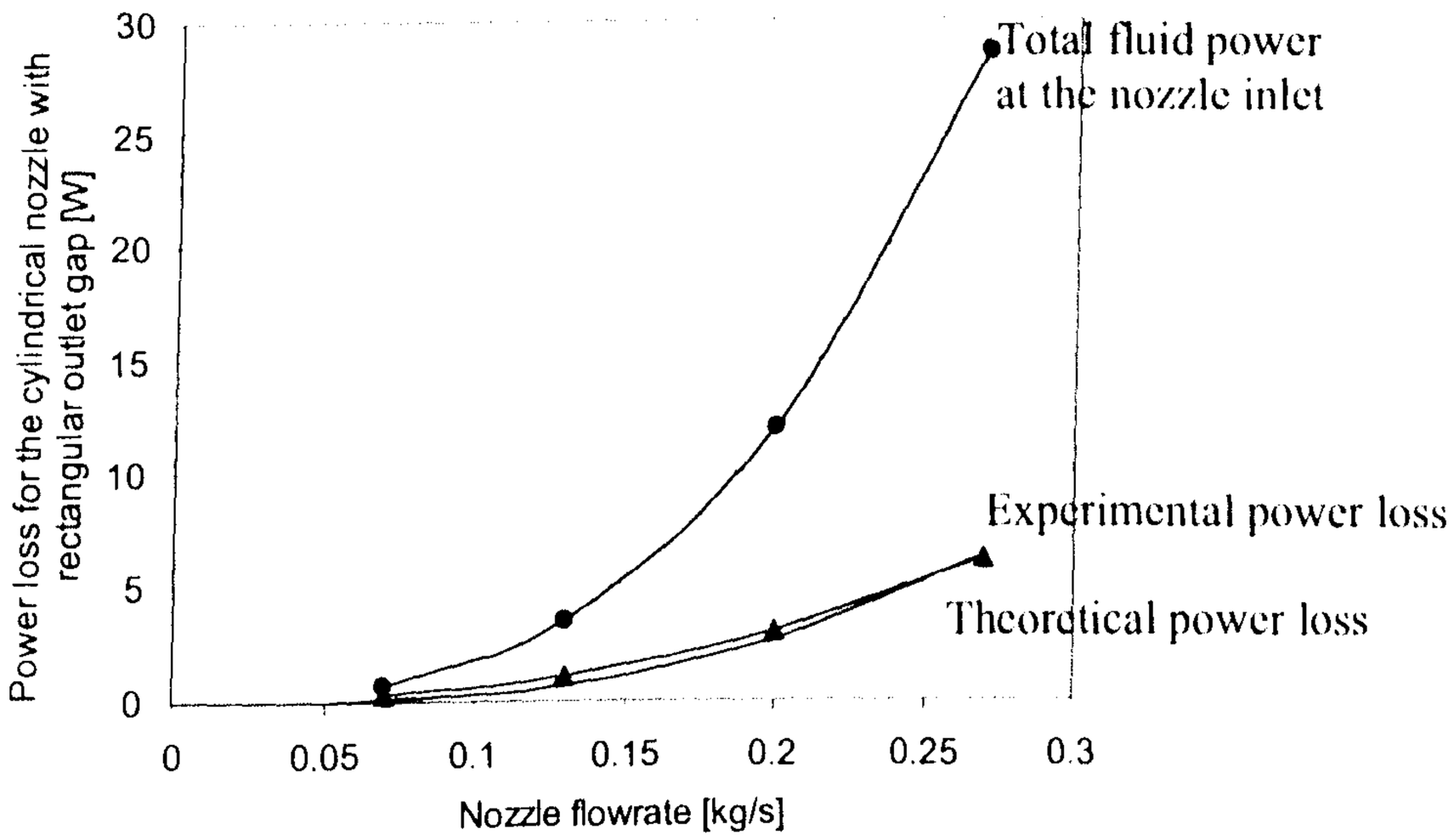

Figure 76. Theoretical and experimental power losses together with total fluid power at the inlet of a cylindrical nozzle having a rectangular outlet gap *(Line of best fit)*.

Total power, experimental and theoretical power losses are plotted in Figure 76 for the cylindrical nozzle having a rectangular outlet gap. A schematic drawing of the nozzle is shown in Figure 94.

The total power and power losses for a cylindrical nozzle with an orifice outlet are shown in Figure 77. A schematic drawing of the nozzle is shown in Figure 95.

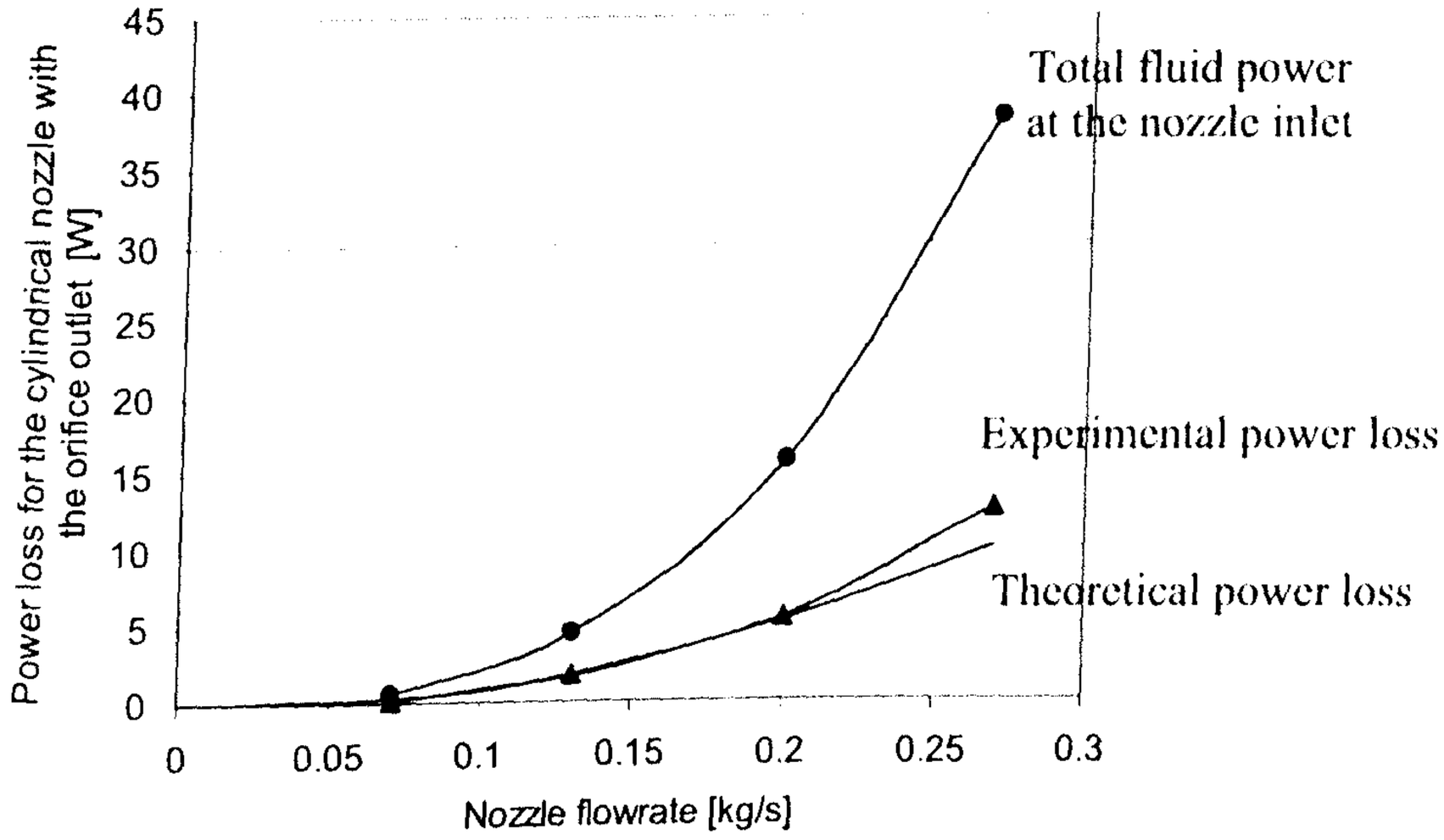

Figure 77. Theoretical and experimental power losses plotted together with total fluid power at the inlet of the cylindrical nozzle having an orifice outlet *(Line of best fit).*

Experiments were conducted to validate Equation 57 for power loss calculation within a gradual contraction. A conical nozzle was manufactured having one section with a 5° gradual contraction. Pressure was measured just before the tapered shape. Flowrate through the nozzle was measured. Experimental power loss and power loss calculated from Equation 57 are plotted in Figure 78. The large discrepancy between these losses suggests that the total loss within the nozzle consists not only of the frictional loss defined by the theoretical method but of losses caused by other effects. It is assumed that the additional loss within the nozzle is caused by turbulence and recirculation of the fluid flow. This additional disturbance of the flow is assumed to be created by the contracted shape of the nozzle walls, which causes swirling motion of the fluid. Extra

motion of the fluid consumes additional energy, which results in reduction of the fluid energy as it passes through the nozzle.

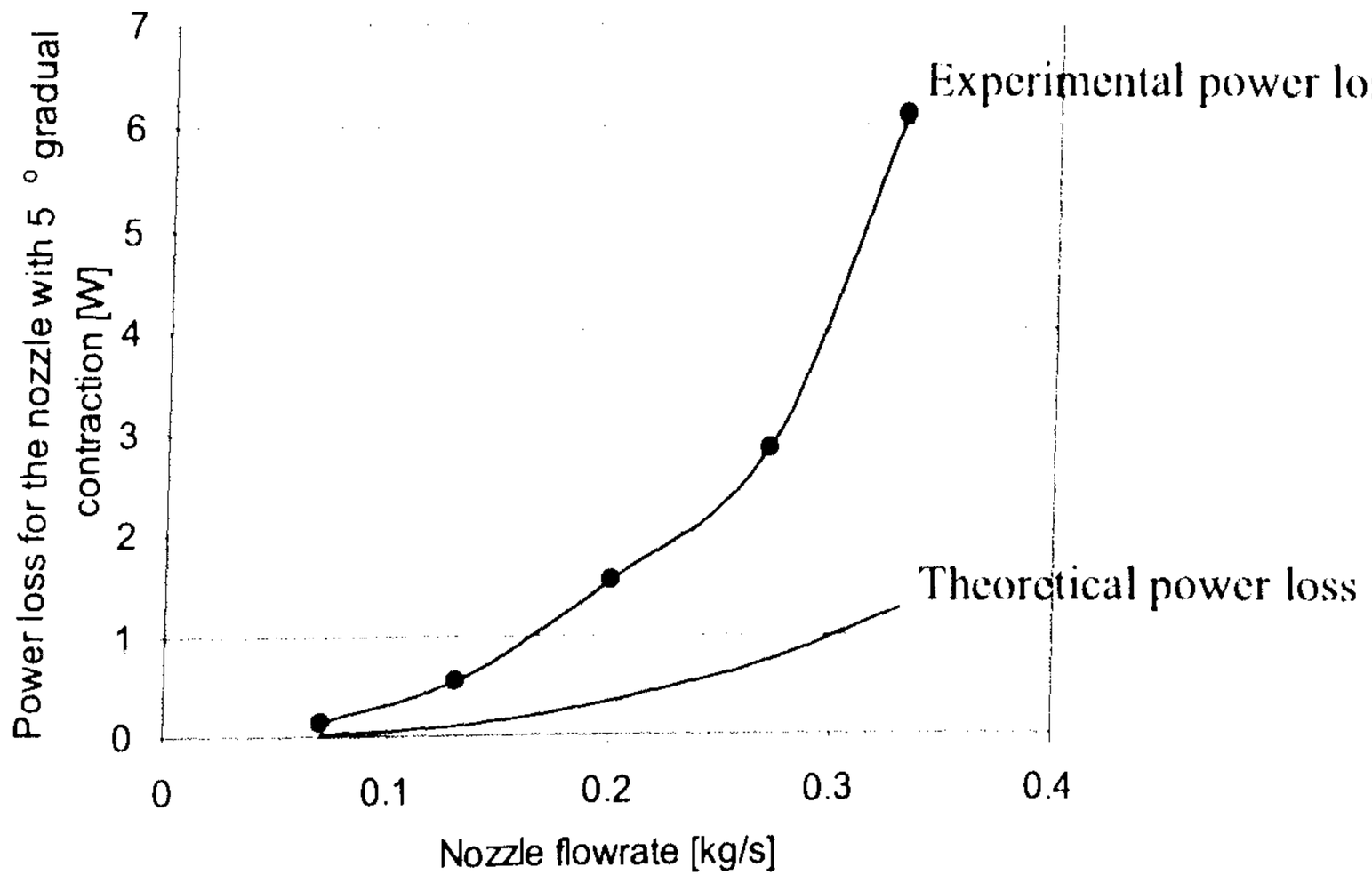

Figure 78. Comparison of theoretical estimated power loss with experimental power loss for a nozzle having a 5^{o} angle of gradual contraction *(Line of best fit)*.

Similar results for the nozzle with 10^{o} gradual contraction are presented in Figure 79.

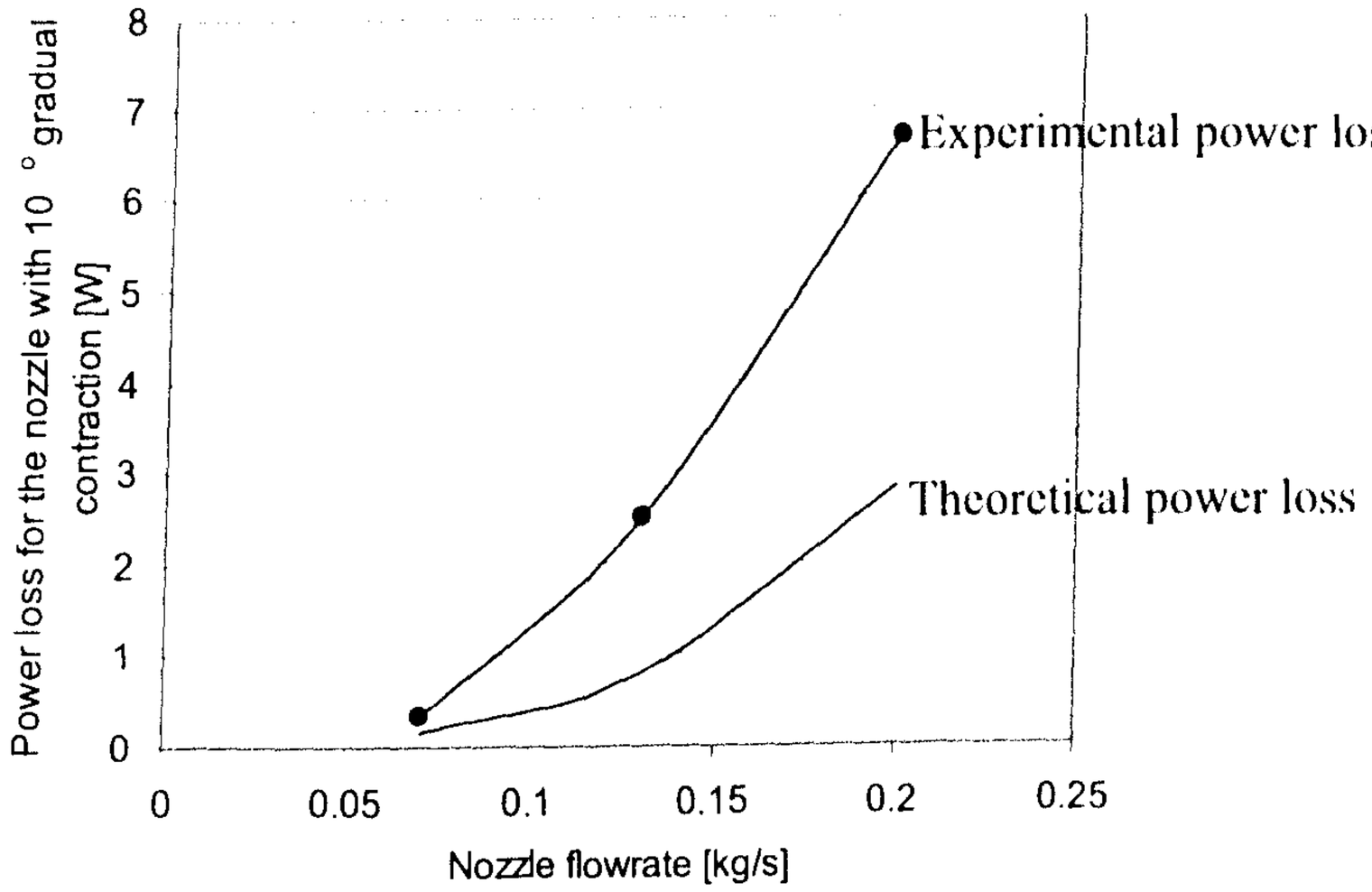

Figure 79. Comparison of theoretical power loss with experimental power loss for a nozzle having 10^{o} angle of gradual contraction *(Line of best fit)*.

Theoretical losses along the nozzle with gradual contraction of 5° were calculated along the nozzle using expressions similar to Equation 57 and plotted in Figure 80.

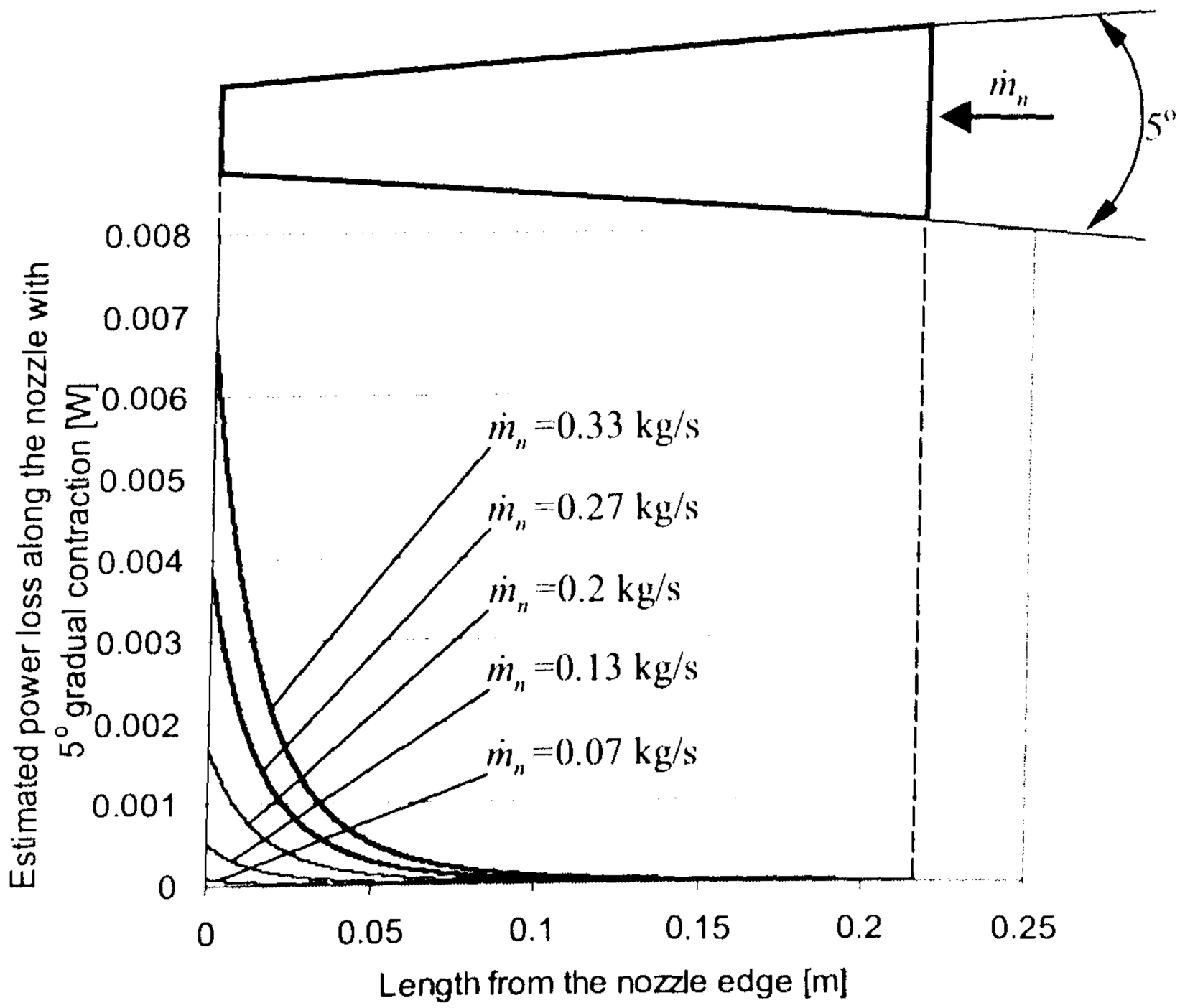

Figure 80. Theoretical estimated power loss along the nozzle having 5° angle of gradual contraction.

From Figure 80 it can be seen that the loss exponentially increases depending on nozzle flowrate and nozzle cross sectional area. This means according to the method that most of the losses occur at the minimum cross sectional area where the fluid velocity is high. In order to prove this experimentally the nozzle was sectioned into six pieces. Losses were determined individually for every piece. For this reason the loss within the whole nozzle was determined similar to the experimental methods described above. Then one piece was cut off the nozzle. Loss for the remaining nozzle was then determined. The difference between these losses gave the loss within this section. The same procedure was repeated for the remaining parts of the nozzle. Schematic illustration of the pieces and the experimental loss within these pieces are shown in Figure 81.

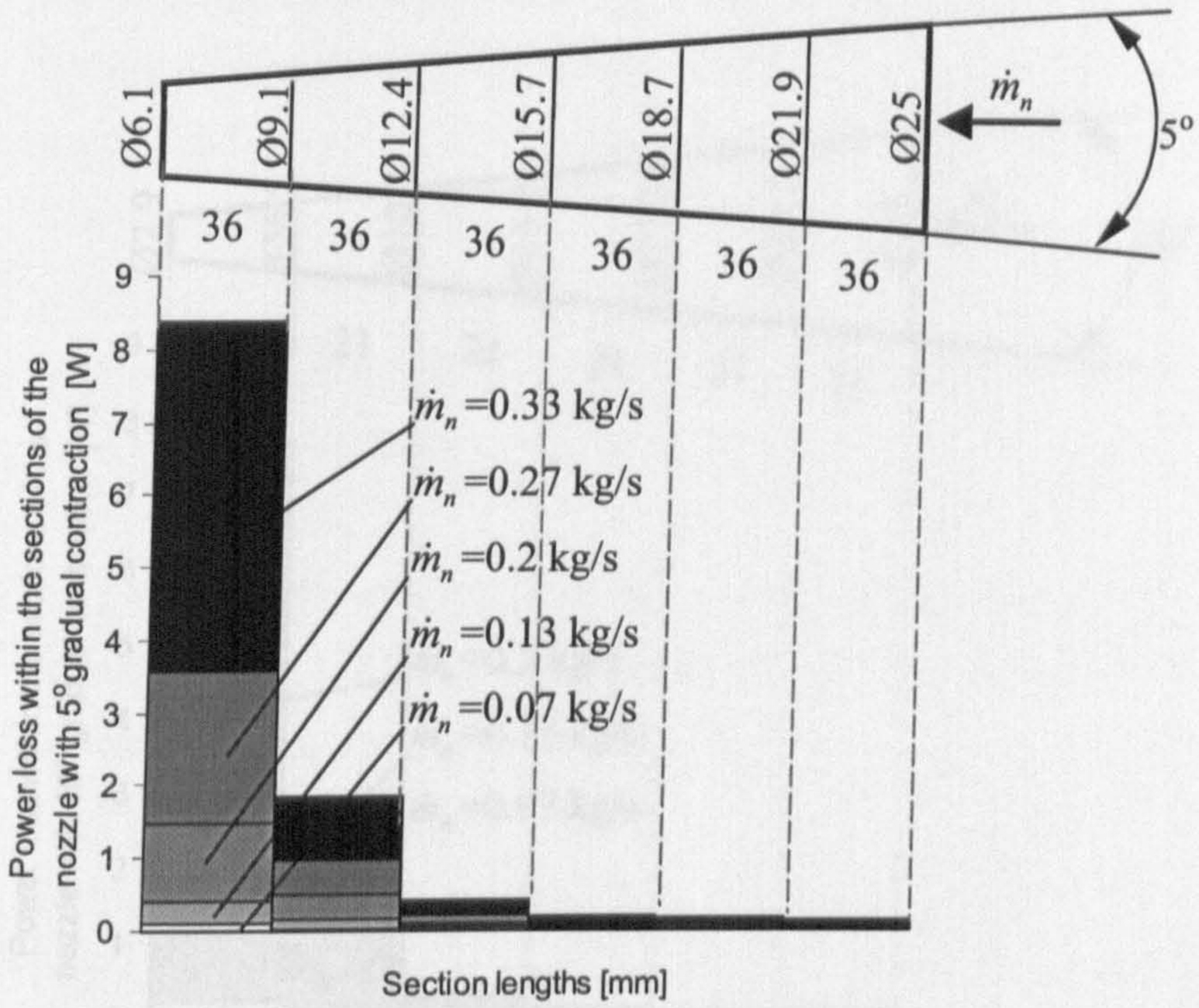

Figure 81. Experimental power loss within the sections along the nozzle having 5° angle of gradual contraction.

It can be seen that the losses calculated from the theoretical method are identical to the losses determined from the experiments. The experimental chart shows the sum of the losses along the section of 36mm length, whereas the theoretical method defines the loss on an infinitely small length. The described method shows the partial solution to the problem for loss calculation within the section of the nozzle having a gradual contraction. However nozzles may have concave, convex or other contracted shapes. This does not allow a similar approach to be used to the problem due to the flow complexity inside the nozzle.

Similar experiments were conducted for the nozzle with 10° gradual contraction. The results are shown in Figure 82. The measurements for this nozzle were discontinued after the maximum nozzle flowrate achievable due to the power limitation of the fluid delivery system.

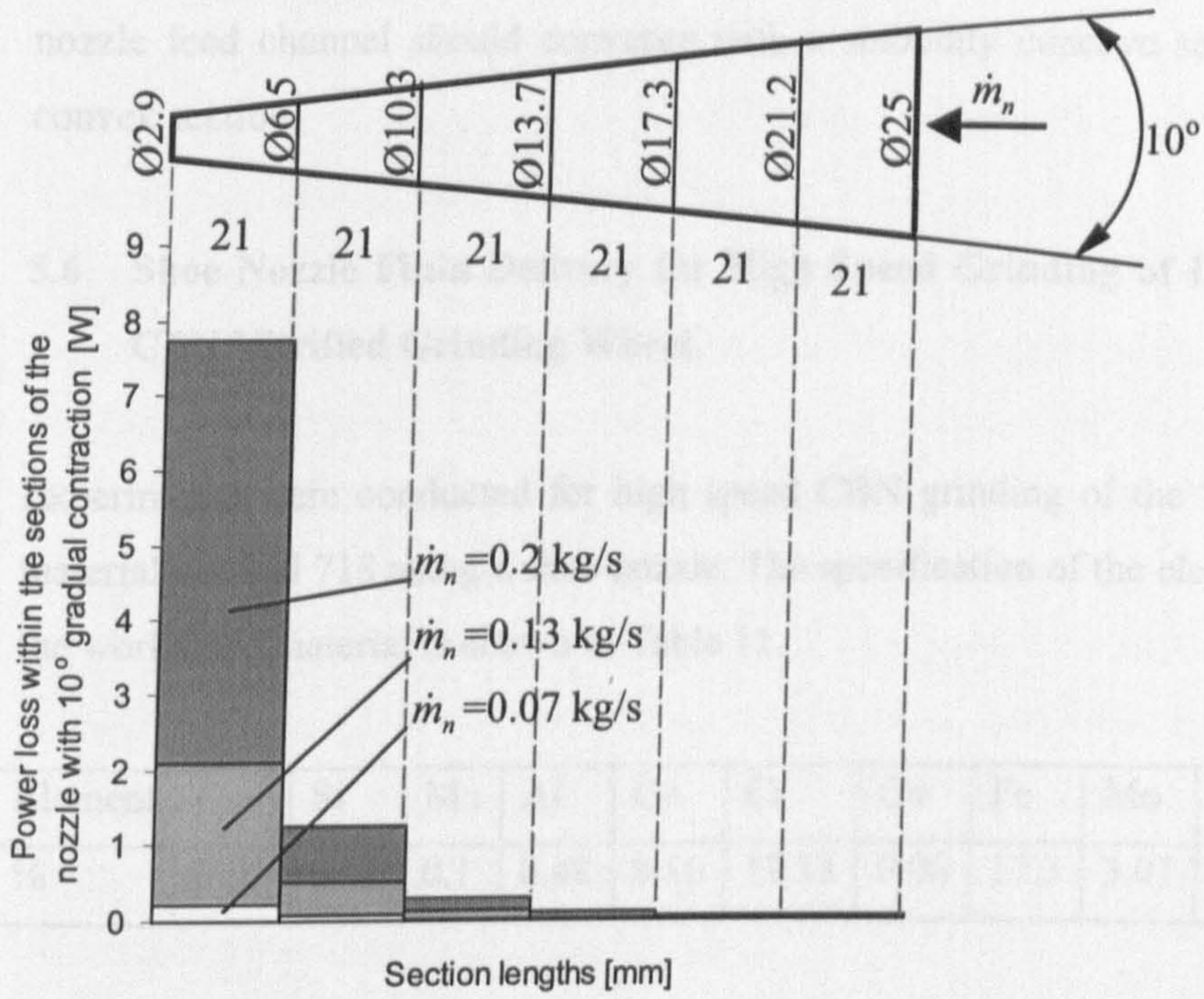

Figure 82. Experimental power loss within the sections along the nozzle having 10° angle of gradual contraction.

Comparing all the nozzles, generally it can be seen that the small size of cross sectional area of the nozzle and the fluid velocity through the nozzle are the main factors in nozzle design that cause high energy loss. Of course it is assumed that inner walls of the nozzle are smooth and the fluid properties are constant. The nozzle with the thinnest and longest slot gave the highest power loss in comparison to other nozzles at equal nozzle flowrate. This is caused because high flowrate through the nozzle produces high fluid velocity, which results in exponential increase in frictional loss. In contradiction of this, the thinnest outlet gap from the nozzle gave the best performance in terms of flowrate through the grinding zone. Therefore it is necessary to formulate an optimal solution to the problem taking into account both aspects including loss minimisation within the nozzle and fluid flow requirements in the wheel-workpiece interface. For this reason it is recommended to design the nozzle with an outlet gap size to produce the required jet velocity and jet flowrate, whereas the other part of the nozzle has to have as large a cross sectional area as possible without sharp transition from one shape to another. The

fluid supply channel to the nozzle and the rest of the system must also satisfy the same requirements to minimise the total power consumed due to the whole fluid process for the grinding operation. Following the design guidance of Webster [51], the internal nozzle feed channel should converge with a smoothly concave section rather than a convex section.

5.6 Shoe Nozzle Fluid Delivery for High Speed Grinding of Inconel 718 with a CBN Vitrified Grinding Wheel.

Experiments were conducted for high speed CBN grinding of the "difficult to grind" material Inconel 718 using a shoe nozzle. The specification of the elements contained in the workpiece material is shown in Table 11.

Element	C	Si	Mn	Al	Co	Cr	Cu	Fe	Mo	Nb	Ni	Ti
%	0.03	0.12	0.1	0.48	0.16	19.13	0.06	17.3	3.01	5.18	53.54	0.94

Table 11. Elements of Inconel 718.

The aim of the experiment was to investigate the effect of delivery fluid minimisation on grinding performance for the particular example using a shoe nozzle. Unfortunately, it was not possible to relate grinding performance to useful flowrate for this application due to the impossibility of incorporating a useful flowrate rig into the cylindrical grinding set-up for this operation. This example was chosen to be of relevance to the project funding and to demonstrate effects of fluid minimisation on grinding performance. The requirement included investigation of power demand by the whole process, specific energy, the workpiece temperature, size holding, roughness, roundness and workpiece hardness.

Eight specimens comprising five diameters were ground at various nozzle flowrates. Flowrate was reduced gradually for each specimen. Average values of experimental results from five diameters were determined. Results are presented in terms of flowrate and power per unit width of the wheel. The comparison of total power with the spindle power required to accelerate fluid within the shoe nozzle are shown in Figure 83. The

total power is the sum of grinding power, power required for the fluid acceleration through the grinding zone and fluid power consumption due to the shoe nozzle. Power consumption due to the shoe nozzle includes fluid power at the nozzle inlet and spindle power consumed due to the fluid acceleration within the shoe. The fluid power at nozzle inlet is the sum of pressure energy per unit time and the fluid kinetic energy per unit time. Fluid power at nozzle inlet was negligible in comparison to the spindle power. The fluid pressure at nozzle inlet was nearly atmospheric since the fluid is pumped from the delivery pipe into the shoe nozzle by the grinding wheel rotating at a high speed. Most of the fluid power demand for the shoe nozzle consists of the spindle power due to fluid acceleration within the shoe, which depends on the mass flowrate accelerated. The pumping power is necessary only for overcoming losses within the supply system in order to deliver fluid to the shoe nozzle inlet. From Figure 83 it can be seen that spindle power consumed due to the shoe nozzle tends to be reduced with reduction of delivery flowrate. This also results in a relatively small reduction of total power. However very low nozzle flowrate caused an increase in total power, which is attributed to insufficient lubrication and cooling in the grinding zone.

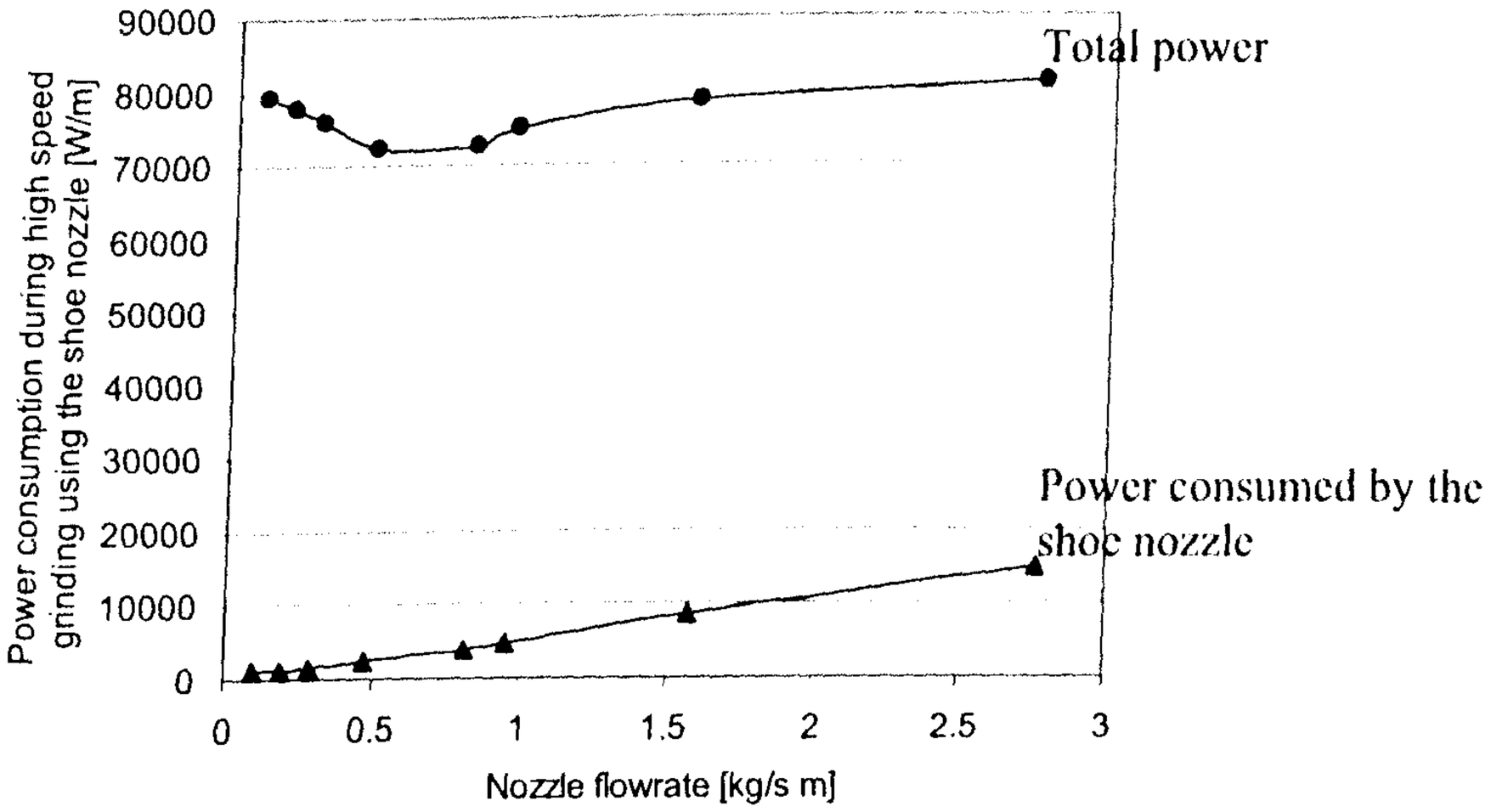

Figure 83. Power consumption in high speed CBN grinding of Inconel 718 using the shoe nozzle *(Line of best fit)*.

Accordingly, this also results in increase of specific energy shown in Figure 84, which is defined as grinding power in per unit volume of material removed. Grinding power is the cutting power of the material without fluid.

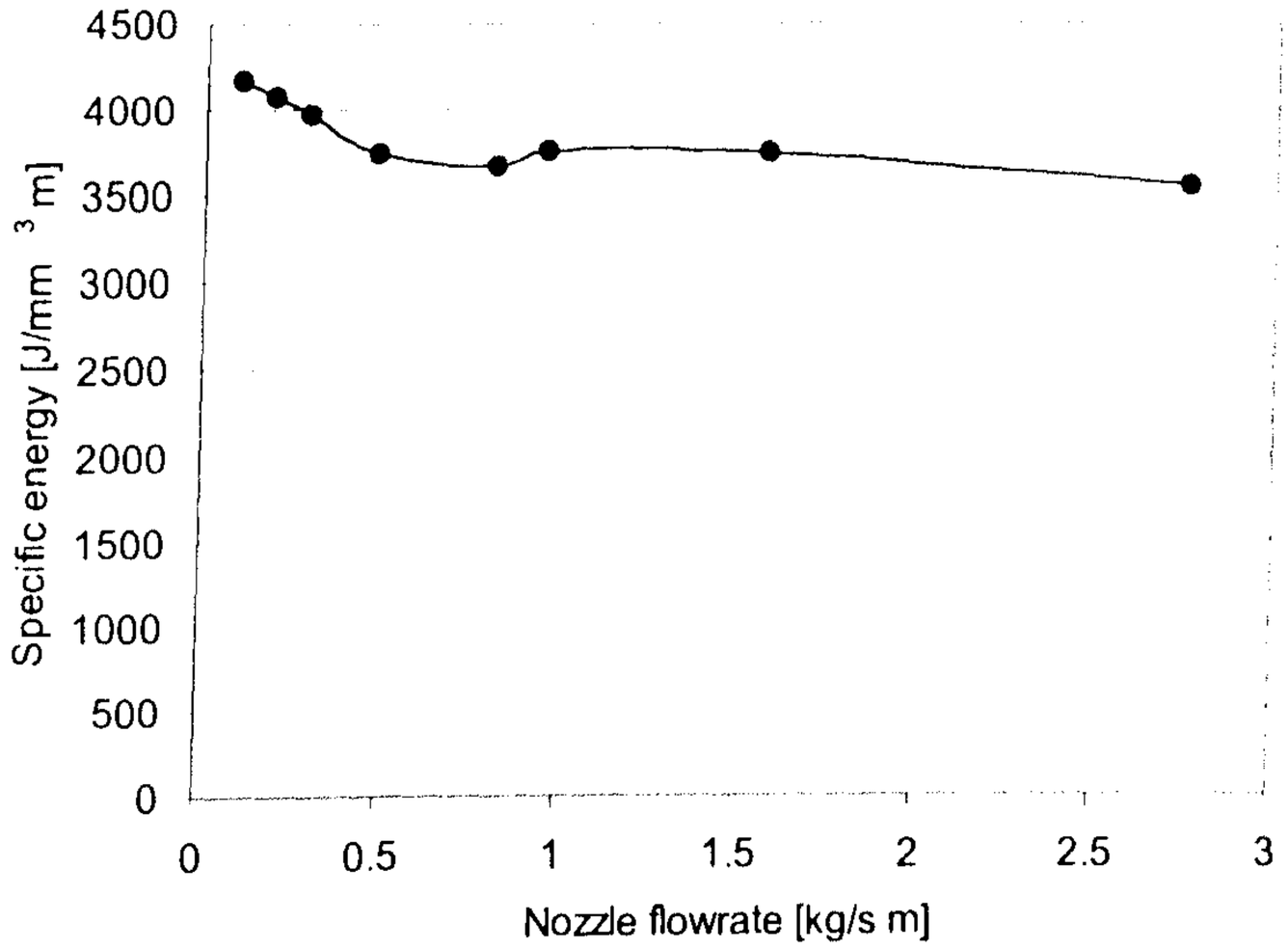

Figure 84. Specific energy during high speed CBN grinding of Inconel 718 using the shoe nozzle *(Line of best fit)*.

Figure 85 shows that the reduction of nozzle flowrate did not significantly affect the workpiece temperature until a particular point was reached. However after this point the dramatic rise of temperature is observed especially beyond the boiling temperature of the grinding fluid, which is of the order of 100 °C or slightly higher.

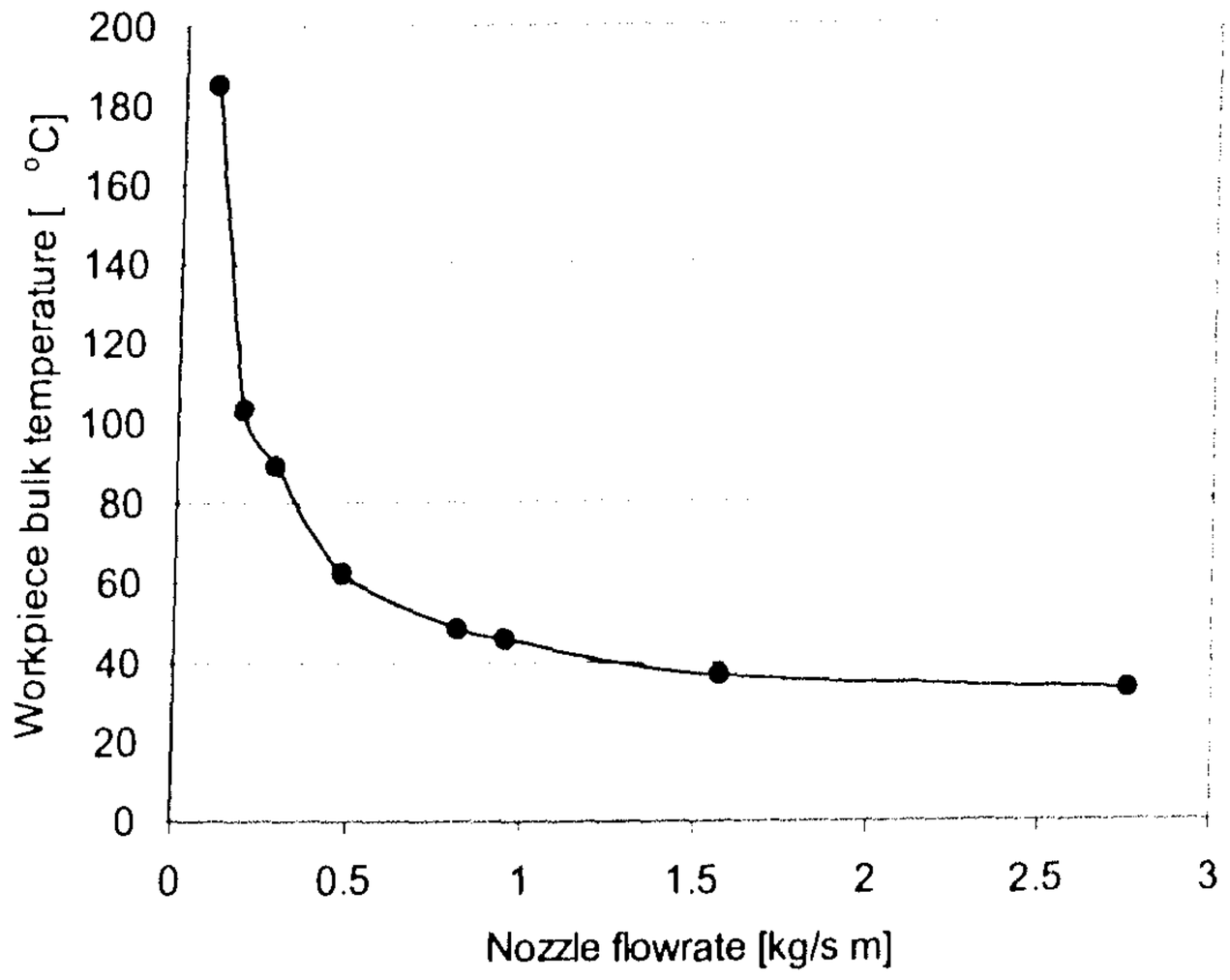

Figure 85. Bulk temperature of the workpiece during high speed CBN grinding of Inconel 718 using the shoe nozzle *(Line of best fit)*.

Increase in temperature resulted in expansion of the workpiece diameter. This caused deviation in the size of ground parts, which is shown in Figure 86. The diameter of the first workpiece was set as zero. The difference in subsequent diameters gave scatter from the first value.

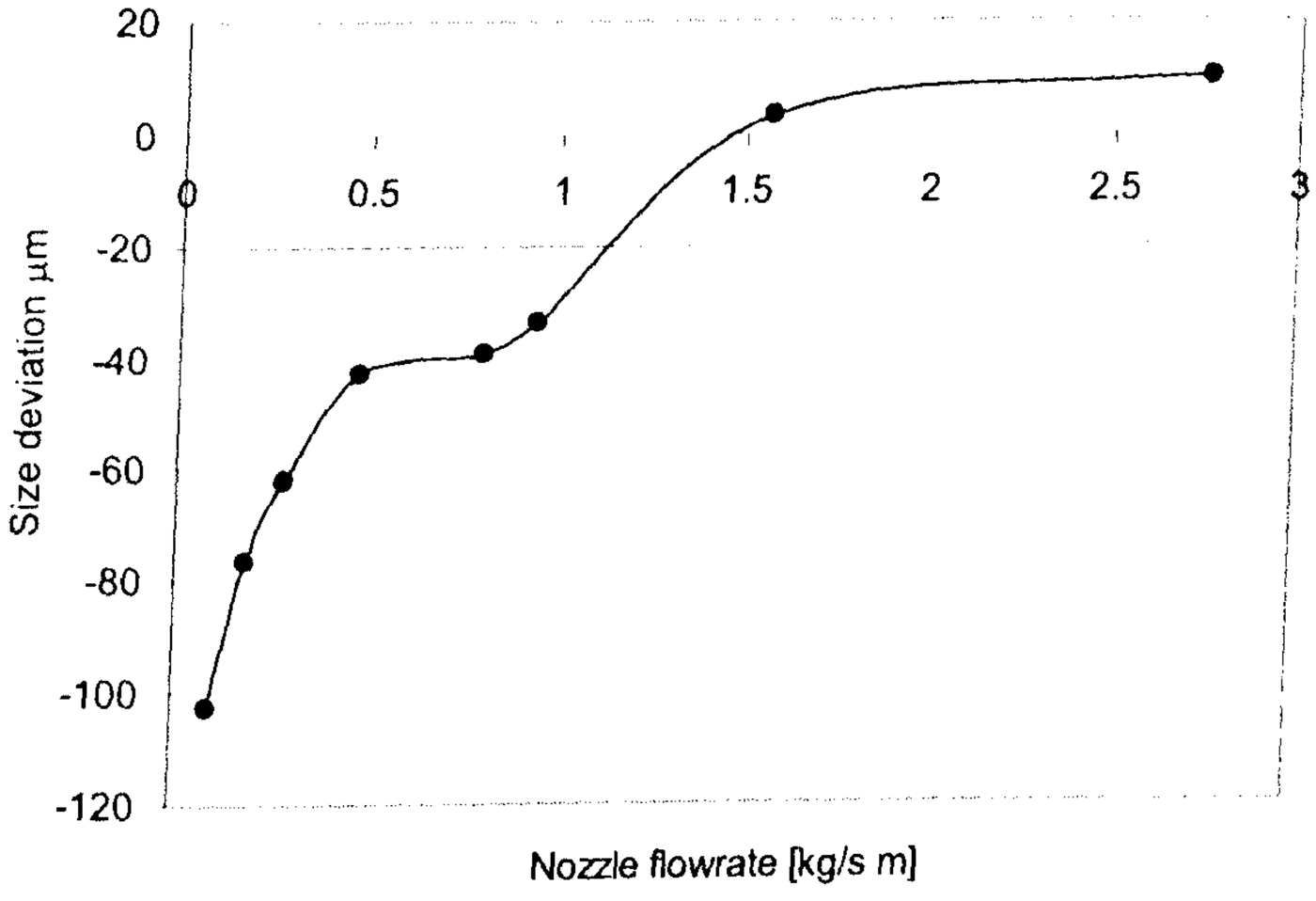

Figure 86. Size deviation of the workpiece after high speed CBN grinding of Inconel 718 using the shoe nozzle *(Line of best fit)*.

As a result of insufficient fluid in the contact zone, rapid wheel loading was observed which is shown in Figure 103. This occurred at a delivery flowrate of approximately 0.5 kg/sm. Insufficient fluid in the grinding zone also resulted in increase of the workpiece roundness errors as illustrated in Figure 87.

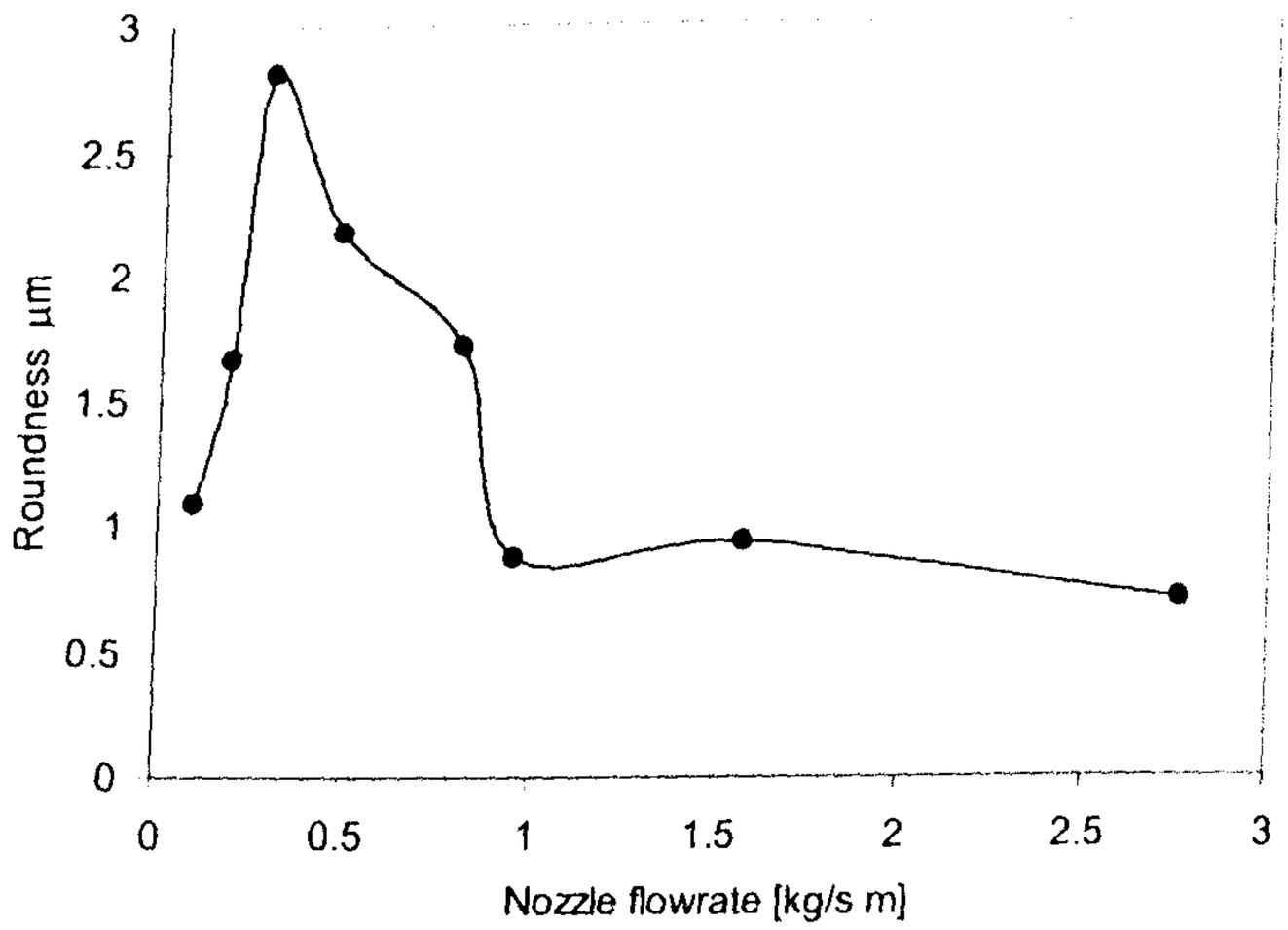

Figure 87. Workpiece roundness after high speed CBN grinding of Inconel 718 using the shoe nozzle *(Line of best fit)*.

In Figure 88 it can be seen that reduction in nozzle flowrate did not significantly affect the workpiece surface roughness after the grinding. However better results tended to be achieved at higher nozzle flowrates.

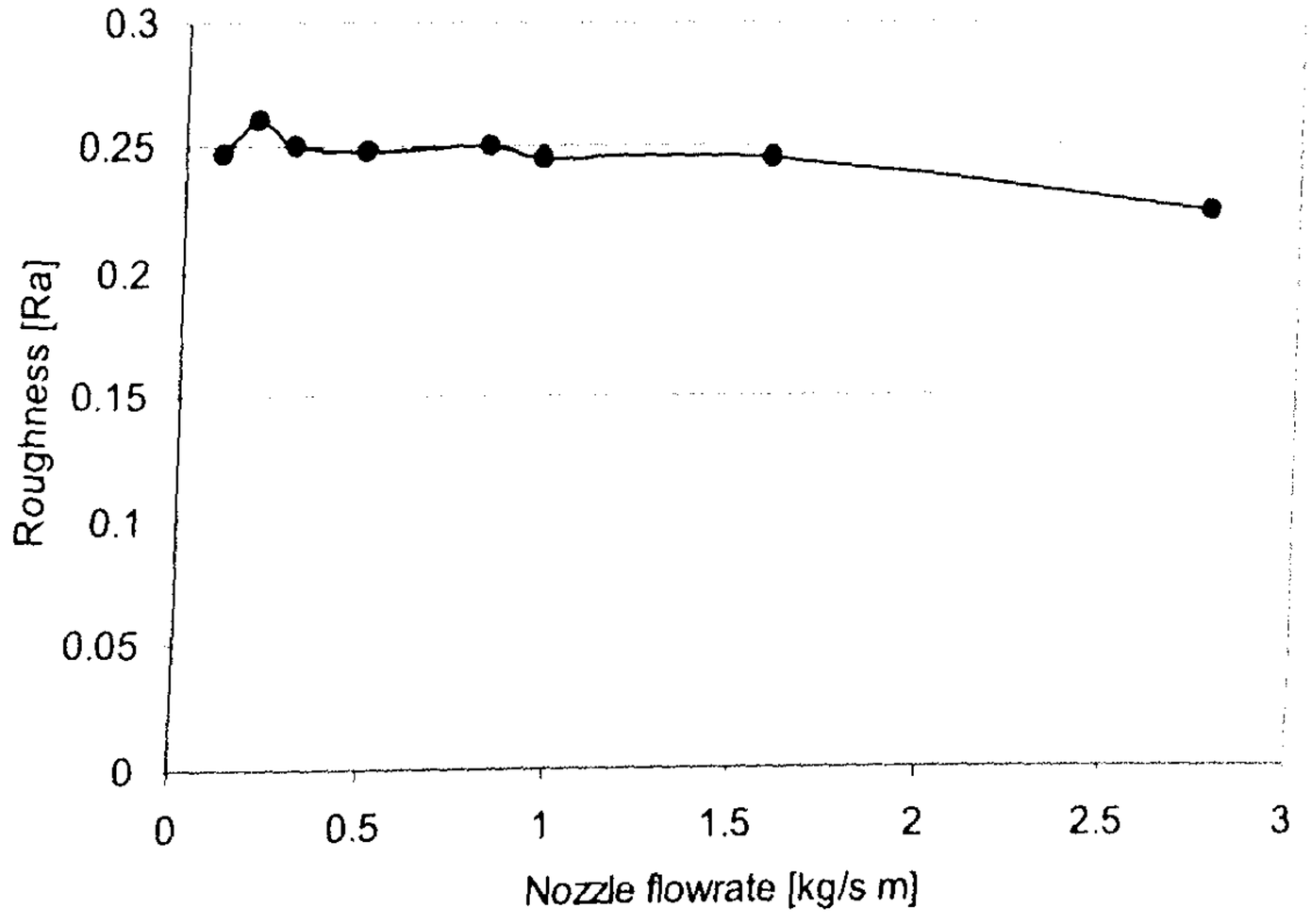

Figure 88. Workpiece roughness after high speed CBN grinding of Inconel 718 using the shoe nozzle *(Line of best fit)*.

The workpiece was sectioned to allow measurement of the hardness from the ground surface towards the workpiece centre. Hardness was measured for the last five diameters of the seven ground specimens. The average values of hardness across the workpiece depth was plotted in the chart, since insignificant change was observed. The results are shown in Figure 89.

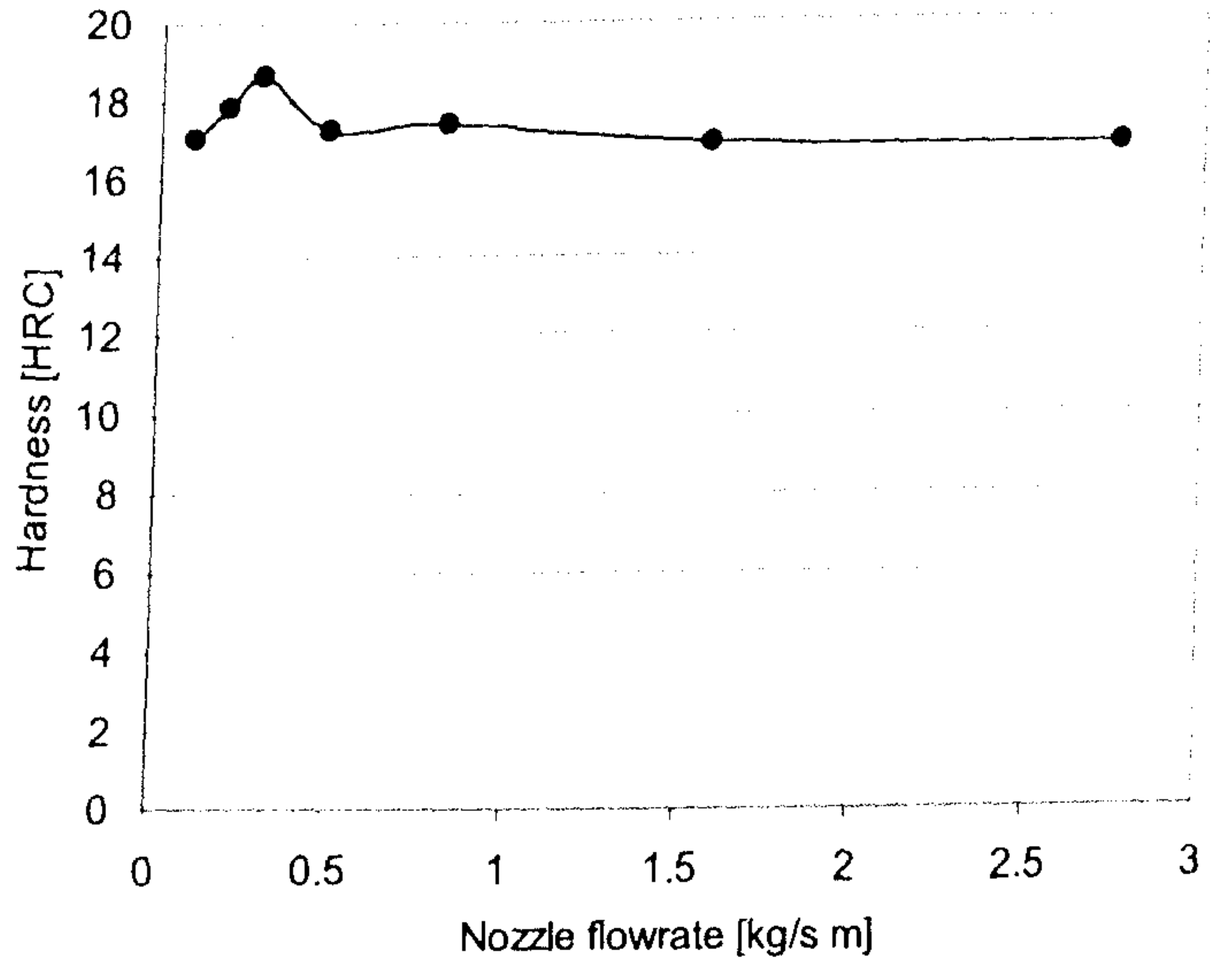

Figure 89. Workpiece hardness after high speed CBN grinding of Inconel 718 using the shoe nozzle *(Line of best fit)*.

Insignificant variation in hardness with workpiece depth can be considered due to the property of the ground material containing high temperature resistant metals such as nickel.

It has been shown that high speed CBN grinding of a "difficult to grind" temperature resistant material can be performed at low delivery flowrate using a correctly designed shoe nozzle. A shoe nozzle minimises power consumption for the whole grinding operation, reduces total cost and improves environmental conditions of the work place. However there is a critical nozzle flowrate after which catastrophic rise of temperature and workpiece damage becomes more likely. Therefore, caution has to be taken to avoid delivery flowrate minimisation below a sufficient quantity essential for the high performance of the grinding operation.

CHAPTER 6. CONCLUSIONS.

Simple and widely applicable models have been developed for useful flowrate through the wheel-workpiece interface. The models relate power, contact pressure between wheel and workpiece, wheel speed, nozzle flowrate, jet velocity, jet power and the required nozzle outlet gap. The models are appropriate for non-porous wheels as well as for high or low porosity wheels. Matching spindle power and fluid delivery power with nozzle jet velocity matched to wheel speed roughly maximises useful flowrate and prevents the total power requirement related to the fluid from becoming excessive. This condition is considered optimal in terms of power requirements for the fluid process.

An optimum jet nozzle should have an outlet gap size to achieve the required jet velocity and jet flowrate. The internal nozzle feed to the outlet gap should have a large cross sectional area with slow shape variation. The fluid supply channel to the nozzle and the rest of the system must also follow these requirements. The following particular conclusions were reached:

1. Insufficient flowrate leads to higher workpiece temperatures and may ultimately lead to thermal damage. Within this limit, it is possible to grind with minimum quantity lubrication as demonstrated in the high-speed CBN grinding of Inconel 718.
2. Useful flowrate is usually much less than supply flowrate. Optimisation of jet nozzle positioning and fluid delivery allows the utilisation ratio to be increased and the following further conclusions to be reached.
3. The energy required to achieve a required useful flowrate using a jet nozzle can be minimised by directing the flow tangentially to the wheel surface with a nozzle positioned close to the grinding contact.
4. Useful flowrate through the grinding contact using jet delivery may be related to spindle power for fluid acceleration by a simple mathematical model. A further model allows useful flowrate to be related to maximum fluid pressure in the contact.
5. Useful flowrate tends to increase with jet velocity and jet flowrate.
6. A small jet nozzle gap gives higher efficiency in the sense of achieving the highest ratio of useful flowrate to delivery jet flowrate. However, the magnitude

of the useful flowrate can be small in comparison to the useful flowrate with a larger gap size.

7. A jet nozzle with a smaller gap size produces a higher jet velocity and lower spindle power. However the nozzle gap thickness should be large enough to satisfy the requirements for a sufficient grinding fluid in the contact zone.

8. Minimum nozzle gap thickness for maximum useful flowrate can be achieved by specifying a nozzle gap thickness according to the required fluid film thickness.

9. Spindle power reaches a maximum when the jet power is approximately equal to the spindle power due to the fluid process. Increasing jet power further reduces spindle power but requires disproportionately increasing jet power.

10. For an impervious wheel, the maximum useful flowrate is always less than the theoretical maximum useful flowrate based on wheel pore size. With sufficient jet flowrate, the maximum useful flowrate practically achievable tends to be approached as jet speed approaches wheelspeed.

11. For a porous wheel, it is possible to exceed the maximum useful flowrate based on the surface porosity of the wheel. This value, termed the optimal useful flowrate, is achievable without undue difficulty or excessive energy to pressurise fluid into the sub-surface of the wheel. With sufficient jet flowrate, the optimal useful flowrate is approached as jet velocity approaches wheel velocity.

12. A shoe nozzle can be very efficient in delivering flowrate with minimum pumping energy loss. However, spindle power is increased compared to jet delivery. At higher wheel speeds, the advantages of jet delivery allow larger values of useful flowrate to be achieved.

13. Losses within the nozzle can be estimated from standard techniques used in hydraulics except non-standard shapes having complex fluid flow. Examples are the shapes having various types of gradual contraction. However, the loss within any nozzle design can be accurately determined from the difference between the fluid energies before and after the nozzle. The shape of the nozzle should be designed to minimise losses.

14. The above conclusions form the basis for optimisation of a jet delivery system.

CHAPTER 7. FUTURE WORK.

The predicted theory show good agreement with the experiments for the range of conditions used during the research. This agreement implies the range of applicability of the empirical coefficients determined from experiment. The broader application of the models requires the loss coefficients to be defined for extended grinding situations.

The proposed equation for the gradual contraction determines only part of the loss within the contracted shape. An investigation is needed in order to predict theoretically the entire loss within such a shape.

Insufficient time was available to investigate fully the application of shoe grinding. Further research is necessary to investigate the utilisation ratio in shoe grinding. Further work is necessary to compare shoe nozzle effectiveness on useful flowrate at a range of wheelspeeds delivery flowrates.

Although the results allow optimisation of fluid delivery systems for useful flow rate in grinding, it does not completely solve all problems in this area. Particularly, there is still a problem of workpiece thermal damage in grinding due to high grinding speed and high removal rates. This sets new requirements for the development of a fluid delivery system to achieve high performance in the grinding operation.

REFERENCES.

[1] **Wagner H. W.,** (1950), "Grinding Fluids, Characteristics and Applications" Annual Meeting, New York, November 26 – December 1, American Society of Mechanical Engineers, pp. 128-132.

[2] **Outwater J. O. and M. C. Shaw,** (1952), "Surface Temperatures in Grinding", Transactions ASME, Vol. 74, pp. 73 – 86

[3] **Tarasov L. P.,** (1961), "Grinding Fluids, Part 1 – What They Are", June, The Tool and Manufacturing Engineer, pp. 67-73.

[4] **Ueno T., Ishibashi A., A. Katsuki,** (1970), "Experiments on the Cooling Ability of Cutting Fluids", JSME, vol. 13, No. 59, pp. 729 - 736.

[5] **Osman M., Malkin S.,** (1972), "Lubrication by Grinding Fluids at Normal and High Wheel Speeds", ASLE Trans., 15, No 4, pp. 261-268.

[6] **Doyle E. D., Turley D. M.,** (1976), 4th North American Metal Working Research Conference, pp. 346.

[7] **Yasui H., Tsukuda S.,** (1983), "Influence of Fluid Type on Wet Grinding Temperature", Bull. Japan Soc. of Prec. Engg., vol. 17, No. 2, pp 133 – 134.

[8] **Ye N E and Pearce T R A,** (1984), "A Comparison of Oil and Water as Grinding Fluids in the Creep Feed Grinding Process", Proc Instn Mech Engrs, Vol. 198 B, No. 14, pp. 229-237.

[9] **Howes T. D., Neailey K., Harrison A. J.,** (1987), "Fluid Film Boiling in Shallow Grinding", Annals of the CIRP, vol. 36, pt. 1, pp. 223 - 226.

[10] **Howes T.,** (1990), "Assessment of the Cooling and Lubricative Properties of Grinding Fluids", Annals of the CIRP, vol. 39, pt. 1, pp. 313 – 316.

[11] **Warren R De Vries,** (1994), "Tribology at the Cutting Edge: Cutting and Grinding Fluids", ASME, PD-Vol. 61,Tribology Symposium, pp. 23-33

[12] **Yokogawa, M.,** (1996) "Study on Air Jet Cooling Grinding Technology without Using Grinding Fluid for Anti-Pollution Measure", International manufacturing engineering conference, Aug., pp. 132 - 136.

[13] **Baheti U., Guo C., and Malkin S.**, (1998), "Environmentally-Conscious Cooling and Lubrication for Grinding", Proceedings of the International Seminar on Improving Machine Tool Performance; presented at the International Seminar on Improving Machine Tool Performance, San Sebastian, Spain, July 6 - 8. Vol. II, pp. 643 - 654

[14] **Walter A.**, (1999), "Formation of Reaction Layers on Ground Surfaces", 3 rd International Machining & Grinding Conference, October 4-7, Westin Hotel, Cincinnati, Ohio, pp. 45-59.

[15] **Shaji S., Radhakrishnan V.**, (2002), "An investigation on surface grinding using graphite as lubricant", International Journal of Machine tools & Manufacture, vol.42, pt.6, pp. 733 – 740.

[16] **Efimov V. V.,** (1980), "Grinding Fluid Flow in the Wheel Workpiece Contact zone", Russian Engineering Journal, vol. 60, pt. 11, pp. 50 – 51.

[17] **Khudobin I. L.** (1981) "The Dumping Action of Coolants in Grinding" Soviet Engineering Research, vol. 61, pt. 5, pp. 51 – 53.

[18] **Akiyama T., Shibata J., and Yonetsu S.**, (1984), "Behaviour of Grinding Fluid in the Gap of the Contact Area Between a Grinding Wheel and a Workpiece – A Study on Delivery of Grinding Fluid", Proceedings of the 5th International Conference on Production Engineering, Tokyo, pp. 52 - 57.

[19] **Maksoud T. M. A., Howes T. D.,** (1989), "Effect of Hydrodynamic Pressure of High Viscosity Coolants on the Stability of the Surface Grinding Process", In: Grinding Fundamentals and Applications, The Winter Annual Meeting of the ASME, San Francisco, 10 –15 Dec., pp. 183 – 199.

[20] **Schumack M. R., J. B. Chung, Schultz W. W., Kannatey-Asibu E.,** (1991), "Analyses of Fluid Flow Under a Grinding Wheel", Transactions of the ASME, May, vol. 113, pp. 190 – 197.

[21] **Engineer F., Guo C., Malkin S.,** (1992), "Experimental Measurement of Fluid Flow Through the Grinding Zone", ASME, Journal of Engineering for Industry, Feb., vol. 114, pp. 61 – 66.

[22] **Guo C., Malkin S.,** (1992), "Analysis of Fluid Flow Through the Grinding Zone", ASME, Journal for Engineering for Industry, Nov., vol. 114, pp. 427 – 434.

[23] **Guo C., Krishnan N., Malkin S.,** (1993), "Matching Forces and Power in Creep-Feed Grinding", SME, 5th International Grinding Conference, Oct. 26 – 28, Cincinnati, Ohio.

[24] **Brinksmeier E., Minke E.,** (1993), "High-Performance Surface Grinding – The Influence of Coolant on the Abrasive Process", Annals of the CIRP, vol. 42, pt. 1, pp. 367 – 370.

[25] **Okuyama Shigeki, Nakamura Yoshinobu, Kawamura Suehisa,** (1993), "Cooling Action of Grinding Fluid in Shallow Grinding", Int. J. Mach. Tools Manufact., Vol. 33, No. 1, pp. 13 – 23.

[26] **Campbell J.D.,** (1993), "An Investigation of the Grinding Fluid Film Boiling Limitation", 5th International grinding conference, Oct. 26-28, Cincinnati, Ohio.

[27] **Campbell J. D.,** (1995), "Optimised Coolant Application", SME, MR95-211, 1st Int. Machining and Grinding Conference, Sept. 12-14, Dearborn, Michigan, pp. 894 – 904.

[28] **Ganesan M., Guo C., Malkin S.**, (1995), "Measurement of Hydrodynamic Forces in Grinding", Transactions of NAMRI/SME, vol. XXIII, pp. 103 – 107.

[29] **Krishnan N., Guo C., Malkin S.**, (1995), "Fluid Flow Through the Grinding Zone in Creep Feed Grinding", 1st International Machining and Grinding Conference, September 12-14, Dearborn, Michigan, pp. 906 – 916.

[30] **Metzger J.**, (1986), "Superabrasive Grinding, Butterworth Press", ISBN 0-48-01586-1.

[31] **Ebbrell, S. Woolley, N. H. Tridimas, Y. D. Allanson D. R. Rowe, W. B.,** (1997), "An Investigation into Coolant Application in Grinding", Proceedings of the 13th Conference on Manufacturing Results, Sept. 9.-11., published by Tylor & Francis as "Advances un Manufacturing Technology.

[32] **Heinzel C., Brinksmeier E.**, (1998), "Optimierung der Kühlschmierung beim Schleifen durch strömungstechnische Methoden", Proceedings of the 11th international colloquium on Tribology, pp. 151 – 163.

[33] **Klocke F., Baus A., Beck T.**, (2000), "Coolant Induced Forces in CBN High Speed Grinding with Shoe Nozzles", Annals of the CIRP, vol.49, pt. 1, pp. 241 – 244.

[34] **Hryniewicz P., Szeri A. Z., Jahanmir S.**, (2001), "Application of Lubrication Theory to Fluid Flow in Grinding: Part 2 – Influence of Wheel and Surface Roughness", ASME, Journal of Tribology, vol. 123, pp. 101 – 107.

[35] **Ganesan M., Guo C., Rafael R., A., Malkin S.,** (1996), "Analysis of hydrodynamic forces in grinding", Transactions of NAMRI/SME, vol. 23, pp. 105 – 110.

[36] **Cui C.**, (1995), "Experimental Investigation of Thermofluids in the Grinding Zone", PhD Dissertation, University of Connecticut.

[37] **Inasaki, I.,** (1998), "Fluid Film in the Grinding Arc of Contact", Contribution on January-CIRP Meeting, Paris, 27 - 31. January.

[38] **Webster J.**, (2002), "Assessment of Grinding Fluid Effectiveness in Continuous-Dress Creep Feed Grinding", Annals of the CIRP, vol. 51, pt. 1.

[39] **T. Jin, D. J. Stephenson and W. B. Rowe,** (2003), "Estimation of Convection Heat Transfer Coefficient of Coolant within the Grinding Zone", Proc. Instn. Mech. Engrs., vol. 217, part B: J. Engineering Manufacture, pp. 397 – 407.

[40] **Pahlitzsch G.,** (1953), "Features and Effects of a Novel Cooling Method Used in Grinding", International Institution for Production Engineering Research, Microtecnic, vol. VIII, No. 4, pp. 199 – 205.

[41] **Sviridov, A. P.** (1960), "The way of Cleaning the Grinding Wheel", Pat. No. 246168.

[42] **Fisher R. C.**, (1965), "Grinding Dry with Water?", Grinding and Finishing, vol. 11, pt. 3, pp. 33 – 35.

[43] **Khudobin, L. V.** (1969), "Cutting Fluids and its Effects on Grinding-Wheel Clogging", Machines & Tools, Volume XL, No.9, pp. 54-59.

[44] **Kaliszer H., Trmal G.,** (1975), "Mechanics of Grinding Fluid Delivery", SME, MR75 - 614, pp. 1 - 16.

[45] **Graham W., Whiston M. G.,** (1978), "Some observations of Through-wheel Coolant Application in Grinding", International Journal of Machine Tool Design & Research, v. 18, No. 1, pp. 9 – 18.

[46] **Satow Yoshikazu,** (1986), "Use of High Pressure Coolant Supply in Precision CBN Grinding", SME, MR86 – 643.

[47] **Rowe, W.B., Morgan, M.N., Allanson, D.A.,** (1991), "An Advance in the Modelling of Thermal Effects in the Grinding Process", Annals of CIRP, 40/1: 339-342.

[48] **Yokogawa Munehiko, Yokogawa Kazuhiko,** (1993), "Improving Grinding Performance of CBN Wheels by Dual-fluid Supply Method", Int. J. Japan Soc. Prec. Eng., vol. 27, No. 1, pp. 11 – 16.

[49] **Okuyama Shigeki, Nakamura Yoshinobu, Kawamura Suehisa,** (1993), "Cooling Action of Grinding Fluid in Shallow Grinding", Int. J. Mach. Tools Manufact., Vol. 33, No. 1, pp. 13 – 23.

[50] **Mindek R. B., Webster J. A.,** (1994), "Minimizing Thermal Damage of Aerospace Components Using Coolant Nozzle and Coolant System Optimisation", Proceedings of the 5th International Gas Turbine Institute of the ASME, vol. 9, pp. 97 – 104.

[51] **Webster J. A.,** (1995), "Selection of Coolant Type and Application Technique in Grinding", Conference Paper of Supergrind'95, Grinding and Polishing with Superabrasives, Nov., pp. 205 – 220.

[52] **Kovacevic R., Mohan R.,** (1995), "Effect of High Speed Grinding Fluid on Surface Grinding Performance", SME, MR95-213, September 12-14, pp. 918 - 931.

[53] **Hiramatsu Hiroyuki,** (1998), "Grinding Fluid Supply Device for Grinder", Patent No.: JP10296633, Application No.: JP19970112145 19970430.

[54] **Brockhoff T., Walter A.,** (1998), "Fluid Minimisation in Cutting and Grinding", Abrasives Magazine, Oct./Nov., pp. 38 – 42.

[55] **Zhang L. C. and Yasunaga N.**, (1998), "Advances in Abrasive Technology", Abrasives Engineering Society.

[56] **Delchev P.G., Gugov L. G., Delijski N. D.,** (2000), "Attachment For Feeding Cooling-Cleaning Fluid to an Abrasive Disc", Patent No.: BG62690, Application No.: BG19970101865 19970829.

[57] **Ramesh K., Yeo S. H., Zhong Z. W., Sim K. C.,** (2001), "Coolant Shoe Development for High Efficiency Grinding", Journal of Materials Processing Technology, vol. 114, pt. 3, pp. 240 – 245.

[58] **Choi H. Z., Lee S. W., Jeong H. D.,** (2001), "A Comparison of the Cooling Effect of Compressed Could Air and Coolant for Cylindrical Grinding With a CBN Wheel", Journal of Materials Processing Technology, vol. 111, pt. 3, pp. 265 – 268

[59] **Furutani K, Ohguro N., Trong Hieu N., Nakamura T.,** (2002), "In-process measurement of topography change of grinding wheel by using hydrodynamic pressure", Int. J. Mach. Tools & Manufact., Vol. 42, pp. 1447 – 1453.

[60] **Suzuki K., Bin Qun H., Mishiro S., Tanaka K., Imai T., Sharma A., Uematsu T. and Iwai M.,** (2003), "Grinding Performance Improvement by a Special Coolant Superimposed with the Megasonic Vibration", Trance Tech Publications, Key Engineering Materials, Vols. 238 – 239, pp. 183 – 188.

[61] **Ninomiya S., Tooe S., Suzuki K. and Uematsu T.,** (2003), "Behaviour of the coolant in Grinding with a Floating Nozzle", Trance Tech Publications, Key Engineering Materials, Vols. 238 – 239, pp. 205 – 210.

[62] **Douglas J. F., Gasiorek J. M., Swaffield J. A.**, (2001), "Fluid Mechanics", 4th Edition, Prentice Hall.

[63] **Rui Cai,** (2002), "Assesment of Vitrified CBN wheels in Precision Grinding", PhD Thesis, Liverpool John Moores University.

APPENDIX

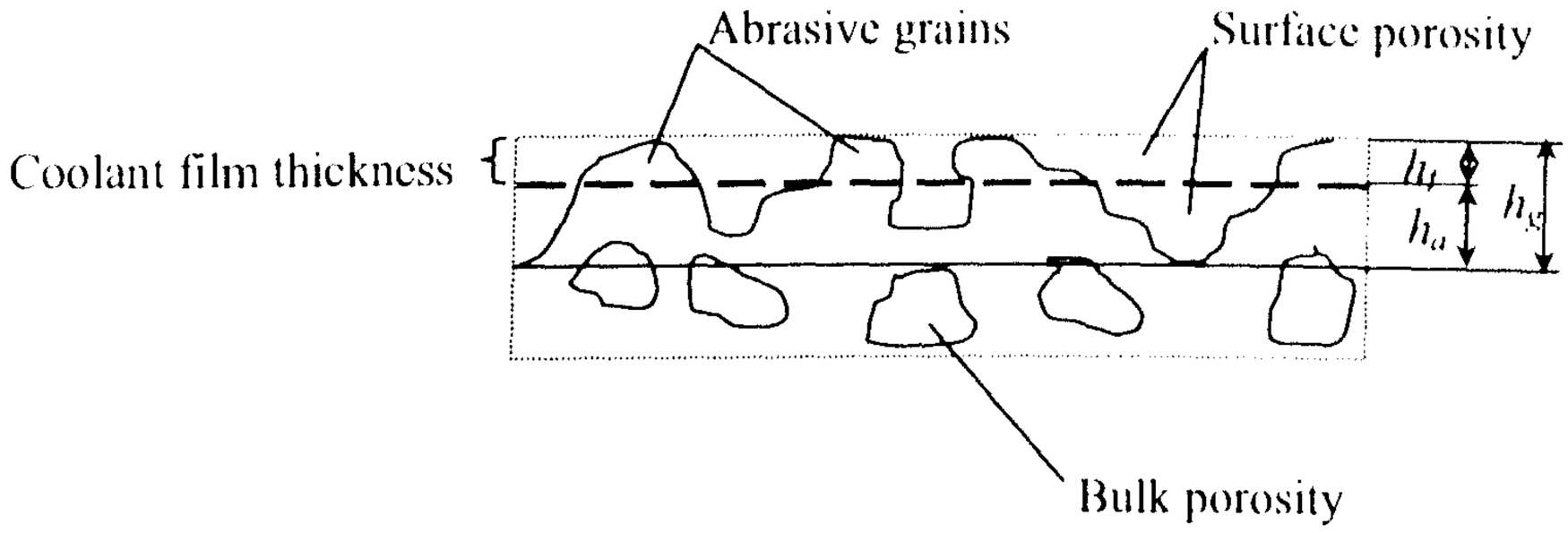

Figure 90. Schematic illustration of the grinding wheel surface porosity.

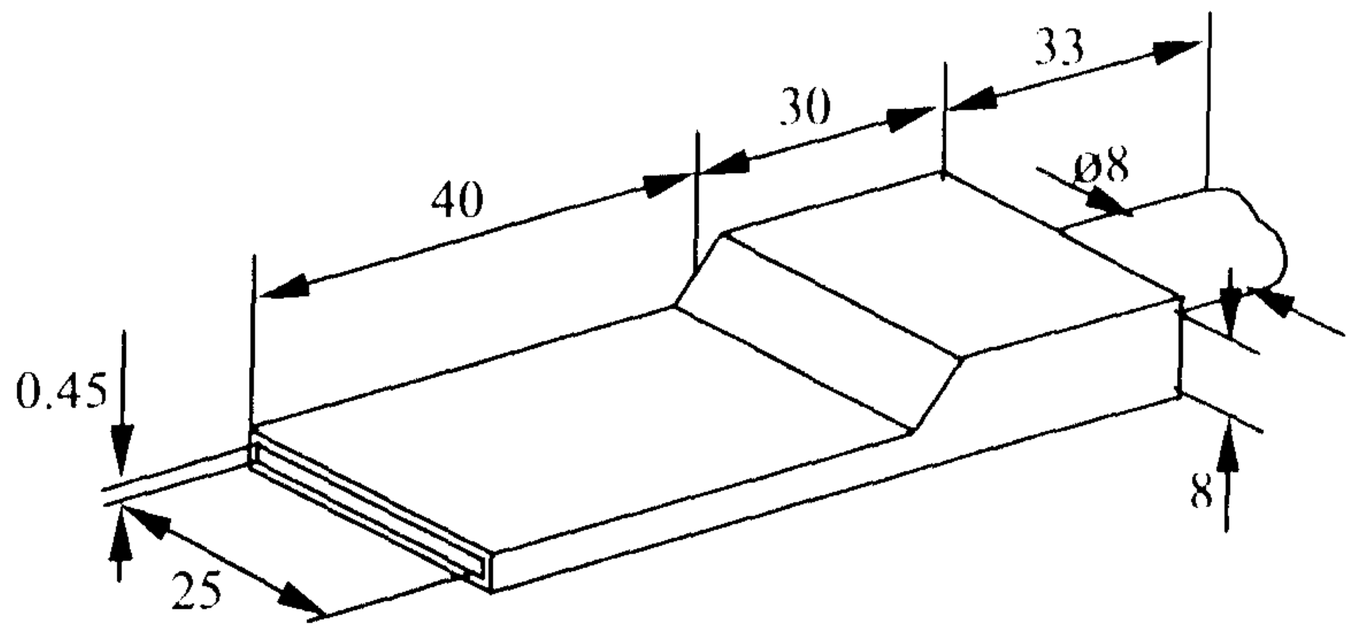

Figure 91. Schematic drawing of the nozzle with long slot and rectangular outlet gap.

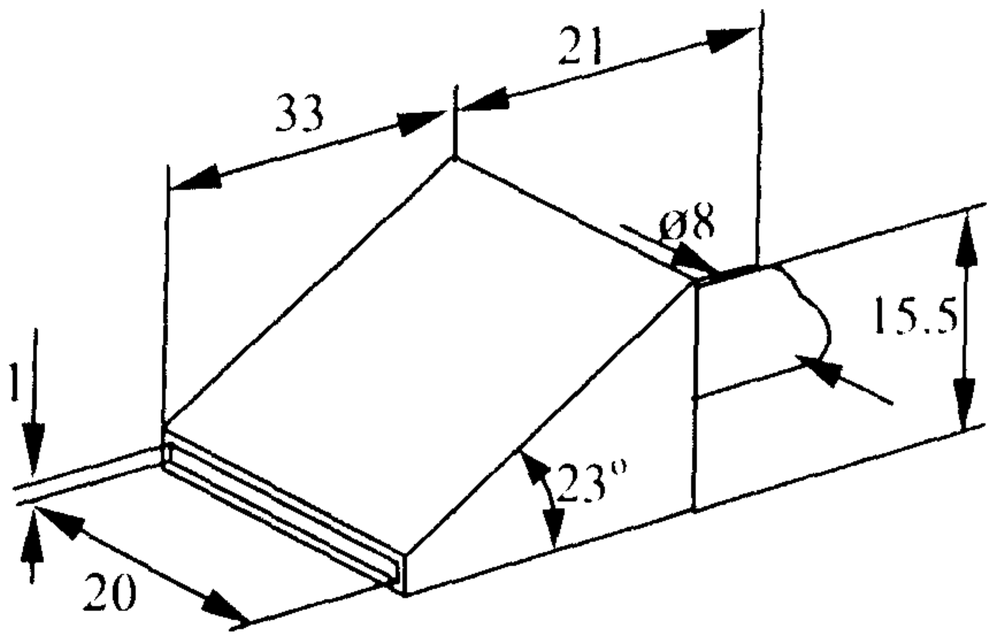

Figure 92. Schematic drawing of the nozzle with rectangular outlet gap and 23° gradual contraction.

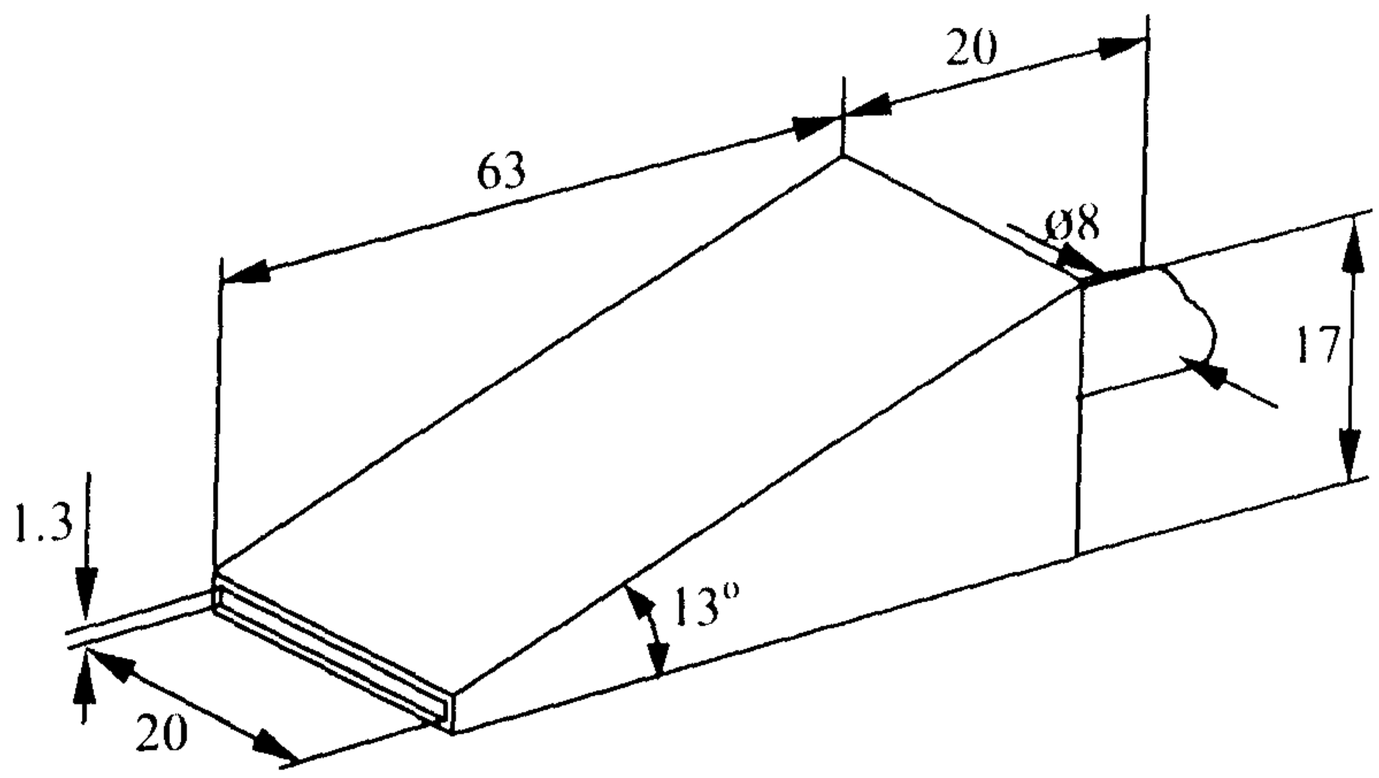

Figure 93. Schematic drawing of the nozzle with rectangular outlet gap and 13° gradual contraction.

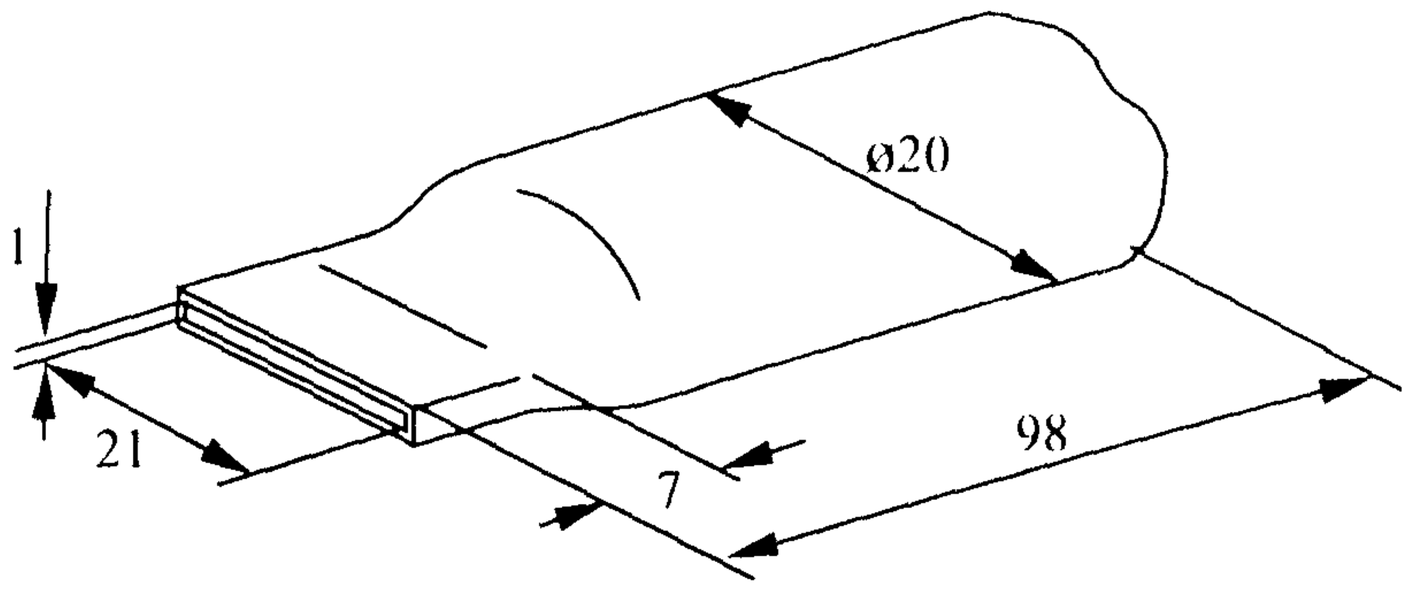

Figure 94. Schematic drawing of the cylindrical nozzle with rectangular outlet gap.

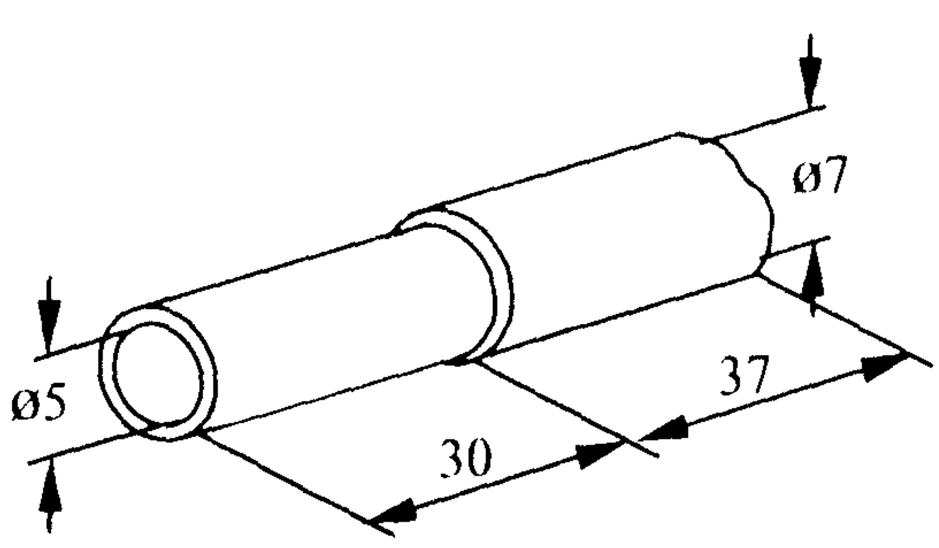

Figure 95. Schematic drawing of the cylindrical nozzle with orifice outlet.

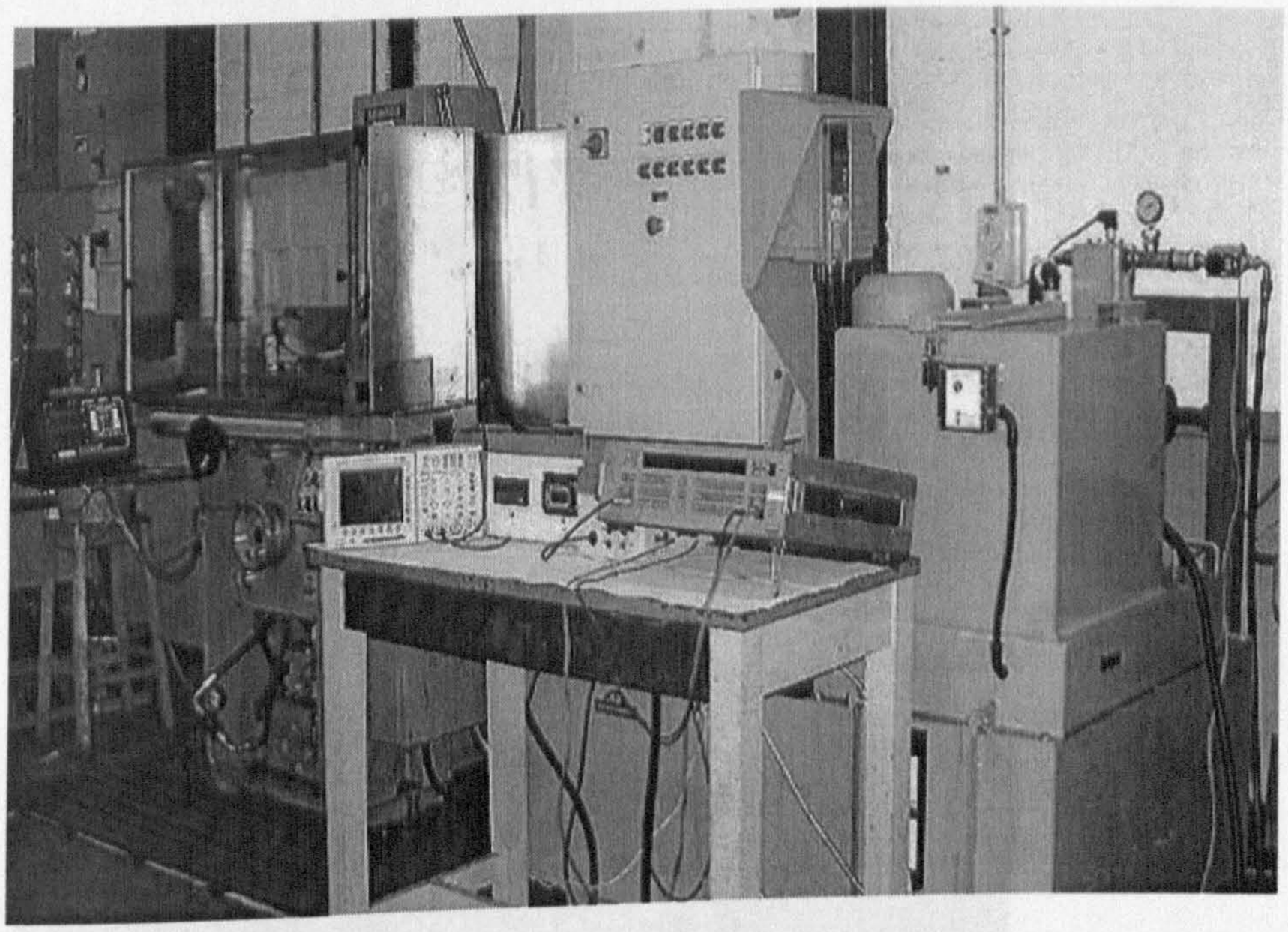

Figure 96. Abwood Series 5020 surface grinding machine and high flowrate fluid delivery system.

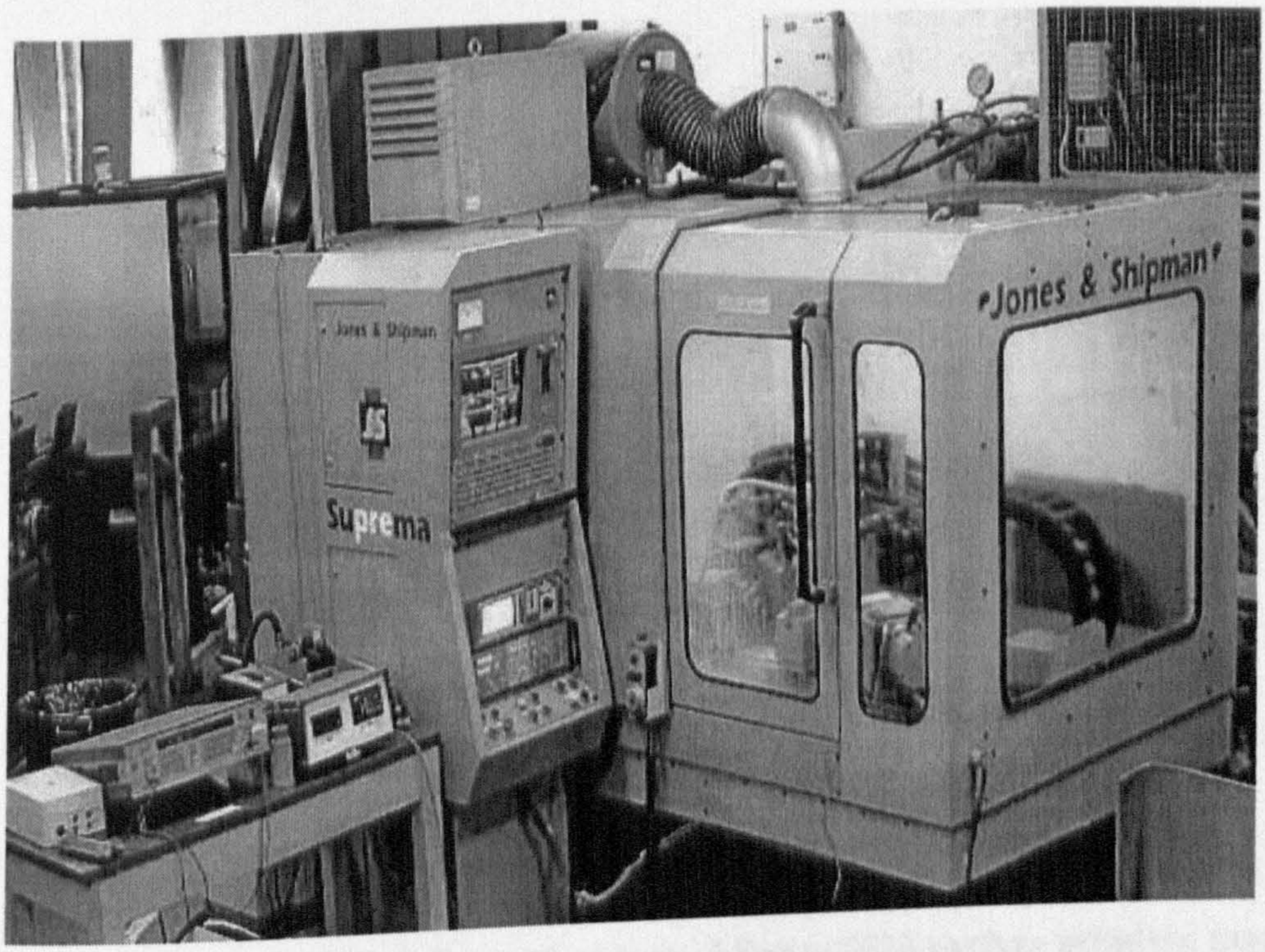

Figure 97. Suprema cylindrical-grinding machine.

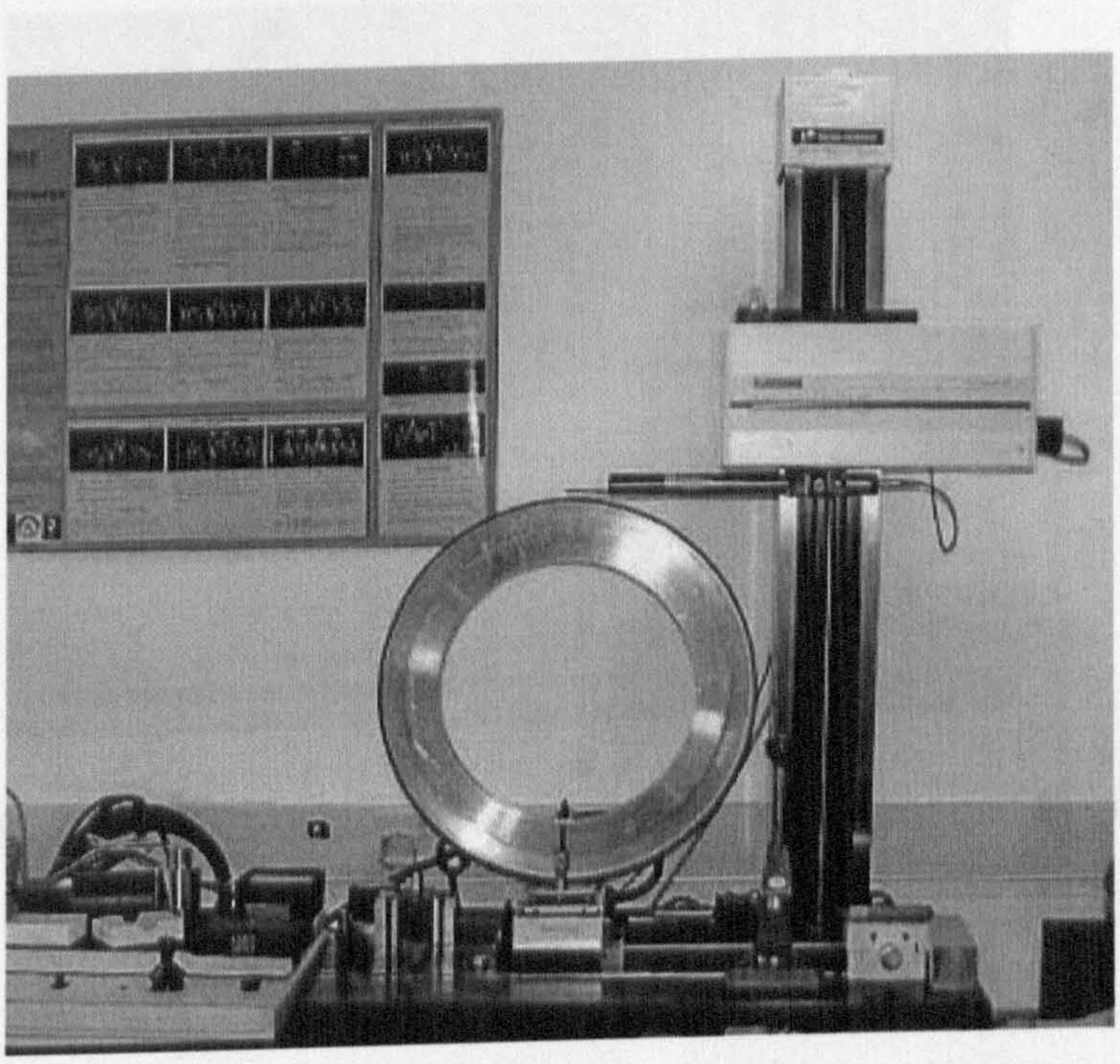

Figure 98. Taylor Hobson Talysurf 120 (3D) instrument.

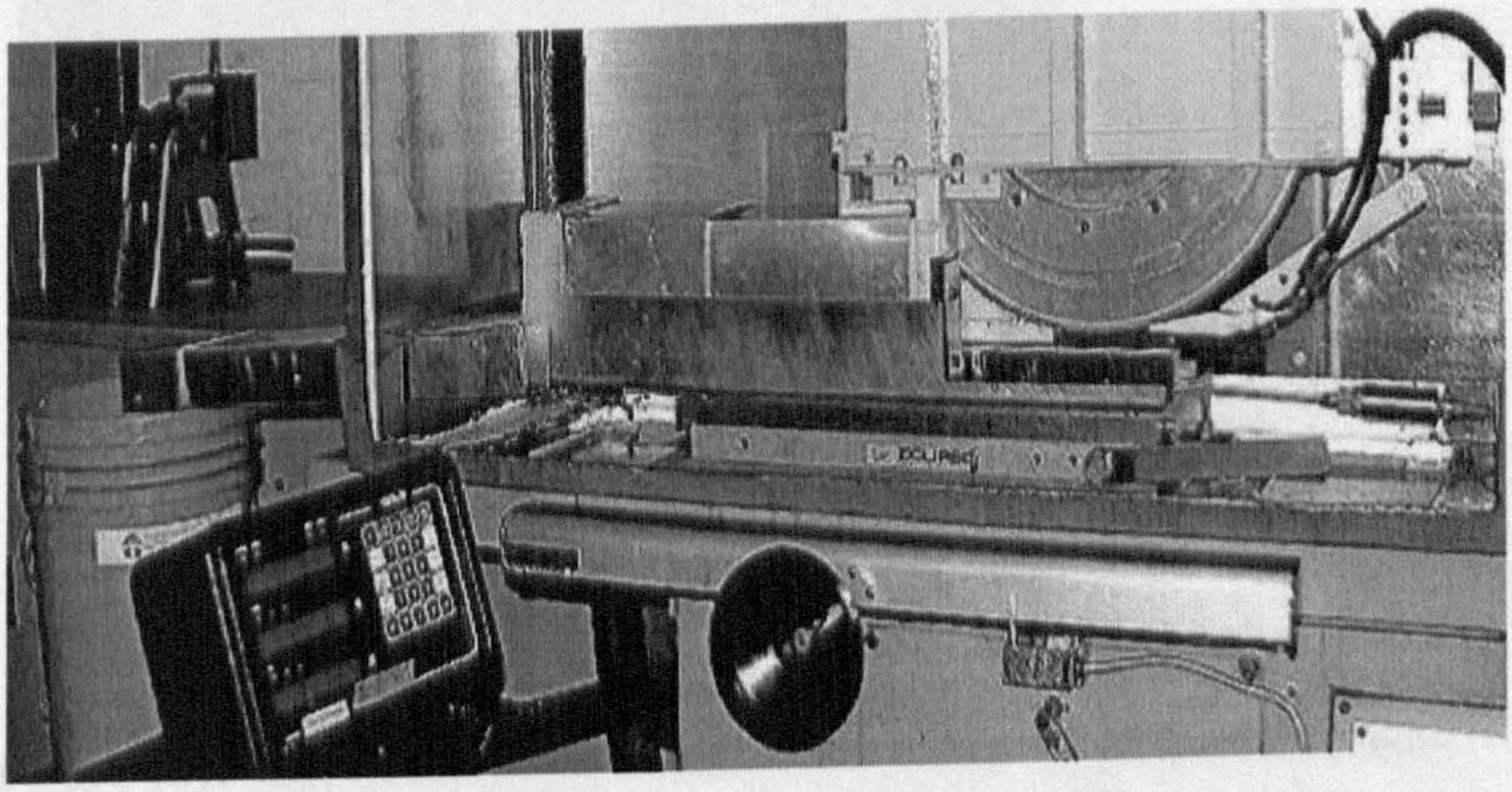

Figure 99. Experimental rig on the Abwood Series 5020 surface grinding machine.

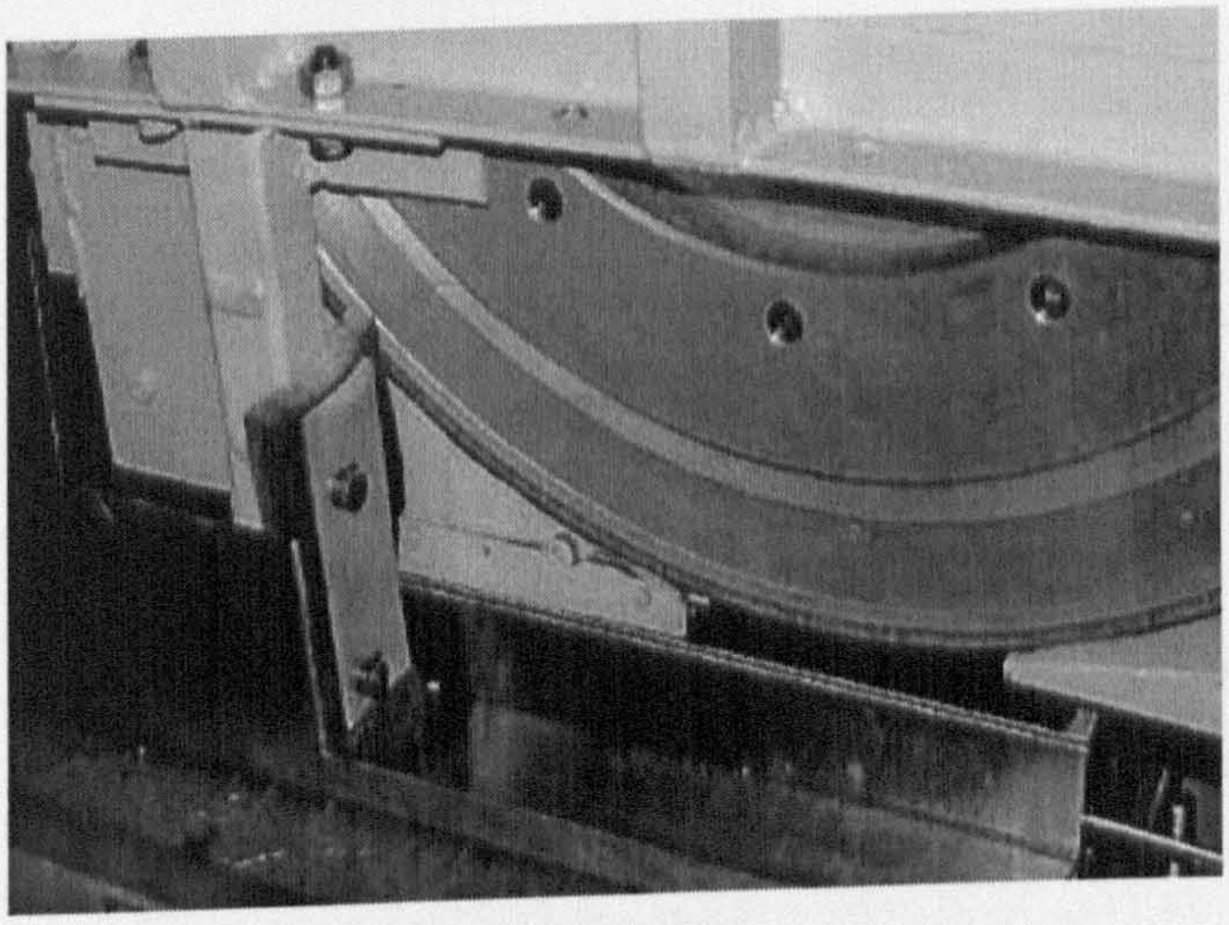

Figure 100. Useful flow separation rig and the carbon workpiece.

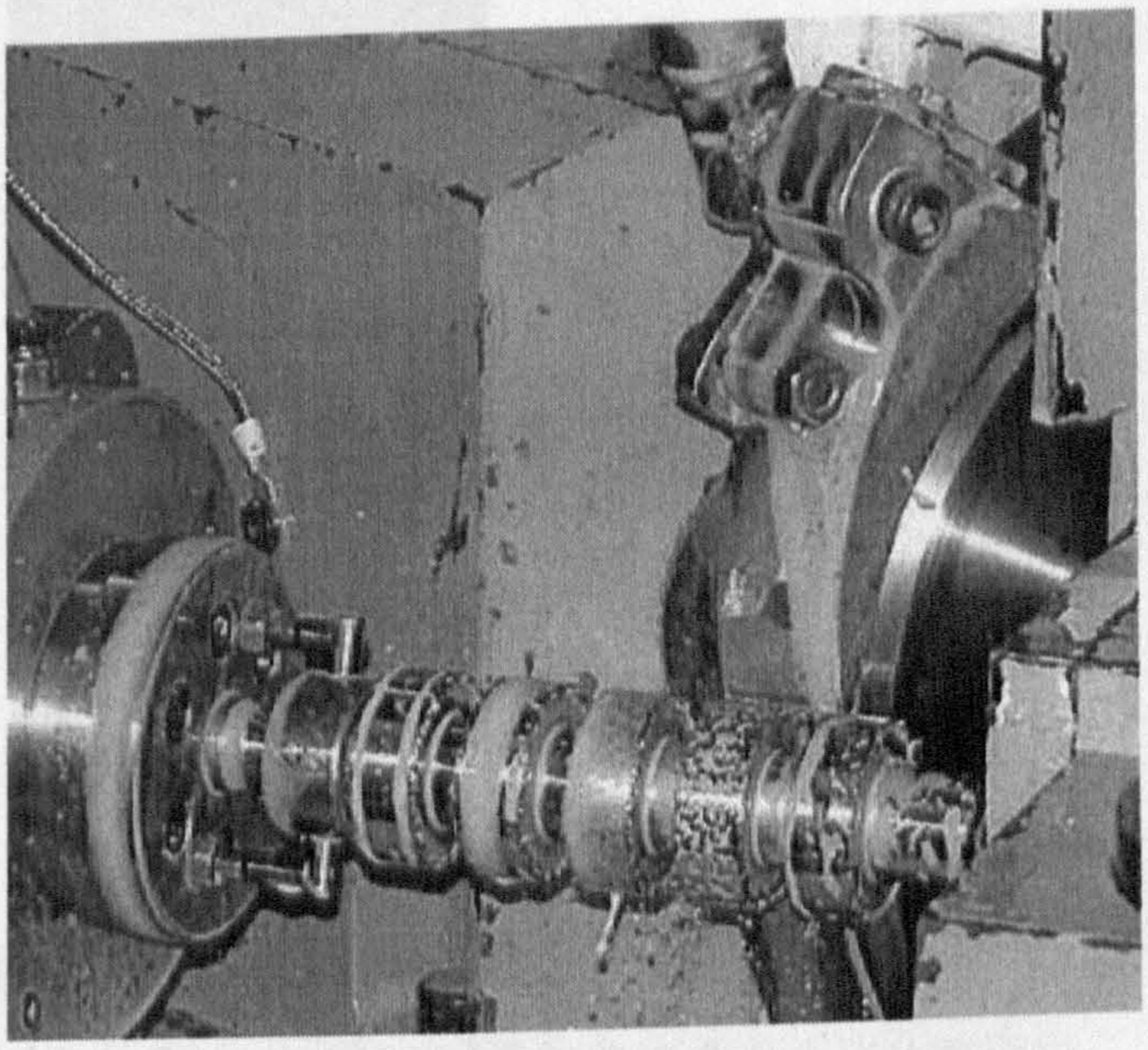

Figure 101. Shoe nozzle with concave plate during high speed grinding.

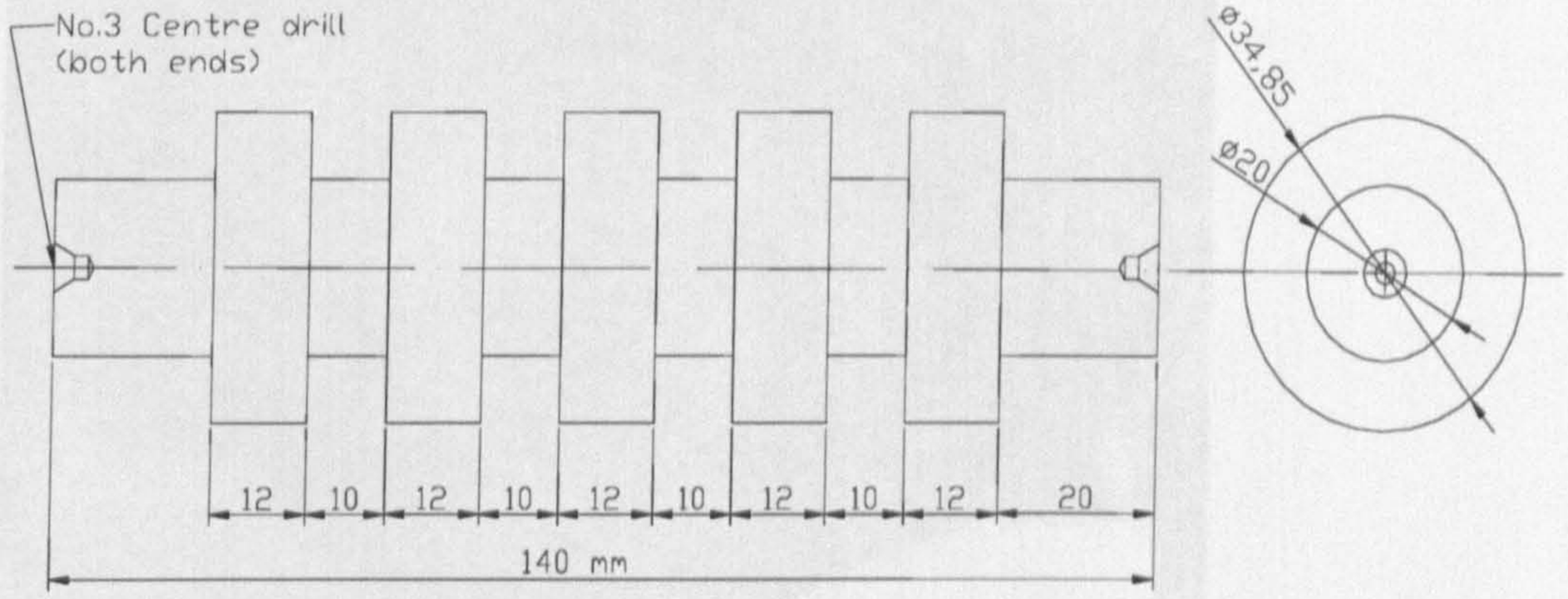

Figure 102. Inconel 718 workpiece.

Figure 103. Loading of the CBN wheel after high speed grinding of Inconel 718 with a shoe nozzle at 0.5 kg/s m delivery flowrate.

Figure 104. Illustration of the reversed air flow from the converging gap.

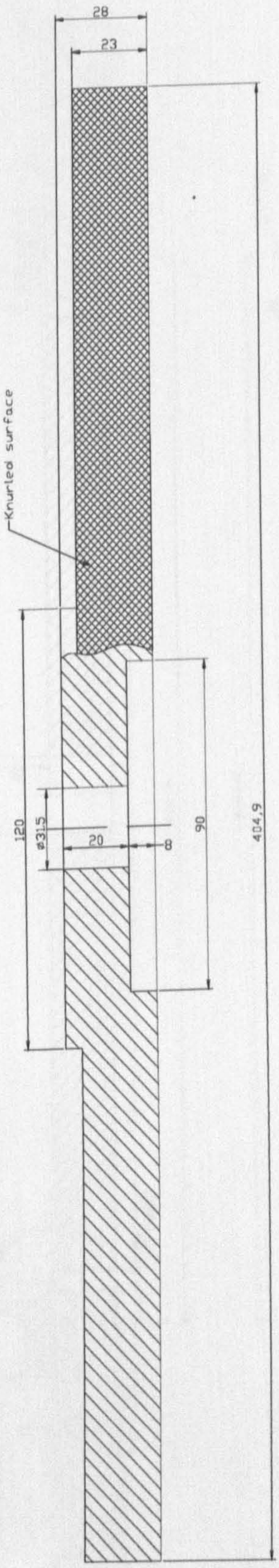

Figure 105. Knurled aluminium disc.

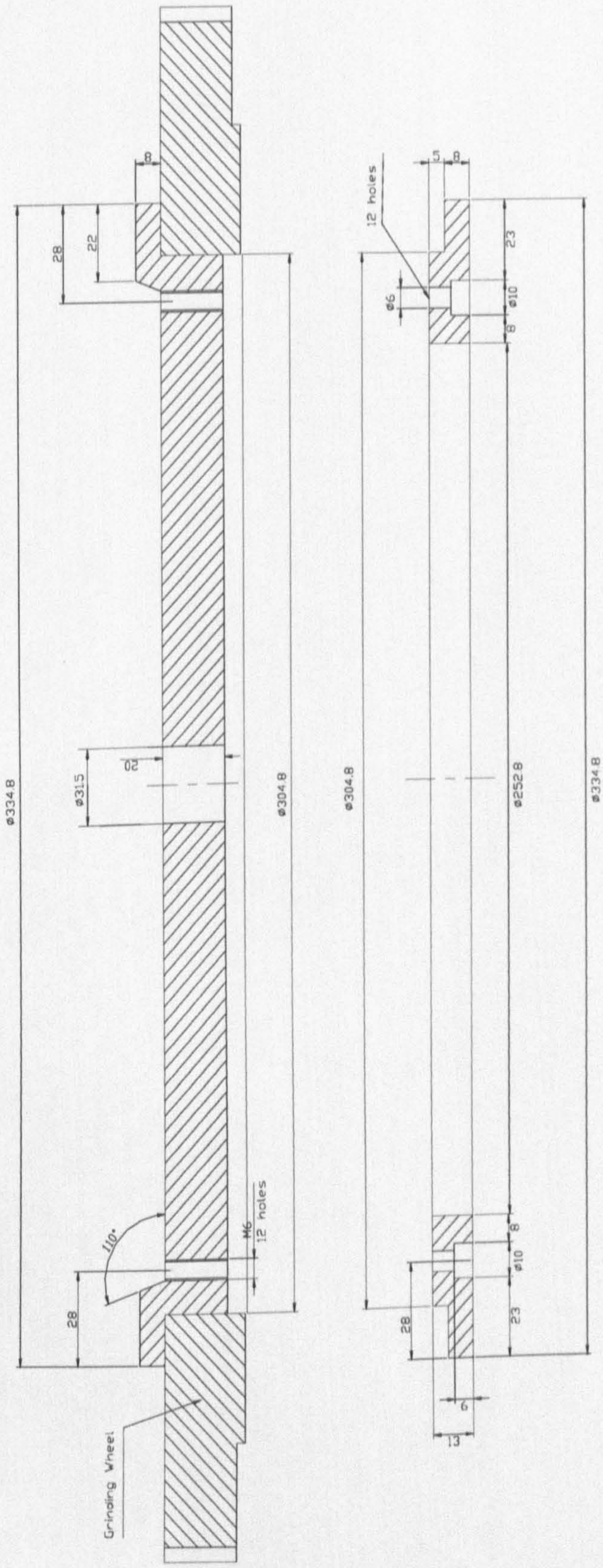

Figure 106. CBN grinding wheel adaptor.